Synucleins and their roles in the pathology of Parkinson's disease as metal binding proteins

Wang, Xiaoyan

Award date:
2009

Awarding institution:
University of Bath

Synucleins and their roles in the pathology of Parkinson's disease as metal binding proteins

Xiaoyan Wang

Thesis submitted for the degree of Doctor of Philosophy

University of Bath

Department of Biology and Biochemistry

July 2009

Abstract

α-synuclein is an abundant and conserved presynaptic brain protein (Uversky 2007). It has been received extensive attention since its aggregation was identified as the main component of Lewy bodies and Lewy neurites, which is the pathological hallmark of several neurodegenerative diseases, collectively known as synucleinopathies, including Parkinson's Disease (PD) (Uversky 2007). Considerable information has been collected about the structural properties and conformational behavior of α-synuclein, although the precise function is still under investigation. Metal ions such as copper and iron, can accelerate the aggregation and fibrillation of α-synuclein. Metal ions may exert their dual physiopathological properties through the interaction with α-synuclein, converting protein structure or/and inducing oxidative stress. In this study, isothermal titration calorimetry and electron paramagnetic resonance were used to determine the metal-binding property of the synuclein proteins, proving the presence of four Cu(II) binding sites per molecular of α-synuclein, with the coordination modes of 1N3O and 2N2O. Furthermore, α-synuclein has a catalytic action on the redox cycling of Cu(II), which was assessed by the application of cyclic voltammetry. However, this property is absent on β-synuclein and γ-synuclein, which belong to the synuclein family and have been suggested to be the physiological regulators of α-synuclein expression. In vivo, immunofluoresence studies revealed that Cu(II) increases the aggregates formation in mammalian doperminergic neuron cells overexpressing α-synuclein and the PD-associated mutants, while no aggregates have been found in cells overexpressing β-synuclein and γ-synuclein.

Acknowledgements

Firstly, I would like to express my sincere gratitude to my supervisor, Professor David R Brown, who has given me invaluable guidance, stimulating suggestions and encouragement in all the time of research for and writing of this thesis. I am deeply grateful of his help in the completion of this thesis.

Secondly, I would like to ackownledge all the scientists who have contributed to this project. I would like to extend my warmest thanks to Dr Josephine Wright and Dr Paul Davies, for their kindest help and support throughout my PhD. I would also like to thank: Dr John viles and Claire Sarell for their assistance with the EPR spectroscopy; Dr Paul Davies and Dr Frank Marken for their help with ITC and CV analysis; Dr Josephine Wright for her supervision on confocal microscopy; Dr Jill Madine for her support on NMR spectroscopy.

Finally, I am greatly indebted to my beloved fiancé Lei Wang, my father Fengchun Wang, my mother Guoping Zhai and my sister Xiaowen Wang for their encouragement and support. I would especially like to thank Lei for his love, friendship, understanding and tolerance. I also owe my sincere gratitude to all my friends who gave me their help and time in listening to me and helping me work out my problems during this period.

Publications

Madine, J., Wang, X., Brown, D. R. and Middelton, D. A. (2009) Evaluation of beta-alanine- and GABA-substituted peptides as inhibitors of disease-linked protein aggregation. ChemBioChem. 2009 Aug 17;10(12):1982-7.

Wright JA, Wang X, Brown DR. (2009) Unique copper-induced oligomers mediate alpha-synuclein toxicity. FASEB J. 2009 Aug;23(8):2384-93. Epub 2009 Mar 26.

Davies P, Fontaine SN, Moualla D, Wang X, Wright JA, Brown DR. (2008) Amyloidogenic metal-binding proteins: new investigative pathways. Biochem Soc Trans. 2008 Dec;36(Pt 6):1299-303.

Wang, X., Moualla, D., Wright, JA and Brown DR. 2009 Copper Binding Regulates Intracellular Alpha-Synuclein Localisation, Aggregation and Toxicity. for submission to J. Neurochem. (In preparation)

Davies, P., Wang, X., Drewitt, A. Marken, F. Brown DR.2009 Synuclein are a family of redox active copper binding proteins. for submission to JACS (In preparation).

Abbreviation

AD	Alzheimer's Disease
AEC	anion exchange chromatography
aS	α-synuclein
bS	β-synuclein
BSA	bovine serum albumin
CD	circular dichroism spectroscopy
CEC	cation exchange chromatography
CSP	cysteine-string protein
CV	cyclic voltammetry
DA	dopamine
DEPC	Diethylpyrocarbonate
DLB	dementia associated with Lewy body disease
DLBD	diffuse Lewy body disease
DNA	deoxyribonucleic acid
DNase	deoxyribonuclease
EDTA	ethylenediaminetetraacetic acid
EM	n-ethylmorpholine
EPR	electron paramagnetic resonance
ERK	extracellular signal-regulated kinase
ESR	electron spin resonance
FBS	fetal bovine serum
FPLC	fast protein liquid chromatography
GCIs	glial cytoplasmic inclusions
gS	γ-synuclein
IEC	ion exchange chromatography
IMAC	immobilized metal affinity chromatography
IPTG	isopropyl β-D-thiogalactopyranoside
IRPs	iron regulatory proteins
ITC	isothermal titration calorimetry
LBs	lewy bodies

LNs	lewy neuritis
MALDI	matrix-assisted laser desorption ionization
MPTP	N-methyl-4-phenyl-1,2,3,6-tetrahydropyridine
MSA	multiple system atrophy
NAC	non-Aβ-component of Alzheimer's Disease amyloid
NET	norepinephrine transporters
NMR	nuclear magnetic resonance
PA	phosphatidic acid
PAGE	polyacrylamide gel electrophoresis
PAK	p21-activated kinase
PC	phosphatidylcholine
PCR	polymerase chain reaction
PD	Parkinson's disease
PK	proteinase K
PKC	protein kinase C
PLD2	phospholipase D2
PMSF	phenylmethylsulphonyl fluoride
PUFA	polyunsaturated fatty acid
PVDF	polyvinylidene fluoride
Q-TOF	Quadrupole time-of-flight
ROS	reactive oxygen species.
SDS	sodium dodecyl sulphate
SNpc	substantia nigra pars compacta
TEMED	tetramethylethylenediamine
TH	tyrosine hydroxylase
WT	wild type

Contents

Contents-Figures

Contents-Tables

Chapter 1. Introduction

1.1 α-synuclein and its family members

1.1.1 α-synuclein

α-synuclein (aS) was first identified as a precursor protein of a peptide termed the non-Aβ-component of Alzheimer's Disease amyloid (NAC), which was discovered and isolated during the investigation of the composition of amyloid plaques of patients with Alzheimer's Disease (AD), which is the most common form of dementia (Ueda, Fukushima et al. 1993; Weinreb, Zhen et al. 1996). This protein was then proven to be a homologue of a protein named synuclein, which was first isolated from the electric organ of the Pacific electric ray (Torpedo californica), where it was found in both nerve terminals and the nuclear envelope (Maroteaux, Campanelli et al. 1988). aS is a highly conserved protein, with at least three isoforms produced in humans by alternative splicing (Clayton and George 1998; Beyer 2006). Two of the isoforms aS-112 and aS-126, are produced resulting from in-frame deletion of exons 3 and 5, respectively (Uversky 2007). Recently, a new isoform aS-98, which lacks exons 3 and exons 5, has been identified as a brain-specific splice variant (Beyer, Domingo-Sabat et al. 2008). The best-known isoform aS-140, which is the whole and major transcript of the protein, is encoded by the human aS gene (SNCA or PARK1) mapping to chromosome 4q21.3-q22 (Chen, de Silva et al. 1995). It is a 140 amino acid protein, which consists of three distinct regions, namely the amphipathic N-terminal domain (residues 1-60), the hydrophobic region (residues 61-95) and the acidic C-terminal part (residues 96-140) (Eliezer, Kutluay et al. 2001)(Fig 1.1). The N-terminal domain of aS is characterized by four 11-amino acid imperfect repeats with a highly conserved hexamer motif (KTKEGV), which is responsible for the lipid binding (Perrin, Woods et al. 2000) and α-helical structure formation when associated with lipid micelles (Weinreb, Zhen et al. 1996; Davidson, Jonas et al. 1998). NMR studies have revealed that this domain of aS bound to lipid-mimicking detergent micelles adopts two separate amphipathic helices, which do not appear to interact with each other although the hinge region between them probably adopts a well-defined structure (Bussell and

Eliezer 2003; Bisaglia, Trolio et al. 2005; Bussell, Ramlall et al. 2005). In addition, this domain is thought to be involved in protein-protein interaction (Weinreb, Zhen et al. 1996; Davidson, Jonas et al. 1998) and dimerization (Jensen, Hojrup et al. 1997). The central hydrophobic region, comprising the NAC sequence, appears to mediate the conformational change of aS from random coil to β-sheet (Serpell, Berriman et al. 2000; el-Agnaf and Irvine 2002) and further to Aβ-like protofibrils and fibrils (Conway, Harper et al. 1998; El-Agnaf, Jakes et al. 1998; Hashimoto, Hsu et al. 1998; Giasson, Uryu et al. 1999; Narhi, Wood et al. 1999; el-Agnaf and Irvine 2002). This part is most likely the amyloidogenic part of aS and is necessary for the aggregation of the protein. It shows mild sequence similarity with domains of the Prion protein and the β-amyloid peptide (Aβ) crucial for aggregation (El-Agnaf, Bodles et al. 1998). Deletion of residues 71-82 within this region prevents aS aggregation in vitro (Bodles, Guthrie et al. 2001; Giasson, Murray et al. 2001). The Carboxyl-terminus of aS, enriched in acidic residues and prolines, does not associate with either vesicles or micelles in solution (Eliezer, Kutluay et al. 2001), however, it is suggested to be primarily involved in the solubilization of the high molecular weight complexes (Park, Jung et al. 2002). Conversely to the hydrophobic region, this portion shows an inhibitory role on the aggregation of aS. Several studies have suggested that C-terminal truncated forms of recombinant aS assemble into filaments more readily than the full-length wild-type (WT) protein (Crowther, Jakes et al. 1998; Serpell, Berriman et al. 2000; Murray, Giasson et al. 2003; Periquet, Fulga et al. 2007). In addition, C-terminal part is essential for the chaperon activity of aS. aS could inhibit the aggregation of model substrates and protect the catalytic activity of alcohol dehydrogenase and rhodanese during heat stress (Kim, Paik et al. 2002) and enzyme activity of microbial esterases in vitro (Ahn, Kim et al. 2006), but deletion of the C-terminal region led to the abolishment of these chaperon activities. Moreover, C-terminal (residues 99-140) portion plays a signal-like role for translocation of aS expressed in *Escherichi coli* (Ren, Wang et al. 2007).

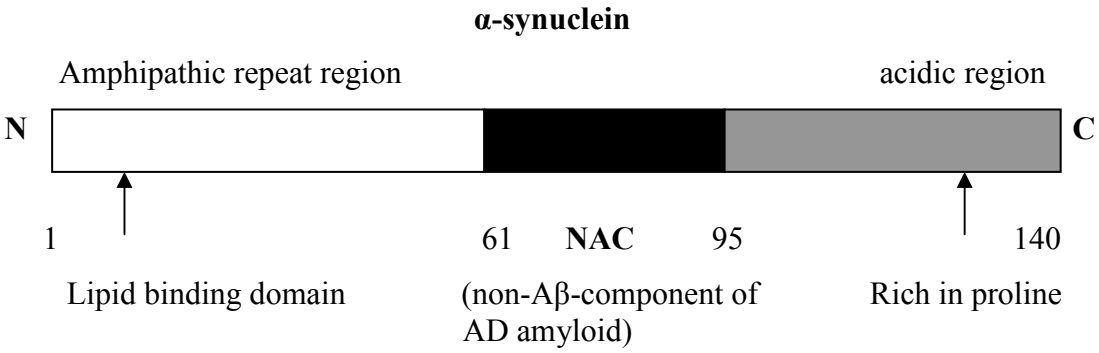

Fig. 1.1 α-synuclein schematic representation.
α-synuclein consists of three distinct regions, namely the amphipathic N-terminal domain, the hydrophobic region and the acidic C-terminal part. The lipid binding domain locates in the N-terminus.

In vivo, aS has been demonstrated to adopt either a highly unstructured free state in the cytoplasm or a highly helical lipid-bound state representing the membrane- or synaptic vesicle-associated protein fraction (Weinreb, Zhen et al. 1996; Eliezer, Kutluay et al. 2001). It's likely that the two conformations are observed in vitro as well. Under physiological condition in vitro, aS is characterized as a natively unfolded protein without any secondary or tertiary structure (Uversky 2003). However, aS can self aggregate when incubated under certain conditions (Uversky, E et al. 2002). Meanwhile, aS can interact with a number of ligands and proteins, such as metals and enzymes, which might alter its native state conformation and lead to aS adopting partially folded conformation (Dev, Hofele et al. 2003). Actually, aS can adopt to a series of different conformations depending on the environment due to its remarkable conformational plasticity (Uversky 2003).

1.1.2 Subcellular localization of aS

aS is expressed in a number of neuronal and non-neuronal cell types including cortical neurons, dopaminergic neurons, noradrenergic neurons, endothelia cells and platelets (Hashimoto, Yoshimoto et al. 1997; Abeliovich, Schmitz et al. 2000; Tamo, Imaizumi et al. 2002). In human, aS is predominantly found in the central nervous system (CNS), including the cerebral cortex, the hippocampus, the amygdala and the olfactory bulb (Maroteaux and Scheller 1991; Iwai, Masliah et al. 1995), notably concentrated in the

presynaptic nerve terminals (Iwai, Masliah et al. 1995). It has been estimated that aS accounts for as much as 1% of the total protein in soluble cytosolic brain fractions (Iwai, Masliah et al. 1995). Recently, aS has also been detected circulating in human body fluids in a soluble form (Borghi, Marchese et al. 2000).

1.1.3 Physiological function of aS

The precise physiological function of aS remains elusive. Nevertheless, many studies have demonstrated that aS plays a crucial role in the regulation of membrane lipid component, synaptic vesicular turnover, synaptic plasticity, ubiquitin-proteasome processing and could act as a molecular chaperon (Dev, Hofele et al. 2003). In addition to binding phospholipid membranes and micelles, aS interacts stably with synthetic phospholipid vesicles containing negatively charged head groups (Davidson, Jonas et al. 1998; Jo, McLaurin et al. 2000; Ramakrishnan, Jensen et al. 2003) and biological membranes, such as crude brain vesicles (Jensen, Nielsen et al. 1998), and has a profound effect on the integrity of these bilayers, resulting in the formation of non-bilayer or small vesicular structures (Madine, Doig et al. 2006). These observations suggest that aS is involved in modulating the organization of membrane lipid components (Uversky 2007). In addition, it was found that when bound to the lipid membrane, monomeric aS can function as an antioxidant preventing the oxidation of unsaturated lipid in vesicles via the formation of methionine sulfoxide (Zhu, Qin et al. 2006).

In pre-synaptic termini, monomeric aS exists in either free or plasma membrane-, vesicle-bound states, which are in an equilibrium (McLean, Kawamata et al. 2000). This association with vesicular structure has led to the hypothesis that aS might be the regulatory component of synaptic plasticity and this is supported by several studies: aS antisense oligonucleotide-treated cultures display a significant reduction in the distal pool of synaptic vesicles (Murphy, Rueter et al. 2000). Furthermore, songbird studies indicate that aS is specifically upregulated in a discrete population of presynaptic terminals of the songbird brain during a period of song acquisition (George, Jin et al. 1995; Tofaris and Spillantini 2007). Specifically, aS is thought to be implicated in the regulation of dopamine (DA) neurotransmission, via the effects on vesicular DA

storage (Lotharius, Barg et al. 2002; Lotharius and Brundin 2002) and the inhibitory activity on tyrosine hydroxylase (TH), the rate-limiting enzyme in DA biosynthesis (Perez, Waymire et al. 2002). Enhanced DA release is detected at nigrostriatal terminals in aS knockout mice, in response to paired electrical stimuli (Abeliovich, Schmitz et al. 2000). Recent study has also indicated that aS regulates catecholaminergic neurotransmission via mediating the activity and surface expression of the norepinephrine transporters (NET) in a manner that is dependent on interaction with the microtubule cytoskeleton (Jeannotte and Sidhu 2007). Another function that could link aS to effects on presynaptic vesicle dynamics and synaptic membrane biogenesis is its inhibitory activity on phospholipase D2 (PLD2), a protein that hydrolyzes phosphatidylcholine (PC) to phosphatidic acid (PA) (Xia, Rohan de Silva et al. 1996; Jenco, Rawlingson et al. 1998). Indeed, besides its ability to bind to PLD2, aS appears to interact with many other proteins, including the microtubule associated protein Tau, 14-3-3, protein kinase C (PKC) and BAD (Dev, Hofele et al. 2003). Based on these studies, aS has been suggested to have a profound effect on synaptic vesicle formation through regulation of PA metabolism, to anchor cytoskeletal component to plasma membrane or lipid vesicles, and to participate in apoptotic cell death (Eliezer, Kutluay et al. 2001). Interestingly, aS is suggested to be involved in the protection of nerve terminals against injury via cooperation with cysteine-string protein (CSP)-α and SNARE proteins on the presynaptic membrane interface via a downstream mechanism (Chandra, Gallardo et al. 2005). In addition, monomeric aS is implicated in the inhibition of proteasomal activities (Snyder, Mensah et al. 2005).

One of the crucial functions of aS is the effect on cell survival and/or susceptibilities to certain insults, although the effect is still controversial. In brief, effects seem dependent on cell type, the kind of insult applied, and on the aS variant being expressed (Dev, Hofele et al. 2003). In some cases, aS acts as a neuroprotective protein. For example, da Costa C.A. and Lee M. (2003) have shown that overexpression of aS can protect neuronal cells from apoptotic stimuli and can delay cell death induced by serum withdrawal (Dexter, Wells et al. 1989; da Costa, Masliah et al. 2003). In other cases, aS displays neurotoxicity via inducing apoptosis or accelerating cell death by increasing the sensitivity of cells to toxic agents (Dev, Hofele et al. 2003). Expression of certain mutant aS forms significantly enhances the sensitivity of different cell types

such as PC12 and M17 neuroblastoma cell lines to the toxicity by proteasome inhibitors (Stefanis, Larsen et al. 2001; Tanaka, Engelender et al. 2001; Petrucelli, O'Farrell et al. 2002). The protective or/and toxic mechanism remains relatively obscure. Recent researches have shown that MAP kinase signaling pathway (Iwata, Maruyama et al. 2001), c-jun N-terminal kinase stress signaling pathway (Hashimoto, Hsu et al. 2002), the NF-kB signaling pathway (Yuan, Jin et al. 2008) and the extracellular signal-regulated kinase (ERK) signaling pathway (Hashimoto, Takenouchi et al. 2003) have been involved.

Finally, aS also interacts with a number of polyvalent metal cations including Fe^{2+}, Fe^{3+}, Al^{3+}, Zn^{2+}, Co^{2+}, Cu^{2+}, Mg^{2+}, Ca^{2+} et al (Paik, Lee et al. 1997; Souza, Giasson et al. 2000; Nielsen, Vorum et al. 2001; Uversky, Li et al. 2001; Golts, Snyder et al. 2002; Wolozin and Golts 2002; Lowe, Pountney et al. 2004; Binolfi, Rasia et al. 2006; Tamamizu-Kato, Kosaraju et al. 2006). This may lead to the hypothesis that aS plays a necessary role in the homeostasis of these metals.

1.1.4 Synuclein family

aS belongs to a class of intrinsically unstructured proteins family, which also includes β synuclein (bS), also known as phosphoneuroprotein 14 and γ synuclein (gS), also referred to breast cancer-specific gene 1 or persyn (Nakajo, Tsukada et al. 1993; Jakes, Spillantini et al. 1994; Iwai, Masliah et al. 1995; Polymeropoulos, Lavedan et al. 1997). The human β synuclein gene (SNCB), mapping to chromosome 5q35 (Spillantini, Divane et al. 1995), encodes a 134-amino-acid protein, while the human γ synuclein (SNCG) (Jakes, Spillantini et al. 1994), located on chromosome 10q23, encodes a 127-amino-acid protein (Lavedan, Leroy et al. 1998). Concerning the structure of these synucleins, bS and gS show a high level of sequence homology to aS (Fig 1.2). Among the human family members, bS is 62% identical and 79% similar to aS, gS is 50% identical and 74% similar to aS, and bS is 47% identical and 66% similar to gS (Sung and Eliezer 2006). The bS lacks 11 central hydrophobic residues within the middle region compared to aS and gS, while the acidic C-terminal with three identically placed tyrosine residues is conserved, which is missing in the gS (Buchman, Hunter et al. 1998; Goedert 2001).

1.1.5 Localization and structure of bS and gS

The localization of bS is mostly overlapped with aS, predominantly throughout the brain, in the cytoplamic matrix of the presynaptic axon terminals (Nakajo, Shioda et al. 1994). Within hippocampal neurons, bS co-localizes almost exclusively with synaptophysin in presynaptic terminals (Murphy, Rueter et al. 2000). In contrast, gS expression is more prevalent in the peripheral nervous system, but it is also expressed in the brain, including the substantia nigra (Buchman, Hunter et al. 1998; Lavedan, Leroy et al. 1998). Interestingly, it is distributed more widely throughout cell bodies and axons within the neuron cytoplasm than aS and bS (Lavedan, Leroy et al. 1998). The synucleins have been established to be present in other cell types, like bS in Sertoli cells of the testis and gS in the epidermis and in the breast cancer tissue (Nakajo, Tsukada et al. 1996; Ninkina, Alimova-Kost et al. 1998; Ninkina, Privalova et al. 1999).

Unlike aS whose structure and function properties have been extensively studied, relatively less investigation has been done to bS and gS. Although all three synucleins are expressed as natively unfolded proteins, they possess some structural variability and the differences between them are directly related to the variation in their primary amino acid sequences (Sung and Eliezer 2006). The NMR studies have demonstrated a high degree of homology in the N terminus of synucleins, which might be due to the conservation of the amino acids in this domain (Bertoncini, Rasia et al. 2007). However, subtle changes are observed in bS and gS compared to aS. Recent structural studies have reported increased α-helical conformation in this region of bS and gS (Bertoncini, Rasia et al. 2007), and bS possessing the highest propensity to adopt α-helical structure (bS>gS>aS). It is hypothesized that the absence of the central hydrophobic cluster in bS (Fig 1.2), which is present in aS and gS, might contribute to stabilize locally encoded α-helical conformation at the N terminus (Bertoncini, Rasia et al. 2007). At the C terminus, Carlos W. Bertoncini et al found evidence for the transient polyproline II conformations clustered in bS, which is stabilized by the presence of eight proline residues embedded in a polypeptide stretch rich in hydrophilic and negatively charged amino acids (Bertoncini, Rasia et al. 2007). In

general, bS exhibits a higher preference for random coil, whereas aS and gS are slightly more compact and structured (Uversky, Li et al. 2002). Both bS and gS are lack of the long-range contacts that observed in aS (Uversky, Li et al. 2002; Bertoncini, Rasia et al. 2007).

```
      1               10                20                30                40
(aS)  MDVFMKGL  SKAKEGVVAAA  EKTKQGVAEAA  GKTKEGVLYVG
(bS)  MDVFMKGL  SMAKEGVVAAA  EKTKQGVTEAA  EKTKEGVLYVG
(gS)  MDVFKKGF  SIAKEGVVGAV  EKTKQGVTEAA  EKTKEGVMYVG

           50              60              70              80
SKTKEGVVHGV  ATVA  EKTKEQVTNVG  GAVVTGVTAVA  QKTVEGAGSIA
SKTREGVVQGV  ASVA  EKTKEQASHLG  GAVFSG-----  ------AGNIA
AKTKENVVQSV  TSVA  EKTKEQANAVS  EAVVSSVNTVA  TKTVEEAENIAV

90          100                 110         120         130
AATGFVKKDQLGKN-----EEGAPQEGILEDMPVDPDNEAYEMPSEEGYQDYEPEA
AATGLVKREEFPTDLKPEEVAQEAAEEPLIEPLMEPEGESYEDPPQEEYQEYEPEA
TSGVVRKEDLRPSAPQQEGVASKEKEEVAEEAQSGGD------------------
```

Fig. 1.2 The sequence alignment of human aS, bS, and gS.
The imperfect 11-residue repeats are delineated by spaces. The KTKEGV consensus sequence within each repeat is highlighted.

1.1.6 Physiological function of bS and gS

Although the physiological role of bS and gS is not fully understood, some characteristic features of aS have been preserved, while others are missing. A recent study has confirmed the fatty acid binding property of bS, although to a less extent compared to aS, but suggested that gS does not share this same characteristic (Salem, Allsop et al. 2007). Furthermore, bS exhibits chaperon activity more efficiently than aS, which is supported by the observation that bS displays remarkably higher activity in the suppression of the heat- induced aggregation of aldolase, alcohol dehydrogenase and citrate sythase (Lee, Paik et al. 2004). bS has also been known to play a role in the antiapoptotic process and to protect neurons from neurotoxin by regulating protein

kinase B/Akt activity (da Costa, Masliah et al. 2003; Hashimoto, Bar-On et al. 2004). In addition, bS is indicated to reduce proteasomal inhibition induced by aS, through competing with subunit in the proteasome for binding to aS (Snyder, Mensah et al. 2005). Unlike aS, bS does not fibrillate when incubated under the same condition, but it can be forced to fibrillate in the presence of some metals (Zn^{2+}, Pb^{2+}, and Cu^{2+}) and pesticides (Yamin, Munishkina et al. 2005). Compared to aS and bS, very little information is available regarding the biological function of gS. It appears to have the property to fibrillate, while it is weaker than aS (Uversky, Li et al. 2002). It's also shown to be involved in the proteasomal inhibition, which is not reduced by bS (Snyder, Mensah et al. 2005). In addition, gS participates in the heat shock protein-based multichaperon complex involved in estrogen receptor-α activation (Jiang, Liu et al. 2004).

1.2 aS and Parkinson's Disease

Parkinson's Disease (PD) is a common and incurable neurodegenerative disorder, affecting up to 2% of the population over the age of 65 years and 4-5% of those over 85 (Eriksen, Wszolek et al. 2005). This disease is worldwide distributed, with no gender preference, and the risk rises steeply with advancing ages. The clinical symptoms include resting tremor, muscle rigidity and Bradykinesia, which refers to slowness of movement. Concerning the pathological features, PD is characterised by progressive loss of dopaminergic neurons in the substantia nigra and the development of Lewy bodies (LBs) observed in these neurons. LBs are the filamentous inclusions within neurons, which were first described in a PD brain by Dr. Friedrich H. Lewy in 1912. LBs in the substantia nigra typically have a characteristic spherical appearance with a loose radiating array of filaments in the periphery or "corona" surrounding a matted meshwork of filaments in the center or "core". LBs are the pathological hallmarks of PD and other neurodegenerative diseases including dementia associated with Lewy body disease (DLB), diffuse Lewy body disease (DLBD), familial forms of AD, Down syndrome and multiple system atrophy (MSA). These diseases, now collectively known as synucleinopathies (Jellinger 2003), are characterized by progressive neuronal cell death and the accumulation of LBs or/and LNs, which are proteinaceous formations in neurons. A number of proteins, such as Parkin, Hsp70 and UCH-L1,

have been shown to be contained in the LBs. Subsequently, fibrillar aS was found to be the main component of the LBs and LNs (Spillantini, Schmidt et al. 1997).

The cause of PD is not clear. Substantial evidence suggests that aS is linked to the pathogenesis of PD in some cases. Initially, it was identified as a candidate gene for PD (Polymeropoulos, Higgins et al. 1996). In 1997, a missense mutation in the aS gene, characterized by a change from alanine to threonine at position 53, was identified in Italian-American and Greek families with autosomal dominant inheritance for the PD phenotype (Polymeropoulos, Lavedan et al. 1997). In 1998, a further mutation A30P, referred to alanine to proline substitution, was discovered in a German family with an autosomal dominant form of PD (Kruger, Kuhn et al. 1998). More recently, a third mutation E46K, known as glutamic acid to lysine substitution, was found in aS gene in a Spanish family with an autosomal dominant form of PD (Zarranz, Alegre et al. 2004). In addition, duplication and triplication of the aS gene, which leads to three and four functional copies of WT aS, also cause PD (Singleton, Farrer et al. 2003; Bonifati 2005; Nishioka, Hayashi et al. 2006). It's likely that aS has a crucial role in the pathogenesis of PD. The plasma aS levels in PD are significantly elevated compared with levels in controls (Lee, Lee et al. 2006), indicating a possible pathological role of aS. The functions of aS and its mutants have been intensely assessed in valid animal models using transgenic technique and viral infection. Overexpression of aS in Drosophila leads to the accumulation of LB-like aS aggregates in DA neurons and a PD-like phenotype (Feany and Bender 2000). Meanwhile, the first transgenic mice overexpressing human aS, generated in 2000 by Masliah et al, displayed a progressive accumulation of LB-like inclusions in neurons, which are associated with a loss of DAergic terminals in the basal ganglia and with motor impairments (Masliah, Rockenstein et al. 2000). Transgenic mice overexpressing the mutants including A30P and A53T aS, also develop many of the salient features of LB disease such as proteinase-K resistance, neuritic pathology and formation of aS inclusions with increasing age (Neumann, Kahle et al. 2002). Coincidently, in the adeno- or lentiviral-mediated rats models, overexpression of either WT or mutant aS led to cellular and axonal pathology accompanied by the loss of nigral neurons and significant motor impairment (Kirik, Rosenblad et al. 2002). In addition, elevated level of aS expression has been detected in other models of PD, including MPTP and 1BnTIQ treatment (Shavali, Carlson et al. 2004; Purisai, McCormack et al. 2005).

Interestingly, down-regulation of aS expression in a viral vector modulated PD rat model, rescues dopaminergic cells from cell death in the substantia nigra, indicating the direct effects of increased level of aS to neuronal cell loss (Hayashita-Kinoh, Yamada et al. 2006). Based on these observations, aS is thought to play an important role in the disease progression. However, the precise role is still under investigation.

It was suggested that the conversion of aS from soluble monomers to insoluble aggregates in the brain is a key event (El-Agnaf and Irvine 2000), and the aggregated forms of aS play a crucial role in the pathogenesis of PD. However, the molecular mechanisms underlying aS monomers into aggregation and further into filamentous inclusions remain unclear.

In contrast to aS, neither bS nor gS is detected in LBs (Biere, Wood et al. 2000), and no mutations of either of them is identified related to familial PD (Lavedan, Buchholtz et al. 1998). Nevertheless, bS mutants have been found in DLB patients (Ohtake, Limprasert et al. 2004) and a very recent study suggests bS gene might modify the age at onset of PD (Brighina, Okubadejo et al. 2007), indicating bS is also linked to diseases.

1.3 Pathological property of synucleins:

1.3.1 α-synuclein aggregation mechanisms

aS aggregation is thought to be a key pathogenic event in the neurodegenerative diseases, because the predominant composition of LBs and LNs is identified to be fibrillar aS (Spillantini, Schmidt et al. 1997; Spillantini, Crowther et al. 1998). aS inclusions are also found in several more disparate neurodegenerative diseases that are not commonly referred to as synucleinopathies (Dev, Hofele et al. 2003), indicating the pathological role of aS aggregation in various diseases. A great deal of research has been reported assessing the mechanism regulating aS fibril formation and the factors triggering this process. It is believed that the conversion of aS into insoluble fibrils is initiated by a conformational modification that leads to an altered structural state. This is particularly evident from analysis of aS in LBs from patients, where an increase in

β-sheet content was observed (Hashimoto, Hsu et al. 1998). It has been reported that aS aggregation is a nucleation-dependent phenomenon in which the initial insoluble seed allows the selective deposition of the inclusions (Wood, Wypych et al. 1999). The process initially forms oligomeric species that are relatively soluble; these oligomers might then self-assemble into fibrillar structures that are insoluble (Cookson and van der Brug 2007; Cookson and van der Brug 2008). This theory regarding aS is that aS has an intrinsic property to form amyloid fibrils, which is increased by raising the effective protein concentration (Greenbaum, Graves et al. 2005). Actually, recombinant aS readily assembles into filaments in vitro, which are similar to aS filaments extracted from diseased brains in terms of morphology, staining, and structure (Wright and Brown 2008). The dynamic studies indicate a multi-step process in the fibril formation, which involves multistate folding (Ferreon and Deniz 2007) and five or nine transient intermediates formation (Kamiyoshihara, Kojima et al. 2007). Molecular modeling and molecular dynamics simulations based on the micelle-derived structure of aS showed that aS homodimers can adopt nonpropagating (head-to-tail) and propagating (head-to-head) conformations. Propagating aS dimers on the membrane incorporate additional aS molecules, and lead to the formation of pentamers and hexamers which then form fibrils (Tsigelny, Bar-On et al. 2007). This observation fits well in the nucleation-dependent mechanism.

Although the precise events responsible for aS aggregation are not fully understood, accruing evidence suggests a complex mechanism encompassing phenomena as diverse as structure perturbation, alternative splicing and posttranslational modification (Beyer 2006).

1.3.1.1 Amino acid determinants

As discussed above, aS is prone to form aggregates even in the absence of other proteins, suggesting this propensity is mainly related to its structure, which is directly correlated with its amino acid sequences. The central NAC region has been implicated to play a critical role in aS aggregation by several lines of evidence. As is known, NAC, the second major component of amyloid plaques in AD brain, readily forms ordered fibrils in vitro (Ueda, Fukushima et al. 1993; Han, Weinreb et al. 1995; Iwai, Masliah

et al. 1995). Moreover, NAC can seed Aβ amyloidogenesis and Aβ can also seed amyloid formation by NAC (Han, Weinreb et al. 1995). Finally, aS aggregation was impaired after the substitution of Ala76 with charged amino acids (either Arg or Glu) and was abolished after the deletion of amino acids residues 71-82 in this region (Giasson, Murray et al. 2001). In contrast to NAC region, C-terminus is suggested to play a role of intramolecular chaperon preventing aS from fibrillation. Apart from full-length aS, accumulated C-terminally truncated aS was found in the LBs and LNs in sporadic PD and LBD, as well as the glial cytoplasmic inclusions (GCIs) of multiple system atrophy (Baba, Nakajo et al. 1998; Gai, Power et al. 1999). Initial perikaryal aS accumulation also seems to be specifically constituted by aS112, a major aS isoform without C-terminus (Beyer, Lao et al. 2004). Several studies have revealed that C-terminus truncated aS constructs are more prone to fibrillate in vitro than the full-length protein (Crowther, Jakes et al. 1998; Serpell, Berriman et al. 2000; Murray, Giasson et al. 2003). According to these observations, it is clear that the C-terminus of aS is a negative regulator of self-assembly. Therefore, modification in this region, such as oxidation, nitration and phosphorylation (Hashimoto, Takeda et al. 1999; Giasson, Duda et al. 2000; Fujiwara, Hasegawa et al. 2002), may affect the propensity of aS to aggregate in vivo in a similar way to truncation. In addition, the tendency of aS to aggregate in vitro is proven to be accelerated by the PD-related point mutations, A30P and A53T, which are present in the N-terminus of aS. Both of the mutations increase the rate of aS oligomerization, whereas the rate of mature fibrils formation was increased by one (A53T) and decreased by the other (A30P) (Conway, Harper et al. 1998; Narhi, Wood et al. 1999; Rochet, Conway et al. 2000; Li, Uversky et al. 2001; Uversky, Li et al. 2001; Li, Uversky et al. 2002). Detailed conformational analysis revealed that the two mutants possess similar structural properties with WT aS, remaining to be natively unfolded (Conway, Harper et al. 1998; El-Agnaf, Jakes et al. 1998; Giasson, Uryu et al. 1999; Del Mar, Greenbaum et al. 2005). Interestingly, both mutations show reduced hydrophobicity in the vicinity of the substitution, which is assumed to be important in aggregation. Concurrently, the propensity to form α-helical structure was shown to be somewhat diminished in the N-terminal region of both mutants, whereas the internal susceptibility to form β-sheets was predicted to be slightly enhanced (Li, Uversky et al. 2001). Taking into account these observations it has been assumed that the increased tendency for A30P and A53T to form β-structure may not be strong enough to alter the structure of the monomeric proteins, but may

affect their aggregation behavior through specific stabilization of an intermolecular β-structure (Uversky 2007). In addition, high-resolution NMR analysis has revealed that A30P aS abolished a significant helical propensity in the N-terminus compared to WT aS, whereas A53T aS led to a preference for extended backbone conformation (Bussell and Eliezer 2001; Eliezer, Kutluay et al. 2001). Recently research has established that E46K mutation is also able to increase the propensity of aS to fibrillate, but to a less extent than A53T mutation (Greenbaum, Graves et al. 2005).

Concerning the structure disruption, both of bS and gS inhibit aS fibril formation and complete inhibition was observed at 4:1 molar excess of bS and gS over aS (Uversky, Li et al. 2002), although the mechanism is not fully elucidated. bS inhibits the generation of aS aggregation in doubly transgenic mice too (Hashimoto, Rockenstein et al. 2001). These findings have provided important sights into the possible effects of structure perturbation on aS aggregation.

1.3.1.2 Post-translational modifications

There is emerging evidence showing that several conditions that are involved in post-translational modification of proteins are relevant in promoting aS aggregation. Oxidative stress appears to be one of these candidates. Free-radical generators such as iron and hydrogen peroxide can accelerate the generation of aS and ubiquitin-positive intracytoplasmic inclusions in cells overexpressing aS under certain conditions (Ostrerova-Golts, Petrucelli et al. 2000). Similarly, pesticide rotenone induces formation of aS inclusions in the substantia nigra, which closely resemble LBs, by inhibiting mitochondrial complex I in rats (Sherer, Betarbet et al. 2001). Reactive species may interact with cellular proteins, thus altering their folding properties and function. Abnormal phosphorylation is proven to be another factor. aS has been established to be selectively and constitutively phosphorylated at mainly serine 129 within the C-terminal domain in synucleinopathy such as PD (Okochi, Walter et al. 2000), where phosphorylation of aS stimulated fibril formation in vitro (Fujiwara, Hasegawa et al. 2002). It seems that aberrant protein degradation is another mechanism that has been implicated in the formation of LBs. This is evident from the marked inhibition of proteasomal activity induced by aS (Snyder, Mensah et al. 2003).

The reduction may lead to the potential for increased proteinaceous aggregates in the substantia nigra of PD patients (McNaught and Jenner 2001). Meanwhile, the role of lipid membranes in the conversion of WT aS to a pathogenic protein has been intensely investigated. Upon exposure to vesicles containing certain polyunsaturated fatty acid (PUFA) acyl groups, recombinant aS forms multimers in vitro (Perrin, Woods et al. 2001). Furthermore, exposure of mesencephalic neurons to PUFA also stimulates the protein to form oligomers in vivo (Sharon, Bar-Joseph et al. 2003), which precede the insoluble fibrilar aggregates formation. However, more recent research has revealed that association of aS with biological membranes can also impede the aggregates formation by protecting the protein from oxidation and nitrosylation (Trostchansky, Lind et al. 2006). Finally, several environmental conditions and ligands have been recognized as triggers for aS aggregation in vitro, such as high temperature, low pH, polyamines, and metal ions (Binolfi, Rasia et al. 2006).

1.3.2 Toxicity of aS aggregates

The fundamental mechanism underlying the toxicity of aS and its aggregation to neurons is not entirely clear. A possible culprit is the transient oligomeric species formed along the way (Volles and Lansbury 2003). Much work has been developed to interpret this concept. aS oligomers are speculated to form pores on intracelluar membranes such as the plasma membrane based on the fact that some oligomeric species are annular or pore-like and aS is a lipid-associated protein (Volles and Lansbury 2002; Zhu, Li et al. 2003). This contention is supported by the evidence that aS aggregates formed ring-like structures under in vitro cell-free condition, and the cells expressing aS displayed increased ion current activity consistent with the formation of Zn^{2+}-sensitive nonselective cation channels (Furukawa, Matsuzaki-Kobayashi et al. 2006; Tsigelny, Bar-On et al. 2007). Incubation with globular aS oligomers significantly inhibited autophosphorylation of p21-activated kinase (PAK4) (Danzer, Schnack et al. 2007), which might contribute to the neuronal damage. aS is reported to be involved in the neuroinflammation by up-regulating interleukin (IL)-6 and ICAM-1 in human astrocytes and astrocytoma cells. This is confirmed by the study that demonstrated early activation of microglial and

consequent increases in proinflammatory molecules in the model of PD (Su, Maguire-Zeiss et al. 2008). Finally, aS aggregating is implicated to induce formation of hydrogen peroxide in vitro (Turnbull, Tabner et al. 2001), which is particularly harmful in the elderly where the antioxidant defences are known to be deceased.

1.4 Metals and synuclein

Both redox-active metals such as copper, iron and manganese, and redox-inactive metals are essential in most biological reactions e.g., in the synthesis of DNA, RNA, and proteins, and as cofactors of numerous enzymes, particularly those involved in respiration. Thus their dyshomeostasis can lead to disturbances in central nervous system and other organ function (Sayre, Moreira et al. 2005). Elevated levels of several of these metals such as copper and iron, have been reported in the neurodegenerative diseases, including PD, which is dyshomeostasis of both redox-active and redox-inactive metal ions. Accruing evidence suggests that abnormal iron handling may be involved in the pathogenesis of PD. The first report of increased iron levels in the Parkinsonian substantia nigra pars compacta (SNpc) of PD was in 1924 followed by another report in 1967 (Sayre, Moreira et al. 2005). Since then, the increased levels of iron in the PD midbrain have been verified by a great deal of research developed using several diverse methods, broadly classified as either postmortem or non-invasive studies. Moreover, analysis of LBs in the parkinsonian substantia nigra showed abnormal accumulation of iron and the presence of aluminum (Dexter, Carayon et al. 1991; Hirsch, Brandel et al. 1991), indicating they might be correlated with aS in the etiology of the disease. Similar alterations in metal homeostasis were observed in toxin-induced animal models of PD. N-methyl-4-phenyl-1,2,3,6-tetrahydropyridine (MPTP) and 6-hydroxydopamine-induced neurodegeneration in rodents and nonhuman primates is associated with increased presence of iron and aS in the SNpc, which are abolished by iron chelators (Mandel, Maor et al. 2004). Several pieces of epidemiological and biochemical data has suggested that iron accumulation might be a primary event in the degenerative process. Occupational exposure to specific metals, especially copper, iron, has been established to be a risk factor for PD (Zayed, Ducic et al. 1990). Dietary intake of iron and manganese above median levels also conferred a nearly doubled risk

of PD (Sayre, Moreira et al. 2005). Meanwhile, unilateral injection or infusion of Fe^{3+} into the SNpc of rats results in neuronal loss and progressive SNpc atrophy accompanied by both depletion of striatal dopamine and decreased motor function. These effects could be prevented by infusion of iron chelator desferrioxamine (Youdim, Ben-Shachar et al. 1993; Sayre, Moreira et al. 2005). In addition, altered levels of metal ions in bodily fluids of live patients were detected, with significant decreases in Al in both early and severe PD compared to controls, lower levels of Fe and Zn in severe PD, and higher levels of several other elements including K, Mg and Cu (Hegde, Shanmugavelu et al. 2004). Nevertheless, the mechanism how metals contribute to the pathogenesis of neurodegenerative diseases is elusive. One of the most popular concepts is that metals increase the levels of oxidative stress associated with the disease. The idea was supported by the shift in the Fe^{2+}/Fe^{3+} ratio in favor of Fe^{3+} and a significant elevation in the Fe^{3+}–binding protein, ferritin (Riederer, Sofic et al. 1989). Another mechanism, which indicates metals such as copper, promote aS aggregation either directly or via increasing levels of oxidative stress and in turn lead to neurodegeneration, is receiving more and more attention. In addition, Fe^{2+} was reported to induce DNA damage in aS transfected human neuroblastoma cells and the susceptibility to toxic effects of Fe^{2+} was enhanced with mutant aS associated with inherited forms of PD (Martin, Williamson et al. 2003).

1.4.1 Metal binding

Metals have been suggested to play a role in the pathogenesis of synucleinpathies as aS was identified as a metal-binding protein. There is cumulative evidence showing aS binds copper although the identification of the binding sites and affinities is still under debate (Fig 1.3). Initial studies suggested that aS binds to 5-10 copper ions with a K_d of 45-60 μM (Paik, Shin et al. 1999; Lee, Lee et al. 2003). However, Rasia et al showed that aS tightly binds to 2 copper ions per monomer with a dissociation constant in the range of 0.1-50 μM and is able to ligate more copper ions with significant lower affinity (400-500 μM) (Rasia, Bertoncini et al. 2005). Binolfi et al showed Cu(II) binds aS with high affinity K_d <0.1 μM (Binolfi, Rasia et al. 2006). A complete study using isothermal titration calorimetry technique determined the Cu(II) binding affinities to aS monomer (WT and mutant forms) to be K_B 10^5 and 10^4 M respectively,

and Fe(III) binding affinities to be 10^5 M (Bharathi and Rao 2007). There is consensus that aS binds Fe(II), nevertheless, the binding affinities reported are different (Golts, Snyder et al. 2002; Binolfi, Rasia et al. 2006). The more recent study suggested that the affinity is around K_d ~1mM (Binolfi, Rasia et al. 2006). There is evidence showing aS binds other metals such as Mn(II), Co(II), and Ni(II), however, with low affinity K_d ~1mM (Binolfi, Rasia et al. 2006). aS has also been reported to bind calcium, magnesium, zinc and aluminum, although the affinities are not determined yet (Paik, Lee et al. 1997; Nielsen, Vorum et al. 2001; Golts, Snyder et al. 2002; Lowe, Pountney et al. 2004).

There has been some controversy in the identification of metal-binding sites. Initial studies claimed C-terminus of aS is responsible for copper binding (Paik, Shin et al. 1999; Paik, Shin et al. 2000). Nevertheless, the following analysis characterized two distinct Cu(II)-binding motifs in aS. The high-affinity binding site encompassing a complex conformational array is located in the N-terminus of the protein, while the low-affinity site sits in the C-terminal region (Rasia, Bertoncini et al. 2005) (Fig 1.3). It was demonstrated that the high affinity site coordinates residues 3-9 and 49-52, which form a long-range interface with His50 as the anchoring residue. This conclusion relied on the observation that the N-terminal region is unable to interact with Cu(II) after modification of aS by DEPC treatment, which prevents histidine side chains from being able to coordinate copper. Therefore, it was reasoned that DEPC treatment would selectively inhibit copper binding to His50, and should not affecting binding to the N-terminus unless such binding required the participation of His50. However, a similar study reported that DEPC treatment modified the protein at multiple sites and eliminated copper binding to both the site around His50 and to the N-terminal site in full-length aS, but that it also eliminated copper binding to the N-terminal site in the H50A mutant, where modification of His50 is not possible (Sung, Rospigliosi et al. 2006). This indicates that copper-binding by aS does not involve long-range interaction and the N-terminus of aS and the site involving His50 are capable of binding copper independently of one another (Sung, Rospigliosi et al. 2006). This analysis suggested that although it is unlikely to occur in vivo, aS has 16 sites capable of binding copper because of the prevalence of negatively charged side chains, one histidine, and the primary amino group, particularly in the unstructured polypeptide. Further analysis utilizing peptides showed that Cu(II) ions appear to be

coordinated by the N-terminal amine group of methionine (residue 1), the amide nitrogen, and the β-carboxylic group of aspartic acid (residue 2) (Kowalik-Jankowska, Rajewska et al. 2005). They also demonstrated that copper binding is pH dependent. It was confirmed by a similar analysis using modified peptides, which showed that above pH6, the coordination of Cu(II) by His50 may involve the lateral NH_2 group of lysine residues upstream of His50 (Kowalik-Jankowska, Rajewska et al. 2006). In contrast to copper, other metals appear to favour C-terminus of aS, which is more likely to be involved in low-affinity and nonspecific binding to metals. NMR spectroscopy demonstrated that many divalent metal ions such as Fe(II), Mn(II), Co(II) and Ni(II) bind preferentially with low affinity (millimolar) to the C-terminal domain of aS, the primary binding site being the motif encompassing residues 119-124, in which Asp121 acts as the main anchoring residue (Binolfi, Rasia et al. 2006). In addition, calcium was reported to bind aS and bS at the C-terminus comprising residues 109-140 (Nielsen, Vorum et al. 2001). So far, there is no evidence showing gS bind any metals.

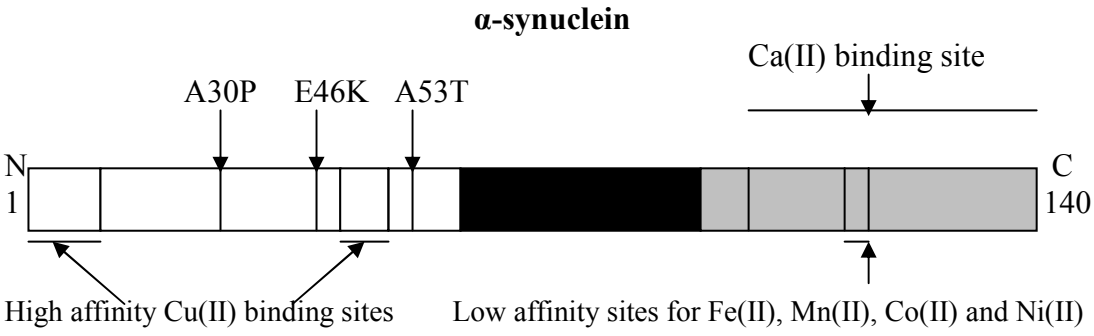

Fig. 1.3 Linear representation of α-synuclein.

The location of binding sites for various metals are indicated in the N-terminus and C-terminus of the protein. Three mutations A30P, E46K, A53T associated with PD are also shown.

1.4.2 Metals and synuclein induced neurotoxicity

1.4.2.1 Conformational changes

Neurodegenerative disorders possess a variety of pathological conditions, which share similar critical metabolic processes such as protein aggregation and oxidative stress, both of which are associated with the involvement of metal ions. Like other amyloidogenic proteins, abnormal folding of aS has been linked to the disease state. Several possible mechanisms for metal-stimulated fibrillation of aS can be envisaged. The simplest would involve direct interactions between aS and the metal, leading to structural changes in aS, and resulting in the enhanced propensity to aggregate (Uversky, Li et al. 2001). Little is currently known about how elevated levels of metals affect the conformational change of aS. As is known, aS is a natively unfolded protein. At neutral pH it is calculated to have 24 negative charges (15 of which are localized in the last third of the protein sequence), leading to strong electrostatic repulsion, which contributes to the lack of folding of aS (Uversky, Li et al. 2001). It has been assumed that the enhancement of fibrillation by metals can be attributed to the masking of the Coulombic charge-charge repulsion associated with the highly acidic C-terminus of the protein (Paik, Shin et al. 1999; Uversky, Lee et al. 2001). Analysis of far-UV circular dichroism at pH 7.5 with 35 μM aS and 2 mM metals indicated that Na(I), K(I), Li(I), Cs(I) and Ca(II) had no effect on the substantially unfolded nature of aS, while Cd(II), Zn(II), Mg(II), and Mn(II) resulted in a small increase in negative ellipticity around 222nm, which was a greater increase with Al(III), Fe(III), Cu(II) and Co(III), suggesting an increase in secondary structure change (Uversky, Li et al. 2001). This observation suggests that an important factor which affects polyvalent cations to induce aS conformational change might be the cross-linking, or bridging, between two or more carboxylates (Uversky, Li et al. 2001; Wright and Brown 2008), and the effectiveness of metal cations to induce fibrillation may be correlated with the increasing ion charge density and with their ability to induce fibrillation-prone partially folded species (Uversky, Li et al. 2001). In fact, aluminum was reported to participate in the pathological process in AD via the structural modifications of aS, which experienced the conformational alterations in the presence of aluminum such as the secondary structure transition to generate about 33% α-helix (Paik, Lee et al. 1997).

In contrast, recent study showed that Cu(II) does not affect the structural features inherent to the spontaneous aggregation of aS, and copper-induced fibrils exhibit the same morphology as those formed in the absence of the cation (Rasia, Bertoncini et al. 2005). In addition, circular dichroism spectroscopy revealed no structural changes after calcium binding (Weinreb, Zhen et al. 1996; Nielsen, Vorum et al. 2001). These conflicts raise the idea that metal induced aS aggregation and neurotoxicity may not due to the conformational alteration, although it is not always necessary for metal ions to cause gross structural changes for functional effects to arise (Nielsen, Vorum et al. 2001).

1.4.2.2 Oxidative stress

Redox-active transition metals such as copper and iron, may play an important role in the pathogenesis of neurodegenerative diseases by participating in an array of cellular disturbances characterized by oxidative stress and increased free radical production (Sayre, Moreira et al. 2005). Metal-catalyzed oxidation of proteins require metals to be bound to the protein and involves the reduction of metals such as Fe(III) and Cu(II), the reaction of Fe(II) and Cu(I) with hydrogen peroxide to generate hydroxyl radicals via a Fenton-like reaction, and oxidation of neighbouring amino acids (Wright and Brown 2008). The ability of these amino acids to form complexes with metal ions directly influences the susceptibility to metal-catalyzed oxidation. Oxidatively modified protein could increase its own tendency toward protein aggregation may due to the generation of reactive oxygen species (ROS). It turns soluble protein into insoluble form by either inhibiting intracellular proteolysis or causing unusual posttranslational modifications. These may then provide the covalent modifications of amino acid residues in proteins and formation of protein-protein cross-linkages (Kowalik-Jankowska, Rajewska et al. 2006). aS has been shown to be a potential target of intracellular oxidants by the identification of posttranslational modifications of synuclein within intracellular aggregates that accumulate in PD brains. It has been demonstrated that in the presence of copper and hydrogen peroxide, aS experienced Cu(II)-catalyzed oxidation and self-oligomerization, which may lead to possible protein aggregation and neurodegeneration (Paik, Shin et al. 2000). This could be almost suppressed by the addition of ascorbic acid or EDTA, indicating that

oligomerization was dependent upon not only metal binding but also its subsequent redox reaction in the presence of hydrogen peroxide (Paik, Shin et al. 2000). Similar effects of iron and hydrogen peroxide on aS aggregation were also observed (Hashimoto, Hsu et al. 1999). However, combination of copper and hydrogen peroxide forms soluble oligomers rather than filaments as examined by thioflavin T fluorescence, while iron and hydrogen peroxide led to filament formation but did not result in aS oligomerization (Hashimoto, Hsu et al. 1999; Cole, Murphy et al. 2005). This suggests that oxidation of aS can affect the aggregation and morphology of aggregate formed and various metals might involve different kinetics and modifications of the aggregate formation. In addition, the biochemically specific copper- or iron-mediated oxidative oligomerization was turned out to be dependent upon the acidic C-terminus of aS because the C-terminally truncated proteins were not affected by both metals and hydrogen peroxide (Paik, Shin et al. 2000). Analysis on Cu(II)-catalyzed oxidation of the N-terminal fragments of aS reported the cleavage of the peptide bond M1-D2 for all peptide studied, indicating the coordination of Met1 and Asp2 residues to the Cu(II) ions, and the fragmentations of these peptides near the Lys residues, supporting the participation of this residue in the coordination of the metal ions (Kowalik-Jankowska, Rajewska et al. 2006). This observation to some extent correlates the oxidation with interaction between metal ions and synuclein protein.

So far, no evidence has shown that bS and gS are capable of binding to metals with high affinities, or forming fibrils. However, certain metals (Zn^{2+}, Pb^{2+}, and Cu^{2+}) have been shown to induce a partially folded conformation of bS that triggers rapid fibrillation (Yamin, Munishkina et al. 2005), indicating that synuclein might be involved in the homeostasis of metals.

1.5 aS: a potential therapeutic target for PD

The aggregated forms of aS play a crucial role in the pathogenesis of PD and the concept that metals substantially regulate aggregation and fibrillation of aS has been widely accepted, while various metals have variable effects during the process. Previous study showed that Cu(II) was the most effective metal ion in promoting aS

oligomerization (Paik, Shin et al. 1999). A recent systematic analysis examining effects of various metals on the kinetics of fibrillation of recombinant aS revealed that Al(III) was the most effective, along with Cu(II), Fe(III), Co(III) and Mn(II) (Uversky, Li et al. 2001). Metal ions are capable of regulating the aggregation and fibrillation of aS, indicating they may exert their dual pathogenic effects through the interaction with aS, inducing protein transformation or/and oxidative stress. Therefore, chelation therapy could be a valuable therapeutic approach towards the treatment of neurodegeneration (Gaeta and Hider 2005). In fact, initial studies suggest that chelators will be effective in treating PD if the neurotoxic side effects can be overcome (Gaeta and Hider 2005). Further research into the definition of metal-binding sites and the mechanism of subsequent damaging events such as oxidative stress, is required to provide more specific therapy. In the other hand, aS is one of the members of synuclein family, including bS and gS, which have been suggested to be the physiological regulators of aS expression. Both of bS and gS inhibit aS fibril formation and neither of them has been shown to bind any redox active metals for high affinities. Thus, determination of the physiological function of synuclein proteins may help finding the way to cure PD.

1.6 Aim of the project

This project tested the roles of metals in the pathological property of synuclein regarding to the metal-binding induced aggregation and toxicity. This work is aim to:

1. Develop methods for the purification of recombinant synuclein proteins and their mutants
2. Determine the Cu(II) binding sites and affinities on synuclein proteins by looking at the stoichiometry of Cu(II) binding to synuclein
3. Investigate the coordination modes between Cu(II) and synucleins, and compare the differences among aS, bS and gS
4. Explore the electrochemical properties of synuclein by analyzing the redox activities catalyzed by synuclein-copper complexes
5. Characterize the effects of metals on mammalian cells stably overexpressing aS and PD-associated mutants

Chapter 2. Materials and Methods

2.1 Media and reagents

All media and reagents were obtained from Sigma-Aldrich, Fisher and Melford Laboratories unless otherwise stated. Media and buffers which appeared in the following materials and methods chapter are detailed in Table 2.1.

Media / Buffers	Details
LB	LB medium: 10g tryptone, 5g yeast, 10g NaCl in 1L dH_2O, pH7.5 and autoclaved. LB agar: LB medium + 1.5% (w/v) agar and autoclaved.
Antibiotics	Carbenicillin: 50mg/ml in dH_2O, filtered through 0.22uM filter and stored at -20°C.
isopropyl β-D-thiogalactopyranoside (IPTG)	1M in dH_2O, filtered through 0.22uM filter and stored at -20°C.
Phenylmethylsulphonyl fluoride (PMSF)	100mM in ethanol, stored at -20°C.
deoxyribonuclease (DNase)	1mg/ml in 5mM $CaCl_2$, stored at -20°C.
TAE buffer	50 x stock solution: 242g Tris base, 57.1ml glacial acetic acid, 1.86g EDTA, dH_2O to 1L.

Media / Buffers	**Details**
SDS-PAGE sample loading buffer	4 x stock solution: 20% Mercaptoethanol, 40% glycerol, 240mM Tris pH6.8, 8% SDS, 0.2% Bromophenol blue
SDS-PAGE running buffer	10 x stock solution: 30.3g Tris, 188g Glycine, 10g SDS, dH_2O to 1L, pH 8.3.
Coomassie blue staining solution	0.25g coomassie blue, 45ml methanol, 10ml glacial acetic acid, 45ml dH_2O.
Urea buffer	1kg urea, 23.2g NaCl, 21.1g Tris-HCl, dH_2O to 2.08L, pH7.5.
Destaining solution	100ml methanol, 140ml acetic acid, dH_2O to 2L
Transfer buffer	0.5 x Running buffer, 20% Methanol
PBS	20 x stock solution: 160g NaCl, 4g KCl, 4g KH_2PO_4, 23g Na_2HPO_4, dH_2O to 1L
Buffer A	20 mM Tris-HCl, 1 mM EDTA, pH 8.0
Buffer B	20 mM Tris-HCl, 1 mM EDTA, 2M NaCl, pH 8.0
Buffer C	10 mM NaAcetate, 1mM EDTA, pH 4.0
Buffer D	10 mM NaAcetate, 1mM EDTA, 2M NaCl, pH 4.0
Buffer E	20mM Tris-HCl pH 7.4, 2.5mM EDTA, 100mM NaCl, 0.1% Triton X-100

Table 2.1 Media and solutions

2.2 Plasmids and oligonucleotides used

The constructs, pDFP1a, pDFP2, pDFP3 and pDFP4a were provided by the University of Lancaster. The coding sequences and amino acids sequences for human aS, bS, gS and their mutants are shown in appendix A. The aS and its mutant DNA was cloned into Xho I/Kpn I in pTrcHis vector, and bS, gS DNA was cloned into Nde I/Bam HI in pET15b vector. The plasmid DNA was used to transform XL-2 blue competent cells, from which permanent bacterial stocks were prepared in 15% sterile glycerol. bS and gS were subcloned into pET3a plasmid from pET15b plasmid. The proteins were expressed in host cells BL-21(DE). pcDNA3.1(-) plasmid was used for transfection in mammalian cells. The mutations were introduced into Kpn I/Xho I in the plasmids by using site-directed mutagenesis. Constructs pDEP4f, pDEP4g, pDEP4h, pDEP5e, pDEP46a, pDEP6f, pDEP6g and pDEP6i were kindly provided by Dr. Josephine Wright. The information about pTrcHis, pET15b, pET11a, pET3a and pcDNA3.1(-) vectors are indicated in appendix B. All the oligonucleotides and plasmids used in this project are detailed in Table 2.2 and Table 2.3.

Oligos	**Use**	**Primer sequences 5'→ 3'**
A30P (aS)	Introduce mutation	GGCAGAAGCA**CCA**GGAAAGAC
A30P (aS) antisense	Introduce mutation	GTCTTTCC**TGG**TGCTTCTGCC
E46K (aS)	Introduce mutation	GCTCCAAAACCAAG**AAG**GGAGTGGTGCATG
E46K (aS) antisense	Introduce mutation	CATGCACCACTCC**CTT**CTTGGTTTTGGAGC
A53T (aS)	Introduce mutation	GTGGTGCATGGTGTG**ACA**ACAGTGGCTGAGAAG
A53T (aS) antisense	Introduce mutation	CTTCTCAGCCACTGT**TGT**CACACCATGCACCAC

Oligos	**Use**	**Primer sequences 5'→ 3'**
H50A (aS)	Introduce mutation	GAGGGAGTGGTG**GCT**GGTGTGGCAACAG
H50A (aS) antisense	Introduce mutation	CTGTTGCCACACC**AGC**CACCACTCCCTC
H65A (bS)	Introduce mutation	CAAGGAACAGGCCTCA**GCT**CTGGGAGGAGC TGTG
H65A (bS) antisense	Introduce mutation	CACAGCTCCTCCCAG**AGC**TGAGGCCTGTTCC TTG
△2-9 (aS)	Introduce mutation	GAAGGAGATATACATATGAAGGCCAAGGAGG GAGTTG
△2-9 (aS) antisense	Introduce mutation	CAACTCCCTCCTTGGCCTTCATATGTATATCTC CTTC
△1-9 (bS)	Introduce mutation	AGGAGATATACATATGATGGCCAAGGAGGGC GTTGTGG
△1-9 (bS) antisense	Introduce mutation	CCACAACGCCCTCCTTGGCCATCATATGTATAT CTCCT
△119-126 (aS)	Introduce mutation	CTGGAAGATATGCCTGTGATGCCTTCTGAGGA AGGG
△119-126 (aS) antisense	Introduce mutation	CCCTTCCTCAGAAGGCATCACAGGCATATCTT CCAG
bS Nde1	Amplication of bS cDNA	GACGAGTCATATGGACGTGTTCATGAAGGG
bS BamH1	Amplication of bS cDNA	AAATATGGATCCTTACTACGCCTCTGGCTCATA C
gS Nde1	Amplication of gS cDNA	GACGAGTCATATGGATGTCTTCAAGAAGGG
gS BamH1	Amplication of gS cDNA	AAATATGGATCCTTACTAGTCTCCCCCACTCTG

Table 2.2 Oligonucleotides

Plasmid	Description	Source
pTrcHis A	Vector for expression of N-terminal $(His)_6$-tag proteins in *E.coli* followed by an enterokinase cleavage site	Invitrogen
pET15b	Vector for expression of N-terminal $(His)_6$-tag proteins in *E.coli* followed by a thrombin cleavage site	Novagen
pET11a	Vector for expression of untagged proteins in *E.coli*	Novagen
pET3a	Vector for expression of untagged proteins in *E.coli*	Novagen
pcDNA 3.1(-)	Vector for expression of untagged proteins in mammalian neuroblast (SHSY5Y) cells	Invitrogen
pDFP1a	Plasmid derived from pTrcHis A for expression of $(His)_6$-aS	University of Lancaster
pDFP1b	Plasmid derived from pTrcHis A for expression of $(His)_6$-aS A30P	This project
pDFP1c	Plasmid derived from pTrcHis A for expression of $(His)_6$-aS E46K	This project
pDFP1d	Plasmid derived from pTrcHis A for expression of $(His)_6$-aS A53T	This project
pDFP1e	Plasmid derived from pTrcHis A for expression of $(His)_6$-aS H50A	This project
pDFP2	Plasmid derived from pET15b for expression of $(His)_6$-bS	University of Lancaster
pDFP3	Plasmid derived from pET15b for expression of $(His)_6$-gS	University of Lancaster
pDFP4a	Plasmid derived from pET11a for expression of untagged aS	University of Lancaster
pDFP4b	Plasmid derived from pET11a for expression of untagged aS H50A	This project
pDFP4c	Plasmid derived from pET11a for expression of untagged aS△1-9	This project
pDFP4d	Plasmid derived from pET11a for expression of untagged aS△1-9 H50A	This project
pDFP4e	Plasmid derived from pET11a for expression of untagged aS△119-126	This project
pDFP4f	Plasmid derived from pET11a for expression of untagged aS△1-9 H50A △119-126	Dr Josephine Wright

Plasmid	Description	Source
pDFP4g	Plasmid derived from pET11a for expression of untagged aS10-100 H50A	Dr Josephine Wright
pDFP4h	Plasmid derived from pET11a for expression of untagged aS1-100	Dr Josephine Wright
pDFP5a	Plasmid derived from pET3a for expression of untagged bS	This project
pDFP5b	Plasmid derived from pET3a for expression of untagged bS H65A	This project
pDFP5c	Plasmid derived from pET3a for expression of untagged bS△1-9	This project
pDFP5d	Plasmid derived from pET3a for expression of untagged bS△1-9 H65A	This project
pDFP5e	Plasmid derived from pET3a for expression of untagged bS10-100 H65A	Dr Josephine Wright
pDFP5f	Plasmid derived from pET3a for expression of untagged gS	Dr Josephine Wright
pDFP6a	Plasmid derived from pcDNA3.1(-) for expression of untagged aS	Dr Josephine Wright
pDFP6b	Plasmid derived from pcDNA3.1(-) for expression of untagged aS A30P	This project
pDFP6c	Plasmid derived from pcDNA3.1(-) for expression of untagged aS E46K	This project
pDFP6d	Plasmid derived from pcDNA3.1(-) for expression of untagged aS A53T	This project
pDFP6e	Plasmid derived from pcDNA3.1(-) for expression of untagged aS H50A	This project
pDFP6f	Plasmid derived from pcDNA3.1(-) for expression of untagged aS△1-9	Dr Josephine Wright
pDFP6g	Plasmid derived from pcDNA3.1(-) for expression of untagged aS△1-9 H50A	Dr Josephine Wright
pDFP6h	Plasmid derived from pcDNA3.1(-) for expression of untagged aS△119-126	This project
pDFP6i	Plasmid derived from pcDNA3.1(-) for expression of untagged aS10-100 H50A	Dr Josephine Wright
pDFP7	Plasmid derived from pcDNA3.1(-) for expression of untagged bS	Dr Josephine Wright

Table 2.3 Plasmids

2.3 **Site-directed mutagenesis**

The following reactions were set up in 0.5 ml thin-wall PCR tubes to introduce mutations: 50 ng template DNA, 1 μl of 25 μM of each primer, 2.5 μl of 25 mM of dNTPs, 6 μl or 8 μl $MgSO_4$ stock solution, 5 μl of 10x buffer (without $MgSO_4$) and 2.5U of Pwo polymerase (Roche applied science) were added. Reactions were set up to a final volume of 50 μl with nuclease free water. The PCR programme, utilising a Thermo Hybaid PCR Sprint thermal cycler, was as follows: 1, one cycle of 95°C for 90 seconds (separating the parental DNA); 2, 5 cycles of 95°C for 30 seconds, followed by 50°C for 1 minute, and then 68°C for 10 minutes; 3, 5 cycles of 95°C for 30 seconds, followed by 55°C for 1 minute, and then 68°C for 10 minutes; 4, one cycle of 68°C for 15 minute. Hold temperature was 4°C. Following PCR, samples were digested by Dpn1 at 37°C for 1 hour to remove the remaining parental DNA.

2.4 **Preparation of competent bacterial cells**

XL-2 Blue Ultra Competent Cells (Stratagene) and BL21 (DE3) pLysS competent cells (Promega) were plated on two LB agar plates and incubated overnight at 37°C. A single colony was inoculated into 10 ml LB medium and incubated overnight at 37°C. The 10 ml overnight culture was added to 200 ml LB medium and incubated at 37°C shaking at 200 rpm until the optical density at 600 nm was 0.6. The culture was centrifuged at 4000 rpm at 4°C for 10 minutes. Cell pellets were resuspended in 200 ml ice cold 0.1 M sterile $MgCl_2$ with plugged pipettes. Then the mixture was centrifuged as previous and the cell pellets were resuspended in 100 ml ice cold 0.1 M sterile $CaCl_2$. The mixture was incubated on ice for 20 minutes and centrifuged as previous. The cell pellets were resuspended in 10 ml ice cold 0.1 M $CaCl_2$ with 15% glycerol and dispensed into 200 μl aliquots in pre-chilled 1.5 ml tubes. The cells were rapidly frozen and stored at -80°C. Everything was done by the flame and all the solution and tubes were sterilized by autoclaving.

2.5 Transformation

XL-2 Blue and BL21 competent cells were used. Cells were thawed on ice and resuspended by gentle flicking the tube. 50 μl aliquot of cells was transferred into pre-chilled 1.5 ml sterile tubes. Either 50 ng of plasmid DNA or 5 μl PCR mutagenesis DNA digested by Dpn1 was added and the cells were then incubated on ice for 30 minutes. After that, cells were heat shocked for 60 seconds at 42°C, and then returned to the ice for 2 minutes. 300 μl LB broth was added to the cells/DNA solution and then incubated at 37°C shaking for 1 hour at 200 rpm. The solution was then centrifuged at 4000 rpm for 5 minutes. The cell pellets were resuspended in 100 μl supernatant and plated on LB agar plates containing 50 μg/ml carbenicillin. The plates were incubated at 37°C overnight.

2.6 Plasmid DNA purification and quantification

2.6.1 Mini-preps

Three to six colonies from each of the transformation plates (XL-2 blue cells) were picked and added to three to six 15 ml Falcon tubes containing 5 ml LB broth with 50 μg/ml carbenicillin. Cultures were incubated at 37°C shaking overnight at 200 rpm. The three to six inoculum cultures were centrifuged at 4000 rpm for 10 minutes, and the supernatant was discarded. Plasmid DNA was purified by using a QIAprep Spin Miniprep Kit according to the manufacturers protocol (QIAGEN).

2.6.2 Agarose gel electrophoresis

5 μl of the plasmid DNA from mini-prep was analyzed in the 1% agarose gel/TAE with 0.5 μg/ml ethidium bromide to confirm the DNA purification. Gel was run at 100 volts for 1 hour using a BioRad mini-sub®cell GT gel tank and BioRad power pac 300. Gels were photographed under long wave UV light. The DNA concentration was determined by the absorbance at 260 nm wavelength in a UV spectrophotometer.

2.7 DNA sequencing

5 μl of 100 ng/ul of purified plasmid DNA from mini-prep DNA and 5 μl of 3.2 pmol/μl of appropriate primers were sent to Geneservice in Cambridge for each sequencing reaction.

2.8 Subcloning

2.8.1 PCR amplification

The coding sequences of bS and gS were amplified from the template DNA in pET15b vector by PCR in a Thermo Hybaid PCR Sprint thermal cycler. The reactions were set up in 0.5 ml thin-wall PCR tubes: 100 ng template DNA, 1 μl of 25 μM of each primer, 1 μl of 10 mM of dNTPs, 5 μl of 10x buffer (with $MgSO_4$) and 2.5U of Pwo polymerase (Roche applied science) were added. Reactions were set up to a final volume of 50 μl with nuclease free water. The PCR programme was as follows: 1, one cycle of 96°C for 60 seconds; 2, 35 cycles of 96°C for 15 seconds, followed by 63°C for 30 seconds, and then 72°C for 90 seconds; 3, one cycle of 72°C for 5 minutes. Hold temperature was 4°C. Following PCR, samples were digested by restriction enzymes.

2.8.2 Restriction enzyme digestion

The digestion reactions were set up as follows: 3 μg of vector DNA or diagnostic DNA, 5 μl of 10x buffer and 0.5 μl of each restriction enzyme were transferred to a 1.5 ml tube. MilliQ H_2O was added to set up a final volume of 50 μl. The contents in the tube were mixed properly and centrifuged. Then the digest reaction was incubated at 37°C for 1 hour or overnight.

2.8.3 Dephosphorylation of vector DNA

The digested vector DNA was dephosphorylated by the treatment of shrimp alkaline phosphatase (Roche applied science) to prevent the self-ligation of the plasmid. The mixture of 3 μg digested vector DNA and 2 μl shrimp alkaline phosphatase were incubated at 37°C for 45 minutes. The enzyme was then inactivated at 65°C for 15 minutes.

2.8.4 DNA extraction

The digest reaction mixtures were loaded into a 1% agarose gel/TAE with 0.5 μg/ml ethidium bromide. Gel was run at 100 volts for 1 hour to make the DNA fragments separated. The DNA was visualized under a UV transilluminator and the fragments of interest were cut off from the gel by a clean, sharp razor blade. The DNA was extracted from the gel slices by using the QIAquick Gel Extraction Kit according to the manufacturers protocol (QIAGEN). The purified DNA was stored at -20°C.

2.8.5 Ligation

2 μl of the purified vector DNA and insert DNA was loaded into a 1% agarose gel/TAE with 0.5 μg/ml ethidium bromide to estimate the relative concentration of the DNA. The ligation reaction was carried out in a 1.5 ml tube by adding vector DNA and insert DNA in a ratio of 1:3. 1 μl T4 DNA ligase (Promega), 2 μl 10x ligase buffer and MilliQ H_2O were added to make a final volume to 20 μl. The reaction was incubated at room temperature for 1 to 3 hours.

2.9 Induction of protein expression

A single colony of BL21 (DE) cells transformed with plasmid DNA was used to inoculate 25 ml of LB broth supplemented with 50 μg/ml carbenicillin in a 50 ml Falcon tube. The culture was incubated at 37°C overnight shaking at 200 rpm, and

then was used to inoculate 1 L of LB broth supplemented with 50 μg/ml carbenicillin in a sterile 2 L conical flask. The culture was grown at 37°C shaking at 200 rpm in an incubator until OD_{600} reached 0.4-0.6 (about 2-3 hours). A 1 ml sample was taken out of the culture for the uninduced control in polyacrylamide gel. Then IPTG from 1 M stock was added to make a final concentration of 1 mM. The cultured was induced for a further 3-5 hours and 1 ml sample was removed to check the level of protein expression in polyacrylamide gel. These samples were centrifuged at 6000 rpm for 5 minutes. The cell pellets were resuspended in 2% (w/v) SDS and heated at 100°C for 5 minutes, 5 μl of which was then mixed with SDS-PAGE sample loading buffer and heated at 100°C for 5 minutes before being loaded into a SDS gel for analysis. At the end of induction, the cells were harvested by centrifuged at 6000 rpm for 10 minutes and resuspended in appropriate buffers before being stored at -80°C.

2.10 **Polyacrylamide gel electrophoresis**

A 10% or 12% (w/v) polyacrylamide separating gel was made by pouring the acrylamide solution into the gap between the glass plates. After polymerization, a 4% (w/v) polyacrylamide stacking gel solution was poured above the separating gel. For gradient gels, a 5% acrylamide solution and a 20% acrylamide solution were mixed individually in the Pouring Stand before they were mixed together and poured into the gap between the glass plates. The plates were fixed in a tank. The SDS-PAGE running buffer was placed between the plates and at the bottom of the tank. Protein samples were mixed with 4x loading buffer and dH_2O to make a total volume of 20 μl. Protein samples were heated at 100°C for 5 minutes and loaded into the stacking gel. The gels were run at constant current 35 mA per gel until the dye reached the bottom of the gels. Under denaturing conditions, proteins in the gels were separated by molecular weight while the negatively charged proteins migrated towards the anode. Protein fractions were observed by either Coomassie blue staining or western blotting. Recipes to make up separating gel and stacking gel are shown in Table 2.4.

Stock solutions	**Separating gel(ml)**		**Stacking gel(ml)**	**Gradient gel(ml)**	
	10%	12%		5%	20%
dH_2O	2.6	2.1	3.6	2.25	0
30% 35.1:1 bis acrylamide	2.7	3.2	0.63	0.75	3
1 M Tris pH8.8	2.6	2.6		1.45	1.45
1 M Tris pH6.8			0.63		
10% SDS	0.08	0.08	0.05	0.045	0.045
10% APS	0.024	0.024	0.03	0.008	0.008
TEMED	0.01	0.01	0.005	0.0045	0.0045

Table 2.4 Recipes for acrylamide gels

2.11 **Coomassie blue staining**

Coomassie blue staining is based on the binding of the dye Coomassie Brilliant Blue, which binds nonspecifically to virtually all proteins via physisorption to arginine, the aromatic amino acids, and histidine. Any dye that is not bound to protein diffuses out of the gel during the destain steps. Generally, the polyacrylamide gels were soaked in the coomassie staining solution and gently rocked for 5 minutes or overnight (depending on the freshness of the coomassie staining solution) after heated in microwave for 15 seconds. Then the staining solution was poured out and the gels were soaked in the destaining solution, which was then gently rocked until the blue bands were visualized against a clear background. The gels were then photographed.

2.12 **Western blotting**

Western blotting, also referred to be immunoblotting, is an analytical technique used to detect specific proteins in a given sample of protein fractions or tissue homogenate. It uses gel electrophoresis to separate denatured proteins by the molecular weight. Then the proteins are transferred to a membrane (typically nitrocellulose or PVDF), where they are probed by using polyclonal or monoclonal antibodies specific to the

target proteins.

2.12.1 Protein transfer

PVDF membrane (Millipore) was activated through immersing in 100% methanol solution for 15 seconds. The SDS gel was placed with the membrane between filter papers to form a sandwich structure. All of these were carried out in the transfer buffer. The "sandwich" was placed in a Trans-Blot®Semi-Dry transfer machine (Biorad). The transfer was run at 50 mA per gel for 1.5 hours or 12 mA per gel 6 volts constant overnight for big proteins transferring.

2.12.2 Antigen detection

The membrane was blocked by incubating in 5% milk in PBS-0.1% Tween20 at room temperature for 1 hour or at 4°C overnight. The membrane was then incubated in primary antibody diluted in 1:1000 in 1% milk in PBS-0.1% Tween20 for 2 hours at room temperature or overnight at 4°C. This was followed by 3 times of washing in PBS-0.1% Tween20 for 15 minutes each time. Horseradish peroxidase (HRP) conjugated secondary antibody was diluted 1:3000 or 1:4000 in 1% milk in TBS-0.1% Tween20 and incubated with membrane for 1 hour at room temperature. The membrane was then washed 3 times as before. The membrane was treated with ECL PLUS Western blotting detection kit (Amersham Pharmacia Biotech) for 5 minutes and exposed to film.

2.13 Purification of $(His)_6$-synuclein by Immobilised metal affinity chromatography (IMAC)

Cell lysate was prepared as below: cell pellets were resuspended in urea buffer by shaking at 37°C for 1 hour and cells were broken down by sonication. The cell lysate was centrifuged at 12000 rpm for 20 minutes at 4°C and the supernatant was retained. The supernatant was filtered through a 0.45 μM filter (Millipore) before it was loaded

into the column.

IMAC Column with 5-6 ml metal chelating sepharose was washed with MilliQ H_2O, saturated with 0.3 M nickel sulphate and equilibrated with urea buffer. The cell lysate was loaded into the column at a speed of 1.2 ml/minute, followed by 100 ml urea buffer with 25 mM imidazole washing at a speed of 4 ml/minute. Then protein was eluted with urea buffer with 100 mM or 300 mM imidazole.

2.14 Purification of synuclein by Ion exchange chromatography (IEC)

IEC is a process that allows the separation of ions and polar molecules based on the charge properties of the molecules. It retains analyte molecules based on coulombic interactions and can be subdivided into cation exchange chromatography and anion exchange chromatography. In cation exchange chromatography, positively charge ions bind to a negatively charged resin, while in anion exchange chromatography the binding ions are negative and the resin displays a positively charged functional group. Once the solutes are bound, the column is washed to equilibrate in the starting buffer, which should be of low ionic strength, and then the bound molecules are eluted off using a gradient of a second buffer which steadily increases the ionic strength of the eluent solution. Proteins have numerous functional groups that can have both positive and negative charges. IEC separates proteins according to their net charge, which is dependent on the composition of the starting buffer. By adjusting the pH or the ionic concentration of the buffer, various proteins molecules can be separated.

2.14.1 Anion exchange chromatography (AEC)

Cells pellets were resuspended in buffer A with 1 mM PMSF and 50 μg/ml DNase and shaked at 37°C for 15 minutes. The cells were lysed by sonication (3x 1 minute) and 1% (w/v) of streptomycin sulfate was added to precipitate the ribosomal proteins. The cell lysate was centrifuged at 8000 g for 20 minutes at 4°C and the supernatant

was retained. 30% (w/v) ammonium sulfate was added and stirred at 4°C for at least 1 hour to precipitate the protein. The mixture was then centrifuged at 10000 g for 20 minutes at 4°C and the pellets were retained. Briefly, the pellets were resuspended in buffer A and filtered through a 0.45 μM filter (Millipore) before it was loaded onto a pre-equilibrated Q-Sepharose Fast Flow column connected to a fast protein liquid chromatography (FPLC) system (Amersham Bioscience). Bound proteins were eluted by a linear gradient of buffer B. Fractions containing proteins were identified from the UV chromatogram and analyzed by SDS-PAGE.

2.14.2 Cation exchange chromatography (CEC)

Cells pellets were resuspended in buffer C with 1 mM PMSF and 50 μg/ml DNase and shaked at 37°C for 15 minutes. The cells were lysed by sonication (3x 1minute). The cell lysate was centrifuged at 8000 g for 20 minutes at 4°C and the supernatant was retained. The semi-purified cell lysate was filtered through a 0.45 μM filter (Millipore) before it was loaded onto a pre-equilibrated Hitrap SP HP column (GE healthcare) connected to a fast protein liquid chromatography (FPLC) system (Amersham Bioscience). Bound proteins were eluted by a linear gradient of buffer D. Fractions containing proteins were identified from the UV chromatogram and analyzed by SDS-PAGE.

2.15 Dialysis of protein fractions

The dialysis tubing (Medicell) was prepared as follows: boiled in 2% (w/v) $NaHCO_3$ with 1 mM EDTA for 5 minutes and rinsed in dH_2O. Protein samples were dialyzed in the tubing (MW12-14K for $(His)_6$-synuclein, MW3K for untag synuclein) against chelex treated MilliQ H_2O pH 7. 1 g of chelex was added to 5 liters of MilliQ water and stirred for 1 hour. Then the water was filtered through filter papers to get rid of the chelex, and adjusted to pH 7. Chelex is a styrene-divinylbenzene resin containing iminodiacetic acid groups. It binds metals via ionic interaction.

2.16 Maintenance and growth of mammalian cells

SH-SY5Y (human neuroblastoma) cells were cultured in 50% (v/v) Dulbecco's Modified Eagle Media and 50% (v/v) Ham's F-12 supplemented with 10% (v/v) fetal bovine serum (FBS), 100 U/ml penicillin, 100 μg/ml streptomycin and 2 mM glutamine. All the media and reagents were obtained from Biowhittaker Lonza. Growth conditions were maintained at 37°C and 5% CO_2 in a humidified incubator.

2.17 Transfection

Transfections were performed using FuGene 6 transfection reagent (Roche applied science). For stable transfections, 6-well plates were used and cells were plated at 50% confluency the day before the transfection. To perform the transfection 50 μl of serum free media was transferred into a micro-centrifuge tube; 3 μl of the FuGene 6 reagent was then added directly to this and mixed by gentle flicking. The mixture was incubated for 5 minutes at room temperature. For each cell line, 1 μg of DNA was then added to the mixture, mixed as before, and incubated at room temperature for 15 minutes. After this the transfection mixture was added to the cells, the 6-well plate swirled and returned to the incubator overnight. Cells were selected with 400 μg/ml G418 sulfate (Calbiochem) 24 hours after transfection, and maintained in 100 μg/ml to keep the plasmid in the cells.

2.18 Immunofluorescence

Coverslips (Scientific laboratory supplies), which were sterilized in 100% ethanol beforehand, were put at the bottom of the wells of 6-well plates. The coverslips were covered in Poly-L Lysine for 10 minutes and rinsed with PBS. Cells were cultured on the coverslips overnight and treated with metals for 48 hours. Coverslips were rinsed in Hanks and fixed in 4% paraformaldehyde/PBS for 30 minutes at room temperature. Coverslips were transferred to a new dish and washed 3 times in PBS with 5 minutes each time. Cells were permeabilised by incubating in 0.1% Triton X-100 in PBS for 10

minutes, followed by washing 3 times as before. Coverslips were then incubated in 1% glycine in PBS for 10 minutes, and washed by PBS to remove the excess glycine. Cells were blocked in 10% FBS in PBS for 30 minutes and washed with PBS. Cells were then incubated in primary antibody overnight at 4°C and washed 3 times as before, then incubated with secondary antibody for 1 hour in dark at 37°C and washed as before. Cells were then mounted in mounting media (Vector Lab) on a clean slide and viewed under the Laser Scanning Microscope LSM510 (Zeiss). The data was analyzed by the software LSM510 image examiner provided by the company.

2.19 3-(4,5-Dimethylthiazol-2-yl)-2,5-diphenyltetrazolium bromide (MTT) assay

MTT assay is a colorimetric assay used to determine cytotoxicity. MTT is a yellow tetrazolium salt that is reduced to form dark blue formazan crystals. The reduction is dependent on the mitochondrial enzyme-succinate dehydrogenase and therefore only occurs in viable cells.

Cells were cultured on 96-well plates with same densities overnight and treated with different concentrations of copper in chelexed media for 48 hours. MTT was prepared to 2.5 mg/ml in Dulbecco's Modified Eagle Media/Ham's F-12 and filtered. Then media was removed from the plates and 50 μl of MTT was added per well. Cells were incubated for 30 minutes at 37^{o}C with 95% O_2 and 5% CO_2. MTT was removed carefully before 100 μl propanol was added per well to dissolve crystals and incubated for at least 30 minutes. The absorbance of this colored solution was quantified by measuring at a wavelength of 570 nm by FLUOstar Omega (BMG Labtech). Each treatment was conducted in triplicate.

2.20 Protein concentration determination

2.20.1 Bradford assay

Bradford assay was used to determine the protein concentration of cell lysate. 5 fold Biorad protein assay reagent (Biorad) was diluted 1:5 with dH_2O. Bovine serum albumin (BSA) protein standards were prepared ranging from 0-4 mg/ml from a stock of BSA at 4 mg/ml in dH_2O. 2 µl of BSA standard or cell lysate and 198 µl diluted protein assay reagent were mixed in a 96-well plate and incubated at room temperature for 15 minutes. The absorbance of each well was measured at 595 nm and recorded in a micro-plate reader (FLUOstar Omega). The protein concentration of the cell lysate was determined by analyzing the data in Excel software.

2.20.2 UV absorbance

This method was used to determine the concentration of recombinant proteins. Protein samples (100 µl) and appropriate buffer (900 µl) were transferred to a quartz cuvette and mixed properly. The absorbance at 280 nm was measured in a Cary 50 Bio UV-visible spectrophotometer (Varian) before it was zeroed using the same buffer. Protein concentrations were calculated by using the principles of Beer-Lamberts law: $A_{280} = \log_{10}(P_0 / P) = abc$

where, A_{280} = absorbance at 280 nm, P_0 = the incident light intensity, P= the emergent light intensity, a = the molar absorption coefficient (M/cm), b = the path length of the protein sample (cm) and c = the solute concentration (M). The theoretical molar absorption coefficients were determined by the amino acid sequences of the proteins (us.expasy.org/tools/protparam.html).

2.21 Isothermal Titration Calorimetry (ITC)

ITC experiments were carried out in a Microcal titration calorimeter (Microcal VP-ITC). Protein samples and metal solutions were adjusted to an appropriate concentration in chelex-treated MilliQ H_2O or 10 mM MES buffer pH 7. All solutions

were filtered through a 0.22 μM filter and degassed before use. All reactions and measurements are performed in an enclosed cell maintained at 25°C. A time course of 30 injections of 4 μl or 8 μl metal solution was titrated into a cell containing protein stirring at 300 rpm. Injections were separated by 120 seconds to allow temperature equilibration. The instrument measured the heat change, generated or absorbed, as metals reacted with protein. The data presented as a binding isotherm by the instrument was expressed in terms of the heat change per mole of metal solutions titrated into protein sample against the metal to protein molar ratio. The binding affinities, the change in enthalpies and the change in entropies were obtained by analyzing the data through the Origin 5.0 software from MicroCal.

When analyzing the data, a base-line correction was applied. For each experiment, the data was subtracted from a series of injections of metal solutions into a buffer blank relating to the heat of dilution of the metal into protein samples. After that, a nonlinear least squares method was used to minimize χ^2 values and acquire best fit parameters for the binding constants, K_a and heating change, $\Delta H°$. In all experiments, the optimal values were obtained in the sequential binding sites model, whereby the numbers of binding sites were determined to fit in a sequential manner by the user. In all cases, 1 to 10 binding sites model were tried to ensure that the best-fit model was obtained.

2.22 Electron paramagnetic resonance spectroscopy (EPR)

EPR, also referred to electron spin resonance (ESR), is a technique for studying chemical species that have one or more unpaired electrons, including organic free radicals and transition metal ions. In the presence of an external magnetic field with strength B_0, the electron possesses two energy states. The separation between the lower energy state and the upper state is $\Delta E = g_e \mu_B B_0$, where g_e is the electron's so-called g-factor. An unpaired electron can move between the two energy levels by either absorbing or emitting electromagnetic radiation of energy $\varepsilon = h\nu$ such that the resonance condition, $\varepsilon = \Delta E$, is obeyed. Substituting in $\varepsilon = h\nu$ and $\Delta E = g_e \mu_B B_0$ leads to the fundamental equation of EPR spectroscopy: $h\nu = g_e \mu_B B_0$.

Structural information can be determined by investigating the transition metal ions

and radicals in proteins. Synuclein protein samples were prepared at a concentration of 100 μM in 20 mM N-ethylmorpholine (EM) buffer pH 7.4. Different equivalents of Cu(II) were added into protein samples before they were transferred into the 3 mm internal diameter quartz EPR tubes and frozen in liquid nitrogen. The experiments were performed in a Bruker continuous wave EPR spectrometer at temperature of 20 K. All the spectra were operated at X-band with 100 kHz magnetic field modulation, with modulation amplitude of 0.5 mT and microwave power of 2 W. The data was analyzed and plotted in Peisach-Blumberg plots to assign the structure of copper-binding sites in synuclein proteins.

2.23 Cyclic Voltammetry (CV)

All measurements were conducted in a 50 ml three-terminal cell consisting of a 3 mm diamond boron-doped diamond working electrode (Diafilm^{TM}, Windsor Scientific, UK), a platinum foil counter electrode and a reference electrode saturated with potassium chloride (SCE, REF401, Radiometer). The working electrode was polished on a fresh micro cloth (Buehler, UK) with alumina slurry (1 micron, Buehler, UK) followed by thoroughly rinsing with dH_2O. Then the diamond electrode was immersed into the protein solution for 1 minute to allow the protein deposit on the electrode.

All of the electrochemical measurements were carried out at room temperature in 10 mM MES buffer pH 7.0, which stabilized the reaction solution. Prior to the experiments, solutions were degassed with high-purity nitrogen to deaerate the system, and a continuous flow of nitrogen was conducted to prevent air from coming in to contaminate the reaction solution.

The voltammetric measurement was manipulated by a μ-Autolab III potentiostat system (Eco Chemie, The Netherlands) connected to a personal computer. A current was introduced into the reaction system by the counter electrode. Electrons were absorbed or released from the protein-diamond electrode surface, resulting in the reduction or oxidation reactions, which can be detected by the computer system. All the cycles were scanned within the potential range –0.5 V-0.5 V (step potential 0.0042 mV). The data obtained was analyzed with the Autolab software.

2.24 Mass spectroscopy

Mass spectroscopy is an analytical technique that identifies the chemical composition of a compound or sample based on the mass-to-charge ratio of charged particles. A sample undergoes chemical fragmentation forming charged particles (ions). The ratio of charge to mass of the particles is calculated by passing them through electric and magnetic fields in a mass spectrometer. Synuclein proteins were made at a concentration of 50 μM in chelex treated MilliQ H_2O pH 7. All the experiments were carried out in the Quadrupole time-of-flight (Q-TOF) or matrix-assisted laser desorption ionization (MALDI) mass spectrometers in the University of West England.

2.25 Nuclear magnetic resonance spectroscopy (NMR)

NMR is a powerful technique for studying the structures of proteins in solution. It is a property that magnetic nuclei have in a magnetic field and applied electromagnetic pulse. The nuclei absorb energy from the electromagnetic pulse and radiate this energy back out. The energy radiated back out is at a specific resonance frequency which depends on the strength of the magnetic field and other factors. This allows the observation of specific quantum mechanical magnetic properties of an atomic nucleus. Chemical shift is used to probe the chemical structure of molecules which depends on the electron density distribution in the corresponding molecular orbitals. Synuclein protein samples from different purification methods were prepared at a concentration of 1 mM in chelex treated MilliQ H_2O pH 7. The experiments were performed in the Bruker 600 MHz spectrometer at room temperature by Dr Jill Madine in the University of Liverpool.

2.26 Circular dichroism spectroscopy (CD)

CD spectroscopy measures differences in the absorption of left-handed polarized light

versus right-handed polarized light which arise due to structural asymmetry. Secondary structure can be determined by CD spectroscopy in the "far-uv" spectral region (190-250 nm). At these wavelengths the chromophore is the peptide bond, and the signal arises when it is located in a regular, folded environment. aS protein samples from different purification methods were prepared at a concentration of 50 μM in chelex treated MilliQ H_2O pH 7. The samples were transferred to cuvettes with 1 mm path length. The CD spectra were measured from 180 nm to 270 nm at room temperature. Two scans were averaged and the buffer background was subtracted.

Chapter 3. Expression and Purification of aS

3.1 Introduction

aS and bS were first discovered in the cytosolic extract of human brain by western blotting with anti-tau antibody (Jakes, Spillantini et al. 1994). While their precise function and biochemical features are still not fully understood, there is cumulative evidence showing that aS is a metal-binding protein. In this study, recombinant His-tagged and untag synucleins were used to investigate their metal-binding characteristics. aS was first overexpressed as Hig-tag fusion proteins in *E.coli* and purified by immobilised metal affinity chromatography (IMAC).

IMAC is a common technique used for the purification of recombinant proteins. It is based on the specific co-ordinate covalent binding of amino acids, particularly histidine, to metals. This technique works by allowing proteins with an affinity for metal ions to be retained in a column containing immobilized metal ions, such as cobalt, nickel, copper, zinc, or iron ions. $(His)_6$-tags in the fusion proteins have an affinity for nickel or cobalt ions which are co-ordinated with a chelator for the purposes of solid medium entrapment. The protein of interest is eluted either by changing the pH or by adding a competitive ligand such as imidazole. In this study, His-tag proteins were applied to a Ni(II) charged HiTrap chelating HP column and eluted with a gradient concentration of imidazole.

Untag synucleins were also purified in this project. Presently, two major purification methods are used in other research groups working on aS. The first one, which is the most common one, is to use a boiling step to semipurify the cell lysate during purification. This is based on the heat stability of aS demonstrated by Weinreb et al. (1996), where circular dichroism (CD) spectroscopy indicated that the structural properties of aS were unchanged post boiling (Weinreb, Zhen et al. 1996). Nevertheless, a more recent research by Uversky et al. (2001) showed that

conformational transition in aS from natively unfolded state to a partially folded intermediate with β–sheet is induced by high temperatures (Uversky, Lee et al. 2001). Moreover, the rate of aS fibrillation was shown to be accelerated by high temperatures. This might be due to the β–sheet in the partially folded intermediate, which forms the major part of the secondary structure in aS fibrils (Uversky, Li et al. 2001). The second method involves an acid precipitation step before loading the cell extract onto an ion exchange column during purification. The pH was decreased to precipitate some of the contaminant proteins in the cell lysates; however, it was later shown that acidic conditions influence the structure of proteins (Salt D.J. et al. 1982). In this study, a new, gentler method, involving only ion exchange chromatography (IEC), was designed to purify synucleins. Three various methods were compared in this study.

3.2 Expression and purification of His-tagged aS

Plasmid pDFP1a (Table 2.3), a derivative of pTrcHis A in which the ORF of aS was cloned into Xho I/Kpn I (appendix B), was transformed into BL21(DE) cells to overexpress $(His)_6$-aS. BL21(DE) cells carrying this plasmid were grown in batch culture to OD_{600} of 0.4-0.6, followed by inducing the protein with 1 mM IPTG.. After 3 hours of induction, the cells were harvested by centrifugation, re-suspended in urea buffer and frozen at -20^{o}C. The cell lysate was prepared as discussed before in chapter 2 and loaded onto an IMAC column. $(His)_6$-aS was eluted with 100 mM imidazole/urea buffer. Samples from each fraction were analyzed by 12% SDS-PAGE (Fig 3.1) and western blots.

As can be seen in Fig 3.1, the majority of the protein was washed off from the column in the presence of 25 mM imidazole, whilst a smaller amount of protein remained bound and began eluting at 100 mM imidazole. The protein was present in the eluted fractions but not in the flow-through. The molecular weight of the $(His)_6$-aS is about 18.6 kDa.

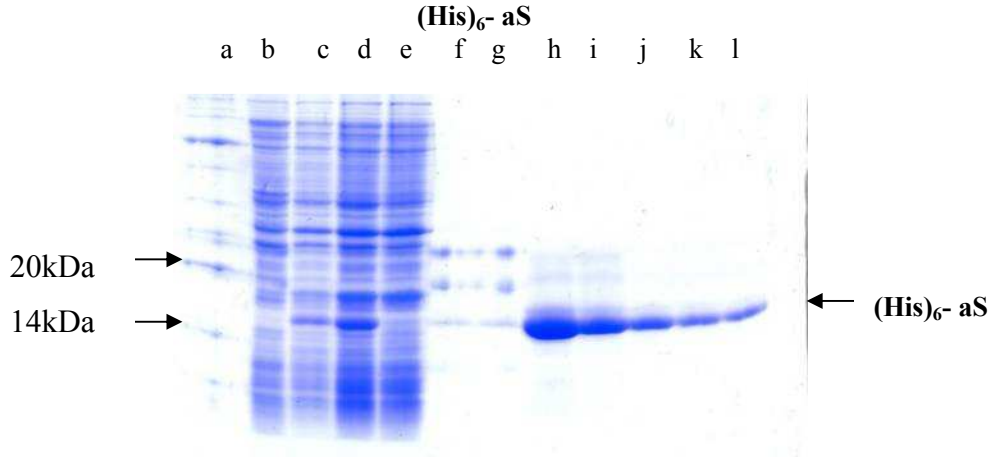

Fig. 3.1 Purification of $(His)_6$-aS and analyzed in 12% SDS-PAGE gel.
Lane a, molecular weight standards (kDa); lane b and c, cellular proteins before and after (3hours) induction with IPTG; lane d, soluble proteins in urea buffer; lane e, protein flow through the IMAC column; lane f, flow through column after 25 mM imidazole wash; lane g-l, fractions eluted with 100 mM imidazole.

All fractions containing the target proteins were pooled and dialyzed against chelex-treated water and 2-6 μg of each sample was applied to SDS-PAGE to check for purity (Fig3.2).

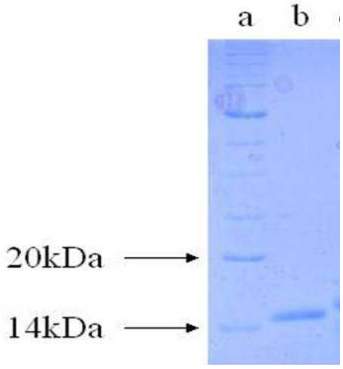

Fig. 3.2 Purified aS was separated on a 12% SDS-PAGE gel.
Lane a, molecular weight standards (kDa); lane b, $(His)_6$-aS.

3.3 Expression and purification of untag aS

Presently, two main strategies are employed for the purification of synuclein; one involves high temperature while the other involves lowering the pH of the cell lysate. As demonstrated, however, these two conditions can potentially cause damage to protein structures, rendering these purification methods less than ideal for the purpose of purifying synuclein. In this study, a milder method was introduced and compared with the two strategies discussed above, where the most approrpaite method was selected for the purification of all proteins used in this project.

3.3.1 Three different purification methods

Plasmid pDFP4a was transformed into BL21(DE) cells to overexpress aS. BL21(DE) cells were grown in batch culture to OD_{600} of 0.4-0.6 where the protein was induced with 1 mM IPTG. After 3 hours of induction, the cells were harvested by centrifugation. The cell lysates were prepared differently using different methods.

3.3.1.1 Boiling and precipitation (Volles and Lansbury 2007)

100 ml of induced cell culture was harvested by centrifuging at 8000 g for 6 minutes. The cell pellets were re-suspended in 750 µl TEN (50 mM Tris pH 8, 10 mM EDTA, 150 mM NaCl), transferred to a 1.5 ml eppendorf tube and freezed at –80^{o}C overnight.

The eppendorf was placed directly into a boiling water bath, boiled for 7 minutes and centrifuged at 21000 g for 4 minutes at room temperature. The yellowish supernatant was removed and placed into a 1.5 ml tube, followed by the addition of 136 µl of 10% streptomycin sulfate. 228 µl glacial acetic acid was then added per ml of supernatant and mixed before it was centrifuged at 21000 g for 2 minutes to precipitate the ribosomal proteins and nucleic acid. The yellowish supernatant was decanted into a 2 ml tube and mixed with the same volume of saturated ammonium sulfate (prepared in MilliQ water at 4^{o}C). The aS protein was precipitated by centrifugation at 21000 g for 2 minutes. The protein pellet was washed with 50%

ammonium sulfate (4°C) by vortexing and centrifugation to get rid of the residual acetic acid. Finally, the protein was re-suspended in 20 mM Tris-HCl pH 8 buffer and dialyzed in chelex-treated MilliQ water for further analysis. Due to the solubility of protein, only the purified aS from last few steps of analysis was analyzed on 12% SDS-PAGE (Fig 3.3). The molecular weight of untag aS is about 14.5 kDa.

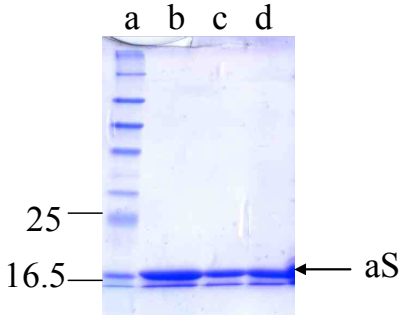

Fig. 3.3 Purified aS was analyzed on a 12% SDS-PAGE.
Lane a, molecular weight standards (kDa); lane b, aS resuspended in Tris-HCl pH 8 buffer; lane c-d, aS after dialysis in chelex treated MilliQ water.

3.3.1.2 Acid precipitation (Conway, Harper et al. 1998)

1 L of induced cell culture of aS was harvested by centrifuging at 8000 g for 6 minutes. The cell pellets were lysed mechanically by sonication in 10 mM NaAcetate, 1 mM EDTA pH 4 (buffer C) with 1 mM PMSF and 50 ug/ml DNase. The cell lysate was spun for 1 hour at 25000 g and the pellets were discarded. The supernatant was acid precipitated on ice by adjusting the pH to 4 using 10% acetic acid. The suspension was stirred on ice for 30 minutes before it was spun for 1 hour at 25000 g. The supernatant was retained and loaded on the 5 ml cation exchange HiTrap SP HP column equilibrated with 2 CV buffer C. The column was then washed with 2 CV buffer C, and a broad gradient elution (10 CVs) from 0 – 60% 10 mM NaAcetate, 1 mM EDTA, 2 M NaCl pH 4 (buffer D) was performed to elute aS. The program was shown in appendix D. As was shown in the UV chromatogram, a peak was observed as semi-purified cell lysate was loaded onto the column (Fig 3.4A). A broad low peak appeared during the flow of a low concentration of buffer D, while a tight high peak

corresponded to the eluted fractions of aS (Fig 3.4A), analyzed on a 12% SDS-PAGE (Fig 3.4B).

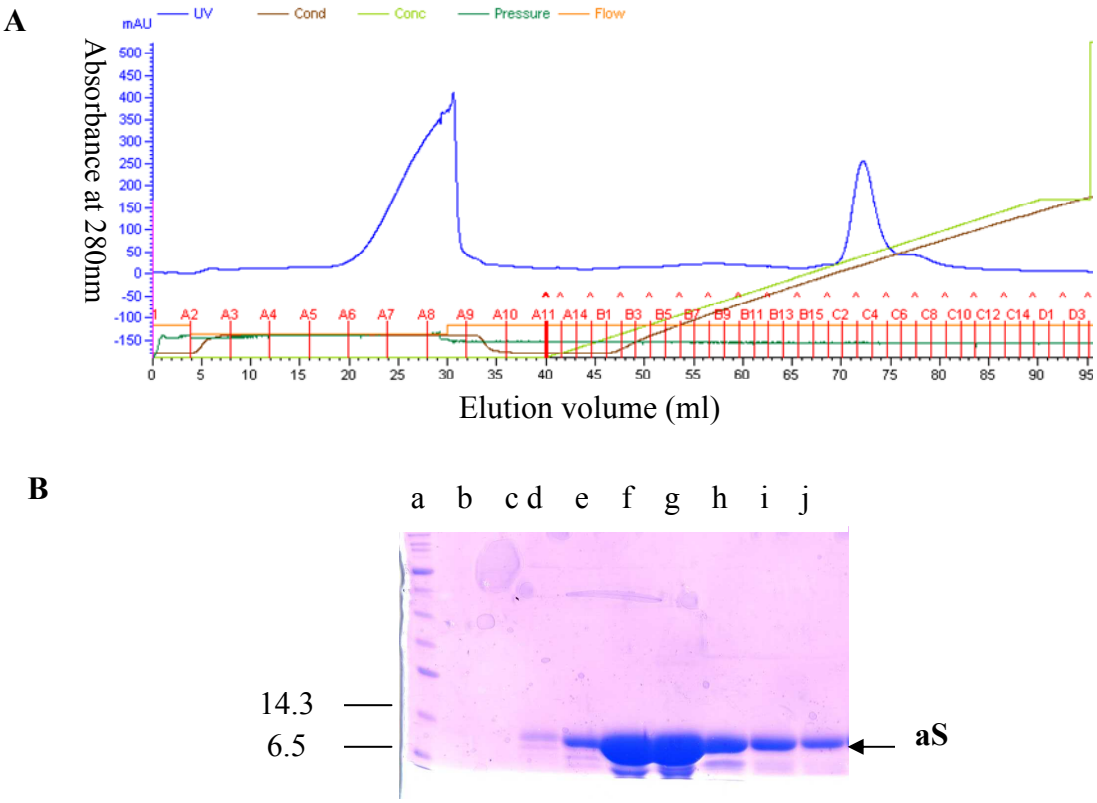

Fig. 3.4 Purification of aS by cation exchange chromatography.
A: UV chromatogram showing the process of protein loading and elution. B: Eluted aS fractions analyzed on a 12% SDS-PAGE. Lane a, molecular weight standards (kDa); lane b-j, eluted aS fractions.

The purified aS was then buffer exchanged to 20 mM Tris-HCl pH 8 buffer through PM10 membrane (Millipore) and dialyzed against chelex treated MilliQ water for further analysis.

3.3.1.3 Anion exchange chromatography

1 L of induced cell culture of aS was harvested by centrifuging at 8000 g for 6 minutes. The cell pellets were lysed mechanically by sonication in 10 mM Tris-HCl, 1 mM EDTA pH 8 (buffer A) with 1 mM PMSF and 0.5 mg/ml DNase. The cell

lysate was spun for 1 hour at 25000 g and the pellets were discarded. The supernatant was loaded on the 50 ml anion exchange Q sepharose column equilibrated with 2 CV buffer A. The column was then washed with 2 CV buffer C and a broad gradient wash (2 CVs) from 0 – 11% 10 mM Tris-HCl, 1 mM EDTA, 2 M NaCl pH 8 (buffer B) was performed followed by 2 CVs of 11% buffer B wash. aS was eluted by 11%-50% buffer B (4 CVs). The program was shown in appendix D. As was shown in the UV chromatogram, a peak was observed as semi-purified cell lysate was loaded onto the column (Fig 3.5A). A broad low peak appeared during the flow of a low concentration of buffer B, while a tight high peak corresponded to the eluted fractions of aS (Fig 3.5A), analyzed on a 12% SDS-PAGE (Fig 3.5B).

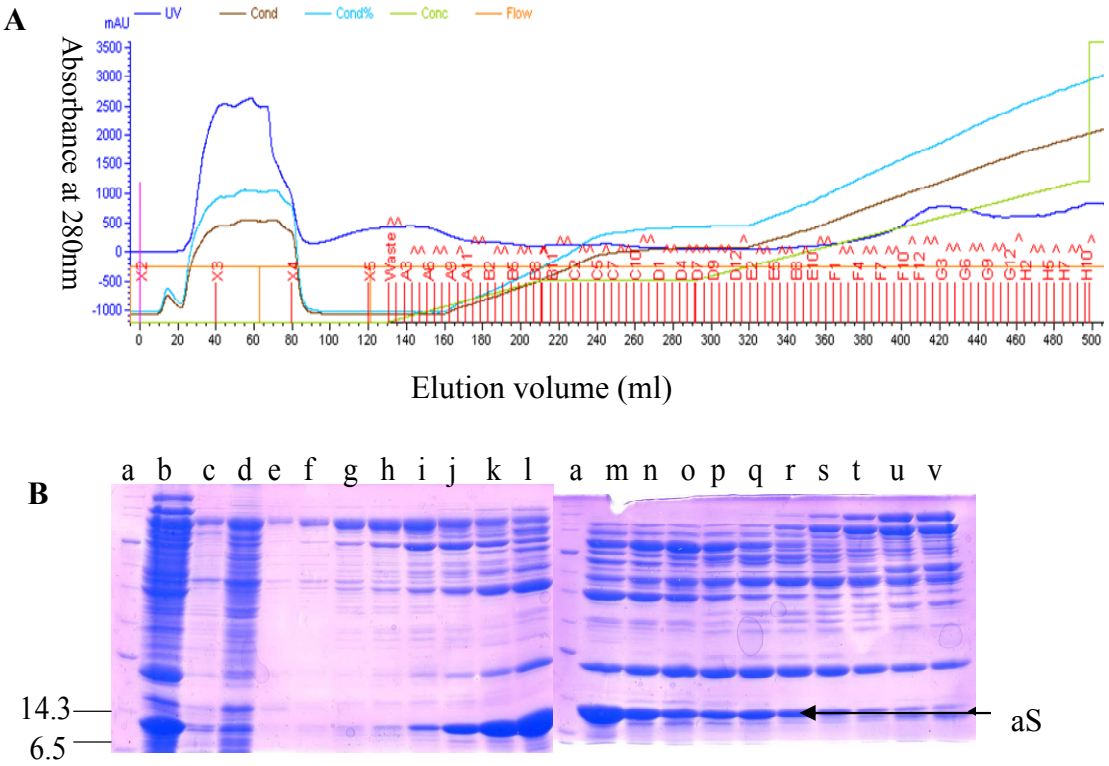

Fig. 3.5 Purification of aS by anion exchange chromatography.

A: UV chromatogram showing the process of protein loading and elution. B: Eluted aS fractions analyzed on a 12% SDS-PAGE. Lane a, molecular weight standards (kDa); lane b, cell lysate; lane c-d, flow through; lane e-v, eluted aS fractions. Lane e-v are from fractions F6-G12.

Fractions containing aS were pooled and filtered through a PM30 membrane (Millipore), where most of the contaminants were trapped above the membrane while the protein passed through the filter (Fig 3.6A). Finally, the purified aS was concentrated and dialyzed against chelex treated MilliQ water (Fig 3.6B).

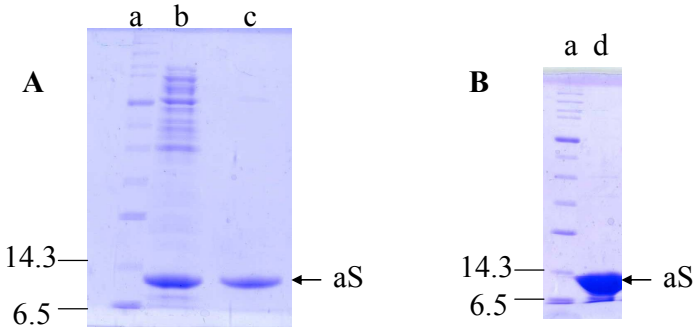

Fig. 3.6 Purified aS by PM30 membrane analyzed on a 12% SDS-PAGE.
A: Lane a, molecular weight standards (kDa); lane b, pooled fractions from anion exchange chromatography; lane c, aS passed through PM30 membrane. B: Lane a, molecular weight standards (kDa); lane d, concentrated aS.

3.3.2 Comparison of aS from different purification methods

Matrix Assisted Laser Desorption Ionisation (MALDI) mass spectrometry indicated that the aS purified from the three methods was of the right size at 14460 dalton and was more than 95% pure (Fig 3.7). Due to the limitation of the technique, no modification was observed.

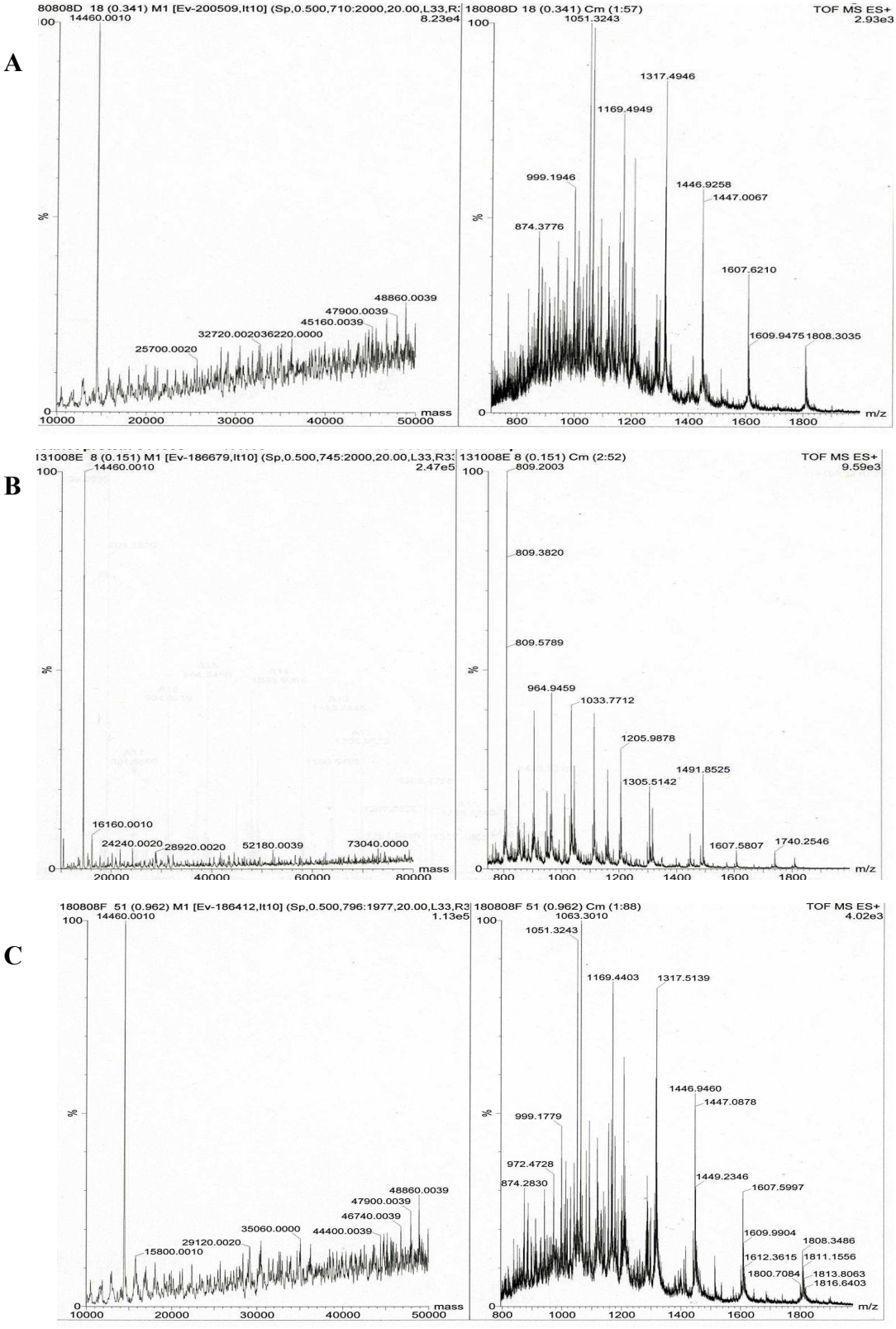

Fig. 3.7 Mass spectrometry of purified aS.

A: aS purified using boiling and precipitation method. B: aS purified using acid precipitation and cation exchange chromatography. C: aS purified using anion exchange chromatography.

Interestingly, two-dimensional nuclear magnetic resonance (NMR) spectroscopy demonstrated slight differences in the structure of aS from the different purification strategies used (Fig 3.8), where the precise changes were unknown because the protein was un-labled on nitrogen, carbon or hydrogen atoms. As seen in Fig 3.8D, few variation in conformations between the two proteins were observed when the data of aS from acid precipitation preparation and anion exchange chromatography were overlayed and compared. The concentration of aS used in this experiment was 1 mM. However, it appeared that the concentration of aS from the boiling and precipitation strategy was much lower in comparison to the other two strategies used (Fig 3.8A). This might have been due to the aggregation of the protein according to the raw data due to the observation of very few crosspeaks in the 2D spectrum. This conclusion was confirmed by loading the sample to a size exclusion column linked with a multiangle light scattering (Fig 3.9). Multiangle light scattering is a technique for measuring, independently, the absolute molar mass and the average diameter of particles in solution, by detecting how it scatters light. The intensity of light scattered at different discrete angles is measured simultaneously by either a single detector on a goniometer, a series of detectors or an array of detectors. Three peaks were detected for aS obtained using the boiling method, whereas two peaks were detected for the aS obtained using the other two purification methods. The extra peak indicated the aggregated aS.

A

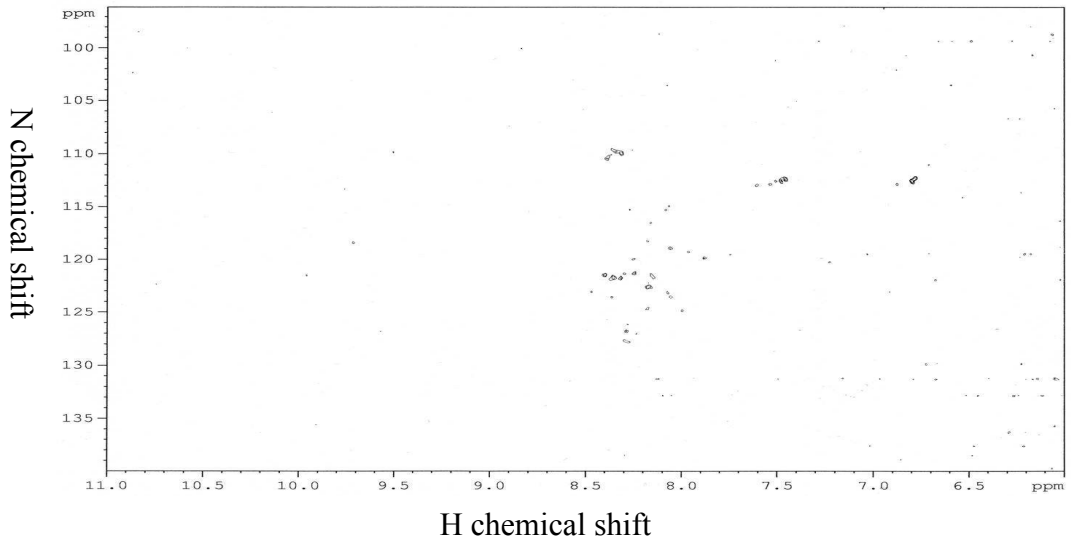

N chemical shift

H chemical shift

B

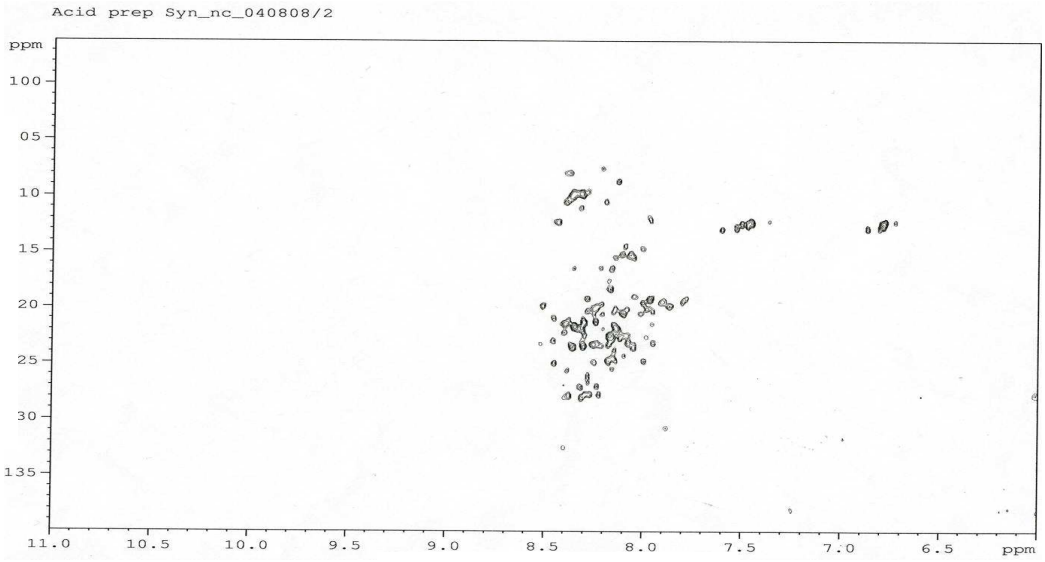

N chemical shift

H chemical shift

C

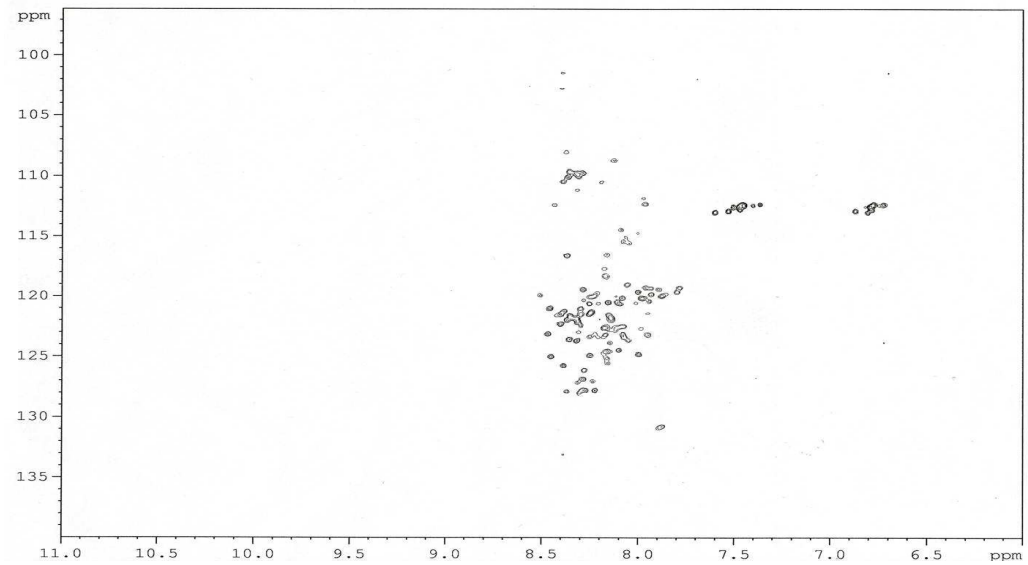

N chemical shift

H chemical shift

D

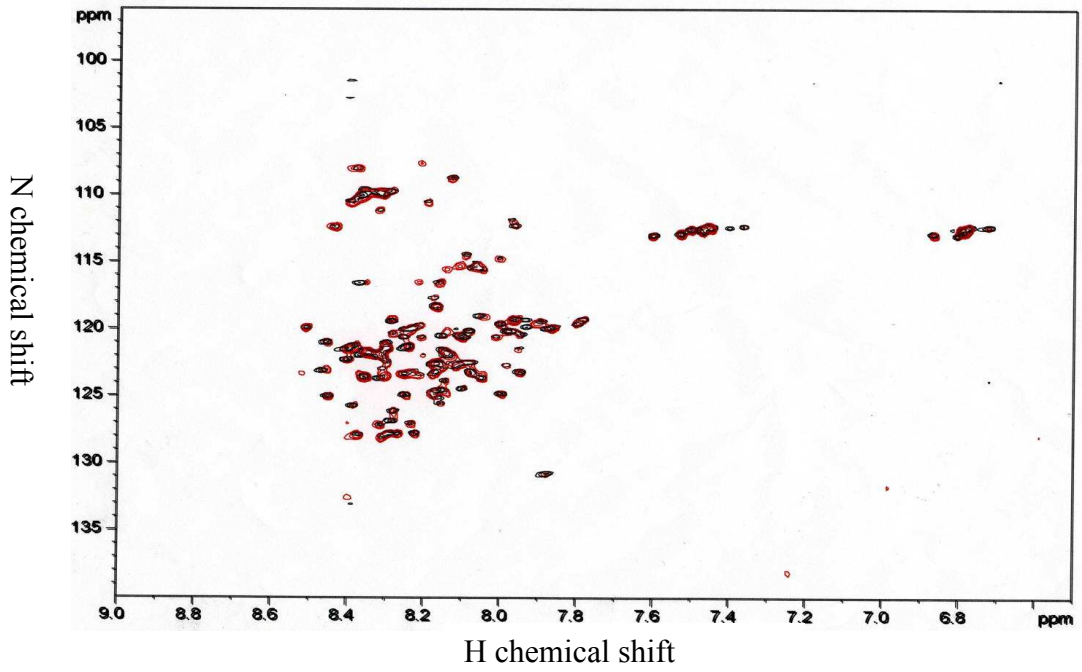

Fig. 3.8 NMR spectroscopy of purified aS.

A: aS purified using boiling and precipitation method. B: aS purified using acid precipitation and cation exchange chromatography. C: aS purified using anion exchange chromatography. D: overlayed data of aS from acid precipitation (red) and anion exchange chromatography.

aS (Boil)

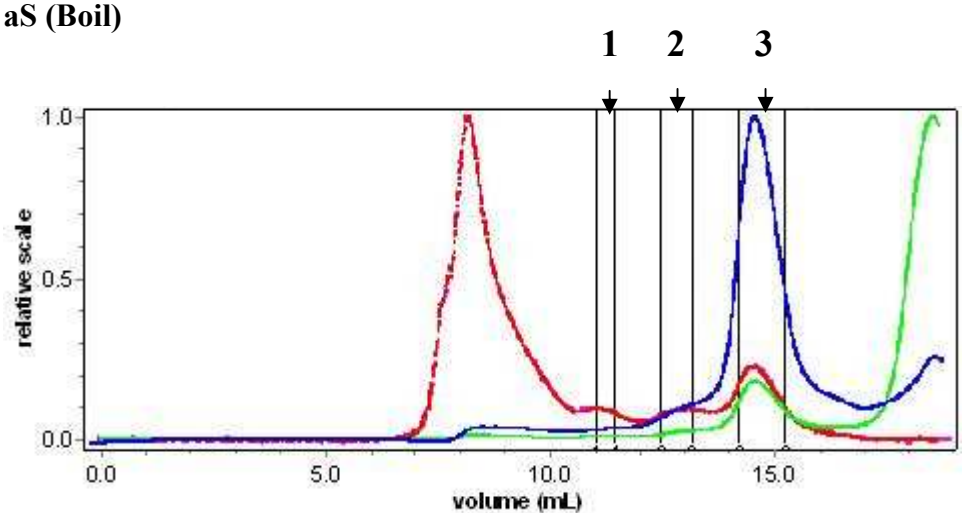

aS (Acid prep)

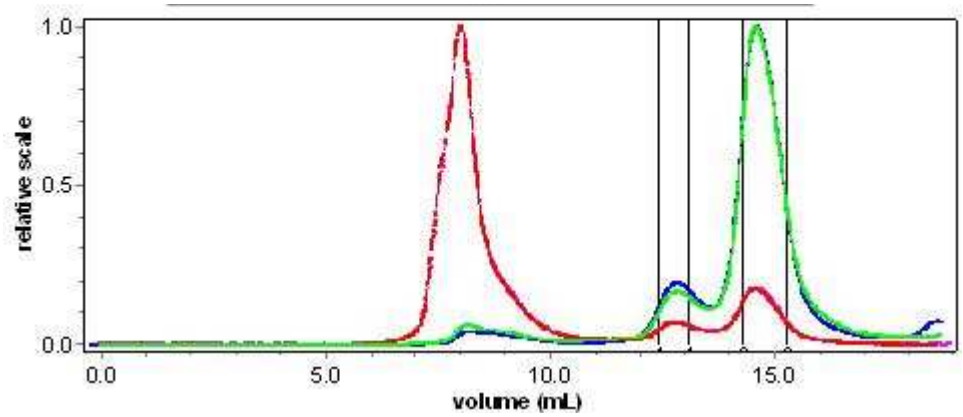

aS (Anion exchange)

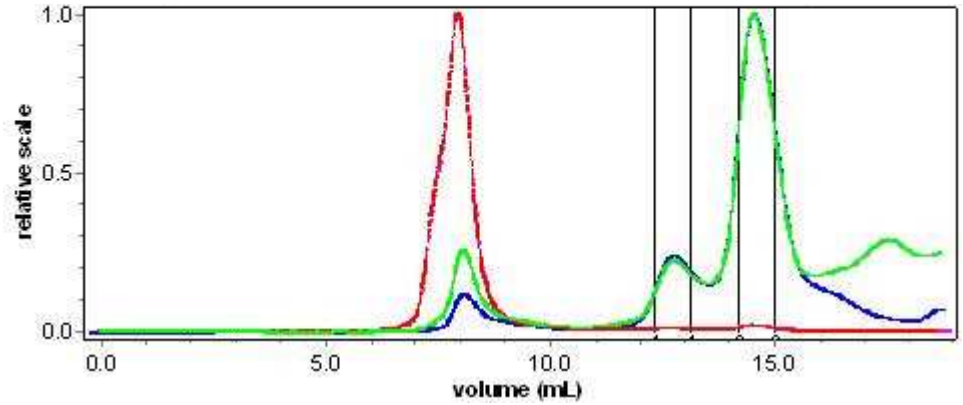

Fig. 3.9 Data from light scattering analysis for Comparison of aS purified with boiling, acid prep and anion exchange methods.

Three peaks are indicated for aS from boiling method. Peak 1 indicates aS aggregates. Green: UV absorbance; Blue: differential refractive index data; Red: count rate.

Similarly, far-UV circular dichroism (CD) spectroscopy showed that the structures of aS purified using acid precipitation and anion exchange chromatography were similar, and were also different from that of the more compacted structure of aS prepared by boiling and precipitation (Fig 3.10). aS obtained from the boiling method demonstrated a more negative value of $[\theta]_{222\ nm}$ than the protein purified by anion exchange chromatography and acid precipitation methods (Fig 3.10), suggesting that aS contained a higher degree of helical secondary structure due to boiling. This explained why the protein sample from the boiling method was more prone to aggregation in the NMR experiment even when the concentrations were identical.

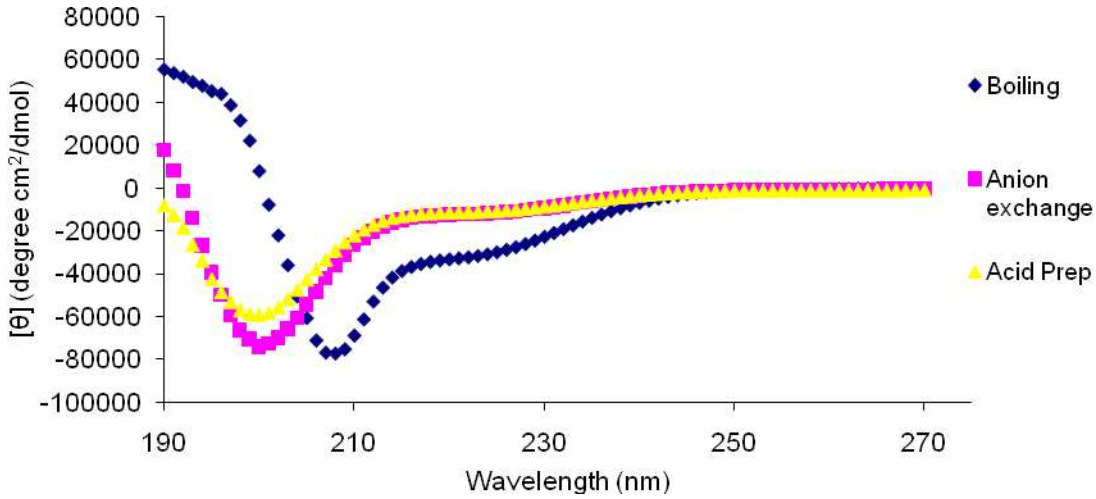

Fig. 3.10 Comparison of far-UV CD spectra on aS from different methods. Measurements were carried out at 25°C. At least three scans were carried out for each experiment.

Considering the results from MALDI mass spectrometry, NMR spectroscopy, light scattering and far-UV CD spectroscopy, aS purified from acid precipitation and anion exchange chromatography techniques were of similar conformation, while the protein that undergone a high temperature resulted in a more compact structure. Consequently, the two methods involving cation exchange and anion exchange chromatography were found to be more reliable, and were used in subsequent purification of the protein.

3.4 Discussion

His-tagged proteins firstly used in the study as fusion protein were widely used in the aS research (Uversky, Lee et al. 2001; Choi, Sung et al. 2002) and the histag showed no adverse effect on copper binding to the prion protein (Thompsett, Abdelraheim et al. 2005). However, the induction of the His-tagged protein was too low for purification. The matter was further complicated by the presence of extra amino acids, excluding the $(His)_6$ tag, in the N-terminus region of the target protein. This may be problematic if the protein was to be used for characterization analyses, as the presence of extraneous amino acids may affect protein features with regard to copper binding. As a consequence, untagged version of the protein was introduced to avoid this potential problem.

Until recently, the most common forms of purification of aS involve either a boiling step or acid precipitation during the preparation of the cell extracts (Jakes, Spillantini et al. 1994; Weinreb, Zhen et al. 1996; Giasson, Uryu et al. 1999; Narhi, Wood et al. 1999; Hoyer, Antony et al. 2002; Lee, Paik et al. 2004). The protein extraction was prepared at high temperature owing to the protein's apparent heat stability (Weinreb, Zhen et al. 1996). However, Uversky et al. (2001) demonstrated that aS experienced a transition from a natively unfolded state to a partially folded conformation with some β–sheet, forming the main component of secondary structures in aS fibrils. Whilst the rate of aS aggregation was accelerated by high temperature, the structural changes induced by heating were found to be reversible (Uversky, Lee et al. 2001). In this study, conformation variations were detected by CD, NMR spectroscopy and light scattering for aS produced by the boiling protocol. More secondary structures were observed in the protein compared to those from the other two purification protocols (Fig 3.8, Fig 3.9 and Fig 3.10), suggesting that the accumulation of aS might be due to the more compacted structure. This explained the reason for protein aggregation observed in NMR spectroscopy. However, far-UV CD spectra demonstrated an essentially unfolded polypeptide chain for aS, including the characteristic minimum in the vicinity of 196 nm and the absence of bands in the 210-230 nm region (Uversky, Li et al. 2002). In that experiment, aS was extracted from the human brain tissue and purified by boiling and chromatography system. In

this study, the negative peak of the far-UV spectra for aS purified by the boiling protocol was around 208 nm and the $[\theta]_{222\,nm}$ intensity was much higher, illustrating a higher degree of secondary structure. This may be due to the freezing and re-thawing of the protein, making it more prone to assembly as boiling may have caused an alteration to protein conformation. Having said this, the structure was even more unfolded straight after purification. This hypothesis was confirmed by the observation from NMR analysis. NMR chemical shifts were frequently applied to investigate the propensity of natively unfolded proteins to probe the different regions of conformational space (Eliezer, Kutluay et al. 2001; Bertoncini, Rasia et al. 2007; Sung and Eliezer 2007). The distribution of the dots in the 2D plot (Fig 3.8) was in close agreement with that demonstrated by other groups (Eliezer, Kutluay et al. 2001; Wu, Kim et al. 2008). As the majority of studies employing the boiling step in protein purification were mainly concerned with the investigation of synuclein aggregation, this may explain why the changes in protein properties causing aggregation were not realized during these studies. (Giasson, Uryu et al. 1999; Narhi, Wood et al. 1999; Hoyer, Antony et al. 2002). Interestingly, aS purified using acid precipitation showed a similar structure to that of aS prepared by anion exchange chromatography, a very common and mild technique for protein purification.

In the protocol for anion exchange chromatography, PM30 membranes (Millipore) were used in the last step to trap the high molecular contaminants. Gel filtration chromatography was initially used to separate aS from the contaminant species but was unsuccessful. aS was shown to behave abnormally on FPLC gel-filtration chromatography with the apparent molecular mass of 70 kDa, which might due to its unfolded structure (Paik, Lee et al. 1997). This provides an explanation as to why some molecules of 35-45 kDa in size always eluted with the target protein during gel filtration chromatography. These molecules were retained by the PM30 membrane while the synucleins were filtered through; this is most likely due to the differences in cellulose material between the membrane and the gel filtration mechanism.

To maintain the results in this project in a comparable manner, acid precipitation and cation exchange chromatography were utilized to purify most of the proteins in this study. Additionally, the anion exchange chromatography was found not to be practical for the purification of some of the proteins, such as aS1-100 and aS1-100

H50A, due to the high isoelectric points (pI). The pI of synuclein proteins purified and used in this study was shown in appendix E.

Chapter 4. Cu(II) binding modes of synucleins determined by EPR spectroscopy

4.1 Introduction

Several possible mechanisms for metal-stimulated fibrillation of aS can be envisaged. The simplest would involve direct interactions between aS and the metal, leading to structural changes in aS, and resulting in the enhanced propensity to aggregate (Uversky, Li et al. 2001). Analysis of far-UV CD at pH 7.5 with 35 μM aS and 2 mM metals indicated that Cu(II) resulted in a large increase in negative ellipticity around 222 nm, suggesting an increase in secondary structure change (Uversky, Li et al. 2001). In contrast, a recent study showed that Cu(II) does not affect the structural features inherent to the spontaneous aggregation of aS, and copper-induced fibrils exhibit the same morphology as those formed in the absence of the cation (Rasia, Bertoncini et al. 2005). These conflicts create the necessity for the examination of aS-Cu interaction. NMR mapping revealed that there are two affected regions in the protein when binding to copper. The first one is located in the N-terminus, comprising residues 3-9 and the histidine within sequence 48-52, while the second region which is less effective is within the C-terminus of aS involving residues 119-124 (Binolfi, Lamberto et al. 2008). Later EPR spectroscopy studies showed that aS binds Cu(II) via two N-terminal binding modes at physiological pH (Drew, Leong et al. 2008). The controversy of copper coordination to the regions of aS deserves a more detailed study to elucidate the degree of contribution of the individual motifs to the overall binding modes. Currently it is still unclear about the mechanism of how copper increases aS aggregation. The details of the binding specificity of Cu(II) to aS, i.e., the identity of the binding sites and the nature of the anchoring domain, may provide important and practical insights into the process. Unlike aS, its homologue bS does not fibrillate when incubated under the same condition, but it can be forced to fibrillate in the presence of some metal ions (Zn^{2+}, Pb^{2+}, and Cu^{2+}) and pesticides (Yamin, Munishkina et al. 2005). In addition, both of bS and gS inhibit aS fibril formation and complete inhibition was observed at 4:1 molar excess of bS and gS over aS (Uversky,

Li et al. 2002), although the mechanism is not fully elucidated. In this chapter, Cu(II) binding modes of the full length synucleins and their mutants were deconvoluted by spectroscopic analyses at physiological pH through the Continuous-Wave (CW) EPR technique. It provides an understanding of the role of Cu(II) on the altered structural states of aS associated with disease.

4.2 Cu(II) binding modes of aS, bS and gS at pH 7.4

Synuclein proteins were expressed and purified as described before (Chapter 3) and the purity was checked in SDS-PAGE (appendix E). All the protein samples were prepared at a concentration of 100 μM in 20 mM N-ethylmorpholine (EM) buffer pH 7.4. Different equivalents of Cu(II) were added into protein samples before they were transferred into the 3 mm internal diameter quartz EPR tubes and frozen in liquid nitrogen. Fig 4.1 showed the CW-EPR spectra of aS, bS and gS with 0, 1, 2, 3 and 4 equivalents of copper at pH 7.4.

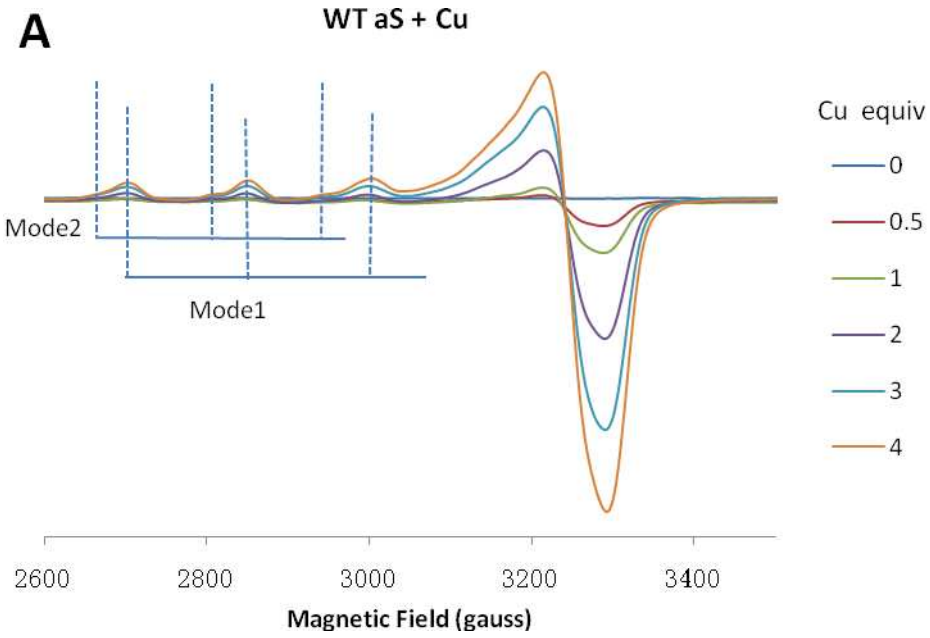

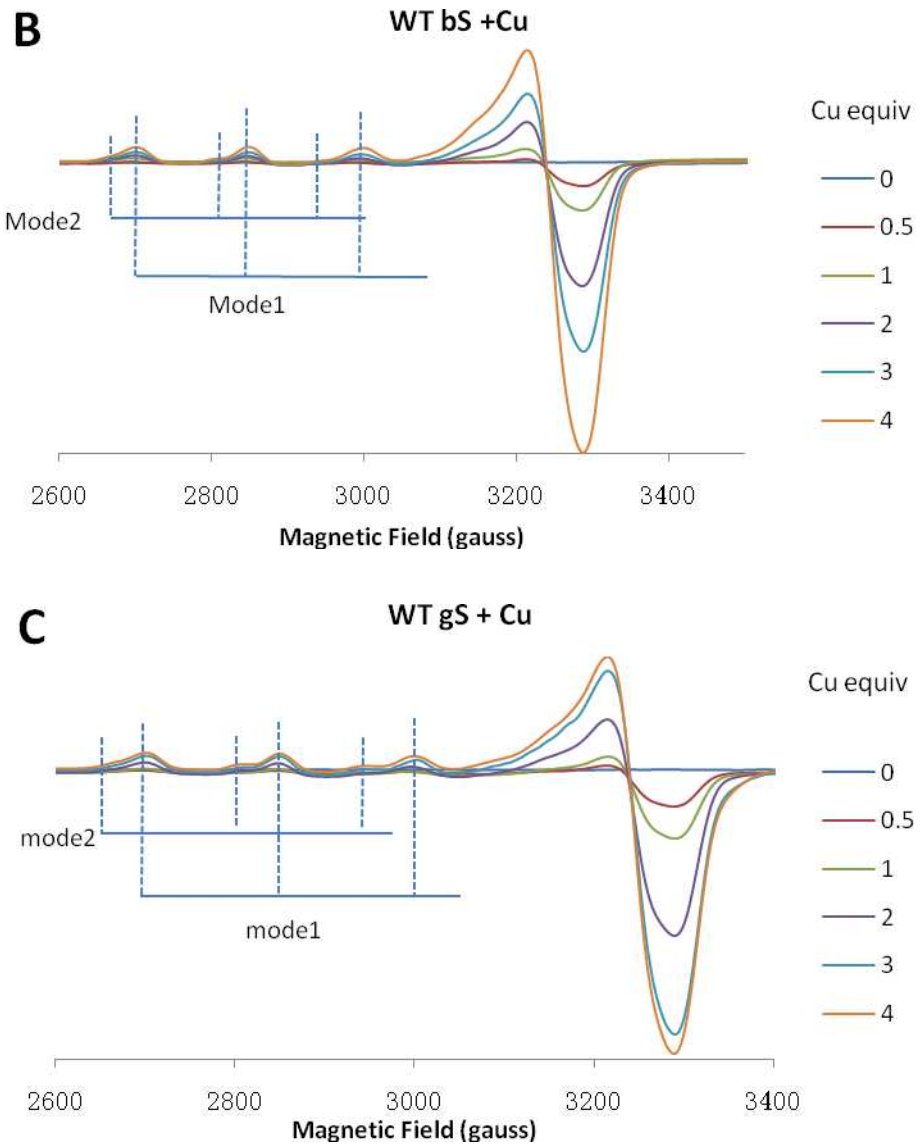

Fig. 4.1 Continuous-wave EPR of Cu(II) binding to WT aS, bS and gS.

EPR spectra at pH 7.4 of (A): aS; (B): bS; and (C): gS bound to 0-4 mol equivalents of Cu(II). Two Cu(II) binding modes were indicated for three proteins. The experiments were performed in a Bruker CW-EPR spectrometer at temperature of 20 K. All the spectra were operated with 100 kHz magnetic field modulation, with modulation amplitude of 0.5 mT and microwave power of 2 W.

All three proteins appeared to have similar binding complexes (Fig 4.1). It was evident that the hyperfine peaks were very wide, which corresponds to two binding modes for each protein, referred as mode 1 and mode 2. The two modes were present at all Cu(II) concentrations, at the same ratio throughout the titration, with mode 1 always the predominant one. Quantification of Cu(II) binding by double integration of the EPR spectra revealed that the proportions of Cu(II) bound by mode 1 and mode 2 in aS were 75% and 25% respectively. Both signals of the parallel hyperfine splitting for the two forms grew upon further addition of Cu(II). The EPR spectra of both modes were typical of type II Cu(II) centers with N and O lignds in a square-planar or tetragonal environment (Peisach and Blumberg 1974). The coordination structure was determined by the $A_{//}$ and $g_{//}$ parameters which were plotted using Peisach-Blumberg diagrams, suggesting 2N2O and 1N3O coordination spheres for all three proteins (Table 4.1).

		$A_{//}$ (mK)	$g_{//}$	Coordination
aS	Mode 1	14.0	2.29	2N2O
	Mode 2	13.0	2.33	1N3O
bS	Mode 1	13.9	2.29	2N2O
	Mode 2	12.9	2.33	1N3O
gS	Mode 1	14.1	2.29	2N2O
	Mode 2	13.2	2.33	1N3O

Table 4.1 Spin Hamiltonian parameters of Cu(II) binding modes for human recombinant aS, bS and gS at pH 7.4.

4.3 Comparison of Cu(II) binding modes of aS and its mutants at pH 7.4

To investigate the contributions of N-terminus and His50, aSΔ1-9 and H50A mutant in which histidine was replaced by alanine were examined. To indentify the residues in aS which were involved in the Cu(II) coordination modes, domain-truncated models of aS were utilized in the EPR experiments. aS and its mutants were expressed and purified as described before (Chapter 3) and the purity was checked in SDS-PAGE (appendix E). All the protein samples were prepared at a concentration of 100 μM in 20 mM EM buffer pH 7.4. Fig 4.2 showed this data.

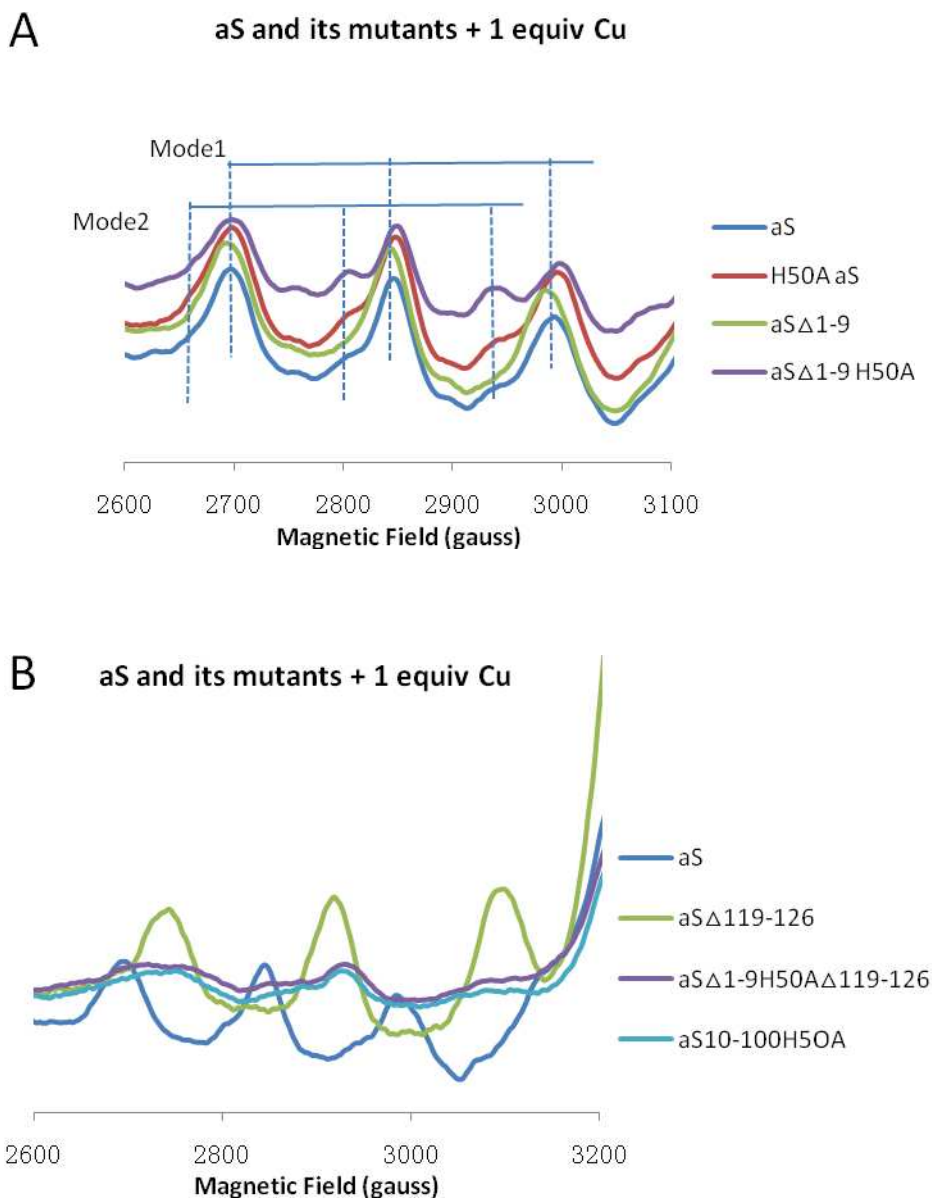

Fig. 4.2 Continuous-wave EPR of Cu(II) binding to aS and its mutants.

EPR spectra at pH 7.4 of (A): aS and the N-terminus mutants; (B): aS and the C-terminus mutants bound to 1 mol equivalent of Cu(II). Two Cu(II) binding modes were indicated for the proteins. The experiments were performed in a Bruker CW-EPR spectrometer at temperature of 20 K. All the spectra were operated with 100 kHz magnetic field modulation, with modulation amplitude of 0.5 mT and microwave power of 2 W.

Fig 4.2 shows the comparisons for the titration of aS and its mutants with 1 mol equivalent Cu(II) followed by CW-EPR at pH 7.4. As reported for aS, at least two different Cu(II) species can be obtained from the EPR spectra for each of the aS mutants on the basis of their $A_{//}$ and $g_{//}$ parameters. In Fig 4.2A, two identical coordination species (mode 1 and mode 2) were detected in aS mutants H50A aS, aS△1-9 and aS△1-9 H50A. The $A_{//}$ and $g_{//}$ values obtained for the main species fell between the range of values associated with Cu(II) complexs with a 2N2O coordination and the values of the other one fell in the range associated with a 1N3O binding mode comparing to the previous data (Binolfi, Lamberto et al. 2008; Drew, Leong et al. 2008) (Table 4.2). A large increase in the proportion of mode 2 was observed in aS△1-9 H50A as the relative signal intensity was stronger (Fig 4.2A). In Fig 4.2B, EPR spectra showed that the $g_{//}$ values decreased in aS mutants aS△119-126, aS△1-9 H50A △119-126 and aS10-100 H50A when binding to Cu(II), and it favoured the 3N1O coordination in the Paisach-Blumberg program comparing to the previous data (Drew, Leong et al. 2008) (Table 4.2). This might be due to the mutation in the C-terminal region of the protein which is responsible for the donation of an oxygen ligand (Rasia, Bertoncini et al. 2005). The proportion of the second mode was much higher in aS△1-9 H50A △119-126 and aS10-100 H50A compared to that in aS△119-126.

		$A_{//}$(mK)	$g_{//}$	Coordination
aS	Mode 1	14.0	2.29	2N2O
	Mode 2	13.0	2.33	1N3O
H50A	Mode 1	13.9	2.29	2N2O
	Mode 2	12.9	2.33	1N3O
aS△1-9	Mode 1	13.9	2.29	2N2O
	Mode 2	12.9	2.33	1N3O
aS△1-9 H50A	Mode 1	14.2	2.29	2N2O
	Mode 2	12.7	2.33	1N3O
aS△119-126	Mode 1	16.4	2.23	3N1O
	Mode 2	15.9	2.26	3N1O
aS△1-9 H50A △119-126	Mode 1	16.2	2.22	3N1O
	Mode 2	15.1	2.27	3N1O
aS10-100 H50A	Mode 1	16.4	2.23	3N1O
	Mode 2	16.5	2.26	3N1O

Table 4.2 Comparison of spin hamiltonian parameters of Cu(II) binding modes for aS and its mutants at pH 7.4.

4.4 Comparison of Cu(II) binding modes of bS and its mutants at pH 7.4

As the homologue of aS, bS was assumed to behave in a similar way while binding copper. Thus, similar site-directed and truncated mutants were designed in this experiment. bS mutants were expressed and purified as described before (Chapter 3) and the purity was checked in SDS-PAGE (appendix E). All the protein samples were prepared at a concentration of 100 μM in 20 mM EM buffer pH 7.4. Different equivalents of Cu(II) were titrated into protein samples before they were transferred into the 3 mm internal diameter quartz EPR tubes and frozen in liquid nitrogen. Fig 4.3 shows this data.

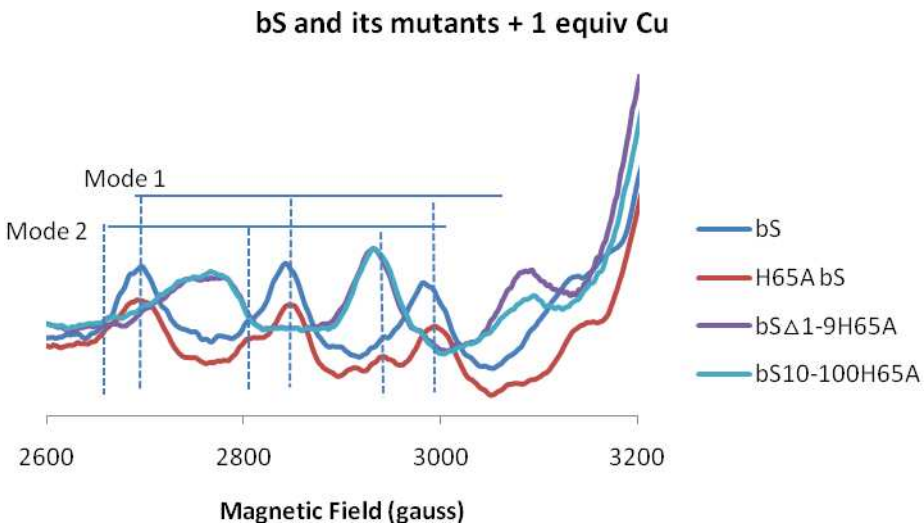

Fig. 4.3 Continuous-wave EPR of Cu(II) binding to bS and its mutants.
EPR spectra at pH 7.4 of bS and its mutants bound to 1 mol equivalent of Cu(II). Two Cu(II) binding modes were indicated for WT bS. The experiments were performed in a Bruker CW-EPR spectrometer at temperature of 20 K. All the spectra were operated with 100 kHz magnetic field modulation, with modulation amplitude of 0.5 mT and microwave power of 2 W.

Two binding components were indicated in Fig 4.3 for WT bS and H65A bS, which suggested that the mutation of His65 had little effect on the change of coordination modes. However, the ratio of mode 2 increased in H65A bS compared to that in WT bS. Two modes were observed for all the mutants although the $A_{//}$ and $g_{//}$ values were slightly different (Table 4.3). The estimation for the structure coordination showed two 3N1O components for bS△1-9 H65A and bS10-100 H65A. It seemed that the shift from 2N2O in bS to 3N1O in the mutants was produced by the truncation of 1-9 amino acids in which Asp2 could provide oxygen ligand.

		$A_{//}$(mK)	$g_{//}$	Coordination
bS	Mode 1	13.9	2.29	2N2O
	Mode 2	12.9	2.33	1N3O
H65A	Mode 1	14.4	2.29	2N2O
	Mode 2	12.9	2.33	1N3O
bS△1-9 H65A	Mode 1	14.7	2.23	3N1O
	Mode 2	15.1	2.27	3N1O
bS10-100 H65A	Mode 1	15.0	2.23	3N1O
	Mode 2	13.8	2.27	3N1O

Table 4.3 Comparison of spin hamiltonian parameters of Cu(II) binding modes for bS and its mutants at pH 7.4.

4.5 Discussion

EPR spectroscopy has been widely used for determining the interaction between Cu(II) and proteins (Klajnert, Cangiotti et al. 2007; Bruschi, De Gioia et al. 2008; Gaggelli, Jankowska et al. 2008; Gralka, Valensin et al. 2008). This study showed how EPR parameters could help in assigning the most favorable structure of Cu(II) complexes in synuclein proteins. EPR spectroscopy identified at least two Cu(II) binding modes for human recombinant aS, bS and gS proteins at physiological pH. Despite the slight differences in the amino acid sequences between synuclein proteins, the three homologues displayed the same Cu(II) binding modes. This result was unexpected, because gS lacks the C-terminal region compared to aS while the carboxylate-rich C-terminal region was originally thought to drive copper binding.

The predominant mode found for aS was 2N2O (mode 1), which was consistent with the study assigning it as $\{NH_2, N^-, \beta\text{-}COO^-, H_2O\}$, involving coordination of the N-terminal amine of Met1 and the deprotonated backbone amide and carboxylate side chain of Asp2 (Drew, Leong et al. 2008). Based on the $A_{//}$ and $g_{//}$ parameters, the second mode was estimated to correlate well with 3N1O coordination, involving

the nitrogen from the imidazole group of His50 (Binolfi, Lamberto et al. 2008). The EPR spectrum of H50A aS indicated identical binding modes with WT aS. This suggested that the coordinating ligand from the His50 could be replaced by that from other amino acid for the Cu(II) coordination mode 2. An analysis using modified peptides showed that above pH 6, the coordination of Cu(II) may involve the lateral NH_2 group of lysine residues upstream of His50 (Kowalik-Jankowska, Rajewska et al. 2006). EPR spectra showing similar coordination components were also observed in both aS△1-9 in which residues 1-9 were knocked out and aS△1-9 H50A aS, although mode 2 was more intense for the double mutant (Fig 4.2A). This implied that Asp2 might be substituted by Glu13 which could also provide a nitrogen and an oxygen ligand in Cu(II) binding modes (Rasia, Bertoncini et al. 2005).

It showed that there was a decrease in the $g_{//}$ values for aS△119-126, in which residues 119-126 were deleted. The spin Hamiltonian parameters suggested two 3N1O coordination components. This implied that amino acids 119-126 contributed to the Cu(II) binding event and the involved amino acids could be substituted because the relative signal intensity was identical to WT aS (Fig 4.2B). This was confirmed by the observation of two identical EPR spectra of aS△1-9 H50A △119-126 and aS10-100 H50A (Fig 4.2B). It was evident that the ratio of second binding species was much higher than that for WT aS, which suggested that the replacement of the amino acids in Cu(II) coordination modes might diminish the binding affinities. Based on these findings, it implied that when binding to copper, synuclein proteins might not act like other type II copper binding proteins such as the prion protein where copper binding sites were assigned to certain amino acids, the binding sites disappeared when certain amino acids missing or mutated (Klewpatinond, Davies et al. 2008). The inconsistence from the other studies might due to the different features of the synuclein proteins, which were purified through different methods. As was shown in chapter 3, the high temperature enhanced the property of aS to aggregate by altering the protein conformation, which could ultimately affect the Cu(II)-binding modes. To further elucidate the details of Cu(II) coordination with aS, more work needs to be done. Future research could focus on studies on model peptides by employing thermodynamic and spectroscopic techniques such as ITC, NMR et al.

The EPR parameters of the bS-Cu(II) complexes estimated at least two different Cu(II) binding modes which were identical to those for aS (Table 4.1). This might be due to the similarity of the amino acid sequences involved in copper coordination, including the Met1, Asp2 and His65. Although two identical binding species were found in H65A bS, the ratio of second mode was increased compared to bS. This implied that substitution of histidine in the coordination made the main mode less significant. Interestingly, the EPR spectra were fairly similar for bS△1-9H65A and bS10-100 H65A apart from a slight reduction on the signal intensity for bS10-100 H65A (Fig 4.3), which implied the contribution of the C-terminus of bS to Cu(II) binding. However, the $A_{//}$ and $g_{//}$ values fell in the range associated with two 3N1O coordination modes, which could be due to the lack of donation of oxygen ligand from Asp121 or Glu125 (Rasia, Bertoncini et al. 2005). This also confirmed that residues 1-9 played a role in the copper-binding event as H65A bS displayed two binding modes of 2N2O and 1N3O (Table 4.3).

Chapter 5. Metal-binding properties of synucleins measured by ITC

5.1 Introduction

Within the last decade, the functional characterization of aS has progressively become an area of extensive study; however, the precise function of aS remains very much elusive. A significant number of studies have demonstrated that aS plays a crucial role in the regulation of membrane lipid component, synaptic vesicular turnover, synaptic plasticity, ubiquitin-proteasome processing and could act as a molecular chaperon (Dev, Hofele et al. 2003). One of the most crucial functions of aS is the effect on cell survival and/or susceptibilities to certain insults involving the co-operation of copper. The idea that aggregated aS is responsible for the pathogenesis of many neurodegenerative diseases where copper acts as an accelerant in the aggregation process is on its way to becoming a universally accepted concept.

Whilst there is cumulative evidence showing that aS binds copper, the identification of the binding sites and affinities is still under debate. Initial studies suggested that aS binds to 5-10 copper ions with a K_d of 45-60 μM (Paik, Shin et al. 1999; Lee, Lee et al. 2003). However, Rasia et al showed that aS tightly binds to 2 copper ions per monomer with a dissociation constant in the range of 0.1-50 μM and is able to ligate more copper ions with significant lower affinity (400-500 μM) (Rasia, Bertoncini et al. 2005). There is consensus that aS binds Fe(II); nevertheless, the binding affinities reported are different (Golts, Snyder et al. 2002; Binolfi, Rasia et al. 2006).

There has been some controversy in the identification of metal-binding sites. Initial studies claimed that the C-terminal region of aS is responsible for copper binding. Nevertheless, the following analysis showed the characterization of two distinct Cu(II)-binding motifs in aS. The high-affinity binding site encompassing a complex conformational array is located in the N-terminal region of the protein, while the low-affinity site sits in the C-terminal region (Rasia, Bertoncini et al. 2005). Further

analysis utilizing peptides showed that Cu(II) ions appear to be coordinated by the N-terminal amine group of methionine (residue 1), the amide nitrogen, and the β-carboxylic group of aspartic acid (residue 2) (Kowalik-Jankowska, Rajewska et al. 2005). They also demonstrated that copper binding is pH dependent. This was confirmed by a similar analysis using modified peptides, indicating that at a pH above 6, the coordination of Cu(II) by His50 may involve the lateral NH_2 group of lysine residues upstream of His50 (Kowalik-Jankowska, Rajewska et al. 2006). In contrast to copper, other metals appear to favour the C-terminus region of aS, which is more likely to be involved in low-affinity and non-specific binding to metals. Although a considerable amount of evidence has been provided for the mechanism of copper binding, there remain several unknowns in this process. The unreliability of many of these studies has also been proven (Thompsett, Abdelraheim et al. 2005), and there exists limited avaibility with regard to information on the study of full length proteins.

In this chapter, isothermal titration calorimetry (ITC) was applied to assess metal affinity for recombinant synuclein proteins. ITC can provide direct information about the thermodynamics of metal-protein interactions. ITC can be used to measure enthalpy and free energy of a reaction and to quantify stoichiometry and affinity; for this reason, it allows quantification of complete metal binding thermodynamics. This is done by directly measuring the energy associated with a chemical reaction when two components are mixed. This is complicated by numerous factors such as heat of dilution, heat from redox, precipitation and hydrolysis. Competition for the metal ion with the buffer and any chelator must be taken into account (Zhang, Akilesh et al. 2000).

5.2 Copper binding to His-tagged synucleins

To test the capability of ITC in analyzing the binding affinities and binding sites of aS to copper, His-tagged synucleins were utilized in the experiment. His-tagged proteins were expressed and purified as described before (Chapter 3) and the purity was checked in SDS-PAGE (appendix E). The complications involved in the study of the coordination chemistry of transition metal ions were taken into account. At pH

7.0, Cu(II) is insoluble due to the formation of oxide species which can alter the protein forms because of their redox activities. It is also important to differentiate between specific binding and non-specific binding. Therefore, copper chelators were applied to chelate the copper ions until they were transferred to the target molecule during the experiments. The coordination of copper with a ligand is physiologically appropriate as metal always appears in chelated form and not free in solution under *in vivo* conditions.

Glycine was proven to be the best chelator in this experiment, which has also been used as a ligand to study copper binding to the prion protein (Thompsett, Abdelraheim et al. 2005). Moreover, the well characterized interaction between glycine and Cu(II) must also be taken into account during data analysis. Cu(II) forms a bis glycine complex, $Cu(Gly)_2$, in the presence of excess copper. Copper: glycine was used in ratio of 1:4 unless otherwise stated. The presence of excess glycine ensured that redundant copper titrated was either chelated or bound to the protein to avoid the inhibition of reaction due to free copper in the solution. Moreover, the excess glycine performed as a competitor to nonspecific protein-copper incorporation. When analyzing the data, the chelator can be taken into account by directly modifying the equations used to fit the data. Alternatively, the chelator can be accounted for post analysis (Zhang, Akilesh et al. 2000; Wells, Jackson et al. 2006), as the chelator only affects the absolute enthalpy change and not the number of binding sites. In this study, data was analyzed using Origin 5.0 with the Microcal software patch installed. Each experimental condition had a blank run with protein present in the chamber replaced with buffer. This data was then subtracted from the run with protein present to take into account any energy of dilution reaction (Davies, Marken et al. 2009). The binding isotherm which fit the data with the lowest X^2 value was taken as the best fit model. From this model, values for K_a and ΔH were calculated along with the most likely number of binding sites involved. The K_a values were then adjusted to factor in the affinity of copper for glycine. Glycine has been shown to bind two atoms of copper with the following affinities: $K_1 = 4.0 \times 10^5\ M^{-1}$ and $K_2 = 1.7 \times 10^4\ M^{-1}$ with $\beta_2 = 6.8 \times 10^9\ M^{-1}$ at pH 7.0 (Davies, Marken et al. 2009). The relative contribution of each of these species at the prevalent pH was then used in the final equilibrium to fully account for the effect of the chelate. The true K_d values of each copper binding events at pH 7.0 were calculated using equation (1), where $K_d(app)$ was the measured

apparent dissociation constant by using Origin 5.0 software, K_d^1 (Gly) and K_d^2 (Gly) were the stepwise dissociation constants for formation of a $Cu(Gly)_2$ complex at pH 7.0 and the concentration of glycine was ［Gly］(Wells, Jackson et al. 2006).

$$K_d = \frac{K_d(app)K_d^1(Gly)K_d^2(Gly)}{[Gly]^2} \qquad (1)$$

His-tagged bS was used in comparison with aS to investigate whether there were any differences in copper binding properties when the amino acid sequences were partially changed. The disease-related mutants, His-tagged A30P, E46K and A53T, were also used for the assessment of their copper binding properties in relation to causing increased aggregation of aS in the presence of copper. All the protein samples, different synucleins and the mutant aS proteins were adjusted to a concentration of 20 μM, proven to be the optimal concentration of His-tagged protein for the experiments. All the experiments were performed at pH 7.0 in chelex treated distilled water at room temperature. The metal solution of $Cu(Gly)_4$ was titrated into all of the protein samples. The final ratio of protein to copper in the reaction cell after each experiment was 1:5. The energy change in molar ratio was indicated by dots in the plots of ITC data (Fig 5.1 and Fig 5.2). All the data has been subtracted from the buffer run, due to heat released from the dilution of metal into the buffer. Each experiment was repeated at least three times, and where possible, separately prepared protein was used. The isotherms obtained from ITC representing the interaction between His-tagged synucleins and copper were shown in Fig 5.1.

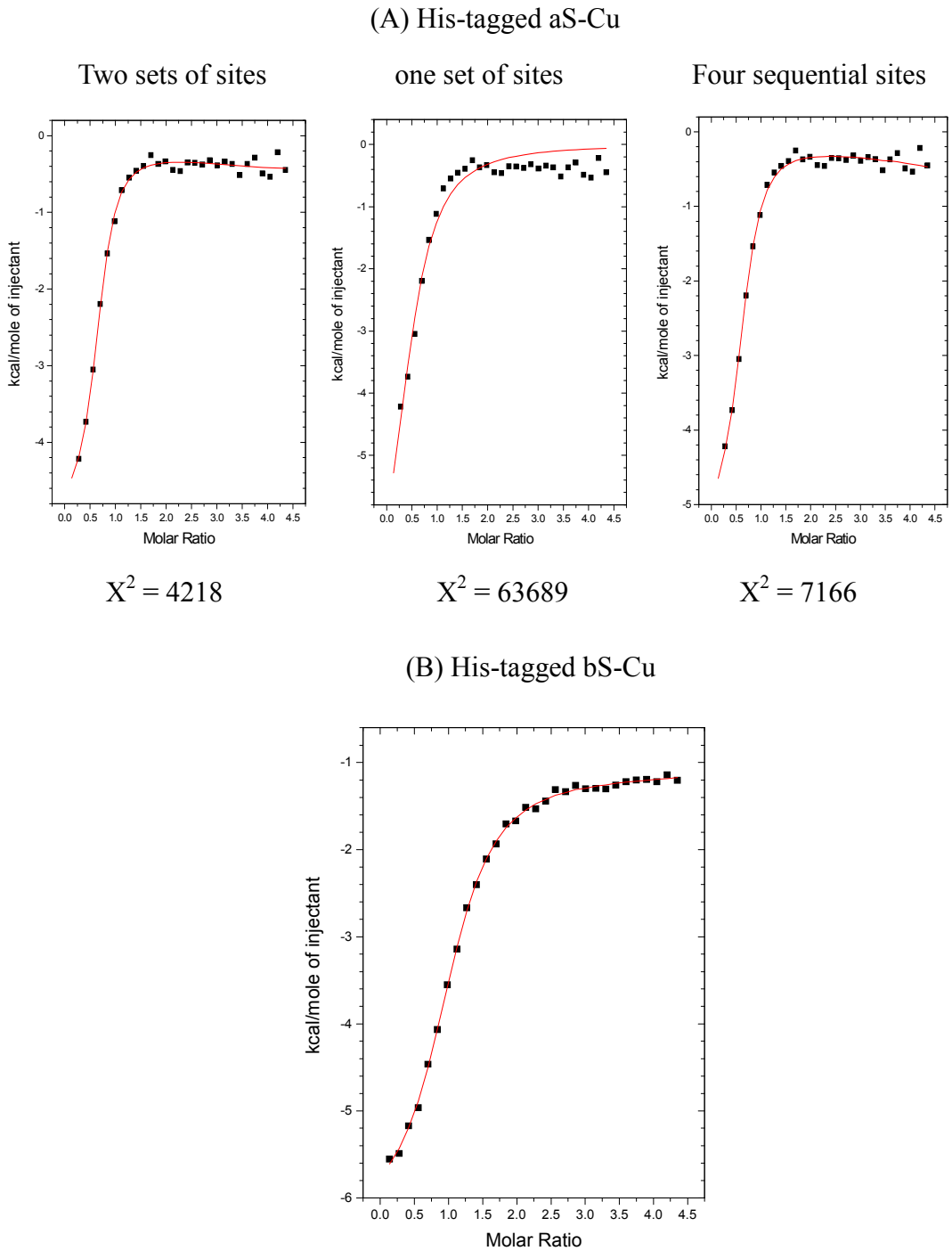

Fig. 5.1 ITC analysis of copper binding to His-tagged aS and His-tagged bS. **The panel shows heat change on addition of the ligand (kcalories/mol). (A) $Cu(Gly)_4$ (1mM: 4mM) titrated into 20 µM $(His)_6$-aS. Three different models were tried. (B) $Cu(Gly)_4$ (1mM: 4mM) titrated into 20 µM $(His)_6$-bS.**

The data was tried to fit all possible models by using the fitting program. Fig 5.1(A) compared the fitting of three models for His-tagged aS. X^2 value is equal to the sum of the squares of the deviations of the theoretical curves from the experimental points divided by the number of degrees of freedom. The two sets of sites model gave the lowest X^2 value and the errors which were less than 10%. The 'two sets of sites' model uses regression to fit a binding isotherm model that assumes two groups of single or multiple independent sites of similar affinity and enthalpy. Table 5.1 showed the stoichiometry and stability constants for the His-tagged aS and His-tagged bS at pH 7.0, where logK values were adjusted to account for the contribution of the chelator species to the overall equilibrium at pH 7.0.

	n_1	$\log K_1$	n_2	$\log K_2$
His-tagged aS	1.92±0.03	6.76	3.30±1.29	3.11
His-tagged bS	2.03±0.08	5.90	5.60±1.72	3.02

Table 5.1 Comparison of log stability constants and number of binding sites for copper between His-tagged aS and His-tagged bS.
The experiments were carried out at pH 7.0 at 25^0C. n_1 and n_2 represent the number of sites detected within each group of binding sites. Therefore the total number of sites was n_1 and n_2.

The number of sites from the second group (n_2) varied for His-tagged aS and His-tagged bS and the errors were more than 30% for both of them. K values were calculated from the mean of at least two independent experiments, with errors less than 10% for K_1 and more than 10% for K_2. This observation implied that the second group of sites was likely located in the His tag with low affinities. The variation in number of sites and high errors might be due to the mobility and the instable coordination of His tag. There were two copper binding sites (n_1) in both His-tagged aS and His-tagged bS, where His-tagged bS showed lower binding affinity compared to His-tagged aS.

(A) His-tagged A30P aS-Cu

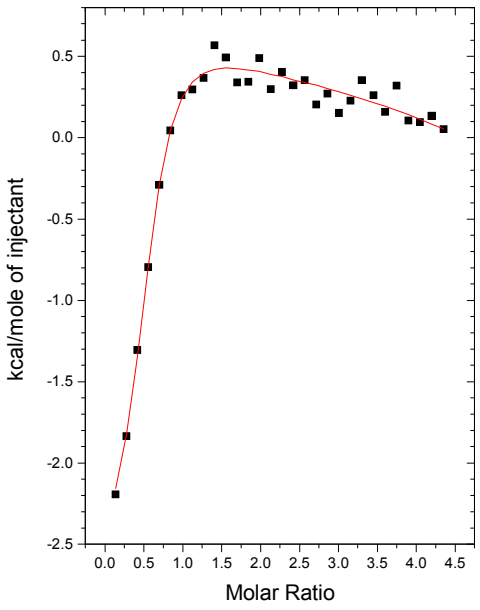

(B) His-tagged A53T aS-Cu

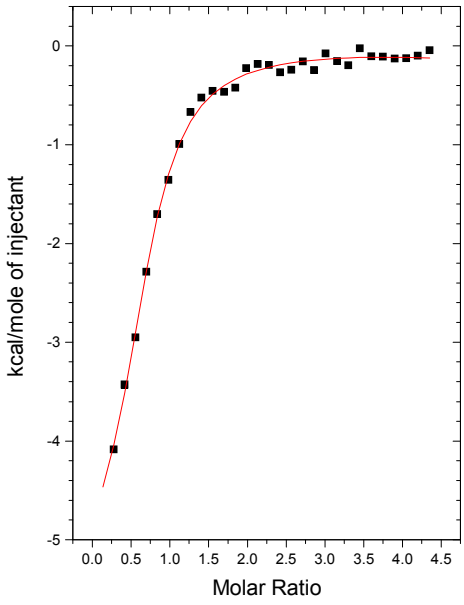

(C) His-tagged E46K aS-Cu

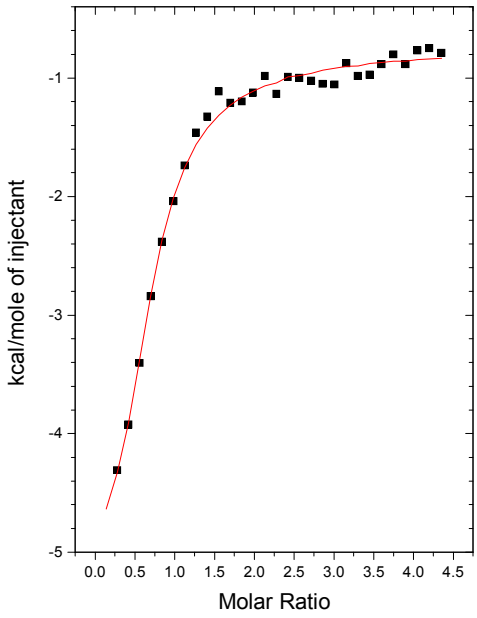

Fig. 5.2 ITC analysis of copper binding to PD-related mutants at pH 7.0.

The panel shows heat change on addition of the ligand (kcalories/mol). (A) $Cu(Gly)_4$ (1mM: 4mM) titrated into 20 µM $(His)_6$-A30P aS. (B) $Cu(Gly)_4$ (1mM: 4mM) titrated into 20 µM $(His)_6$-A53T aS. (C) $Cu(Gly)_4$ (1mM: 4mM) titrated into 20 µM $(His)_6$-E46K aS.

Again, the two sets of sites model gave the lowest X^2 value and the errors were less than 10%. Table 5.2 showed the stoichiometry and stability constants for the His-tagged aS and the disease mutants at pH 7.0. LogK values were adjusted to account for the contribution of the chelator species to the overall equilibrium at pH 7.0.

His-tagged protein	n_1	$logK_1$	n_2	$logK_2$
aS	1.92±0.03	6.76	3.30±1.29	3.11
A30P	3.40±0.01	3.21	0.94±0.11	7.16
E46K	1.93±0.06	6.19	6.79±0.05	3.76
A53T	0.97±0.08	5.97	4.11±0.16	2.45

Table 5.2 Comparison of log stability constants and number of binding sites for copper between His-tagged aS and the mutants.
The experiments were carried out at pH 7.0 at 25^0C. n_1 and n_2 represent the number of sites detected within each group of binding sites. Therefore the total number of sites was n_1 and n_2.

There was a group of sites with high stability constants, representing the copper binding sites on the protein. The other group with low log stability represented the nonspecific interaction between His tag and copper. The number of sites in this group varied in each mutated protein and the errors for K values were more than 20%. According to the observation, it seemed that the analysis using the Origin 5.0 software could only separate the two groups in terms of the binding events caused by the disruption of His tag during its interaction with copper in the ITC experiment. Therefore, untagged proteins were used in the next experiment.

5.3 Copper binding to untagged aS and bS at pH 7

Recombinant aS and bS proteins were expressed and purified as described in Chapter 3 and the purity was checked on SDS-PAGE. $Cu(Gly)_2$ was titrated into the protein

solution with 10 mM MES as buffer. Fig 5.3 showed the thermodynamic data for aS and bS following subtraction of buffer energies of dilution.

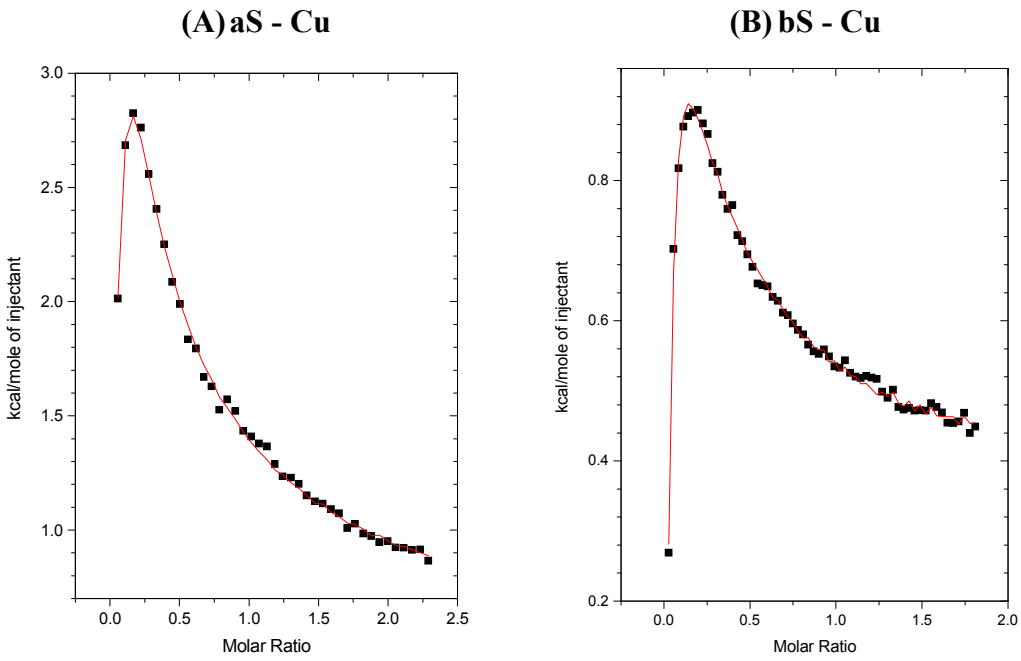

Fig. 5.3 Thermodynamic plots of synuclein titrated with Cu/Gly at pH 7, 25^{0}C. Data was after subtraction of the buffers. 10 mM MES was used to stabilize the pH throughout the experiment. (A) Plot of aS-Cu reaction. (B) Plot of bS-Cu reaction.

The data fitted well into the sequential binding model which assumes that sites are filled sequentially and each site is affected by the previous binding event. The sequential binding model was used under circumstances where sites within a group of sites were not identical, leading to the degeneracy within the two sites (Zhang, Akilesh et al. 2000). The model was supplied in the Origin software by Microcal and the chelator effect was factored to the overall equilibrium and potentially error prone according to equation (1). This was previously demonstrated to be a feasible model for the studies of Prion protein (Davies, Marken et al. 2009). Table 5.3 compared the values from aS and bS analyzed by a sequential binding model. The means of three independent experiments were calculated, with errors between K values not exceeding 10%.

		logKa	ΔGº (kcal/mol)
aS	K_1	7.022	-5.618
	K_2	7.274	-5.934
	K_3	6.661	-5.441
	K_4	7.356	-4.411
bS	K_1	7.749	-6.649
	K_2	7.869	-6.800
	K_3	8.033	-7.018
	K_4	7.998	-6.972

Table 5.3 Comparison of log stability constants and number of binding sites for copper binding to aS and bS at pH 7.0, 25^0C.
Sequential binding model was applied to fit the data. LogK values have been adjusted to account for the relative contribution of the chelator species to the overall equilibrium. Errors between K values were not exceeding 10%.

Four binding events were detected for both aS and bS with three events of similar affinity constants. The binding sites on bS showed higher affinity than those on aS.

5.4 Copper binding to aS mutants

To investigate the details of copper binding to aS, site-directed and domain-truncated mutants were applied for the ITC analysis. The recombinant proteins were expressed and purified as described in Chapter 3. The experiments were conducted as before. Fig 5.4 showed thermodynamic data for aS mutants following subtraction of buffer energies of dilution.

(A) aSΔ1-9-Cu

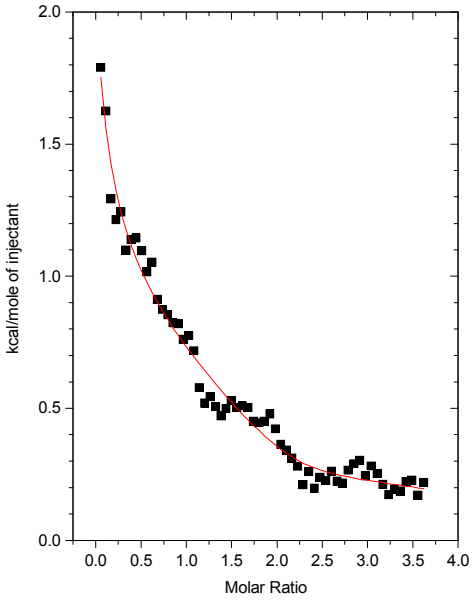

(B) H50A aS-Cu

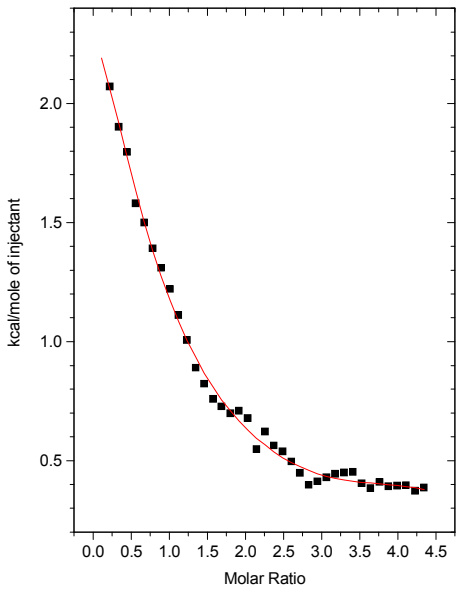

(C) aSΔ1-9 H50A-Cu

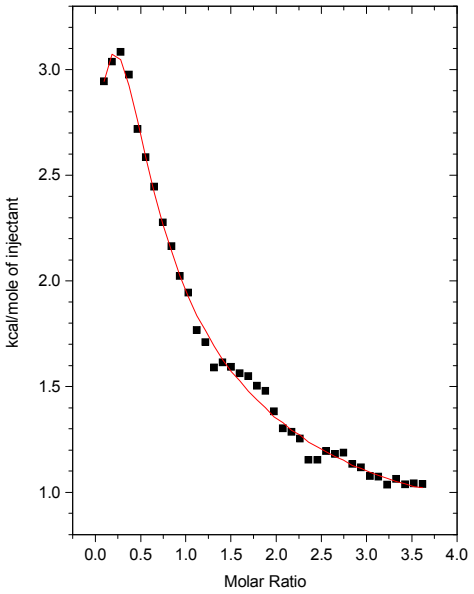

(D) aS1-100-Cu

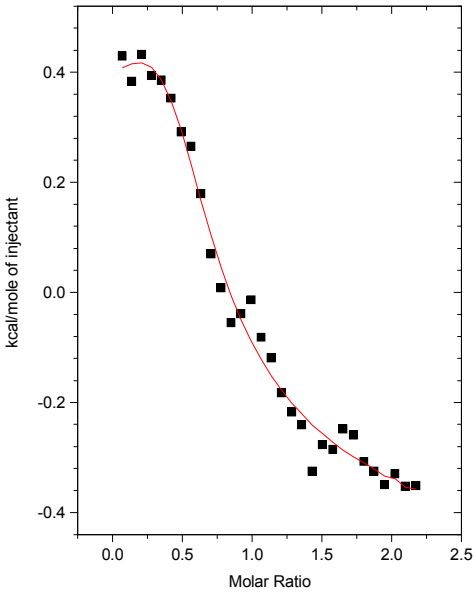

(E) aS10-100 H50A-Cu

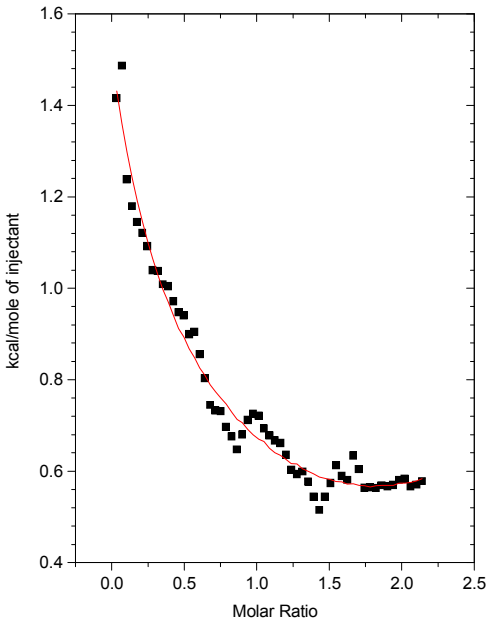

Fig. 5.4 Thermodynamic plots of aS mutants titrated with Cu/Gly at pH 7, 25^{0}C. Data was after subtraction of the buffers. 10 mM MES was used to stabilize the pH throughout the experiments. (A) Plot of aSΔ1-9-Cu reaction. (B) Plot of H50A aS-Cu reaction. (C) Plot of aSΔ1-9 H50A-Cu reaction. (D) Plot of aS1-100-Cu reaction. (E) Plot of aS10-100 H50A-Cu reaction.

Again, the data fitted well using the sequential binding model. The chelator effect was factored to the overall equilibrium and potentially error prone as before. Table 5.4 compared the values from aS and its mutants analyzed by the sequential binding model. The means of three independent experiments were calculated, with errors between K values not exceeding 10%.

		logKa	ΔGº (kcal/mol)
aS	K_1	7.022	-5.618
	K_2	7.274	-5.934
	K_3	6.661	-5.441
	K_4	7.356	-4.411
aSΔ1-9	K_1	7.340	-6.514
	K_2	7.817	-7.167
	K_3	6.802	-5.784
	K_4	7.073	-6.152
aS H50A	K_1	7.520	-5.134
	K_2	5.750	-4.998
	K_3	7.070	-5.526
	K_4	7.460	-5.333
aS Δ1-9 H50A	K_1	6.980	-4.720
	K_2	6.320	-4.962
	K_3	6.830	-5.009
	K_4	6.910	-5.142
aS 1-100	K_1	6.340	-4.600
	K_2	6.180	-4.409
	K_3	7.040	-5.391
	K_4	6.410	-5.004
aS 10-100 H50A	K_1	6.320	-5.371
	K_2	6.320	-5.304
	K_3	5.910	-4.949
	K_4	6.490	-5.581

Table 5.4 Comparison of log stability constants and number of binding sites for copper binding to aS and its mutants at pH 7.0, 25^0C.

Sequential binding model was applied to fit the data. LogK values have been adjusted to account for the relative contribution of the chelator species to the overall equilibrium. Errors between K values were not exceeding 10%.

Table 5.4 demonstrated that the affinity value of the second binding site was 1.5 magnitudes less when the His50 was replaced with alanine. In contrast, the affinity constants of the first and third events were slightly increased. However, the number of sites remained the same, indicating the involvement of His50 in the interaction with copper. The amino acid vicinity might substitute the histidine for the binding to copper and affect the copper coordination of the other sites in H50A aS mutant. It seemed that the log stability constants of the last three binding events were diminished in the double mutant aSΔ1-9 H50A, although the number of binding sites remained to be four. This suggested that the amino group and His50 were both responsible for the copper coordination. Similarly, for aS1-100, the log stability constant was enhanced for the third binding site and decreased for the other three and the affinity values were reduced for all four sites in aS10-100 H50A. This implied that the C-terminal region of aS contributed to the interaction with copper.

5.5 Copper binding to bS mutants

To investigate the details of copper binding to bS, site-directed and domain-truncated mutants were applied for the ITC analysis. The recombinant proteins were expressed and purified as described in Chapter 3. The experiments were conducted as before. Fig 5.5 showed thermodynamic data for bS mutants following subtraction of buffer energies of dilution.

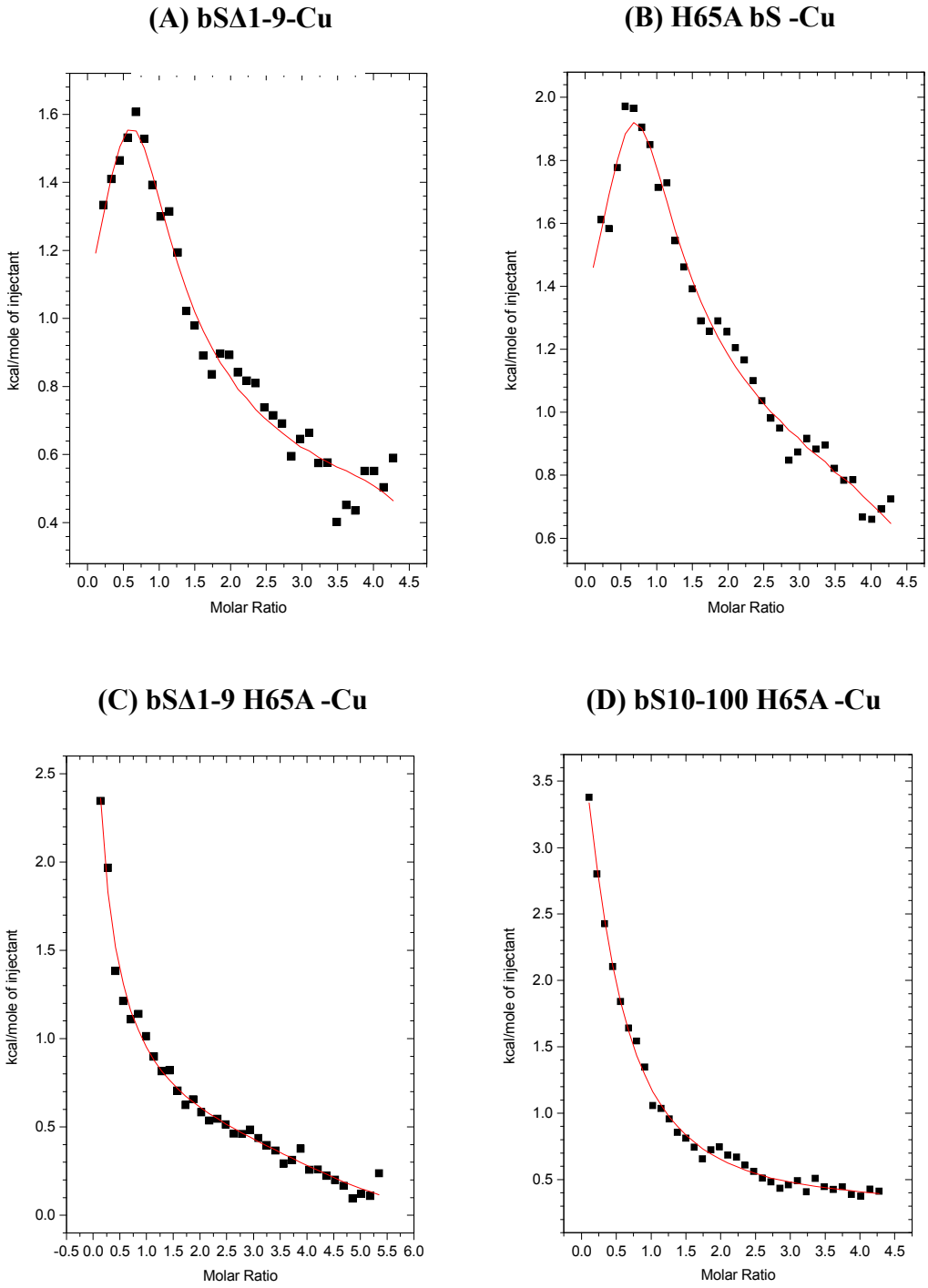

Fig. 5.5 Thermodynamic plots of bS mutants titrated with Cu/Gly at pH 7, 25^{0}C. Data was after subtraction of the buffers. 10 mM MES was used to stabilize the pH throughout the experiments. (A) Plot of bSΔ1-9-Cu reaction. (B) Plot of H65A bS-Cu reaction. (C) Plot of bSΔ1-9 H65A-Cu reaction. (D) Plot of bS10-100 H65A-Cu reaction.

The data was analyzed by using a sequential binding model. The chelator effect was

factored to the overall equilibrium and potentially error prone as before. Table 5.5 compared the values from aS and its mutants analyzed by a sequential binding model. The mean of three independent experiments were calculated, with errors between K values not exceeding 10%.

		logKa	ΔGº (kcal/mol)
bS	K_1	7.749	-6.649
	K_2	7.869	-6.800
	K_3	8.033	-7.018
	K_4	7.998	-6.972
bSΔ1-9	K_1	7.100	-6.149
	K_2	5.830	-4.811
	K_3	7.050	-6.309
	K_4	7.290	-6.576
bS H65A	K_1	7.600	-5.771
	K_2	6.450	-5.201
	K_3	7.890	-5.766
	K_4	6.960	-5.900
bSΔ1-9 H65A	K_1	7.810	-6.981
	K_2	7.640	-6.733
	K_3	5.100	-4.591
	K_4	6.210	-5.755
bS10-100 H65A	K_1	7.230	-6.590
	K_2	5.350	-4.777
	K_3	5.170	-4.349
	K_4	Not detected	Not detected

Table 5.5 Comparison of log stability constants and number of binding sites for copper binding to bS and its mutants at pH 7.0, 25^0C.
Sequential binding model was applied to fit the data. Errors between K values were not exceeding 10%.

Four binding events were observed in the WT bS and the N-terminal mutants, while the affinity constants varied. The logK values of the second and third binding sites were two and one magnitude less, respectively, when residues 1-9 were knocked out. This occurred on the second and fourth site when the His65 was substituted with alanine. However, this variation was shifted to the third and fourth site for the double mutant bSΔ1-9 H65A. One binding site was missing when the C-terminus was deleted and the affinities of the first and second site were decreased. According to these observations, residues 1-9, His65 and the C-terminal region were all involved in copper coordination.

5.6 Discussion

The role of metal binding in the physiological and pathological function of aS has been the focus for a number of studies on aS protein. However, there have been some inconsistencies with regard to previous publications on the copper binding sites and affinities for aS (Paik, Shin et al. 1999; Lee 2003; Rasia, Bertoncini et al. 2005). In this chapter, a thorough thermodynamic study of copper binding to aS was presented to explain the fundamental knowledge of copper binding stoichiometry for the metalloprotein.

In order to examine the feasibility of ITC on assessing the aS-Cu interaction, $(His)_6$-tag proteins were applied first. It appeared that there was a huge variation on the number of binding sites that was most likely contributed by the His tag. This could be due to the mobility and instability of the His tag. In addition, there was a disadvantage for the use of His-tagged synucleins. The purified protein contained additional amino acids at the N-terminus region even when the His-tag was cleaved by specific proteinases. This might interrupt the copper interaction as the amino acids might be potential factors in stopping copper binding. However, ITC was proven to be a feasible method for exploring copper binding to aS despite the inaccuracy in the number of binding events caused by the presence of the His tag.

There were four independent copper binding sites detected on untagged aS at pH 7, 25^{o}C through the application of ITC. The logK values were in the range of 6.66-7.36

which was in close agreement with current literature (Rasia, Bertoncini et al. 2005; Binolfi, Lamberto et al. 2008). Previous studies by other groups have claimed that three regions are associated with metal binding to aS: the N-terminus, a region near the C-terminus and a histidine at position 50 (Murray, Giasson et al. 2003; Rasia, Bertoncini et al. 2005; Sung, Rospigliosi et al. 2006). In this study, single amino acid mutated and domain-truncated recombinant proteins were produced and examined by ITC for copper binding properties. Four binding events were observed in all the aS mutants including aS10-100 H50A at pH 7. This result was unexpected because it was previously suggested that copper bound exclusively to the negatively charged C-terminal region (Paik, Shin et al. 1999; Uversky, Li et al. 2001). Subsequent studies indicated the involvement of the N-terminus and His50 with the high-affinity binding site assigned to the N-terminal region (Rasia, Bertoncini et al. 2005). However, the affinity constants varied when the amino acid was mutated or deleted and the affinity values of four sites were reduced in the absence of the three regions (Table 5.4 and Table 5.5). According to this observation, the three domains were responsible but not essential for copper incorporation. In their absence, other residues became dominant and replace them in the coordination with copper; this explained the presence of four binding sites with variable logK constants. The finding on the significant reduction in the affinity of second binding site on H50A aS indicated that His50 was assigned for the high-affinity anchoring site on aS. A CD and EPR spectroscopic analysis using modified peptides showed that above pH6, the coordination of Cu(II) may involve the lateral NH_2 group of lysine residues upstream of His50 (Kowalik-Jankowska, Rajewska et al. 2006), showing that lysine could act as a copper anchoring site in the absence of histidine. While the majority of the literature suggest for the presence of at least two copper binding sites on aS, there is no strong, solid evidence for such inference. CD spectra revealed that aS was not saturated even with four equivalents of Cu(II), and spectra of the aS1-108-Cu complex was similar to that of the WT protein (Rasia, Bertoncini et al. 2005). In addition, the purification of aS from other studies involved the high temperature, which was proven to alter the protein conformation in this study. This explained why only two binding sites were detected in those researches (Rasia, Bertoncini et al. 2005). In the recent study showing two Cu(II)-binding sites on aS, no chelators were used in the ITC experiment when copper was titrated into the protein solution at pH 7 (Bharathi and Rao 2007). As is known, at pH 7.0, Cu(II) is insoluble due to the

formation of oxide species which can alter the protein forms because of their redox activities. This could affect the copper-protein interaction.

Unlike aS, its homologue bS has attracted less attention and the metal-binding features have remained largely unexplored. It was reported for the first time that bS binds two copper atoms per monomer with the K_d in the range of 0.2-50 μM (Binolfi, Lamberto et al. 2008). In this study, four binding sites with higher affinities than aS were detected by analyzing the ITC data for bS-Cu interaction. Similarly, residues 1-9 and His65 were involved in the copper binding but they were not essential as the number of sites remained unchanged without their participation. However, one site was missing in the absence of the C-terminal region (Table 5.5), indicating that it is the only essential contributor for one binding site. The affinity constants were altered when any of the three regions was mutated or deleted. This suggested that the three regions contributed to the copper binding event. Moreover, there was a manifest decrease in the affinity on second binding site on bSΔ1-9, implying that the higher-affinity site on bS was allocated on the residues 1-9 not on histidine. This finding was in close agreement with the literature showing the higher-affinity site was assigned to the N-terminal amino group of Met1 (Binolfi, Lamberto et al. 2008). In general, the four sites on bS displayed higher affinity for copper than aS (Table 5.5). The evidence presented here might provide some insight into the mechanism by which bS inhibit aS aggregation. This study implied that the preventive effect of bS on aS aggregation might be related to the higher affinities for copper. In that case, bS competes with aS for copper binding and acts as a copper-sequestering protein, playing the role of a copper chelator, hence preventing or attenuating the subsequent aggregation of aS.

Chapter 6. Electrochemistry of Cu(II) bound synuclein proteins

6.1 Introduction

Accumulating evidence has demonstrated that metals, especially copper, are one of the triggers for the aggregation of aS (Atwood, Moir et al. 1998; Paik, Shin et al. 1999; Shin, Lee et al. 2000; Uversky, Li et al. 2001). Redox-active transition metals such as copper and iron, may play an important role in the pathogenesis of neurodegenerative diseases by participating in an array of cellular disturbances characterized by oxidative stress and increased free radical production (Sayre, Moreira et al. 2005). Metal-catalyzed oxidation of proteins require metals to be bound to the protein and involves the reduction of metal ions such as Fe(III) and Cu(II). Fe(II) and Cu(I) can react with hydrogen peroxide to generate hydroxyl radicals via a Fenton-like reaction, and oxidation of neighbouring amino acids (Halliwell and Gutteridge 1986; Wright and Brown 2008). The ability of these amino acids in the protein to form complexes with metal ions directly influences the susceptibility to metal-catalyzed oxidation. Oxidatively modified protein could increase its own tendency toward protein aggregation due to the generation of reactive oxygen species (ROS), which exert pro-aggregatory effects and turn soluble protein into insoluble forms by either inhibiting intracellular proteolysis or causing unusual posttranslational modifications. These may then provide the covalent modifications of amino acid residues in proteins and formation of protein-protein cross-linkages (Kowalik-Jankowska, Rajewska et al. 2006).

aS has been shown to be a potential target of intracellular oxidants by the identification of posttranslational modifications of synuclein within intracellular aggregates that accumulate in PD brains. It has been demonstrated that in the presence of copper and hydrogen peroxide, aS experienced Cu(II)-catalyzed oxidation and self-oligomerisation, which may lead to possible protein aggregation and neurodegeneration (Paik, Shin et al. 2000). This could be almost suppressed by the

addition of ascorbic acid or EDTA, indicating that oligomerisation was dependent upon not only metal binding but also its subsequent redox reaction in the presence of hydrogen peroxide (Paik, Shin et al. 2000). Similar effects of iron and hydrogen peroxide on aS aggregation were also observed (Hashimoto, Hsu et al. 1999). Therefore, it is important to explore the biochemical features of the protein-metal complex, which might shed light on the molecular basis of the aS aggregation. There have been no attempts to directly characterise the redox chemistry of as so far. Electrochemical analysis was employed for the first time to investigate the amyloid formation of aS (Palecek, Ostatna et al. 2008). In traditional electrochemical system, protein is analyzed in free solution within a three electrode cell where the effect of protein migration through the solution on the electrode potential has to be corrected. In addition, the signal from the copper bound protein might be buried due to the high background. In this study, a new electrochemical method cyclic voltammetry (CV) was designed to describe the electrochemistry properties of copper charged synuclein proteins.

Recombinant bS and gS were utilized to compare the redox activities with aS by the application of CV experiments. Among the human family members, bS is 62% identical and 79% similar to aS, gS is 50% identical and 74% similar to aS (Sung and Eliezer 2006). Both bS and gS inhibit aS fibril formation and complete inhibition was observed at 4:1 molar excess of bS and gS over aS (Uversky, Li et al. 2002), although the mechanism is not fully elucidated. The electrochemical properties investigation of bS and gS might provide a better understanding for the effects of the homologues on aS aggregation.

6.2 Electrochemical system

The CV system was set up and all measurements were conducted in a 50 ml three-terminal cell consisting of a 3 mm diamond boron-doped diamond working electrode (Diafilm^{TM}, Windsor Scientific, UK), a platinum foil counter electrode and a reference electrode saturated with potassium chloride (SCE, REF401, Radiometer) as described before in chapter 2. 10 mM MES buffer was used to stabilize the system at pH 7 as this was proven to make minimal background to the voltammagram. The

working electrode was prepared as previously described in chapter 2 and immersed in the voltammetric cell for recording background signal. The electrode was then immersed in apo protein or copper-bound protein samples for one minute before being rinsed thoroughly in buffer to eliminate any loosely bound protein. Synuclein proteins were shown to be able to adhere strongly to the negatively charged surface of the working electrode due to the positively charged regions on the proteins (http://mobyle.pasteur.fr/cgi-bin/portal.py). The distribution of charges on synuclein proteins were presented in appendix F. All the protein samples were prepared at a concentration of 100 μM at pH 7. The electrode was then placed in the CV cell and the voltage ramped from 450 mV to -450 mV. Each experiment was scanned at least twice and the data represented the second scan. Fig 6.1 shows a typical cyclic voltammogram of WT aS bound to copper recorded at a scan rate of 60 mVs^{-1}.

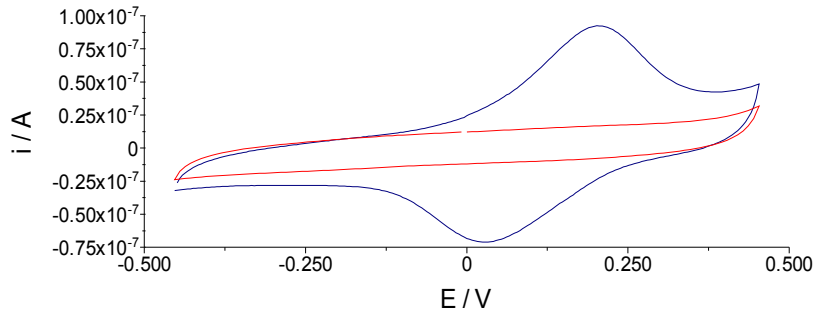

Fig. 6.1 Representative cyclic voltammogram of WT aS bound to copper recorded at scan rate of 60 mVs^{-1}.
Blue line indicates that reduction and re-oxidation of aS-Cu complex absorbed on the 3 mm diamond boron-doped diamond working electrode. Red line represents the background signal of aS without copper bound. The experiment was conducted in 10 mM MES buffer pH 7. The step potential was 0.0042 mV.

The background current in Fig 6.1 (red line) was obviously different from the signal of aS-Cu complex. A stable redox cycle (blue line) was observed over the background. This suggested that the reduction and re-oxidation processes were assigned to the copper centres in the aS-Cu complex. Each experiment was scanned twice and the signal remained the same, implying the processes were reversible and reproducible. The voltammograms were recorded at different scan rates to examine the reliability of the redox process (Fig 6.2).

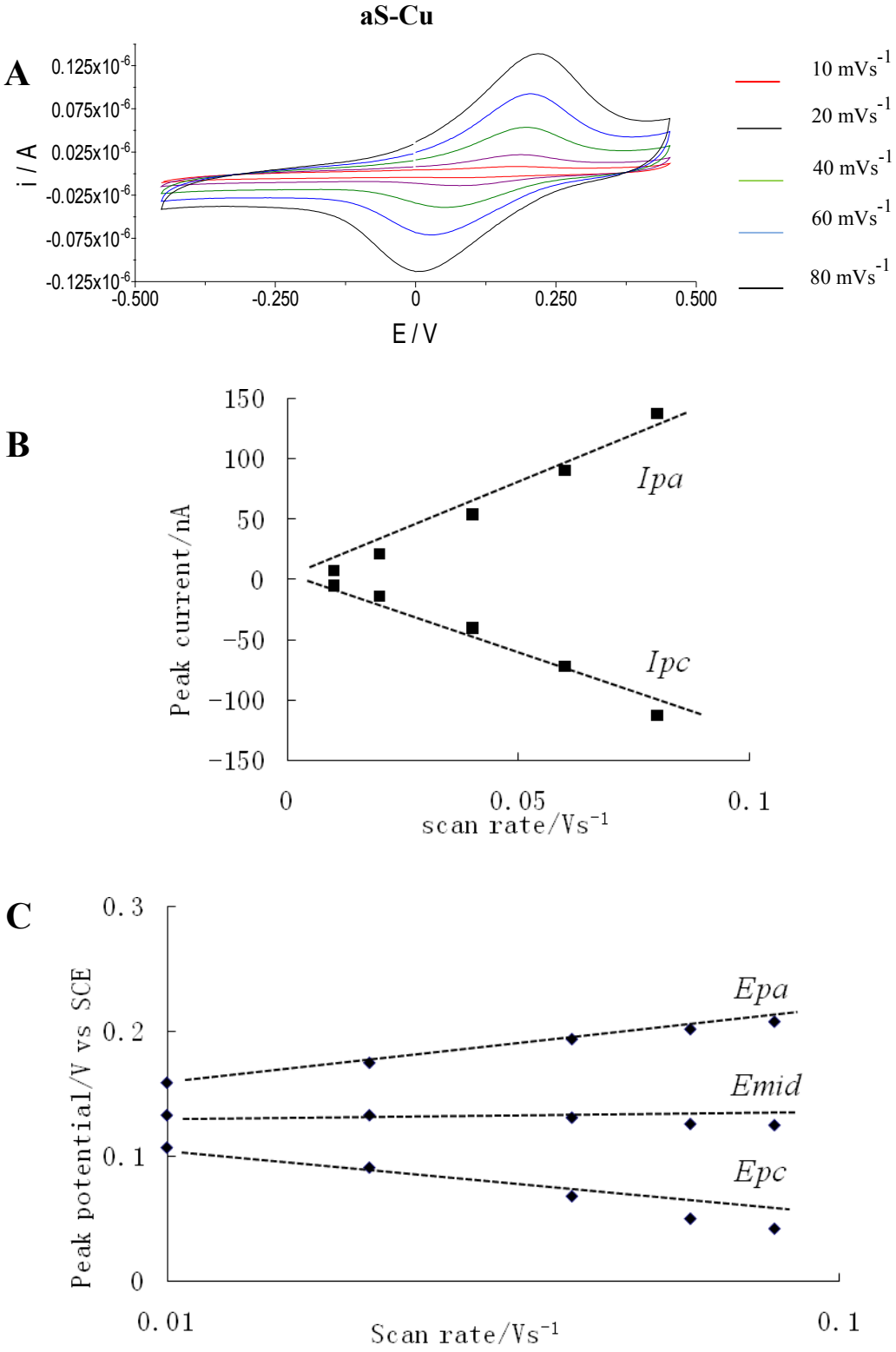

Fig. 6.2 Comparison of voltammograms of aS-Cu complex at five different scan rates. A. Comparison of voltammograms of aS-Cu obtained at different scan rates. B. Plot of the peak current versus the scan rate. C. Plot of the peak potentials versus the scan rate (in logarithmic scale).

Fig 6.2 showed the comparison of voltammetric data of aS-Cu complex at five different scan rates and the peak current and potential were plotted against the scan rates. Fig 6.2 B presented a linear relationship between peak current and scan rate. Ipa and Ipc indicated the peak current of oxidation and reducation respectively. This confirmed a permanently surface bound protein and electron transfer directly into the protein bound copper (Davies, Marken et al. 2009). This proved that the adsorption of the protein was stable and the current responses were highly reproducible and reversible. Fig 6.2 C demonstrated the effect of scan rates on the peak potentials. Epa and Epc indicated the peak potential of oxdaiton and reduction respectively. Emid was the average of Epa and Epc. The characteristic logarithmic dependence was consistent with an electron transfer rate limited process, which was represented by the equation (Davies, Marken et al. 2009),

$$E_p = E_{mid} + \frac{RT}{nF} \ln \frac{[O]}{[R]}$$

(R, gas constant; T, temperature; n, number of electrons transferred; F, Faraday constant; O, oxide on the electrode surface; R reducer on the electrode surface).

It suggested that the peak potential was related to the midpoint potential, the number of transferred electrons and the protein-copper complex.

6.3 Redox activities of synuclein-copper complexes

Synuclein proteins were expressed and purified as described before (Chapter 3) and the purity was checked in SDS-PAGE (appendix E).

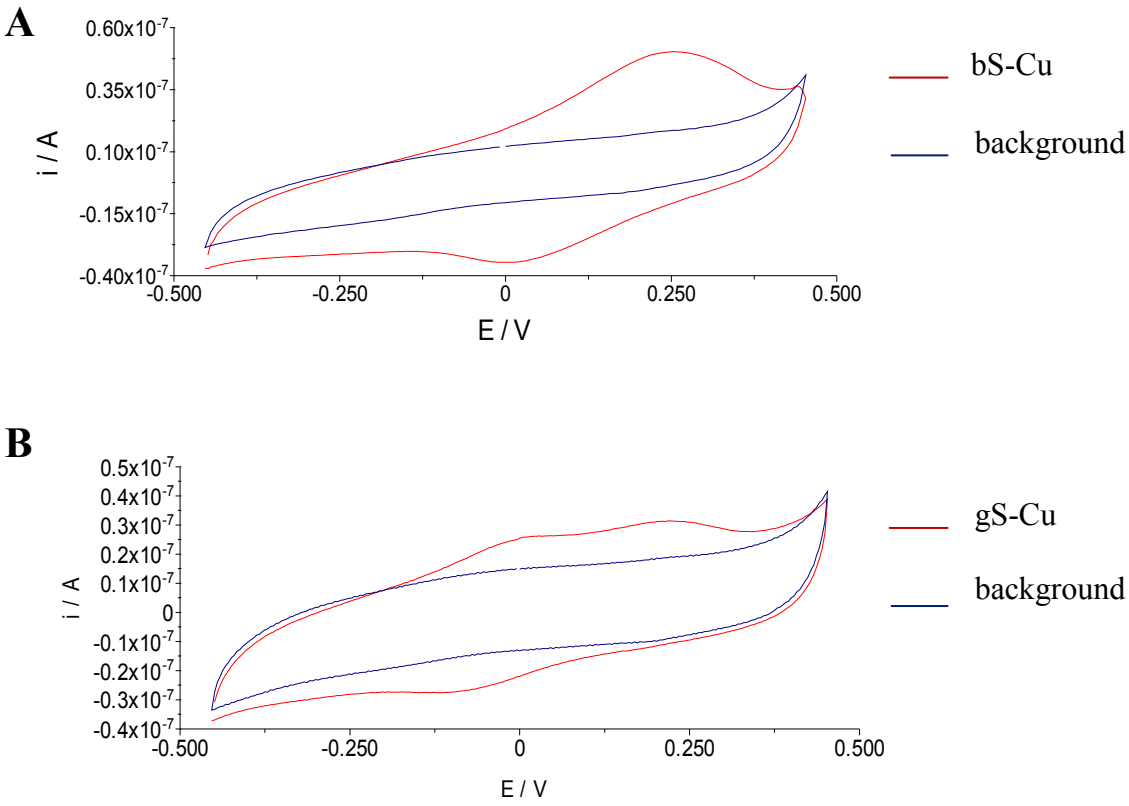

Fig. 6.3 Voltammograms of synuclein-Cu obtained at scan rate of 60 mVs^{-1}. The experiments were conducted in 10 mM MES buffer pH 7. The step potential was 0.0042 mV.

Fig 6.3 demonstrated different copper centres in three synuclein proteins showing different midpoint potentials (Table 6.1). The different copper centres on each protein might be electronically distinct but coupled and therefore might not be individually resolved. Nevertheless, there was a second small oxidation peak of gS-Cu complex, which might indicate an individual copper centre. The midpoint potentials were analyzed by using GPES manager software (Table 6.1).

	Midpoint potential E_{mid} (V vs SCE)	
	1st	2nd
aS	0.130±0.003	Not detected
bS	0.140±0.007	Not detected
gS	-0.045±0.005	0.065±0.006

Table 6.1 Comparison of the midpoint potentials from aS, bS and gS.

The midpoint potentials of aS and bS were quite close and were quite different from that of gS (Table 6.1). The peak current of oxidation and reduction was nearly identical for aS (Fig 6.1), which suggested that the redox cycling was fully reversible. However, the current response of reduction was less than the oxidation peak for bS and gS (Fig 6.3). This indicated two possibilities: the oxidation was not reversible and part of the copper or protein might be oxidized permanently; the reduced Cu(I) fell off due to the weak binding to protein. Two oxidation peaks were detected for gS-Cu, suggesting the existence of two independent redox process.

6.4 Comparison of electrochemical features of synucleins and their mutants

6.4.1 aS and its mutants

Previous studies by other groups have suggested three specific regions are associated with metal binding to aS. These include the N-terminus, a region near the C-terminus and a histidine at position 50. In order to explore the dependence on copper for the protein's apparent redox state, aS mutants lacking the candidate residues for copper binding were applied to the cyclic voltammetry experiments. The voltammograms of these mutants-Cu complexes were obtained at scan rate of 60 mVs^{-1} and compared with WT aS-Cu in Fig 6.4.

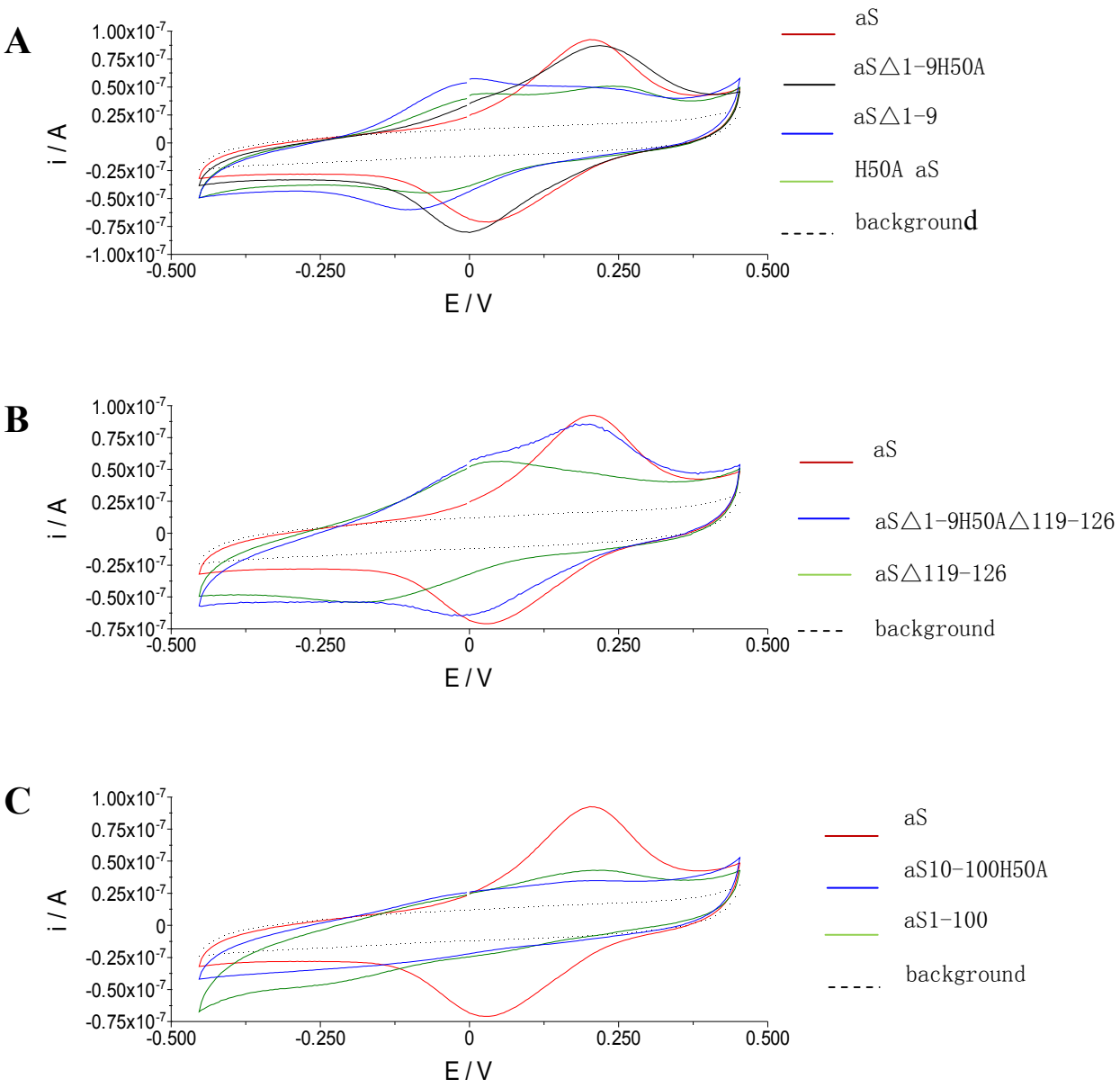

Fig. 6.4 Comparison of voltammograms of site-directed and domain-truncated aS mutants-Cu with WT aS-Cu obtained at scan rate of 60 mVs^{-1}.
The experiments were conducted in 10 mM MES buffer pH 7. The step potential was 0.0042 mV.

The voltammograms in Fig 6.4 were obtained from the proteins with the same equivalents of copper added. In Fig 6.4 A, the voltammograms exhibited a second oxidation peak for the mutant aS△1-9 and H50A, which suggested that the coupled copper centres in these proteins might be split into two due to the mutation. However,

the double mutant aS△1-9 H50A showed similar redox potential to that for WT aS. The fact that mutation of either of the regions on aS caused a redox shift without the loss of this redox centre strongly suggests that both regions were involved in copper coordination without being the main binding residue for redox chemistry. This may also point towards a fundamental change in protein structure when these coordinating ligands were not present and therefore when copper bound to the protein. The midpoint potentials and integrated current peak charges were compared in Table 6.2.

To explore the effect of C-terminus on the copper-dependent redox properties of aS, the cyclic voltammetry signals of C-terminal mutated or truncated mutants were presented in Fig 6.4 B and C. The oxidation and reduction peaks were eminently reduced on aS10-100 H50A and aS1-100, where C-terminus was deleted. Meanwhile, the redox peak for aS△119-126 was much higher compared to these two mutants. In addition, the redox potential was shifted when the 119-126 residues were knocked out, which suggested that this region was involved in copper coordination. The redox peak charges were compared in Table 6.2. The plots for the comparison of voltammetric data of aS10-100 H50A-Cu complex at different scan rates are shown in appendix F, confirming a permanently surface bound protein and electron transfer directly into the protein bound copper (Davies, Marken et al. 2009). This proved that the adsorption of the protein on the electrode surface was stable.

	Midpoint potential E_{mid} (V vs SCE)		Integrated oxidation peak charge (nC)	Integrated reduction peak charge (nC)
	1st	2nd		
aS	0.130±0.003	Not detected	3592±222	-3638±85
H50A	-0.030±0.008	0.089±0.006	2839±140	-1167±89
aS△1-9	-0.044±0.007	0.077±0.004	3788±314	-2408±71
aS△1-9 H50A	0.103±0.002	Not detected	4082±91	-4195±155
aS△ 119-126	-0.063±0.005	Not detected	2500±318	-1241±56
aS1-100	-0.024±0.002	Not detected	1007±29	-236±12
aS△1-9 H50A △119-126	0.092±0.003	Not detected	4775±47	-2971±24
aS10-100 H50A	0.032±0.002	Not detected	668±12	-110±3

Table 6.2 Comparison of the midpoint potentials and integrated peak charges from aS and its mutants.

The voltammograms showed without doubt that WT aS was capable of cycling electrons when bound to copper. However, when the His50 was replaced with alanine, which was proven not to bind copper, the integrated oxidation peak charge was diminished by 20% and the reduction peak charge was reduced by nearly 70% (Table 6.2). There was no obviously change of oxidation peak for aS△1-9, while the reduction was about half of the oxidation charge. It was interesting to note that the redox activity was restored on the double mutant aS△1-9 H50A (Table 6.2).

Similarly, the oxidation peak charge was slightly reduced on aS△119-126, while the reduction was only half of the oxidation charge. Nevertheless, for the C-terminus truncated mutants aS1-100 and aS10-100 H50A, only 1007±29 nC and 668±12 nC

of responsive oxidation charge was observed respectively, and the reduction peak was almost eliminated (Table 6.2). These findings indicated that although the copper centres were combined, some of them were not redox reversible or some copper was lost from the protein when it was reduced.

6.4.2 bS and its mutants

The physiological function of bS still remains to be elucidated. Nevertheless, bS has been found to inhibit the aggregation of aS and the formation of aS protofibrils (Hashimoto, Rockenstein et al. 2001; Park and Lansbury 2003), indicating that bS may be an internal regulator of aS. The electrochemistry of bS and its mutants lacking candidate residues for copper binding were applied to the CV experiments. The voltammograms of these mutant-Cu complexes were obtained at scan rate of 60 mVs^{-1} and compared with WT bS-Cu in Fig 6.5.

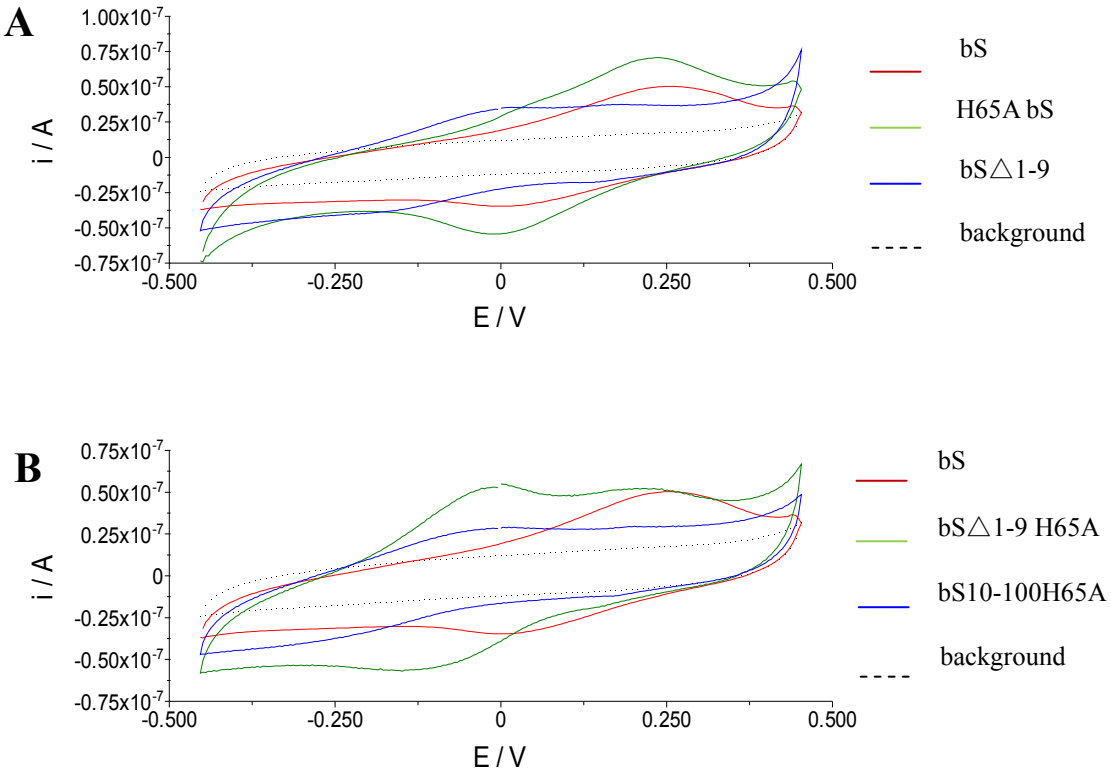

Fig. 6.5 Comparison of voltammograms of site-directed and domain-truncated bS mutants-Cu with WT bS-Cu obtained at scan rate of 60 mVs^{-1}.
The experiments were conducted in 10 mM MES buffer pH 7. The step potential was 0.0042 mV.

It seemed that the redox activity of bS was enhanced when the His65 was substituted with alanine, while no increase was detected when residues 1-9 were knocked out although the peak potential was shifted (Table 6.3). The ability of bS to exchange electrons in the electrode system was greatly decreased when the C-terminal region was completely deleted (Fig 6.5).

	Midpoint potential E_{mid} (V vs SCE)		Integrated oxidation peak charge (nC)	Integrated reduction peak charge (nC)
	1st	2nd		
bS	0.140±0.007	Not detected	1719±89	-931±45
H65A bS	0.117±0.002	Not detected	2417±74	-2389±13
bS△1-9	-0.083±0.007	Not detected	1208±67	-307±50
bS△1-9 H65A	-0.055±0.006	0.066±0.002	3113±106	-1178±49
bS10-100 H65A	-0.135±0.001	Not detected	1454±44	-184±4

Table 6.3 Comparison of the midpoint potentials and integrated peak charges from bS and its mutants.

It seemed that only half of the copper centres on bS-Cu complex were redox reversible because the integrated reduction peak value was about 50% of oxidation charge. His65 might inhibit the redox activity especially the reduction of bS-Cu because the H65A bS mutant showed reversible electron cycling (Table 6.3). The reduction peak was greatly diminished for bS△1-9, indicating amino acids 1-9 contributed to the reduction process. It was interesting that the oxidation intensity was regained for the double mutant bS△1-9 H65A, while the calculated reduction charge was not. This finding further confirmed that His65 inhibited the redox activity while the region 1-9 activated it. The lack of C-terminus on bS10-100 H65A led to a further descend in redox activity especially in reduction process compared to bS△1-9 H65A, suggesting the C-terminus of the protein was involved in the electrochemistry. The calculated charge response in oxidation was 1454±44 nC for bS10-100 H65A, which was about half of that for bS△1-9 H65A (3113±106 nC). This suggested that C-terminus contributed to half of the electron transfers in the process.

6.5 Discussion

The voltammograms showed that aS was capable of exchanging electrons when bound to copper. The electrochemistry was completely dependent on the interaction with copper because no redox signal was detected on the apo protein. The redox cycling was fully reversible (Table 6.1), suggesting that the protein was unaffected by continuous oxidation and reduction. However, this was not the case for bS and gS, where the reduction peaks were much less than the oxidation peaks (Table 6.1).The finding indicated that some of the copper or protein might be oxidized permanently, which could prevent the protein from aggregating or Cu(I) was not stable on the protein and was lost during the change in oxidation state. Interestingly, there were two independent redox centres on gS, while only one was detected on aS or bS (Table 6.1). Regarding the decreased reduction peak, one of the copper centres might be reduction silent. This implied that bS and gS could act as internal regulators for aS aggregation by oxidative and reductive modifications rather than structural interruption. This observation may open new avenues for the research on bS and gS functions.

The electrochemical property of aS was further examined by investigating the mutants lacking potential proposed copper-binding sites. Only one oxidation and reduction peak was observed for the WT aS-Cu species, suggesting the copper centres were electronically coupled as ITC data in chapter 5 showed that there were more than one copper bound. The imidazole ring of His50 was believed to be involved in the copper coordination (Kowalik-Jankowska, Rajewska et al. 2006). However, the midpoint potential and responsive current peak during the redox process on the mutant aS△1-9 H50A was quite close to that for WT aS, indicating the amino acids in the proximity might fill in the position and form the identical coordination geometry which is consistent with the EPR data in chapter 4. There is evidence showing that lysine residues upstream of His50 could act as a copper anchoring site in the absence of histidine (Kowalik-Jankowska, Rajewska et al. 2006). Similarly, Asp2 might be substituted by Glu13 which could also provide nitrogen and oxygen ligand in Cu(II) binding mode (Rasia, Bertoncini et al. 2005). It was interesting that the single mutation caused the split of the copper centres and one of

them lost the reductive feature, because two oxidation peaks were obtained on H50A aS and aS△1-9 but the number of electrons transferred during reduction process were about half of that during oxidation (Table 6.2). Similarly, aS△119-126 showed slightly decreased oxidative activity but large diminished reductive response (Table 6.2). This implied that the electrochemistry was mostly dependent on the feature but not on the number of the copper centres, because some of the copper centres were redox-silent when the original copper-binding sites were replaced. According to the observation, the redox capability of aS was contributed by copper bound to the residues 1-9, His50 and the C-terminus. The integrated reduction peak charge was enormously reduced on aS1-100, indicating the presence of the C-terminal region of aS was essential for the reductive electrochemistry, which might be involved in the mechanism of inhibition of aS aggregation, providing evidence showing C-terminus of aS is a negative regulator of self-assembly. The protein might be partially oxidized permanently without the C-terminal region, which could lead to self-oligomerization and hence possible protein aggregation and neurodegeneration (Paik, Shin et al. 2000). It fits the hypothesis that C-terminus truncated aS constructs are more prone to fibrillate in vitro than the full-length protein (Crowther, Jakes et al. 1998; Serpell, Berriman et al. 2000; Murray, Giasson et al. 2003). This is confirmed by a recent research revealing that the ^{125}YEMPS^{129} motif in aS can modulate DA inhibition of aS fibrillization. However, aS ending before the ^{125}YEMPS^{129} motif (residues 1-124) could still form soluble oligomers (Leong, Pham et al. 2009). In addition, the biochemically specific copper- or iron-mediated oxidative oligomerization was turned out to be dependent upon the acidic C-terminus of aS because the C-terminally truncated proteins were not affected by both metals and hydrogen peroxide (Paik, Shin et al. 2000).

In contrast to aS, mutation of His65 on bS enhanced the redox activity especially the reduction current, producing reversible electron cycling (Table 6.3). This demonstrated that His65 was responsible for the inhibition of the electrochemical activity of the protein. This was contrast to aS, where His50 contributed to the redox activity especially the reduction response which was thought to inhibit the protein aggregation (Table 6.2). In addition, there was research showing the mutation on His50 could slow down the copper induced aS aggregation. The difference of the

electrochemical features on the two proteins indicated two distinct mechanisms for the protein aggregation, as no study has reported inhibition of aggregation on the His65 mutant. The reductive response was enormously diminished for bS△1-9 and bS10-100 H65A, indicating the involvement of residues 1-9 and the C-terminus on the redox activity. Little has been investigated about bS, this new technique might provide new insight into the role of bS on the inhibition of aS aggregation.

This is the first time CV is employed to investigate the electrochemical property of aS. More work needs to be done to confirm some of the hypothesis and uncertainties. For example, Cu(I)-aS could be used in the experiment to see if the signal is still detectable as Cu(I) was speculated to fall off the protein when Cu(II) was reduced. In addition, the number of redox active coppers could be calculated by using the integrated oxidation peak charge and weighing the electrode with protein-Cu bound. In that case, the electrochemistry of the protein could be investigated in a quantitative way.

Chapter 7. Characterization of metal effects on synuclein aggregation in mammalian cells

7.1 Introduction

Two neuropathological hallmarks of PD are LBs and LNs that can occur in the dopaminergic neurons of the substantia nigra. These are intracytoplasmic protein inclusions whose main components are implicated to be aggregated aS (Goedert 1999). The etiology of PD is still unknown. The concept that aS aggregation is involved in the pathology of PD is widely accepted. LB-like inclusions and neuronal cell loss were found in some transgenic, adenoviral, lentiviral-based animal models overexpressing aS (Masliah, Rockenstein et al. 2000; Kirik, Rosenblad et al. 2002; Lee, Stirling et al. 2002; Lo Bianco, Ridet et al. 2002; Martin, Pan et al. 2006), and the dopaminergic cell death was resuced with down-regulation of aS expression in the substantia nigra of a PD rat model (Hayashita-Kinoh, Yamada et al. 2006). However, the mechanism by which the amyloid-like aggregated aS is formed and causes cell death remains unclear. Three potential factors which may contribute to the formation of aS aggregates in cells have been identified. First of all, most in vitro studies using recombinant proteins suggest that three different missense mutations in the aS gene lead to increases in aS aggregation because of an increase in the rate of aggregation of mutant proteins compared with WT aS (Conway, Harper et al. 1998; Takeda, Hashimoto et al. 1998; Giasson, Uryu et al. 1999). These mutations include A30P, E46K and A53T substitutions in aS identified in autosomal dominantly inherited, early onset PD (Polymeropoulos, Lavedan et al. 1997; Kruger, Kuhn et al. 1998). These findings indicate that the mutations of aS might be involved in the mechanisms of aS aggregation. Secondly, transition metals are another possible trigger involved in the pathogenesis of aS misfolding. There is a great increase in the accumulation of aS aggregates and vulnerability to toxicity induced by iron in BE-M17 neuroblastoma cells overexpressing aS (Ostrerova-Golts, Petrucelli et al.

2000). Binolfi A et al. demonstrated that Cu(II) binds specifically to aS and triggers its aggregation by establishing a hierarchy in aS-metal ion interaction. Nevertheless, whether the metals promote aS aggregation directly by binding and inducing structure change or via increasing levels of oxidative stress is still obscure. Finally, aS is a protein which can self aggregate under certain conditions, especially when the cellular concentration of aS increases which appears in both familial and sporadic forms of PD (Wu, Kim et al. 2008). Thus, it is a key challenge for neuron cells to maintain the intracellular levels of aS in a steady state and below the critical concentration. Consequently, this brings up the importance of protein transport and localization, which has not been intensely investigated. Abnormal accumulation of aS in specific cellular organelles may increase local concentration of this protein, which may induce the protein self-aggregation, even without altering the total level. For example, paraquat treatment promotes nuclear localization of aS and amino acids 134-139 of aS seem to be responsible for this localization (Goers, Manning-Bog et al. 2003; Yu, Li et al. 2007). Additionally, translocation of aS to the mitochondria was shown to be caused by exposure of cells to various stresses (Cole, Dieuliis et al. 2008; Parihar, Parihar et al. 2008; Shavali, Brown-Borg et al. 2008).

The survival of neurons with intracellular LBs shows that intracytoplasmic aS aggregates are not toxic to all cells (Spillantini, Schmidt et al. 1997). Considerable evidence suggests the loss of homeostasis of the redox active transition metals copper and iron plays a role in many neurodegenerative diseases. High levels of iron are found in the substantia nigra (Dexter, Wells et al. 1989) and high levels of copper in the CSF in PD brains (Pall, Williams et al. 1987). In addition, aS was shown to bind to copper and iron (Golts, Snyder et al. 2002; Rasia, Bertoncini et al. 2005; Binolfi, Rasia et al. 2006) and aS aggregation is stimulated in the presence of these metals (Uversky, Li et al. 2001; Rasia, Bertoncini et al. 2005). These findings suggest that the examination of the links between intracellular synuclein proteins and metals is desirable.

In this chapter a cell culture system was used to investigate intracellular synuclein aggregation in the presence or absence of metals. Aggregates in mammalian dopaminergic neuron cells overexpressing synucleins or their mutants were detected and assessed by western blotting and confocal microscopy. Cells stably transfected

with mutant forms of aS were also created to investigate the potential amino acid determinants involved in the translocation of aS. Cell toxicity induced by synuclein overexpression was examined in the presence of copper.

7.2 Creation of cell lines overexpressing aS and bS

SH-SY5Y cells were stably transfected with pcDNA3.1(-) (control), pcDNA3.1(-) aS and bS as described in chapter 2. The overexpression of aS and bS was detected by western blotting (Fig 7.1).

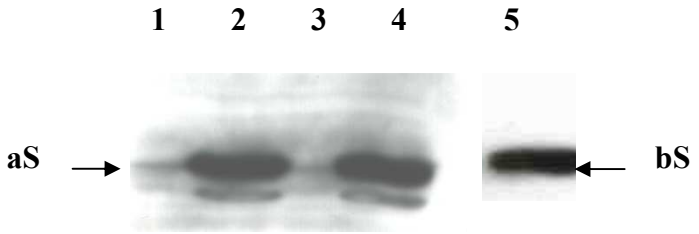

Fig. 7.1 Western Blotting of cells overexpressing aS and bS.
Lane 1 and 3, cells transfected with pcDNA3.1(-). Lane 2 and 4, cells transfected with pcDNA3.1(-) aS. Lane 5, cells transfected with pcDNA3.1(-) bS. aS and bS were detected using the mouse primary aS antibodyB (Zymed Laboratories Inc.) and the mouse primary bS antibody (Upstate) respectively.

The overexpression of aS and bS was also confirmed under microscope (Fig 7.2).

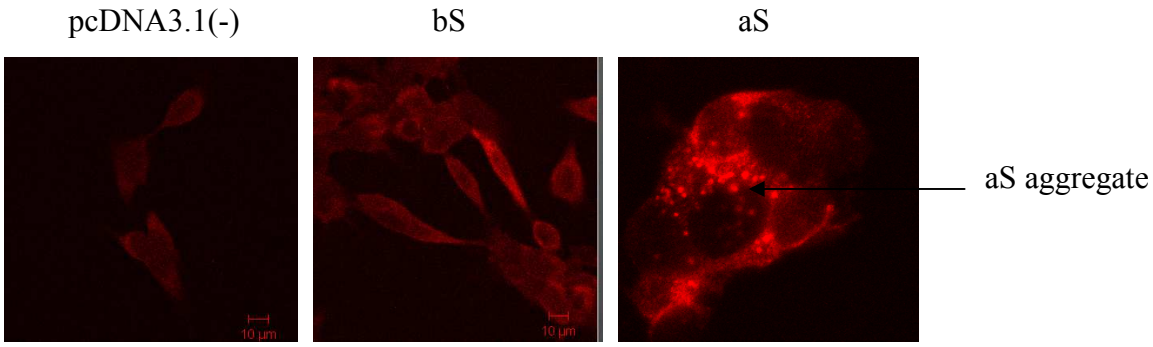

Fig. 7.2 Immunofluorescence of SHSY5Y cells expressing vector, aS and bS. aS and bS were detected using the mouse primary aS antibodyB (Zymed Laboratories Inc.) and the mouse primary bS antibody (Upstate) respectively, and visualized with a secondary Rhodamine Red-x goat anti-mouse antibody (Invitrogen). aS aggregate was indicated.

7.3 Quantitative analysis of aS aggregates in cells

7.3.1 Immunofluorescence

The major axis length of the aggregate was more than approximately one-twenty fifth of the cell nucleus diameter. As shown above, aggregates were formed in cells overexpressing aS but not in cells overexpressing pcDNA3.1(-) or bS. To investigate the role of metals in the induction of aggregates, cells were treated with different concentrations of copper and iron before they were visualized under confocal microscope (Fig 7.3).

(A)
nontreated
media

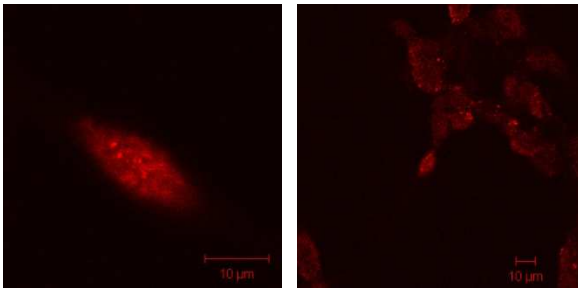

(B)
CM

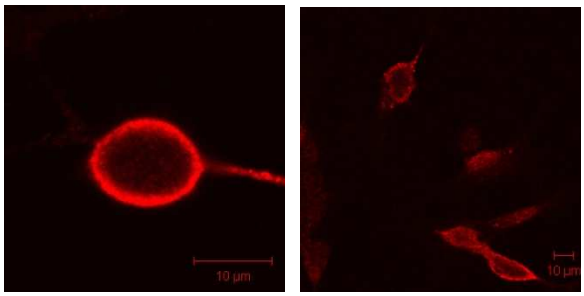

(C)
CM+
10 μM $CuCl_2$

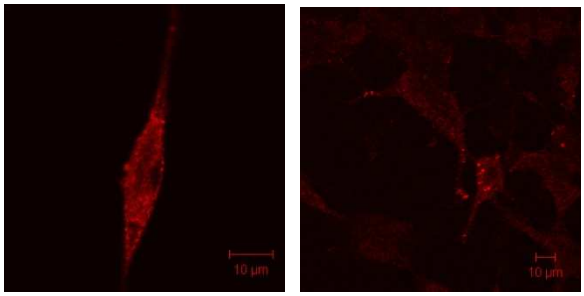

(D)
CM+
300 μM $CuCl_2$

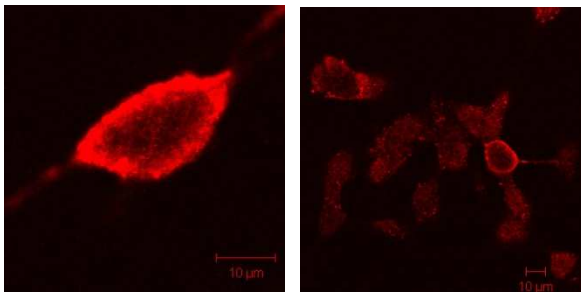

(E)
CM+
10 μM $FeSO_4$

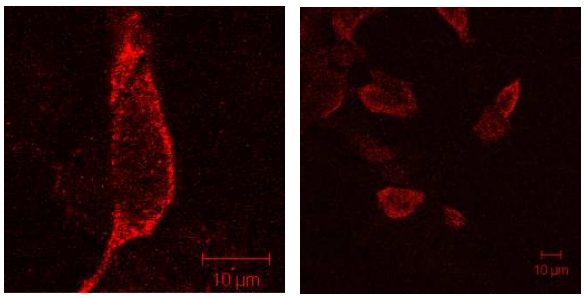

(F)
CM+
300 μM $FeSO_4$

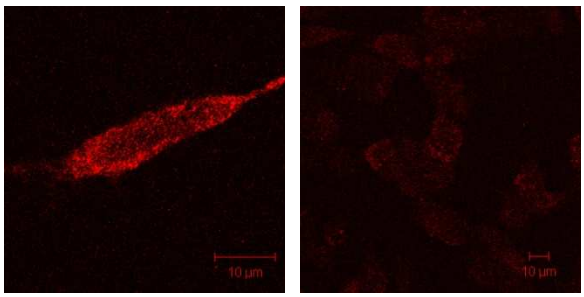

Fig. 7.3 Immunofluorescence of SHSY5Y cells expressing pcDNA3.1(-) aS.
aS was detected using the mouse primary aS antibodyB (Zymed Laboratories Inc.), and visualized with a secondary Rhodamine Red-x goat anti-mouse antibody (Invitrogen). Images were captured using a Zeiss LSM 510 confocal microscope. Cells were treated with six different conditions: A. nontreated media, B. chelex treated media (CM), C. CM+10 μM $CuCl_2$, D. CM+300 μM $CuCl_2$, E. CM+10 μM $FeSO_4$ F. CM+300 μM $FeSO_4$, for 48 hours. Scale bar represents 10 μm. Two images were presented for each treatment: the left for single cell and right for group cells.

The aggregates formed under different conditions were quantified by counting the number of cells with aggregates in at least three groups of cells with each group of at least 30 cells. Table 7.1 represents the percentage of cells with aggregates in different conditions.

	Percentage of cells with aggregates
Nontreated media	12.7% ± 2.7%
Chelexed media (CM)	3.8% ± 0.3%
CM + 10 μM $CuCl_2$	9.8% ± 0.8%
CM + 300 μM $CuCl_2$	37.7% ± 1.8%
CM + 10 μM $FeSO_4$	3.6% ± 0.5%
CM + 300 μM $FeSO_4$	4.5% ± 0.6%

Table 7.1 High concentration of Cu(II) accelerates the formation of aS aggregates.
Data were expressed as the mean ± standard error (S.E.). Statistical analyses were conducted using a two-tailed t-test. Among these conditions, 300 μM $CuCl_2$ induced aggregation most efficiently ($p < 0.001$).

7.3.2 Proteinase K (PK) resistance of aS aggregates

In this study, PK resistance of aS aggregates was analyzed by using western blotting

as a new quantitative technique. Briefly, cells were split into 6-well plates at a density of 2 x 10^5 per well. To investigate the metal triggered aS aggregation, cells were treated with 10 μM $CuCl_2$, 10 μM $FeSO_4$ and 1 mM $FeSO_4$ in chelex treated media for 48 hours. Cells were harvest in buffer E (Table 2.1) and homogenized with 26G needles and centrifuged at 14000 rpm for 10 minutes at 4°C. Cells overexpressing aS were lyzed and the cell lysate concentration was determined by Bradford assay. 20 μg of cell lysate was digested with different concentrations of PK at 37°C for 1 hour and applied to western blotting. Fig 7.4 presents the data of western blotting against aS. The experiments were repeated at least three times. It seems the aggregates were retained in the stacking gels instead of being transferred to the separating gels (Fig7.4).

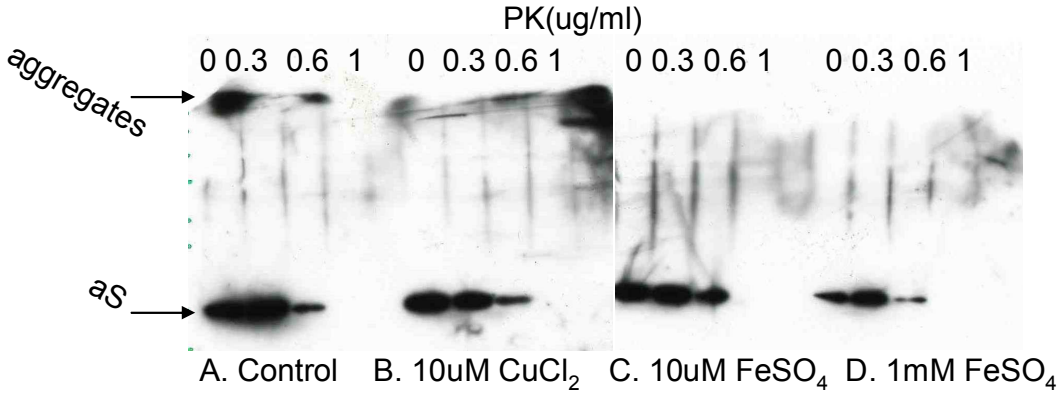

Fig. 7.4 PK resistance of aS aggregates.

A, control cells; B, cells treated with 10 μM $CuCl_2$; C, cells treated with 10 μM $FeSO_4$; D, cells treated with 1 mM $FeSO_4$. PK concentrations were between 0 and 1 μg/ml.

Because the aggregates were retained in the stacking gels, it was very difficult to judge how resistant of the aggregate is to PK. To solve this problem, gradient gels were used instead of normal SDS gels. The cells and cell lysates were prepared as before. Fig 7.5 presents the data of western blotting against aS. The experiments were repeated at least three times. There were no obvious aggregates observed (Fig 7.5).

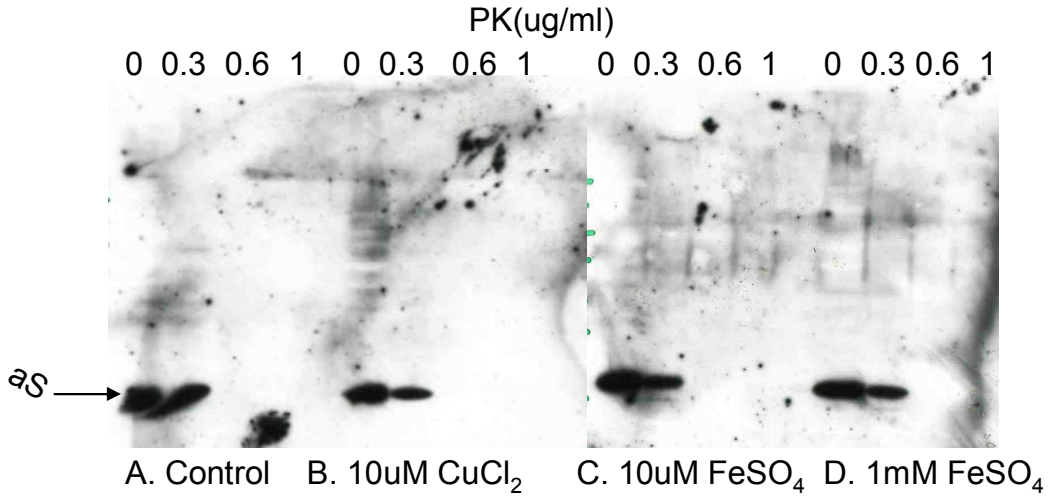

Fig. 7.5 PK resistance of aS aggregates.

A, control cells; B, cells treated with 10 μM $CuCl_2$; C, cells treated with 10 μM $FeSO_4$; D, cells treated with 1 mM $FeSO_4$. PK concentrations were between 0 and 1 μg/ml.

Comparing these two methods, it seems neither of them has successfully demonstrated the PK resistance of aS aggregates formed under different concentrations of metals. Based on this, the method referring to immunofluorescence described above was employed in the following studies.

7.4 Effects of metals on synuclein aggregation

7.4.1 Generation of cell lines overexpressing mutated aS

To investigate whether the potential metal-binding regions of aS are involved in the effects of metal accelerated aS aggregation or whether copper increases the aS aggregation by binding directly to the protein or not, several cell lines overexpressing the related proteins in which the potential copper or iron binding sites were mutated or truncated, were employed. SH-SY5Y cells were stably transfected to generate cell lines overexpressing H50A aS, aS△1-9 H50A, aS△1-9 and bS. The overexpression of proteins in cells was detected and visualized under the confocal microscopy (Fig 7.7).

7.4.2 Quantitative analysis of synuclein aggregates in cells

The overexpression of protein in the stable cell lines were also confirmed by using immunofluorescence under confocal microscope (Fig 7.6). Expression of pcDNA3.1(-) alone served as negative control. Cells overexpressing aS were shown in Fig 7.3. Only images representing single cells were shown in Fig 7.6, images representing groups of cells were presented in appendix C.

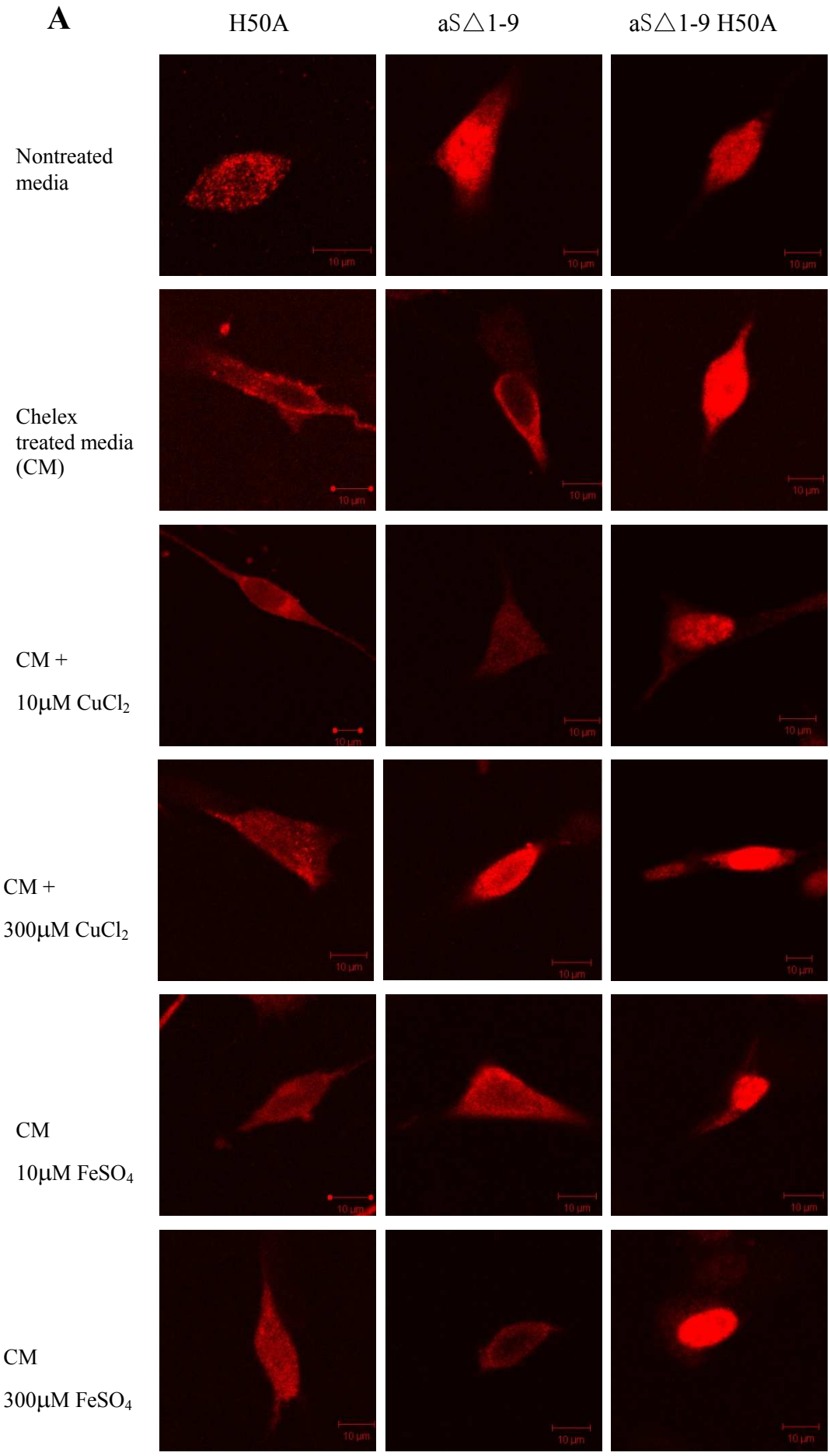
A
H50A
aS△1-9
aS△1-9 H50A
Nontreated media
Chelex treated media (CM)
CM + 10μM $CuCl_2$
CM + 300μM $CuCl_2$
CM 10μM $FeSO_4$
CM 300μM $FeSO_4$

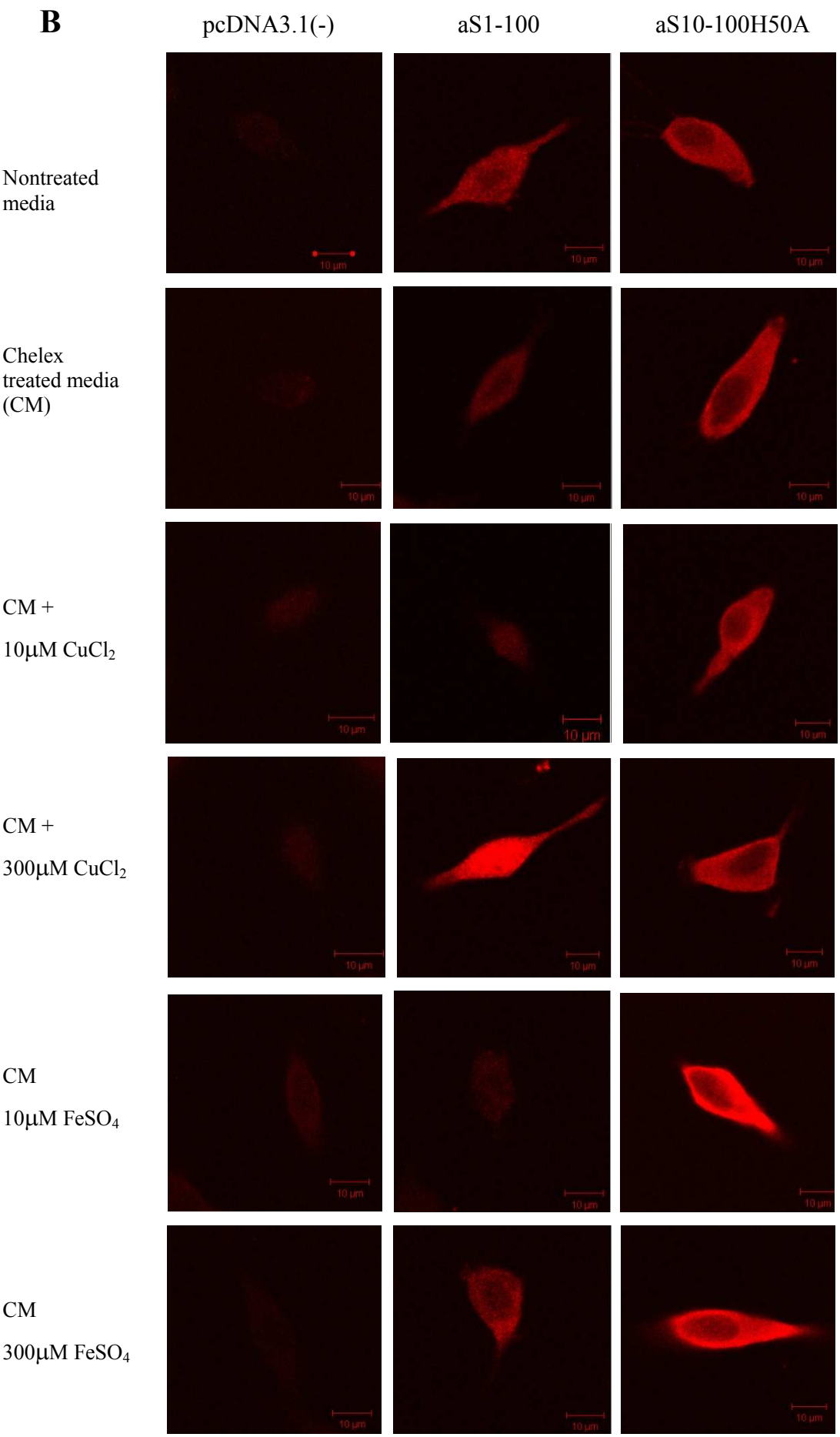
B
pcDNA3.1(-)
aS1-100
aS10-100H50A
Nontreated media
Chelex treated media (CM)
CM + 10µM $CuCl_2$
CM + 300µM $CuCl_2$
CM 10µM $FeSO_4$
CM 300µM $FeSO_4$
10 µm

Fig. 7.6 Immunofluorescence of SHSY5Y cells overexpressing aS mutants.
A: aS was detected using the mouse primary aS antibodyB (Zymed Laboratories Inc.), and visualized with a secondary anti mouse antibody (Invitrogen); B: aS was detected using the sheep primary aS antibodyA (abcam) directed against amino acids 11-26 of aS sequences, and visualized with a secondary anti sheep antibody (Molecular probes). Images were captured using a Zeiss LSM 510 confocal microscope. Shown are six cell lines treated with six different conditions: nontreated media, chelex treated media (CM), CM+10 μM $CuCl_2$, CM+300 μM $CuCl_2$, CM+10 μM $FeSO_4$ CM+300 μM $FeSO_4$, for 48 hours. Scale bar represents 10 μm.

Aggregates were only observed in cells overexpressing H50A aS and aS△1-9 H50A but not in cells overexpressing other mutant forms of aS with or without copper. No aggregates were detected in cells overexpressing aS△1-9, aS△1-9 H50A, aS1-100 or aS10-100 H50A when treated with iron. The aggregates in different cell lines and different conditions were quantified by counting the number of cells with aggregates in at least 3 groups of certain amount of cells. The images of cells were captured under Zeiss LSM 510 confocal microscope. Fig 7.7 represents the differences of percentages of cells with aggregates in different cell lines and conditions.

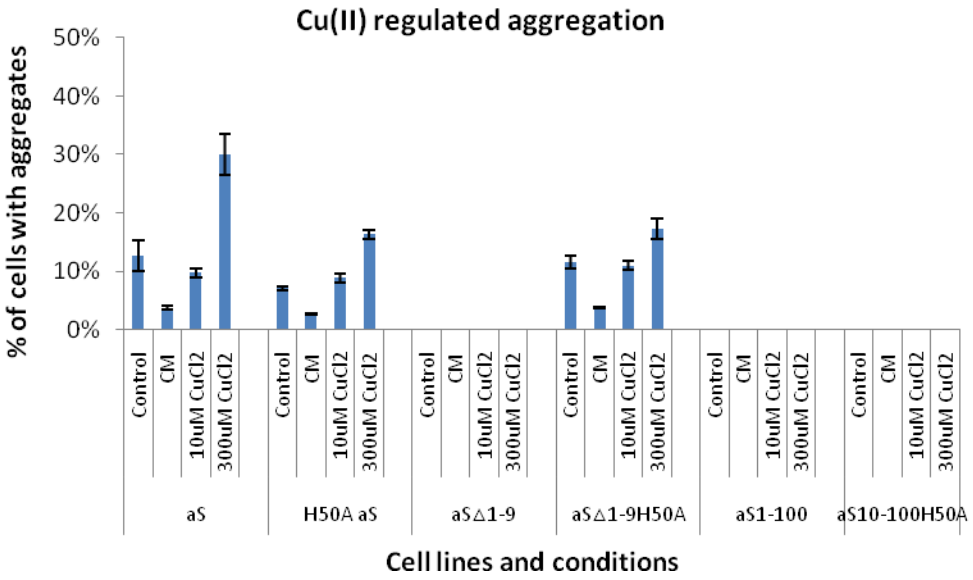

Fig. 7.7 The percentage of cells with aggregates in SHSY5Y cells overexpressing H50A aS and aS△1-9 H50A is decreased and there is no aggregates found for cells overexpressing aS△1-9, aS1-100 and aS10-100 H50A.

The cells were treated with four different conditions: nontreated media, chelex treated media (CM), CM+10 μM $CuCl_2$, CM+300 μM $CuCl_2$ for 48 hours. Data were expressed as the mean ± standard error (S.E.). Statistical analyses were conducted using a two-tailed t-test. Among cells overexpressing aS, H50A aS and aS△1-9 H50A, 300 μM $CuCl_2$ induced aggregation most efficiently compared to the other conditions ($p < 0.001$).

For cells overexpressing aS, the percentage of cells with aggregates was nearly tripled with treatment of 300 μM copper compared to physiological concentration. However, the effect of high concentration of copper was impaired in cells overexpressing H50A aS and aS△1-9 H50A, because the percentage decreased to 16% and 17% respectively compared to 30% in cells overexpressing aS. It seemed that the aggregation was impeded in the absence of metals because the cells with aggregates were significantly decreased in chelex treated media (Fig 7.7). However, the number of cells was restored when 10 μM $CuCl_2$ was added. No aggregates were detected in cells overexpressing aS△1-9, aS1-100, or aS10-100 H50A with or without metal treatments.

7.5 Effects of metals on the aggregation of PD-associated aS mutants

Apart from metals, alterations in the amino acid sequences of aS contribute to the formation of aggregates without the presence of excess metals. It was proven that the tendency of aS to aggregate in vitro is accelerated by the PD-related point mutations, A30P and A53T, which are present in the N-terminus of aS. In this study, immunofluorescence was employed to detect and quantify the aggregates under confocal microscope. Cells overexpressing A30P aS, E46K aS and A53T aS were used to investigate if the three mutations have a role in the metal regulated aggregation.

7.5.1 Creation of cell lines overexpressing PD-associated mutants

SH-SY5Y cells were stably transfected to generate cells overexpressing A30P, E46K and A53T aS. The cells were harvested as before, and the cell extract was applied to western blotting for the confirmation of protein overexpression (Fig 7.8). The concentration of cell extract was determined by Bradford assay. Equal amount of proteins from each cell line were loaded to verify the same expression levels.

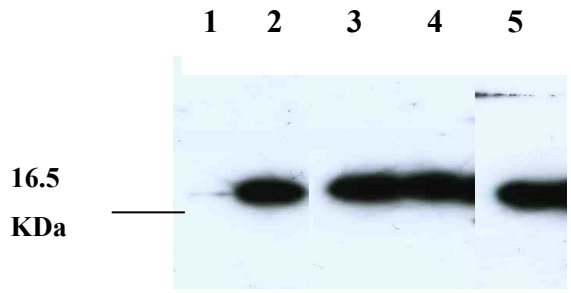

Fig. 7.8 Western blotting of cells overexpressing aS and the disease mutants. Lane 1, cells transfected with pcDNA3.1(-). Lane 2, 3, 4 and 5, cells overexpressing WT aS, A30P aS, E46K aS and A53T aS. aS antibody B (Zymed Laboratories Inc.) was against the C-terminus of aS.

7.5.2 Quantitative analysis of synuclein aggregates in cells

The overexpression of protein in the stable cell lines were also confirmed by using immunofluorescence under confocal microscope (Fig 7.9). Cells overexpressing aS were shown in Fig 7.3. Fig 7.9 represents the images of cells overexpressing PD-associated aS mutants A30P, E46K, A53T under different conditions. Only images representing single cells were shown in Fig 7.9, images representing groups of cells were presented in appendix C.

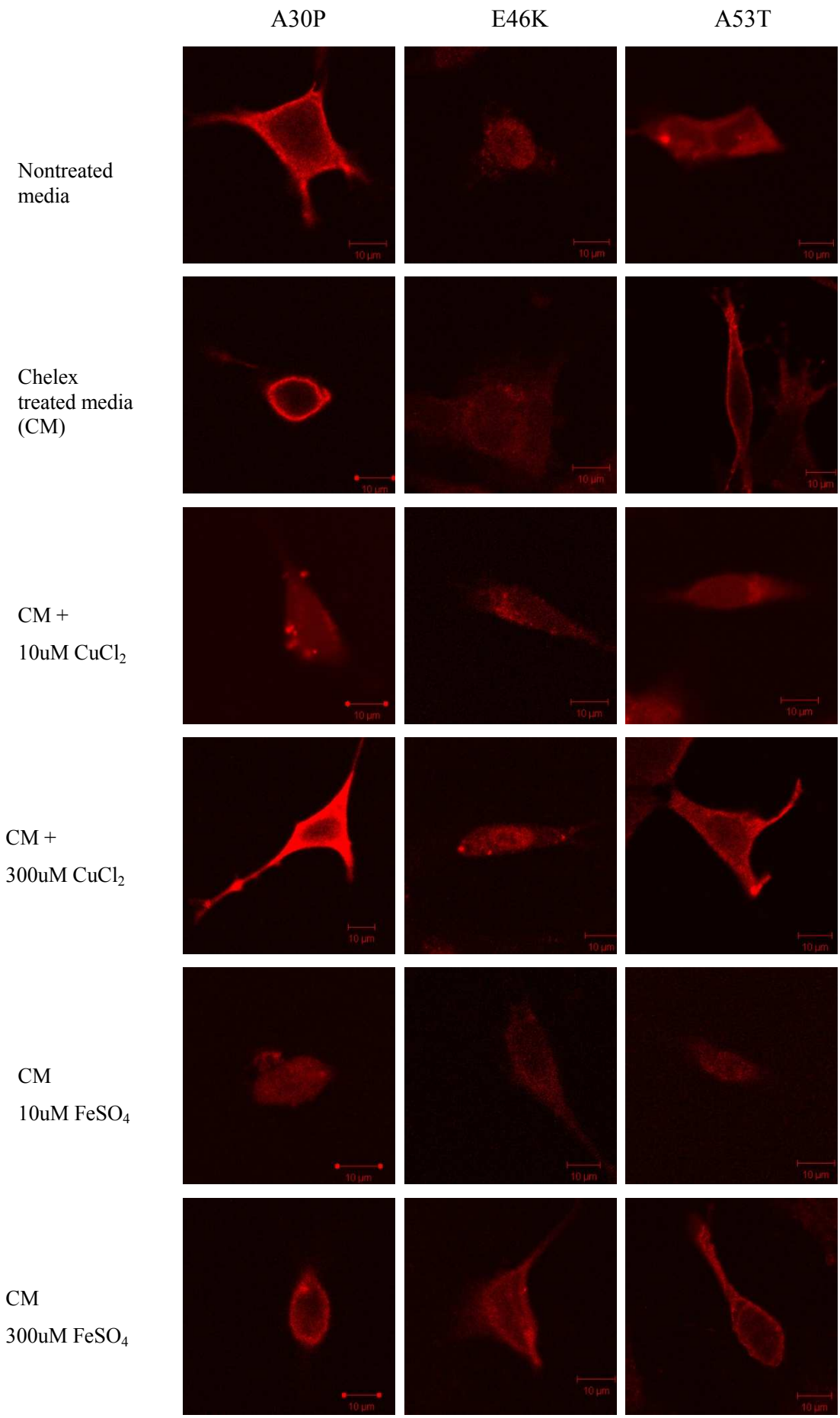
A30P
E46K
A53T
Nontreated media
Chelex treated media (CM)
CM + 10uM $CuCl_2$
CM + 300uM $CuCl_2$
CM 10uM $FeSO_4$
CM 300uM $FeSO_4$

Fig. 7.9 Immunofluorescence of SHSY5Y cells expressing PD-related aS mutant. aS was detected using the mouse primary aS antibodyB (Zymed Laboratories Inc.), and visualized with a secondary Rhodamine Red-x goat anti-mouse antibody (Invitrogen). Images were captured using a Zeiss LSM 510 confocal microscope. Shown are three cell lines treated with six different conditions: nontreated media, chelex treated media (CM), CM+10 μM $CuCl_2$, CM+300 μM $CuCl_2$, CM+10 μM $FeSO_4$ CM+300 μM $FeSO_4$, for 48 hours. Scale bar represents 10 μm.

The aggregates in different cell lines and different conditions were quantified by counting the number of cells containing aggregates in at least 3 groups of certain amount of cells. The images of cells were captured under Zeiss LSM 510 confocal microscope. Fig7.10 represents the differences of percentages of cells with aggregates in different cell lines and conditions.

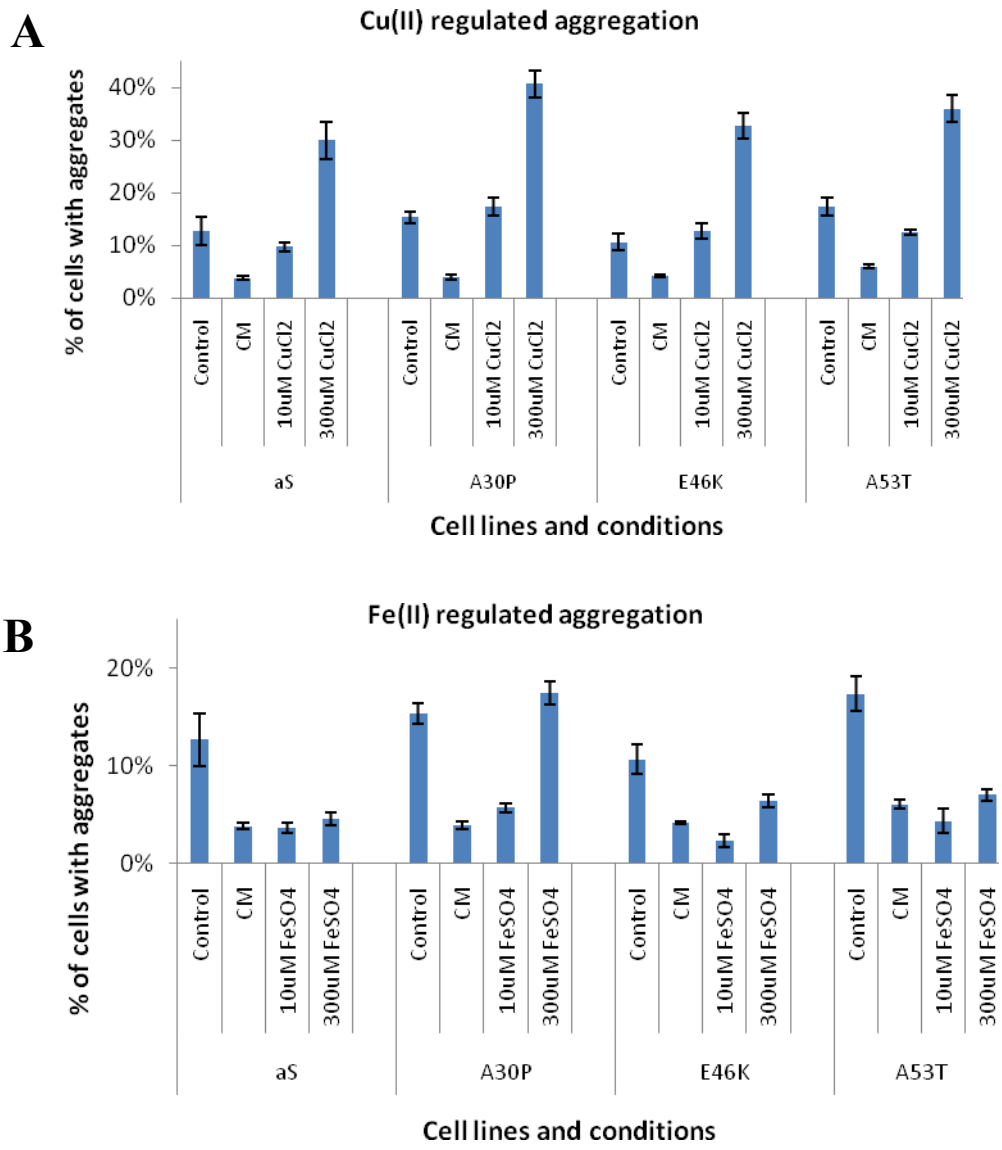

Fig. 7.10 The percentages of cells containing aggregates in SHSY5Y cells overexpressing aS, A30P aS, E46K aS and A53T aS were significantly increased in the presence of 300 μM $CuCl_2$ but not $FeSO_4$.

A: Comparison of cells with aggregates in different cell lines treated with nontreated media, chelex treated media (CM), CM+10 μM $CuCl_2$, CM+300 μM $CuCl_2$ for 48 hours; B: Comparison of cells with aggregates in different cell lines treated with nontreated media, chelex treated media (CM), CM+10 μM $FeSO_4$ CM+300 μM $FeSO_4$ for 48 hours. Data was expressed as the mean ± standard error (S.E.).Statistical analyses were conducted using a two-tailed t-test. Among the varying conditions, 300 μM $CuCl_2$ induced aggregation most efficiently ($p < 0.001$).

There was not an obvious increase of percentages of cells with aggregates in the cells overexpressing A30P, E46K and A53T aS in physiological condition compared to cells overexpressing aS (Fig 7.10). However, the percentages were three times and twice fold higher respectively with the increasing of concentration of copper, which suggested high concentration of copper had a stonger effect on the aggregation of aS mutants. Interestingly, no increase on the percentage of cell with aggregates was observed when iron was added to the chelex treated media (CM) (Fig 7.10). For cells overexpressing WT aS, E46K and A53T aS, the aggregation with treatment of 300 μM $FeSO_4$ was even less than that in control media.

When cells were treated with chelexed media in which metals were removed by binding to the chelex, most of the overexpressed proteins were bound to the cell membranes (Fig 7.3 and Fig 7.10), and this phenomenon disappeared when copper or iron were added back to the media. It indicates that aS might be the physiological copper or/and iron transporters, which insert into the membranes and form influx channels to keep the homeostasis of metals.

7.6 Localization of aS in mammalian cells regulated by different amino acid regions

The distribution of aS in cells is of great importance because abnormal accumulation of aS in specific cellular organelles may increase local concentration of this protein, which may induce the protein self-aggregation, and finally fibrillization. Cells overexpressing aS mutants in which suspicious copper or/and iron binding sites were mutated or truncated, were employed to investigate if these regions were responsible for the transport or/and location of the proteins. Fig 7.11 represents the location of overexpressed proteins in mammalian cells stained by immunofluorescence.

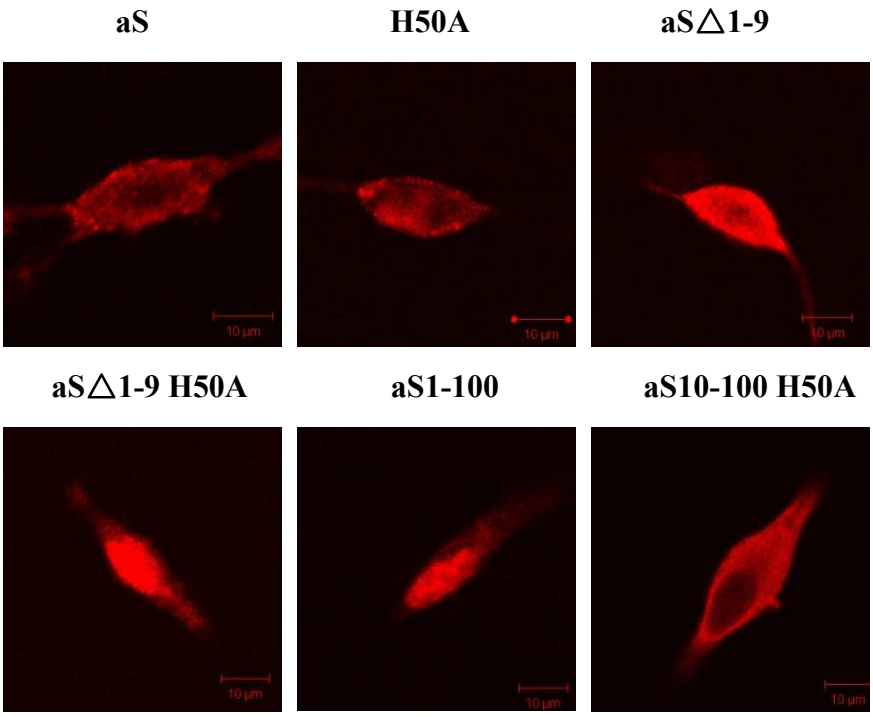

Fig. 7.11 Comparison of location of aS mutants in SHSY5Y cells overexpressing aS, H50A aS, aS△1-9, aS△1-9 H50A, aS1-100 and aS10-100 H50A.
aS was detected using the mouse primary aS antibodyB (Zymed Laboratories Inc.) for aS, H50A aS, aS△1-9 and aS△1-9 H50A or sheep primary aS antibodyA (abcam) for aS1-100 and aS10-100 H50A. Scale bar represents 10 μm.

Cells were observed under non-fluorescence first and the location of nuclei was defined. Overexpressed WT aS and H50A aS was distributed all over the whole cells. In cells overexpressing aS△1-9 and aS△1-9 H50A, aS△1-9 and aS△1-9 H50A was concentrated in the nucleus (Fig 7.6 A). This implied the amino acid sequences of 1-9 in aS were responsible for the translocation of aS. Similarly, this happened to the C-terminus truncated protein aS1-100. The overexpressed protein was concentrated in the nuclues (Fig 7.6 B). Nevertheless, aS10-100 H50A was mostly located in the cytoplasm under all conditions (Fig 7.6 B). This suggests that the residues 1-9 and C-terminal domain of aS were both involved in the transport of aS in mammalian cells. However, the precise amino acid sequences have not been determined yet.

7.7 Synucleins and copper induced cytotoxicity

Overexpressed aS and copper induced aS aggregates were thought to be toxic to cells. In this experiment, MTT assay was employed to analyze the cell toxicity induced by synuclein proteins. Fig 7.12 shows the percentages of survived cells among different cell lines treated with different concentrations of copper in CM for 48 hours. Expression of pcDNA3.1(-) alone served as negative control.

A

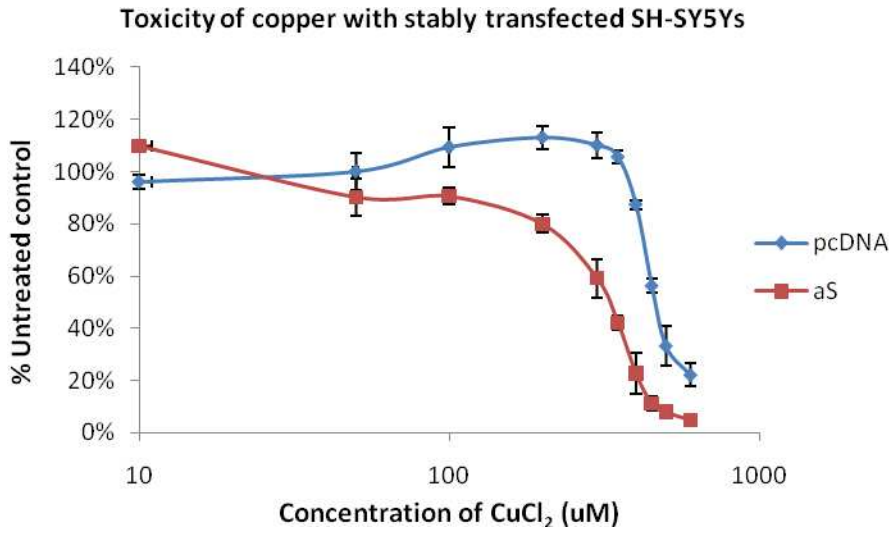

B

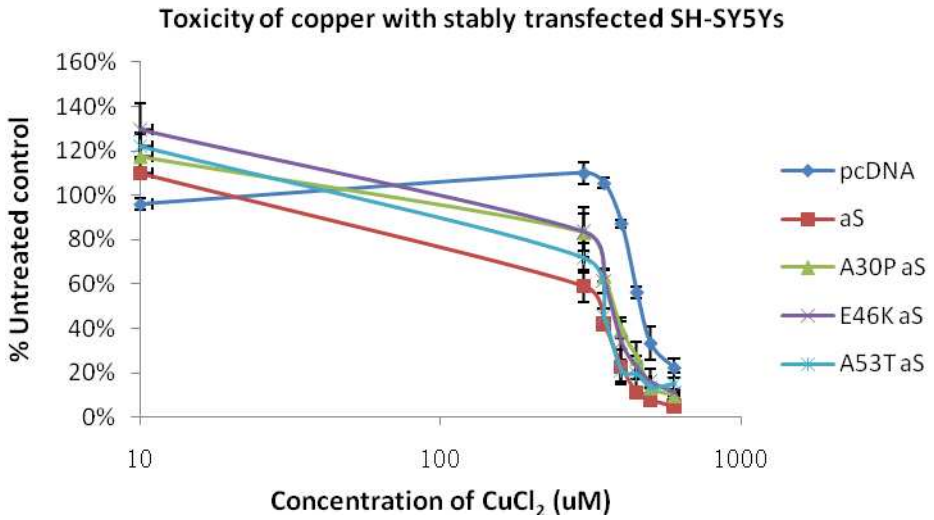

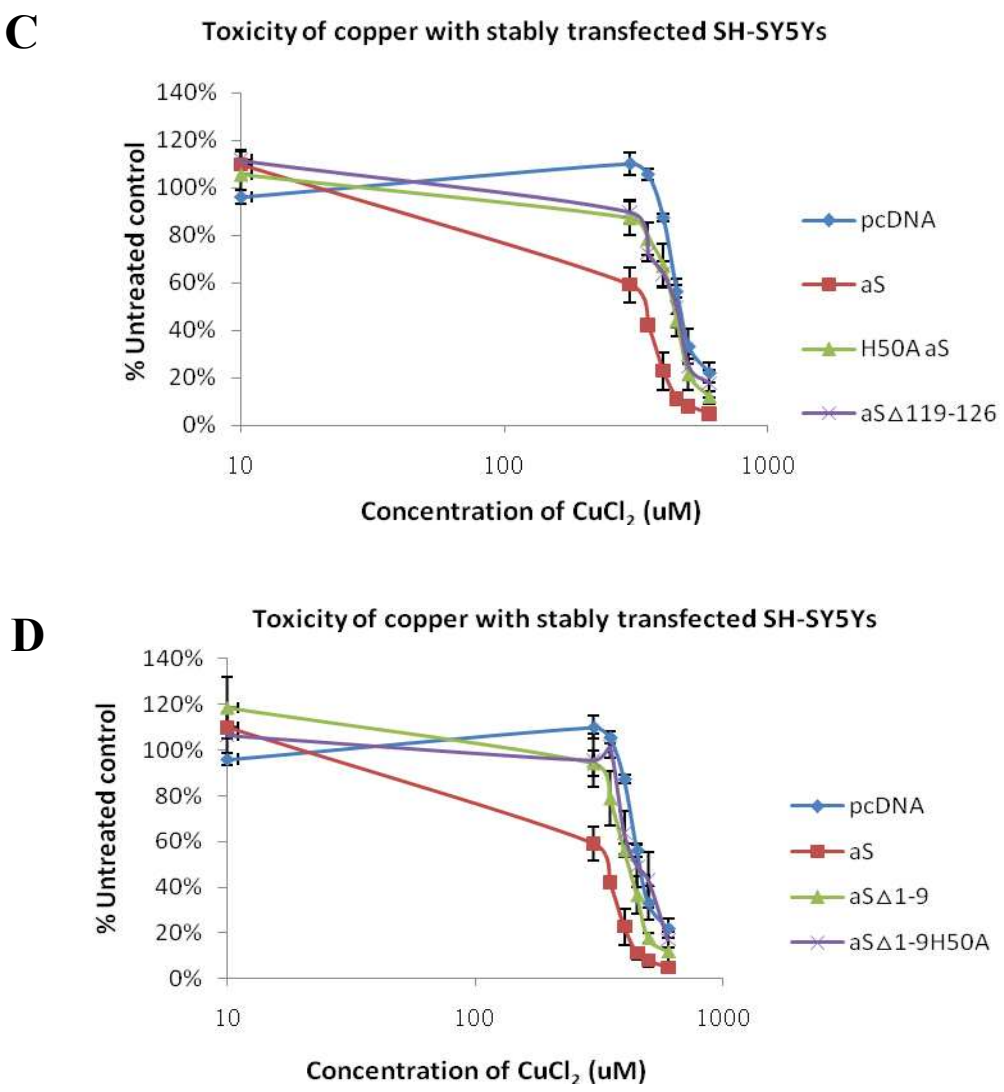

Fig. 7.12 Copper induced cell toxicity is enhanced in cells overexpressing aS and PD-related mutants.

SHSY5Y cells were treated with different conditions in CM: 10 μM, 50 μM, 100 μM, 200 μM, 300 μM, 350 μM, 400 μM, 450 μM, 500 μM and 600 μM $CuCl_2$ for 48 hours. A: Comparison of cells overexpressing pcDNA3.1(-) and aS; B: Comparison of cells overexpressing pcDNA3.1(-), aS, A30P aS, E46K aS, A53T aS; C: Comparison of cells overexpressing pcDNA3.1(-), aS, H50A aS and aS△119-126; D: Comparison of cells overexpressing pcDNA3.1(-), aS, aS△1-9 and aS△1-9 H50A. Each experiment was repeated at least 3 times. Data was expressed as the mean ± standard error (S.E.). Statistical analyses were performed by one-way ANOVA. There was a significant increase in cell toxicity for cells overexpressing aS compared to cells overexpressing pcDNA3.1(-), H50A aS, aS△119-126, aS△1-9 and aS△1-9 H50A ($p < 0.001$).

It seemed physiological concentration of copper favours the growth of all the cells, while it was toxic when the concentration increased to 300 μM or more. 40% of cells death was observed in cells overexpressing aS when treated with 300 μM $CuCl_2$ in CM (Fig 7.12A). This might be due to the disadvantages of this experiment because the floating cells were not counted. More cell death was detected for cells overexpressing the PD-related mutants compared to control cells when treated with high concentration of $CuCl_2$ (Fig 7.12B). However, there was nearly no cell death in cells overexpressing aS mutants where some copper binding sites were mutated or truncated when treated with 300 μM $CuCl_2$ in CM, and there was 10% increase of cell growth for cells transfected with pcDNA3.1(-) vector (Fig 7.12C), which means the copper-aggregate complex might be toxic to the cells. There is no obvious difference in the cell death for cells overexpressing PD-related aS mutants, compared to cells overexpressing WT aS.

7.8 Discussion

aS is a small protein currently regarded to play a role in the pathogenesis of PD. The physiological function of this protein remains unknown. What is known is that point mutations or increased levels of expression of WT aS causes PD. A great deal of literature supports the hypothesis that aS is neurotoxic because it is inherently prone to aggregation and the small oligomers are damaging to neuron cells. In this study, a series of methods were designed and applied to investigate the factors which promote the aggregation and the neurotoxicities induced.

The cell culture system was applied and a method was designed to quantify the aggregates in neuron cells overexpressing aS by analyzing the PK resistance. No obvious difference was observed when treated with different metals (Fig 7.4), and it seemed that the aggregates were retained in the stacking gel due to their stickiness and insolubility. This problem was not solved even in gradient gels (Fig 7.5). Another possibility is that the proportion of the oligomers and monomers is too low that the oligomers could not be detected when certain amount of total protein was loaded. This was proven by Dr Josephine in our lab when she successfully separated the aggregates from the monomeric aS (Wright, Wang et al. 2009).

In this study, immunofluorescence was used to determine the aggregation in synuclein overexpressing cells. As discussed above, aS is prone to form aggregates and aggregates were observed in cells overexpressing aS (Fig 7.3). No aggregate was detected in bS overexpressing cells (Fig 7.2), which might due to the lack of NAC region that is implicated in aS aggregation (Ueda, Fukushima et al. 1993; Han, Weinreb et al. 1995; Iwai, Masliah et al. 1995).

Redox-active metal ions such as Cu(II) and Fe(III) are known to enhance aS fibrillogenesis (Uversky, Li et al. 2001). Nearly 40% of aS overexpressing cells containing aggregates were detected when treated with 300 μM $CuCl_2$ (Table 7.1), while only 12.7% of them was seen in cells in nontreated media. It seemed that Fe(II) has no effect on the formation of aS aggregates (Table 7.1). Copper and iron showed differential binding pattern toward aS revealed by fluorescence (Bharathi and Rao 2008), which might induce the differences in the morphology of aggregates in immunofluorescence. In addition, Fe(III) is more chemically active than Fe(II), which could accelerate the protein aggregation by increasing the levels of oxidative stress.

Intriguingly, in cells transfected with H50A aS, there were only 7.1% of cells including aggregates in nontreated media and 16.3% in 300 μM $CuCl_2$ treated media (Fig 7.6A and Fig 7.7). The percentages were much less than those for cells overexpressing WT aS (12.7% and 37.7% respectively). Again, 17.3% of cells overexpressing aS△1-9 H50A treated with 300 μM $CuCl_2$ were obversed containing aggregates, while none was detected in cells overexpressing aSΔ1-9 or aS10-100 H50A (Fig 7.6 and Fig 7.7). This finding was surprising, as the three regions of aS including residues 1-9, His50 and C-terminus were demonstrated to be responsible for copper binding (Sung, Rospigliosi et al. 2006), which was suggested to promote aggregation. This led to the conclustion that copper mediated aS aggregation was not only relied on direct binding to the protein as four binding sites were detected on all the proteins according to ITC analysis in chapter 5. This indicated that the other hypothesis that metals enhance aS aggregation by increasing the levels of oxidative levels is possible. This hypothesis was further confirmed by CV data in chapter 6 showing fully reversible redox process on copper bound aS and aSΔ1-9 H50A, but

much less reduction peak charge for aSΔ1-9 and aS10-100 H50A, in which case the protein or the metal might be oxidized permenantly.

The PD-related point mutations, A30P and A53T, increase the propensity of aS to aggregate in vitro (Conway, Harper et al. 1998; Narhi, Wood et al. 1999; Rochet, Conway et al. 2000; Li, Uversky et al. 2001; Uversky, Li et al. 2001; Li, Uversky et al. 2002). In this study, more aggregates were visualized in cells overexpressing A30P, E46K and A53T when treated with 300 μM $CuCl_2$ (Fig 7.10). Specifically, the percentages of cells increased by 10%, 3% and 6% respectively compared to that in cells overexpressing WT aS (Fig 7.10A). This is consistant with the literature establishing that E46K mutation is able to increase the propensity of aS to fibrillate, but to a less extent than A53T mutation (Greenbaum, Graves et al. 2005). Nevertheless, there were only slight increased aggregates in cells overexpressing A30P when treated with 300 μM iron, no obvious increase in cells overexpressing E46K and A53T aS was observed (Fig7.10B). This implied that iron mediated aggregation could involve different mechanisms compared to copper. Fe^{2+} was reported to induce DNA damage in aS transfected human neuroblastoma cells and the susceptibility to toxic effects of Fe^{2+} was enhanced with mutant aS associated with inherited forms of PD (Martin, Williamson et al. 2003).

In chelex treated media where metals were removed by binding to the chelex, most of the overexpressed proteins were bound to the cell membranes (Fig 7.3 and Fig 7.6). The proteins were distributed over the cell when copper or iron was added back to the chelex treated media (Fig 7.3 and Fig 7.6). This implies that aS might be one of the copper or/and iron transporters and it is translocated to the membrane when the concentrations of copper or/and iron were different in and out of cells. In addition, immunofluorescence revealed that most of the protein was distributed in the nuclei in cells overexpressing aS△1-9, aS△1-9 H50A and aS1-100 (Fig 7.11). In contrast, most of the proteins were transported to the cytoplasm in cells overexpressing aS10-100 H50A (Fig 7.11). These observations suggested that both of the amino acids 1-9 and the C-terminus were the domains on aS responsible for the transport of protein between the cytoplasm and the nucleus, although the mechanism is still unknown.

The copper induced cytotoxicity was assessed by MTT assay which revealed that overexpressing cells were less resistant to high concentrations of copper than control cells (Fig 7.12). 59% of viabilities were observed in cells overexpressing aS with 300 μM $CuCl_2$ (Fig 7.12A), which might due to the disadvantage of this technique, because floating cells could not be counted in this experiment. No toxicity was observed in the absence of copper in all the cell lines, suggesting that overexpression of synuclein protein was not toxic. This corresponds with that intracytoplasmic aS aggregates are not toxic to cells (Spillantini, Schmidt et al. 1997). It seemed that cells overexpressing WT aS and the PD-related mutants displayed the higher degree of cell death than control cells when treated with high concentration of copper (Fig 7.12B), indicating that the copper-aggregate complex played a role in the cytotoxicity. However, no toxicity was detected in cells overexpressing the aS mutants in which some of the copper-binding sites were mutated or truncated when treated with 300 μM $CuCl_2$, indicating the overexpression of these mutants was not toxic even in the presence of high concentration of copper when there was no aggregate. These findings revealed that overexpression of WT and PD-related aS mutants enhanced Cu(II)-induced neurotoxicity in SHSY5Y cells and copper could mediate the toxicity by interacting with the protein directly which led ultimately to aggregation which triggered cell death. In PD patients, there is increased expression of aS and high levels of copper in the CSF (Pall, Williams et al. 1987). This study collates these observations by suggesting that the combination of increased aS expression and copper levels causes increased toxicity to neuronal cells.

Previous studies have shown that aging A30P or A53T aS increases their toxicity (El-Agnaf, Salem et al. 2006). Accordingly, this study showed that the toxicity of aggregated aS mutants was significantly increased in the presence of high concentration of copper (Fig 7.12B). However, there was no significant difference in the effect of the aS mutants compared to WT aS (Fig 7.12B), which corresponds with the observation that there is no significant difference between the ability of WT aS and aS mutants to bind copper (Bharathi and Rao 2007). In addition, no significant difference was observed in the morphology of fibrils formed from WT aS or mutants, which were the toxic species to cells (Wright, Wang et al. 2009).

Chapter 8. Disscussion

PD is a chronic and progressive neurodegenerative disorder, affecting approximately 2% of the population by the age of 65 years, and up to 4% to 5% of the population by the age of 85 years (Eriksen, Wszolek et al. 2005). This disease is worldwide distributed, with no gender preference, and the risk rises steeply with advancing ages. It is expected by the World Health Organisation that PD, along with other neurodegenerative diseases, will surpass cancer as the second most common cause of death by the year of 2050. As far as we know, there is no cure for PD although medications or surgery can provide transient relief from the symptoms. Furthermore, it is yet unclear about the mechanisms how the abnormal protein deposits are formed and what causes the neuronal cell death in the brain. Therefore, it is important to characterize the proteins which are implicated in the development of the disease, as these may provide potential therapeutic targets.

The clinical symptoms of PD include resting tremor, muscle rigidity and Bradykinesia, which refers to slowness of movement. Neuropathologically PD is characterized by progressive loss of dopaminergic neurons in the substantia nigra and the development of LBs and LNs observed in these neurons (Tofaris and Spillantini 2007). The fact that aS has been linked to PD is based on two observations: the identification of point mutations and gene duplication and triplication of aS in the families with autosomal-dominant early-onset PD and the discovery that the fibrillar form of aS is the major component of LBs (Tofaris and Spillantini 2007). Later on, its homologues bS and gS, were shown to be able to inhibit the aS fibril formation (Uversky, Li et al. 2002), although the mechanism is not fully elucidated. The precise function of aS is unknown. However, there is increasing evidence showing that the process of aS aggregation is the key step during the progression of neurodegeneration. Metals such as copper and iron were proven to be factors accelerating aS fibrillation (Paik, Shin et al. 1999; Uversky, Li et al. 2001), although the mechanisms are not fully understood. There are several hypotheses about the mechanisms for metal-stimulated fibrillation of aS. The simplest would involve direct interactions between aS and the metal, leading to structural changes in aS, and resulting in the enhanced propensity to

aggregate. Another one indicates redox-active transition metals such as copper and iron, may exert their pathogenic effects by participating in an array of cellular disturbances characterized by oxidative stress and increased free radical production (Sayre, Moreira et al. 2005). The aim of this thesis was to further our understanding of the role of synuclein proteins and metals in the pathogenesis of PD by investigating the copper-binding properties of aS and copper induced aggregation and neurotoxicity in doperminergic neuron cells.

To date, there are mainly two strategies for synuclein purification, involving high temperature and acidic condition in the cell lysate preparations respectively. Previous recombinant aS has been purified on the basis that the protein is heat resistant (Jakes, Spillantini et al. 1994; Weinreb, Zhen et al. 1996; Giasson, Uryu et al. 1999). However, high temperature has been shown to cause conformational alteration in aS (Uversky, Lee et al. 2001; Bertoncini, Jung et al. 2005). In this study, three purification protocols including boiling, acid precipitation and anion exchange chromatography, were introduced and compared in chapter 3. The proteins from each protocol were examined by MALDI mass spectrometry, far-UV CD, 2D NMR spectroscopy and light scattering. The methods involving anion exchange chromatography and acid precipitation were shown to be more reliable and selected for the purification of all the proteins used in this project. 2D NMR spectroscopy demonstrated aS from these two protocols was in a native and monomeric form, while protein experiencing boiling procedure was more prone to aggregate (Fig 3.8). This was confirmed by the light scattering technique (Fig 3.9). Furthermore, the negative peak of far-UV CD spectra for aS purified by boiling protocol was shift to 208 nm and the $[\theta]_{222\ nm}$ intensity was much higher, illustrating more secondary structure (Fig 3.10). No aggregates were detected by the MALDI mass spectrometry (Fig 3.7). This might be due to two reasons: the concentration used for MALDI mass spectrometry was only one tenth of that for NMR analysis; the small amount of aggregates could be disassembled during the ionization of the experiment.

aS has been identified as a metal-binding protein. Although there is a consensus that aS binds copper, it is still controversial about the location of the binding sites and the binding affinities. CW-EPR spectroscopy demonstrated that aS bound Cu(II) via two binding modes at physiological pH, corresponding to 2N2O and 1N3O (Table 4.2).

This is consistent with previous studies on truncated model fragments implying the involvement of the N-terminal amine of Met1 and the deprotonated backbone amine and carboxylate side chain of Asp2 for the mode 2N2O (Kowalik-Jankowska, Rajewska et al. 2005) and the nitrogen of imidazole group of His50 for mode 1N3O (Binolfi, Lamberto et al. 2008). However, the modes were not changed for mutants H50A aS and aS△1-9 (Table 4.2), suggesting the amino acids involved in the coordination could be replaced or/and there were more than one binding site for each mode. This was confirmed by the observation that the proportion of the mode 1N3O was greatly increased on aS△1-9 H50A. For the C-terminal mutants aS△119-126, aS△1-9 H50A△119-126 and aS10-100 H50A, the $A_{//}$ and $g_{//}$ parameters were changed and correlated well with two 3N1O coordination sphere (Table 4.2), illustrating the square-planar or tetragonal geometry has been altered. The stoichiometry of copper binding to aS was assessed by ITC, showing four binding sites for all the N-terminal and C-terminal aS mutants although the affinities were different (Table 5.4). This finding confirmed that the residues involved in copper coordination could be replaced by the amino acid in the vicinity. There is evidence showing that the coordination of Cu(II) may involve the lateral NH_2 group of lysine residues upstream of His50 (Kowalik-Jankowska, Rajewska et al. 2006), showing that lysine could act as a copper anchoring site in the absence of histidine. Similarly, Asp2 might be substituted by Glu13 which could also provide nitrogen and oxygen ligand in Cu(II) binding mode (Rasia, Bertoncini et al. 2005). Based on these findings, it implied that when binding to copper, aS might not act as such protein as prion protein where copper binding sites were assigned to certain amino acids, the binding sites disappeared when certain amino acids missing or mutated (Klewpatinond, Davies et al. 2008).

Similar to aS, its homologues bS and gS displayed two identical copper binding modes (Table 4.1). The coordination modes remained the same for H65A bS but shifted to two 3N1O modes for bS△1-9 H65A and bS10-100 H65A, suggesting His65 might not be involved in the interaction with copper. Nevertheless, it was denied by the ITC analysis showing four binding sites for bS and H65A bS with reduced affinities for H65A bS (Table 5.5). The affinity constants were altered when any of the three regions was mutated or deleted. This suggested that the three regions

contributed to the copper binding event. Moreover, there was a manifest decrease in the affinity on second binding site on bSΔ1-9 (Table 5.5), implying that the higher-affinity site on bS was allocated on the residues 1-9 while that was on His50 for aS (Table 5.4). One binding site was missing for bS10-100 H65A (Table 5.5). These observations suggested that the residues in the N-terminus of bS were replaceable for the copper cooperation, but the C-terminus was essential for one binding event. It was noteworthy that the logKa constants for bS were in the range of 7.7-8.0, which were higher than those for aS (6.7-7.4). This finding might provide some insight into the mechanism by which bS inhibit aS aggregation. It implied that the preventive effect of bS on aS aggregation might be related to the higher affinities for copper. In that case, bS competes with aS for copper binding and acts as a copper-sequestering protein, playing the role of a copper chelator and hence preventing or attenuating the subsequent aggregation of aS.

There are several lines of evidence showing redox-active transition metals such as copper and iron, may play an important role in the pathogenesis of neurodegenerative diseases by increasing oxidative stress and free radical production (Sayre, Moreira et al. 2005). The oxidation of proteins could be catalyzed by metals (Cole, Murphy et al. 2005) and oxidatively modified protein could increase its own tendency toward protein aggregation due to the generation of reactive oxygen species (ROS), which exert pro-aggregatory effects and turn soluble protein into insoluble forms by either inhibiting intracellular proteolysis or causing unusual posttranslational modifications (Kowalik-Jankowska, Rajewska et al. 2006). To further explore the role of synucleins in PD, the electrochemical property of the copper bound proteins were assessed by CV in this study. aS displayed capability of exchanging electrons when bound to copper (Fig 6.1). The redox cycling was fully reversible (Table 6.1), suggesting that the protein was unaffected by continuous oxidation and reduction. However, this was not the case for bS and gS, where the reduction peaks were much less than the oxidation peaks (Table 6.1). The finding indicated that some of the copper or protein might be oxidized permanently or Cu(I) was not stable on the protein and fell off. This observation could explain how bS and gS inhibit aS aggregation: Cu(II) was reduced and fell off from bS or gS after it was dragged away from aS and bound to bS and gS as they showed higher binding affinities according to ITC (chapter 5).

Only one oxidation and reduction peak was observed for the WT aS-Cu species, suggesting the copper centres were electronically coupled as four copper were bound per molecular of aS according to ITC (chapter 5). The midpoint potential and responsive current peak during the redox process on the mutant aS△1-9 H50A was quite close to that for WT aS, indicating the amino acids in the proximity might fill in the position and form the identical coordination geometry. This confirmed that lysine residues upstream of His50 could act as a copper anchoring site in the absence of histidine (Kowalik-Jankowska, Rajewska et al. 2006) and Asp2 might be substituted by Glu13 in Cu(II) binding mode (Rasia, Bertoncini et al. 2005). The integrated reduction peak charge was enormously reduced on aS1-100, indicating the presence of the C-terminal region of aS was essential for the reductive electrochemistry, which might be involved in the mechanism of inhibition of aS aggregation, providing evidence showing C-terminus of aS is a negative regulator of self-assembly. The protein might be partially oxidized permanently without the C-terminal region, which could lead to self-oligomerization and hence possible protein aggregation and neurodegeneration (Paik, Shin et al. 2000). It fits the hypothesis that C-terminus truncated aS constructs are more prone to fibrillate in vitro than the full-length protein (Crowther, Jakes et al. 1998; Serpell, Berriman et al. 2000; Murray, Giasson et al. 2003). In contrast to aS, mutation of His65 on bS enhanced the redox activity especially the reduction current, producing reversible electron cycling (Table 6.3). This demonstrated that His65 was responsible for the inhibition of the electrochemical activity of the protein. This was contrast to aS, where His50 contributed to the redox activity especially the reduction response which was thought to inhibit the protein aggregation (Table 6.2). The difference of the electrochemical features on the two proteins indicated two distinct mechanisms for the protein aggregation, as no study has reported inhibition of aggregation on the His65 mutant. The reductive response was enormously diminished for bS△1-9 and bS10-100 H65A, indicating the involvement of residues 1-9 and the C-terminus on the redox activity. Little has been investigated about bS, this new technique might provide new insight into the role of bS on the inhibition of aS aggregation.

To further investigate the role of aS and metals in neurotoxicity, copper and iron induced aggregation and toxicity in doperminergic neuron SHSY5Y cells

overexpressing synucleins were examined by confocal microscopy and MTT assay. High concentration of Cu(II) enhanced the aggregation in aS overexpressing cells while Fe(II) had no effect on the formation of aS aggregates (Table 7.1). Intriguingly, in cells transfected with H50A aS, there were only 7.1% of cells including aggregates in nontreated media and 16.3% in 300 μM $CuCl_2$ treated media (Fig 7.6A and Fig 7.7). The percentages were much less than those for cells overexpressing WT aS (12.7% and 37.7% respectively). Again, 17.3% of cells overexpressing aS△1-9 H50A treated with 300 μM $CuCl_2$ were obversed containing aggregates, while none was detected in cells overexpressing aS△1-9 or aS10-100 H50A (Fig 7.6 and Fig 7.7). This finding pointed to the conclustion that copper mediated aS aggregation was not only relied on direct binding to the protein as four binding sites were detected on all the proteins according to ITC analysis in chapter 5. The other hypothesis that metals enhance aS aggregation by increasing the levels of oxidative levels stands out. This hypothesis was verified by CV data in chapter 6 showing fully reversible redox process on copper bound aS and aS△1-9 H50A, but much less reduction peak charge for aS△1-9 and aS10-100 H50A. This disappearance of aggregation might be due to the alteration of the electrochemical property of aS.

The PD-related point mutations, A30P and A53T, increase the propensity of aS to aggregate in vitro (Conway, Harper et al. 1998; Narhi, Wood et al. 1999; Rochet, Conway et al. 2000; Li, Uversky et al. 2001; Uversky, Li et al. 2001; Li, Uversky et al. 2002). In this study, more aggregates were visualized in cells overexpressing A30P, E46K and A53T when treated with 300 μM $CuCl_2$ (Fig 7.10). Specifically, the percentages of cells increased by 10%, 3% and 6% respectively compared to that in cells overexpressing WT aS (Fig 7.10A). This is consistant with the literature establishing that E46K mutation is able to increase the propensity of aS to fibrillate, but to a less extent than A53T mutation (Greenbaum, Graves et al. 2005). Nevertheless, there were only slight increased aggregates in cells overexpressing A30P when treated with 300 μM $FeSO_4$, and no obvious increase in cells overexpressing E46K and A53T aS was observed (Fig 7.10B). This implied that iron mediated aggregation could involve different mechanisms compared to copper. Fe^{2+} was reported to induce DNA damage in aS transfected human neuroblastoma cells and the susceptibility to toxic effects of Fe^{2+} was enhanced with mutant aS associated with inherited forms of

PD (Martin, Williamson et al. 2003).

aS was demonstrated to be one of the copper or/and iron transporters as most of the overexpressed proteins were bound to the cell membranes in chelex treated media where metals were removed by binding to the chelex (Fig 7.3 and Fig 7.6). In addition, immunofluorescence revealed that most of the protein was distributed in the nuclei in cells overexpressing aS△1-9, aS△1-9 H50A and aS1-100 (Fig 7.11). In contrast, most of the proteins were transported to the cytoplasm in cells overexpressing aS10-100 H50A (Fig 7.11). These observations suggested that both of the amino acids 1-9 and the C-terminus were responsible for the transport of protein between the cytoplasm and the nucleus although the mechanism is still elusive.

The copper induced cytotoxicity was assessed by MTT assay which revealed that overexpressing cells were less resistant to high concentrations of copper than control cells (Fig 7.12). It seemed that cells overexpressing WT aS and the PD-related mutants displayed the higher degree of cell death than control cells when treated with high concentration of copper (Fig 7.12B), indicating that the copper-aggregate complex played a role in the cytotoxicity. However, no toxicity was detected in cells overexpressing the aS mutants in which some of the copper-binding sites were mutated or truncated when treated with 300 μM $CuCl_2$, indicating the overexpression of these mutants was not toxic even in the presence of high concentration of copper when there was no aggregate. These findings revealed that overexpression of WT and PD-related aS mutants enhanced Cu(II)-induced neurotoxicity in SHSY5Y cells and copper could mediate the toxicity by interacting with the protein directly which led ultimately to aggregation which triggered cell death. In PD patients, there is increased expression of aS and high levels of copper in the CSF (Pall, Williams et al. 1987). This study collates these observations by suggesting that the combination of increased aS expression and copper levels causes increased toxicity to neuronal cells.

The mechanism of aS ovexpression induced cell toxicity was not fully defined in this study although copper has been proven to be essential during this process. The most common hypothesis for the mechanism is that aS oligomers can create pores in membranes, which increases permeability of cells to ions from the extracellular space,

leading to cell death (Volles and Lansbury 2002; Danzer, Haasen et al. 2007). The toxic species are the aS oligomers that are annular or porelike, with outer diameters of 10–12 nm and inner diameters of 2 nm (Lashuel, Hartley et al. 2002; Lashuel, Petre et al. 2002). These features may lead to the increased but nonspecific ion permeability observed with aS-expressing cells (Furukawa, Matsuzaki-Kobayashi et al. 2006). This hypothesis is the most popular, particularly given the mechanistic similarity to other proteins involved in neurodegenerative diseases, such as Aβ (Bhatia, Lin et al. 2000; Kawahara, Kuroda et al. 2000; Zhu, Lin et al. 2000). Our research on extracellular aS aggregates showed that the soluble aS oligomers were the toxic species to cells in the presence of copper (Wright, Wang et al. 2009). Concerning the data from CV, it showed unreversible redox chemistry for the aS mutants lacking potential copper-binding sites although ITC analysis demonstrated they were capable of binding the same number of coppers with WT aS. This might contribute to the absence of aggregates in the SHSY5Y cells overexpressing these mutants where the intracellular ROS levels were decreased. CV showed reduced reduction response for these mutants, suggesting Cu(II) might be reduced to Cu(I) and fell off the protein. The reduced copper could interact with H_2O_2 and generate hydroxyl radical (Sayre, Moreira et al. 2005). There was evidence showing that the formation of H_2O_2 from aS was accelerated in the presence of copper (Paik, Shin et al. 2000). Therefore, copper accelerates the formation of aS aggregates by binding to the protein directly and increasing intracellular ROS levels. This then leads to aggregates induced neurotoxicity and cell death through the pore-creation mechanism.

The findings described here illustrate that disruption of the interaction between copper and aS and the inhibition of downstream toxic process could be a potential target for the development of new therapeutics for PD. In fact, initial studies suggested that copper chelators will be effective in the treatment of PD if the neurotoxic side effects can be overcome (Gaeta and Hider 2005). Actually, the chelation therapies have had some success in improving cognition and lowering Aβ levels in Alzheimer's disease (Ritchie, Bush et al. 2003; Adlard, Cherny et al. 2008; Lannfelt, Blennow et al. 2008).

For CV, future research will determine the precise amino acids of aS involved in

Cu(II) induced oxidative stress. Furthermore, the characterization of the electrochemistry of aS will give a better idea about the physiological and pathological functions of the protein. The copper binding property and electrochemistry of bS and gS were shown to be different from aS although they belong to the same family. The future work can explore the details of redox activity of bS and gS, which might provide a novel approach to the treatment for PD. In addition, the effect of Cu(I) will be investigated by CV to confirm the mechanism for redox stress induced aS aggregation. Also, the interaction between aS and Cu(I) will be examined by ITC and EPR to further understand the physiological funcation of the protein. In vivo, the intracellular aggregates will be isolated and imaged by electron microspy to find the toxic species. In addition, cells overexpressing aS will be treated with bS or/and gS to see the effect of the homologues on aS aggregates induced toxicity. This might open a new avenue for the therapy for PD.

Appendix A

1. Coding sequence of α-synuclein

```
1   ATGGATGTAT TCATGAAAGG ACTTTCAAAG GCCAAGGAGG GAGTTGTGGC TGCTGCTGAG
61  AAAACCAAAC AGGGTGTGGC AGAAGCAGCA GGAAAGACAA AAGAGGGTGT TCTCTATGTA
121 GGCTCCAAAA CCAAGGAGGG AGTGGTGCAT GGTGTGGCAA CAGTGGCTGA GAAGACCAAA
181 GAGCAAGTGA CAAATGTTGG AGGAGCAGTG GTGACGGGTG TGACAGCAGT AGCCCAGAAG
241 ACAGTGGAGG GAGCAGGGAG CATTGCAGCA GCCACTGGCT TTGTCAAAAA GGACCAGTTG
301 GGCAAGAATG AAGAAGGAGC CCCACAGGAA GGAATTCTGG AAGATATGCC TGTGGATCCT
361 GACAATGAGG CTTATGAAAT GCCTTCTGAG GAAGGGTATC AAGACTACGA ACCTGAAGCC
421 TAA
```

2. Amino sequence of α-synuclein

```
1   MDVFMKGLSK AKEGVVAAAE KTKQGVAEAA GKTKEGVLYV GSKTKEGVVH GVATVAEKTK
61  EQVTNVGGAV VTGVTAVAQK TVEGAGSIAA ATGFVKKDQL GKNEEGAPQE GILEDMPVDP
121 DNEAYEMPSE EGYQDYEPEA
```

3. Coding sequence of α-synuclein A30P

```
1   ATGGATGTAT TCATGAAAGG ACTTTCAAAG GCCAAGGAGG GAGTTGTGGC TGCTGCTGAG
61  AAAACCAAAC AGGGTGTGGC AGAAGCACCA GGAAAGACAA AAGAGGGTGT TCTCTATGTA
121 GGCTCCAAAA CCAAGGAGGG AGTGGTGCAT GGTGTGGCAA CAGTGGCTGA GAAGACCAAA
181 GAGCAAGTGA CAAATGTTGG AGGAGCAGTG GTGACGGGTG TGACAGCAGT AGCCCAGAAG
241 ACAGTGGAGG GAGCAGGGAG CATTGCAGCA GCCACTGGCT TTGTCAAAAA GGACCAGTTG
301 GGCAAGAATG AAGAAGGAGC CCCACAGGAA GGAATTCTGG AAGATATGCC TGTGGATCCT
361 GACAATGAGG CTTATGAAAT GCCTTCTGAG GAAGGGTATC AAGACTACGA ACCTGAAGCC
421 TAA
```

4. Amino sequence of α-synuclein A30P

```
1   MDVFMKGLSK AKEGVVAAAE KTKQGVAEAP GKTKEGVLYV GSKTKEGVVH GVATVAEKTK
61  EQVTNVGGAV VTGVTAVAQK TVEGAGSIAA ATGFVKKDQL GKNEEGAPQE GILEDMPVDP
121 DNEAYEMPSE EGYQDYEPEA
```

5. Coding sequence of α-synuclein E46K

```
1   ATGGATGTAT TCATGAAAGG ACTTTCAAAG GCCAAGGAGG GAGTTGTGGC TGCTGCTGAG
61  AAAACCAAAC AGGGTGTGGC AGAAGCAGCA GGAAAGACAA AAGAGGGTGT TCTCTATGTA
121 GGCTCCAAAA CCAAGAAGGG AGTGGTGCAT GGTGTGGCAA CAGTGGCTGA GAAGACCAAA
181 GAGCAAGTGA CAAATGTTGG AGGAGCAGTG GTGACGGGTG TGACAGCAGT AGCCCAGAAG
241 ACAGTGGAGG GAGCAGGGAG CATTGCAGCA GCCACTGGCT TTGTCAAAAA GGACCAGTTG
301 GGCAAGAATG AAGAAGGAGC CCCACAGGAA GGAATTCTGG AAGATATGCC TGTGGATCCT
361 GACAATGAGG CTTATGAAAT GCCTTCTGAG GAAGGGTATC AAGACTACGA ACCTGAAGCC
421 TAA
```

6. Amino sequence of α-synuclein E46K

```
1   MDVFMKGLSK AKEGVVAAAE KTKQGVAEAA GKTKEGVLYV GSKTKKGVVH GVATVAEKTK
61  EQVTNVGGAV VTGVTAVAQK TVEGAGSIAA ATGFVKKDQL GKNEEGAPQE GILEDMPVDP
121 DNEAYEMPSE EGYQDYEPEA
```

7. Coding sequence of α-synuclein A53T

```
1   ATGGATGTAT TCATGAAAGG ACTTTCAAAG GCCAAGGAGG GAGTTGTGGC TGCTGCTGAG
61  AAAACCAAAC AGGGTGTGGC AGAAGCAGCA GGAAAGACAA AAGAGGGTGT TCTCTATGTA
121 GGCTCCAAAA CCAAGGAGGG AGTGGTGCAT GGTGTGACAA CAGTGGCTGA GAAGACCAAA
181 GAGCAAGTGA CAAATGTTGG AGGAGCAGTG GTGACGGGTG TGACAGCAGT AGCCCAGAAG
241 ACAGTGGAGG GAGCAGGGAG CATTGCAGCA GCCACTGGCT TTGTCAAAAA GGACCAGTTG
301 GGCAAGAATG AAGAAGGAGC CCCACAGGAA GGAATTCTGG AAGATATGCC TGTGGATCCT
361 GACAATGAGG CTTATGAAAT GCCTTCTGAG GAAGGGTATC AAGACTACGA ACCTGAAGCC
421 TAA
```

8. Amino sequence of α-synuclein A53T

```
1   MDVFMKGLSK AKEGVVAAAE KTKQGVAEAA GKTKEGVLYV GSKTKEGVVH GVTTVAEKTK
61  EQVTNVGGAV VTGVTAVAQK TVEGAGSIAA ATGFVKKDQL GKNEEGAPQE GILEDMPVDP
121 DNEAYEMPSE EGYQDYEPEA
```

9. Coding sequence of α-synuclein H50A

```
1   ATGGATGTAT TCATGAAAGG ACTTTCAAAG GCCAAGGAGG GAGTTGTGGC TGCTGCTGAG
61  AAAACCAAAC AGGGTGTGGC AGAAGCAGCA GGAAAGACAA AAGAGGGTGT TCTCTATGTA
121 GGCTCCAAAA CCAAGGAGGG AGTGGTGGCT GGTGTGGCAA CAGTGGCTGA GAAGACCAAA
181 GAGCAAGTGA CAAATGTTGG AGGAGCAGTG GTGACGGGTG TGACAGCAGT AGCCCAGAAG
241 ACAGTGGAGG GAGCAGGGAG CATTGCAGCA GCCACTGGCT TTGTCAAAAA GGACCAGTTG
301 GGCAAGAATG AAGAAGGAGC CCCACAGGAA GGAATTCTGG AAGATATGCC TGTGGATCCT
361 GACAATGAGG CTTATGAAAT GCCTTCTGAG GAAGGGTATC AAGACTACGA ACCTGAAGCC
421 TAA
```

10. Amino sequence of α-synuclein H50A

```
1   MDVFMKGLSK AKEGVVAAAE KTKQGVAEAA GKTKEGVLYV GSKTKEGVVA GVATVAEKTK
61  EQVTNVGGAV VTGVTAVAQK TVEGAGSIAA ATGFVKKDQL GKNEEGAPQE GILEDMPVDP
121 DNEAYEMPSE EGYQDYEPEA
```

11. Coding sequence of α-synuclein △1-9

```
1   ATG_______ __________ _______AAG GCCAAGGAGG GAGTTGTGGC TGCTGCTGAG
61  AAAACCAAAC AGGGTGTGGC AGAAGCAGCA GGAAAGACAA AAGAGGGTGT TCTCTATGTA
121 GGCTCCAAAA CCAAGGAGGG AGTGGTGCAT GGTGTGGCAA CAGTGGCTGA GAAGACCAAA
181 GAGCAAGTGA CAAATGTTGG AGGAGCAGTG GTGACGGGTG TGACAGCAGT AGCCCAGAAG
241 ACAGTGGAGG GAGCAGGGAG CATTGCAGCA GCCACTGGCT TTGTCAAAAA GGACCAGTTG
301 GGCAAGAATG AAGAAGGAGC CCCACAGGAA GGAATTCTGG AAGATATGCC TGTGGATCCT
361 GACAATGAGG CTTATGAAAT GCCTTCTGAG GAAGGGTATC AAGACTACGA ACCTGAAGCC
421 TAA
```

12. Amino sequence of α-synuclein △1-9

```
1   M________K AKEGVVAAAE KTKQGVAEAA GKTKEGVLYV GSKTKEGVVH GVATVAEKTK
61  EQVTNVGGAV VTGVTAVAQK TVEGAGSIAA ATGFVKKDQL GKNEEGAPQE GILEDMPVDP
121 DNEAYEMPSE EGYQDYEPEA
```

13. Coding sequence of α-synuclein △119-126

```
1   ATGGATGTAT TCATGAAAGG ACTTTCAAAG GCCAAGGAGG GAGTTGTGGC TGCTGCTGAG
61  AAAACCAAAC AGGGTGTGGC AGAAGCAGCA GGAAAGACAA AAGAGGGTGT TCTCTATGTA
121 GGCTCCAAAA CCAAGGAGGG AGTGGTGCAT GGTGTGGCAA CAGTGGCTGA GAAGACCAAA
181 GAGCAAGTGA CAAATGTTGG AGGAGCAGTG GTGACGGGTG TGACAGCAGT AGCCCAGAAG
241 ACAGTGGAGG GAGCAGGGAG CATTGCAGCA GCCACTGGCT TTGTCAAAAA GGACCAGTTG
301 GGCAAGAATG AAGAAGGAGC CCCACAGGAA GGAATTCTGG AAGATATGCC TGTG______
361 __________ _________AT GCCTTCTGAG GAAGGGTATC AAGACTACGA ACCTGAAGCC
421 TAA
```

14. Amino sequence of α-synuclein △119-126

```
1   MDVFMKGLSK AKEGVVAAAE KTKQGVAEAA GKTKEGVLYV GSKTKEGVVH GVATVAEKTK
61  EQVTNVGGAV VTGVTAVAQK TVEGAGSIAA ATGFVKKDQL GKNEEGAPQE GILEDMPV__
121 ______MPSE EGYQDYEPEA
```

15. Coding sequence of α-synuclein 1-100

```
1   ATGGATGTAT TCATGAAAGG ACTTTCAAAG GCCAAGGAGG GAGTTGTGGC TGCTGCTGAG
61  AAAACCAAAC AGGGTGTGGC AGAAGCAGCA GGAAAGACAA AAGAGGGTGT TCTCTATGTA
121 GGCTCCAAAA CCAAGGAGGG AGTGGTGCAT GGTGTGGCAA CAGTGGCTGA GAAGACCAAA
181 GAGCAAGTGA CAAATGTTGG AGGAGCAGTG GTGACGGGTG TGACAGCAGT AGCCCAGAAG
241 ACAGTGGAGG GAGCAGGGAG CATTGCAGCA GCCACTGGCT TTGTCAAAAA GGACCAGTTG
301 TAATGA
```

16. Amino sequence of α-synuclein 1-100

```
1  MDVFMKGLSK AKEGVVAAAE KTKQGVAEAA GKTKEGVLYV GSKTKEGVVH GVATVAEKTK
61 EQVTNVGGAV VTGVTAVAQK TVEGAGSIAA ATGFVKKDQL
```

17. Coding sequence of α-synuclein 10-100 H50A

```
1   ATG_______ __________ _______AAG GCCAAGGAGG GAGTTGTGGC TGCTGCTGAG
61  AAAACCAAAC AGGGTGTGGC AGAAGCAGCA GGAAAGACAA AAGAGGGTGT TCTCTATGTA
121 GGCTCCAAAA CCAAGGAGGG AGTGGTGGCT GGTGTGGCAA CAGTGGCTGA GAAGACCAAA
181 GAGCAAGTGA CAAATGTTGG AGGAGCAGTG GTGACGGGTG TGACAGCAGT AGCCCAGAAG
241 ACAGTGGAGG GAGCAGGGAG CATTGCAGCA GCCACTGGCT TTGTCAAAAA GGACCAGTTG
301 TAATGA
```

18. Amino sequence of α-synuclein 10-100 H50A

```
1  M________K AKEGVVAAAE KTKQGVAEAA GKTKEGVLYV GSKTKEGVVA GVATVAEKTK
61 EQVTNVGGAV VTGVTAVAQK TVEGAGSIAA ATGFVKKDQL
```

19. Coding sequence of β-synuclein

```
1   ATGGACGTGT TCATGAAGGG CCTGTCCATG GCCAAGGAGG GCGTTGTGGC AGCCGCGGAG
61  AAAACCAAGC AGGGGGTCAC CGAGGCGGCG GAGAAGACCA AGGAGGGCGT CCTCTACGTC
121 GGAAGCAAGA CCCGAGAAGG TGTGGTACAA GGTGTGGCTT CAGTGGCTGA AAAAACCAAG
181 GAACAGGCAT CACATCTGGG AGGAGCTGTG TTCTCTGGGG CAGGGAACAT CGCAGCAGCC
241 ACAGGACTGG TGAAGAGGGA GGAATTCCCT ACTGATCTGA AGCCAGAGGA AGTGGCCCAG
301 GAAGCTGCTG AAGAACCACT GATTGAGCCC CTGATGGAGC CAGAAGGGGA GAGTTATGAG
361 GACCCACCCC AGGAGGAATA TCAGGAGTAT GAGCCAGAGG CGTAG
```

20. Amino sequence of β-synuclein

```
1   MDVFMKGLSM AKEGVVAAAE KTKQGVTEAA EKTKEGVLYV GSKTREGVVQ GVASVAEKTK
61  EQASHLGGAV FSGAGNIAAA TGLVKREEFP TDLKPEEVAQ EAAEEPLIEP LMEPEGESYE
121 DPPQEEYQEY EPEA
```

21. Coding sequence of β-synuclein H65A

```
1   ATGGACGTGT TCATGAAGGG CCTGTCCATG GCCAAGGAGG GCGTTGTGGC AGCCGCGGAG
61  AAAACCAAGC AGGGGGTCAC CGAGGCGGCG GAGAAGACCA AGGAGGGCGT CCTCTACGTC
121 GGAAGCAAGA CCCGAGAAGG TGTGGTACAA GGTGTGGCTT CAGTGGCTGA AAAAACCAAG
181 GAACAGGCAT CAGCTCTGGG AGGAGCTGTG TTCTCTGGGG CAGGGAACAT CGCAGCAGCC
241 ACAGGACTGG TGAAGAGGGA GGAATTCCCT ACTGATCTGA AGCCAGAGGA AGTGGCCCAG
301 GAAGCTGCTG AAGAACCACT GATTGAGCCC CTGATGGAGC CAGAAGGGGA GAGTTATGAG
361 GACCCACCCC AGGAGGAATA TCAGGAGTAT GAGCCAGAGG CGTAG
```

22. Amino sequence of β-synuclein H65A

```
1   MDVFMKGLSM AKEGVVAAAE KTKQGVTEAA EKTKEGVLYV GSKTREGVVQ GVASVAEKTK
61  EQASALGGAV FSGAGNIAAA TGLVKREEFP TDLKPEEVAQ EAAEEPLIEP LMEPEGESYE
121 DPPQEEYQEY EPEA
```

23. Coding sequence of β-synuclein △1-9

```
1   ___________ ___________ _______ATG GCCAAGGAGG GCGTTGTGGC AGCCGCGGAG
61  AAAACCAAGC AGGGGGTCAC CGAGGCGGCG GAGAAGACCA AGGAGGGCGT CCTCTACGTC
121 GGAAGCAAGA CCCGAGAAGG TGTGGTACAA GGTGTGGCTT CAGTGGCTGA AAAAACCAAG
181 GAACAGGCAT CACATCTGGG AGGAGCTGTG TTCTCTGGGG CAGGGAACAT CGCAGCAGCC
241 ACAGGACTGG TGAAGAGGGA GGAATTCCCT ACTGATCTGA AGCCAGAGGA AGTGGCCCAG
301 GAAGCTGCTG AAGAACCACT GATTGAGCCC CTGATGGAGC CAGAAGGGGA GAGTTATGAG
361 GACCCACCCC AGGAGGAATA TCAGGAGTAT GAGCCAGAGG CGTAG
```

24. Amino sequence of β-synuclein △1-9

```
1   __________M AKEGVVAAAE KTKQGVTEAA EKTKEGVLYV GSKTREGVVQ GVASVAEKTK
61  EQASHLGGAV FSGAGNIAAA TGLVKREEFP TDLKPEEVAQ EAAEEPLIEP LMEPEGESYE
121 DPPQEEYQEY EPEA
```

25. Coding sequence of β-synuclein 10-100 H65A

```
1   ___________ ___________ ________ATG GCCAAGGAGG GCGTTGTGGC AGCCGCGGAG
61  AAAACCAAGC AGGGGGTCAC CGAGGCGGCG GAGAAGACCA AGGAGGGCGT CCTCTACGTC
121 GGAAGCAAGA CCCGAGAAGG TGTGGTACAA GGTGTGGCTT CAGTGGCTGA AAAAACCAAG
181 GAACAGGCAT CAGCTCTGGG AGGAGCTGTG TTCTCTGGGG CAGGGAACAT CGCAGCAGCC
241 ACAGGACTGG TGAAGAGGGA GGAATTCCCT ACTGATCTGA AGCCAGAGGA AGTGGCCCAG
301 TAGTAA
```

26. Amino sequence of β-synuclein 10-100 H65A

```
1   __________M AKEGVVAAAE KTKQGVTEAA EKTKEGVLYV GSKTREGVVQ GVASVAEKTK
61  EQASALGGAV FSGAGNIAAA TGLVKREEFP TDLKPEEVAQ
```

27. Coding sequence of γ-synuclein

```
1   ATGGATGTCT TCAAGAAGGG CTTCTCCATC GCCAAGGAGG GCGTGGTGGG TGCGGTGGAA
61  AAGACCAAGC AGGGGGTGAC GGAAGCAGCT GAGAAGACCA AGGAGGGGGT CATGTATGTG
121 GGAGCCAAGA CCAAGGAGAA TGTTGTACAG AGCGTGACCT CAGTGGCCGA GAAGACCAAG
181 GAGCAGGCCA ACGCGGTGAG CGAGGCTGTG GTGAGCAGCG TCAACACTGT GGCCACCAAG
241 ACCGTGGAGG AGGCGGAGAA CATCGCGGTC ACCTCCGGGG TGGTGCGCAA GGAGGACTTG
301 AGGCCATCTG CCCCCCAACA GGAGGGTGTG GCATCCAAAG AGAAAGAGGA AGTGGCAGAG
361 GAGGCCCAGA GTGGGGGAGA CTAG
```

28. Amino sequence of γ-synuclein

```
1   MDVFKKGFSI AKEGVVGAVE KTKQGVTEAA EKTKEGVMYV GAKTKENVVQ SVTSVAEKTK
61  EQANAVSEAV VSSVNTVATK TVEEAENIAV TSGVVRKEDL RPSAPQQEGV ASKEKEEVAE
121 EAQSGGD
```

Appendix B

1. pTrcHis vector map

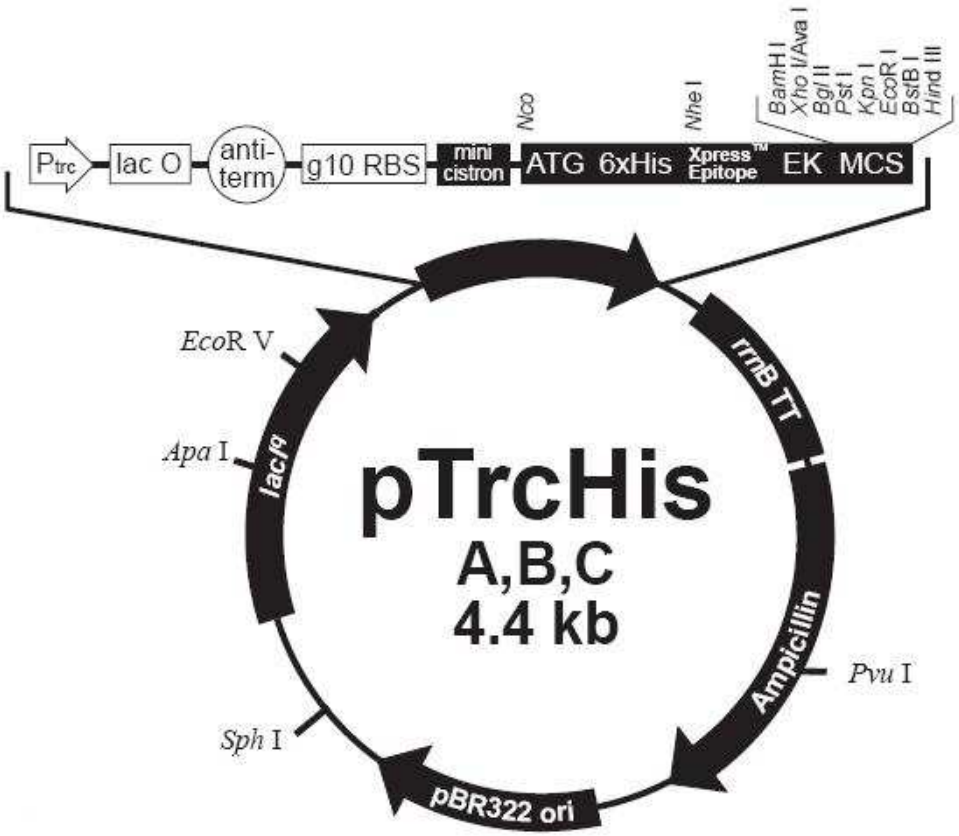

trc promoter: base 191-221

lac operator: base 228-248

Polyhistidine and enterokinase cleavage site: base 425-504

Xpress™ Epitope: base 482-505

Multiple cloning site: base 515-554

Ampicillin resistance ORF: base 1074-1934

Below is the multiple cloning site and EK cleavage site for pTrcHis A. Synclein is cloned between Xho I and Kpn I.

Amino sequence of $(His)_6$-aS

MGGSHHHHHHGMASMTGGQQMGRTLYDDDDKDRWGSE
MDVFMKGLSK AKEGVVAAAE KTKQGVAEAA GKTKEGVLYV GSKTKEGVVH
GVATVAEKTK EQVTNVGGAV VTGVTAVAQK TVEGAGSIAA ATGFVKKDQL
GKNEEGAPQE GILEDMPVDP DNEAYEMPSE EGYQDYEPEA

2. pET15b vector map

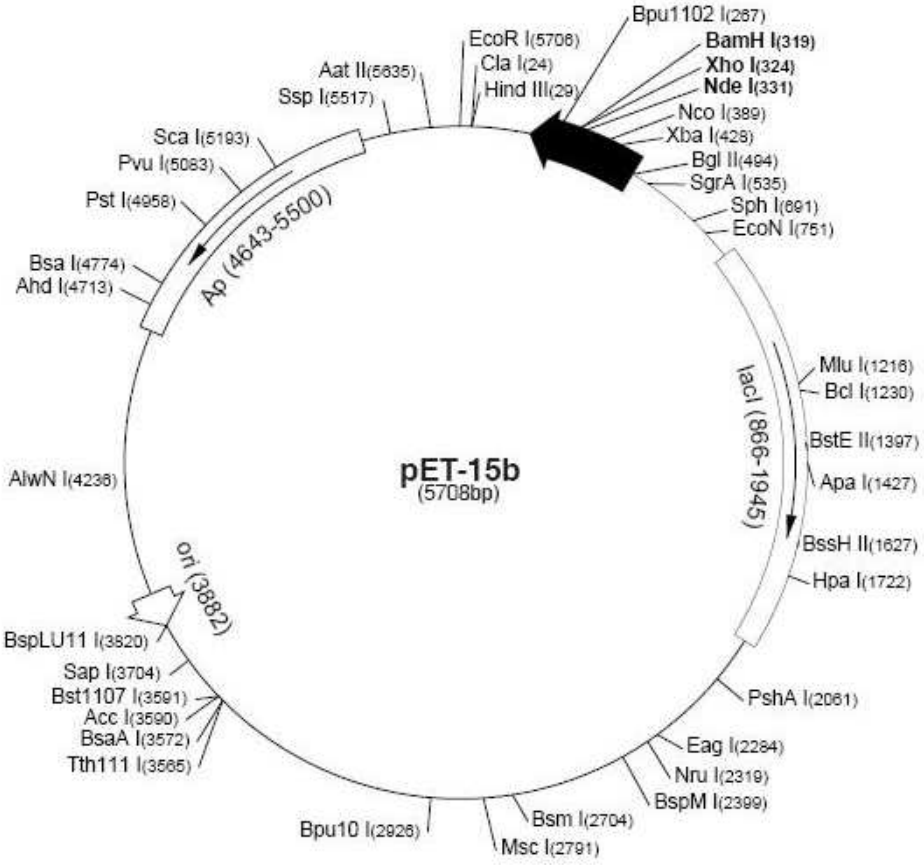

3. pET11a vector map

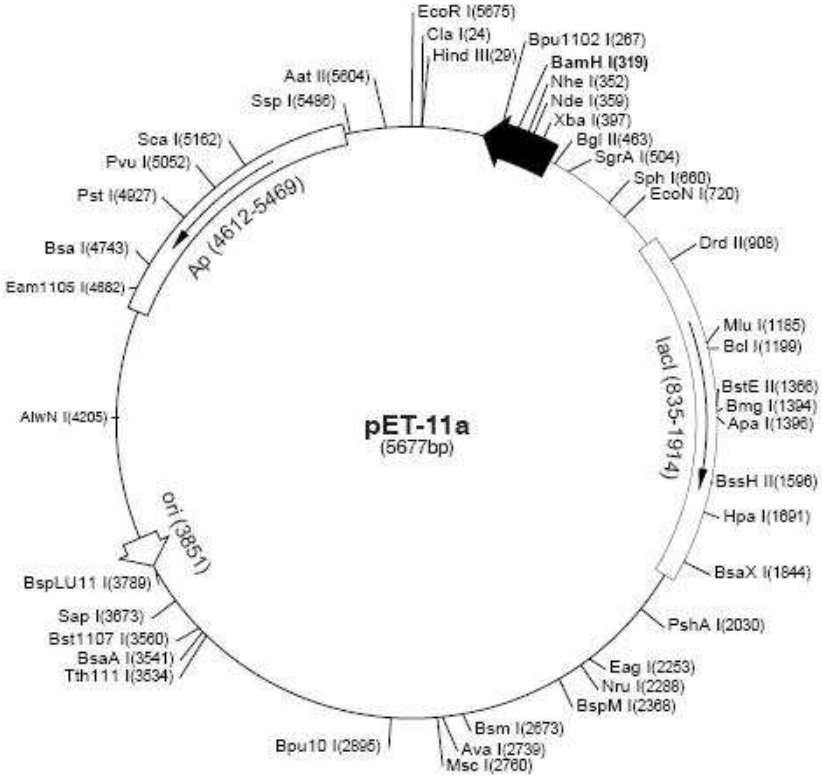

4. pET3a vector map

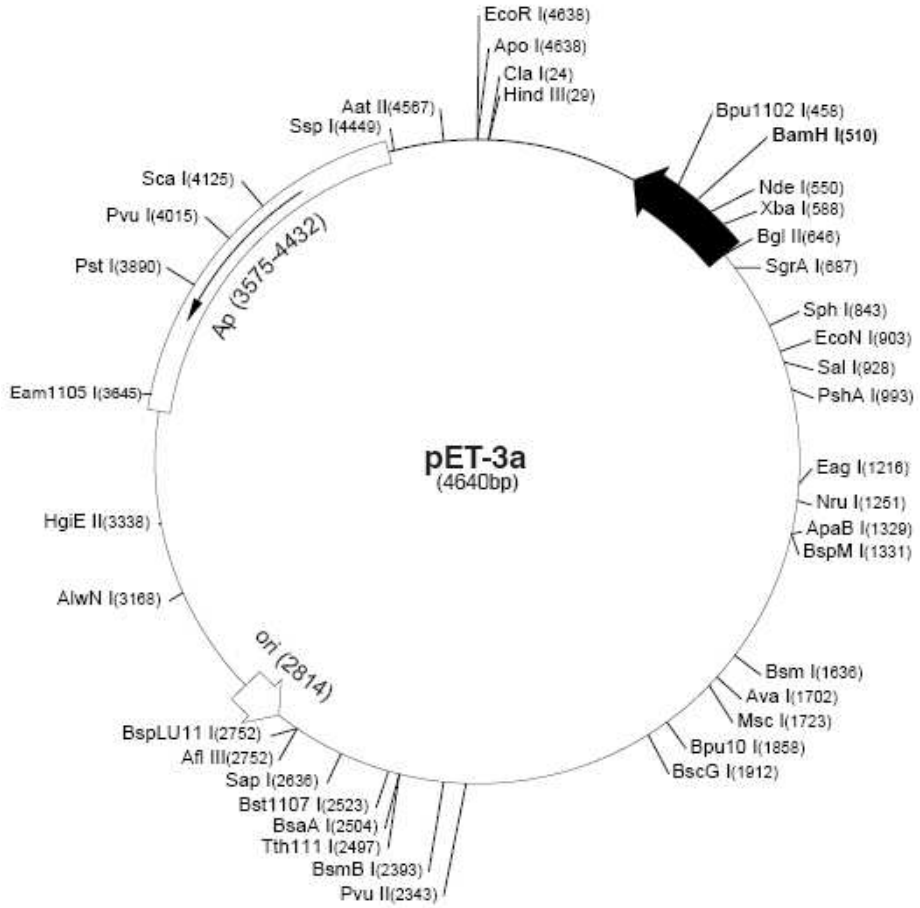

5. pCDNA3.1(-) vector map

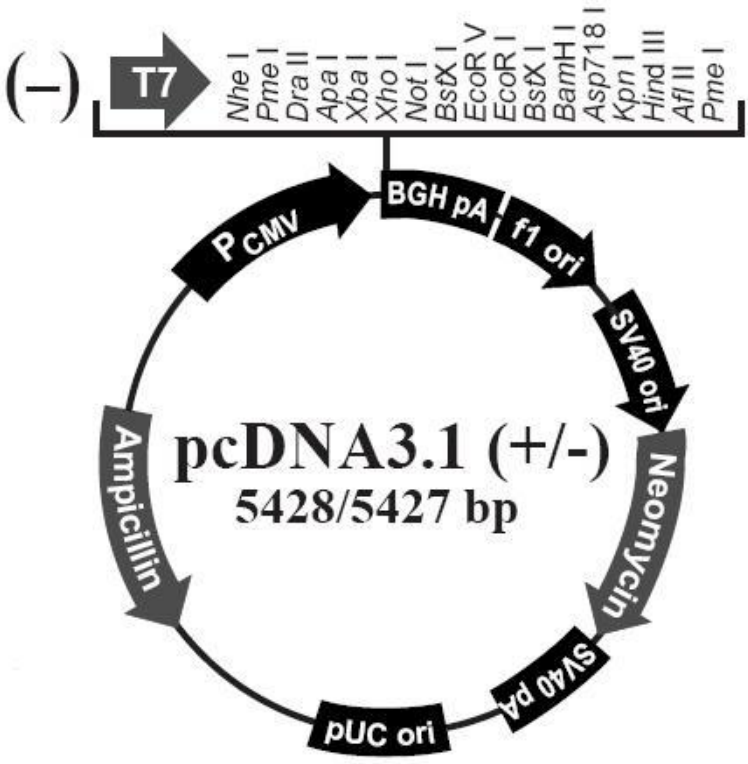

Appendix C

Confocal images

A: Immunofluorescence staining of SHSY5Y cells expressing pcDNA3.1(-) and aS, treated with six different conditions: nontreated media, chelex treated media (CM), CM+10μM $CuCl_2$, CM+300μM $CuCl_2$, CM+10μM $FeSO_4$ CM+300μM $FeSO_4$, for 48hours. aS was detected using the mouse primary aS antibodyB (Zymed Laboratories Inc.). Scale bar represents 10 μm.

B: Immunofluorescence staining of SHSY5Y cells expressing A30P, E46K and A53T aS, treated with six different conditions: nontreated media, chelex treated media (CM), CM+10μM $CuCl_2$, CM+300μM $CuCl_2$, CM+10μM $FeSO_4$ CM+300μM $FeSO_4$, for 48hours. aS was detected using the mouse primary aS antibodyB (Zymed Laboratories Inc.). Scale bar represents 10 μm.

C: Immunofluorescence staining of SHSY5Y cells expressing H50A aS, aS△1-9, and aS△1-9 H50A, treated with six different conditions: nontreated media, chelex treated media (CM), CM+10μM $CuCl_2$, CM+300μM $CuCl_2$, CM+10μM $FeSO_4$ CM+300μM $FeSO_4$, for 48hours. aS was detected using the mouse primary aS antibodyB (Zymed Laboratories Inc.). Scale bar represents 10 μm.

D: Immunofluorescence staining of SHSY5Y cells expressing aS1−100, aS10-100 H50A and pcDNA3.1(-), treated with six different conditions: nontreated media, chelex treated media (CM), CM+10μM $CuCl_2$, CM+300μM $CuCl_2$, CM+10μM $FeSO_4$ CM+300μM $FeSO_4$, for 48hours. aS was detected using the sheep primary aS antibodyA (abcam). Scale bar represents 10 μm.

A

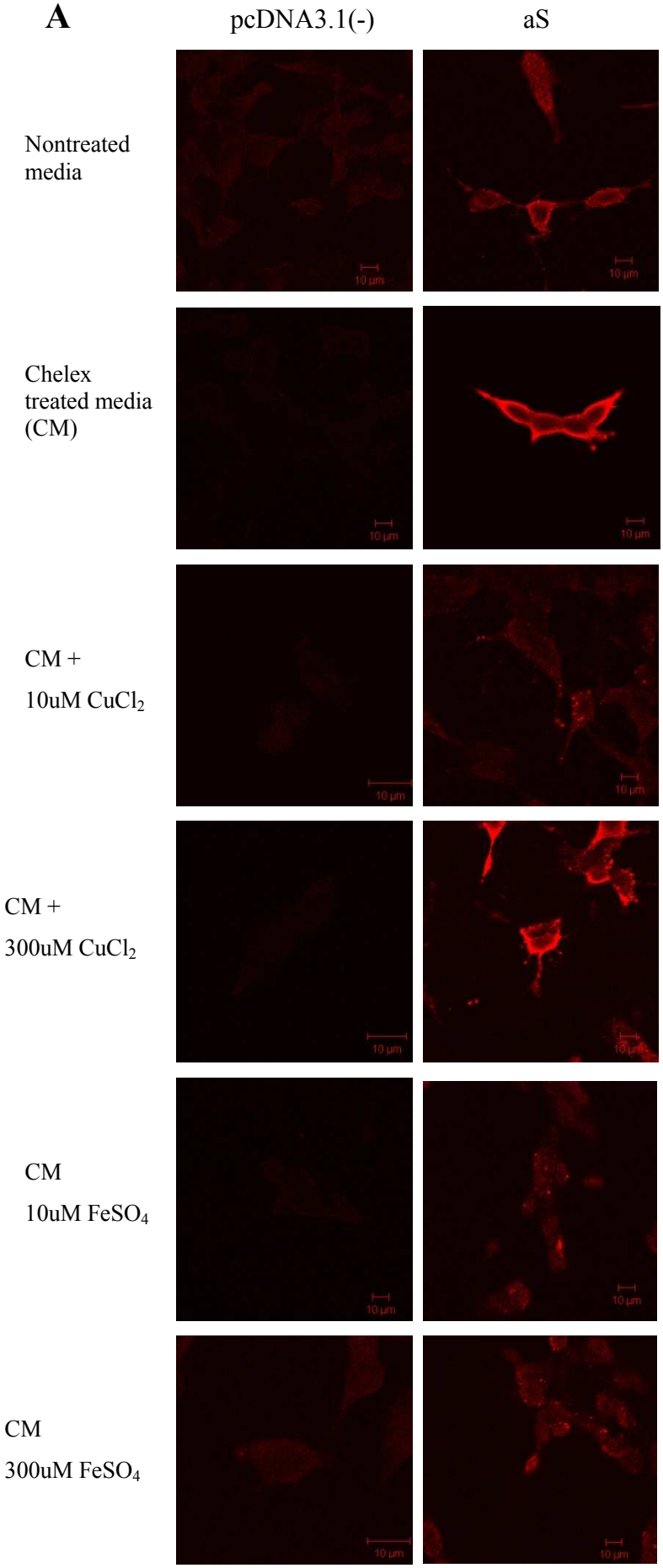
pcDNA3.1(-)
aS
Nontreated media
Chelex treated media (CM)
CM + 10uM $CuCl_2$
CM + 300uM $CuCl_2$
CM 10uM $FeSO_4$
CM 300uM $FeSO_4$
10 µm

B

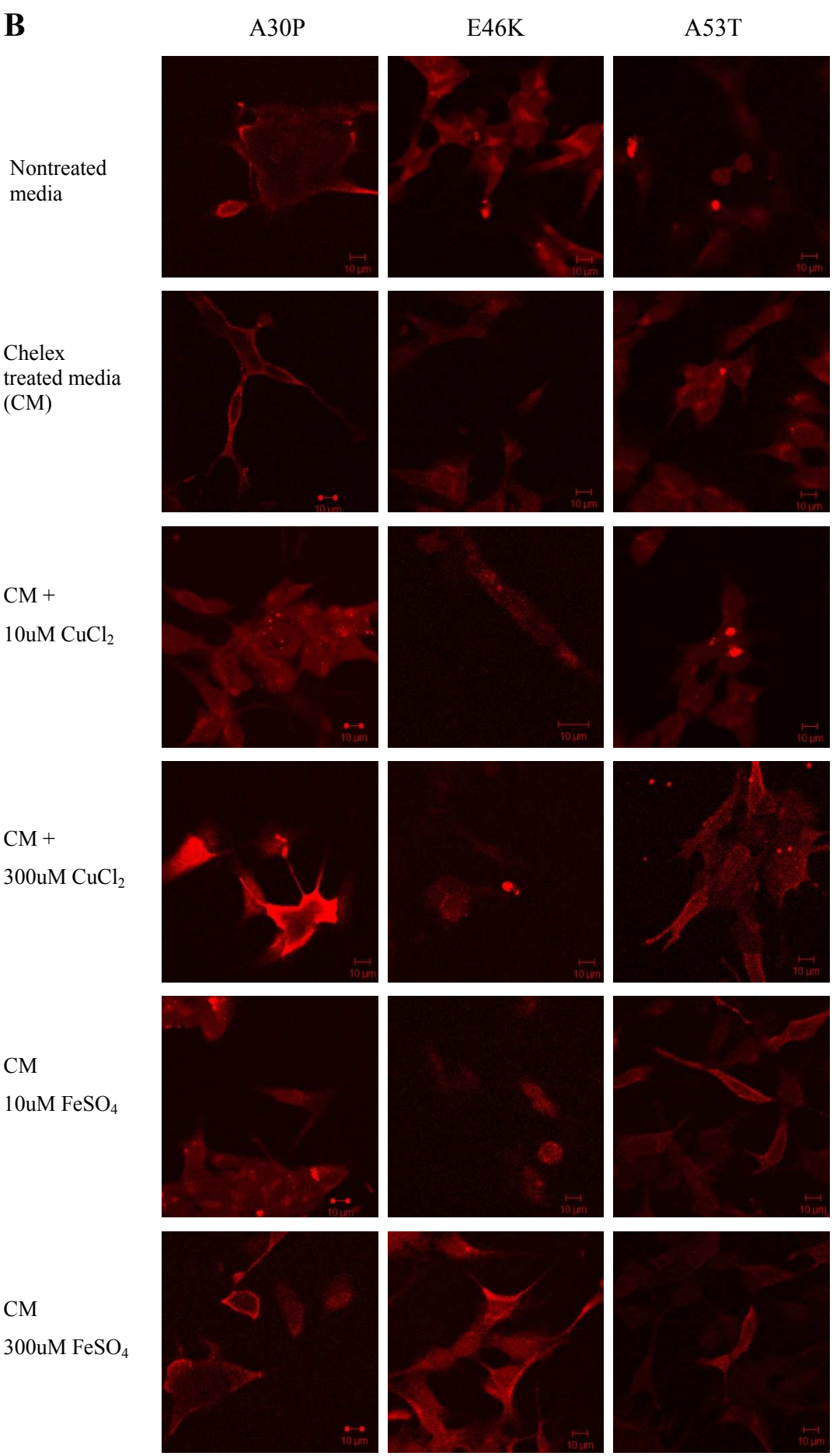
A30P
E46K
A53T
Nontreated media
Chelex treated media (CM)
CM + 10uM $CuCl_2$
CM + 300uM $CuCl_2$
CM 10uM $FeSO_4$
CM 300uM $FeSO_4$

C

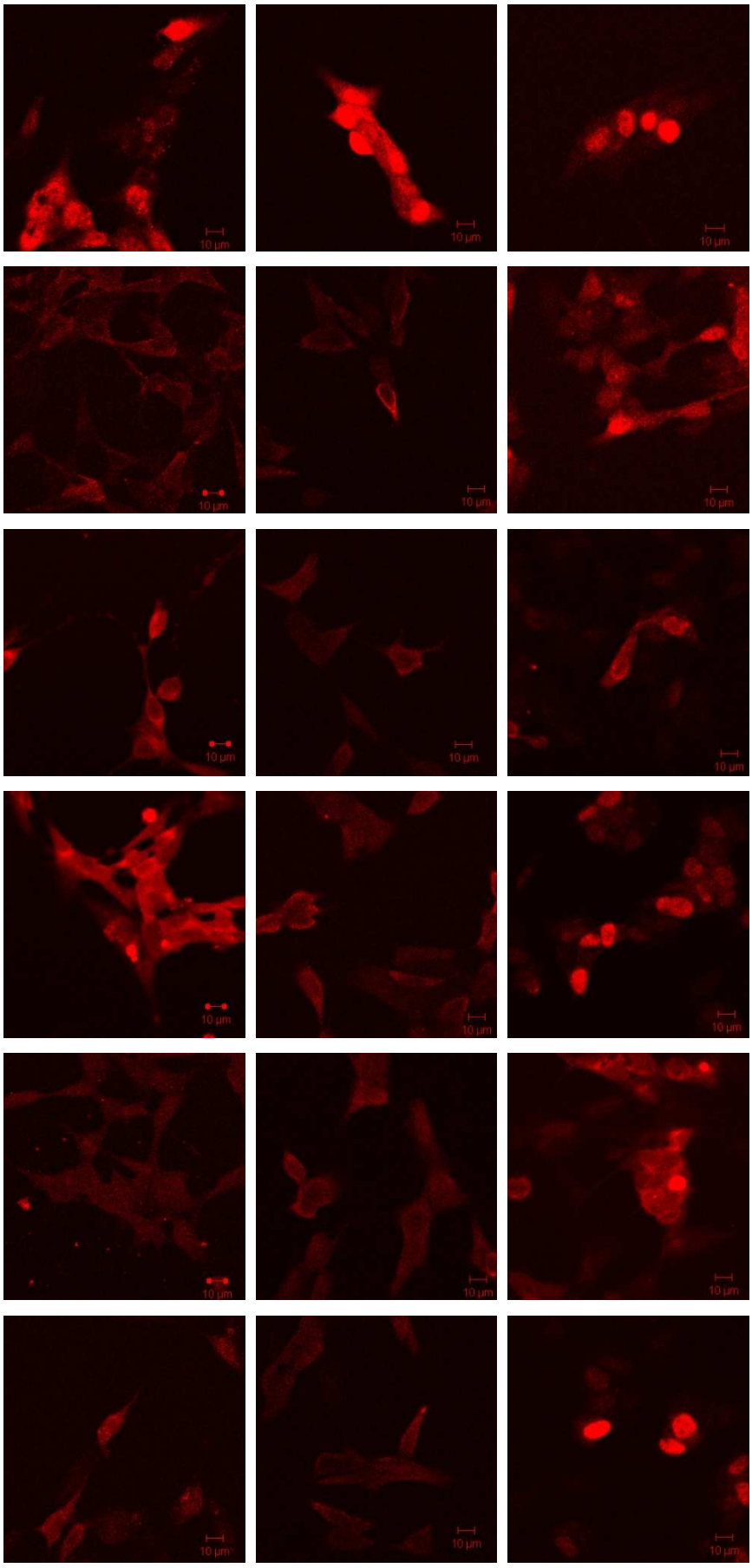
H50A
aS△1-9
aS△1-9 H50A
Nontreated media
Chelex treated media (CM)
CM + 10uM $CuCl_2$
CM + 300uM $CuCl_2$
CM 10uM $FeSO_4$
CM 300uM $FeSO_4$

D

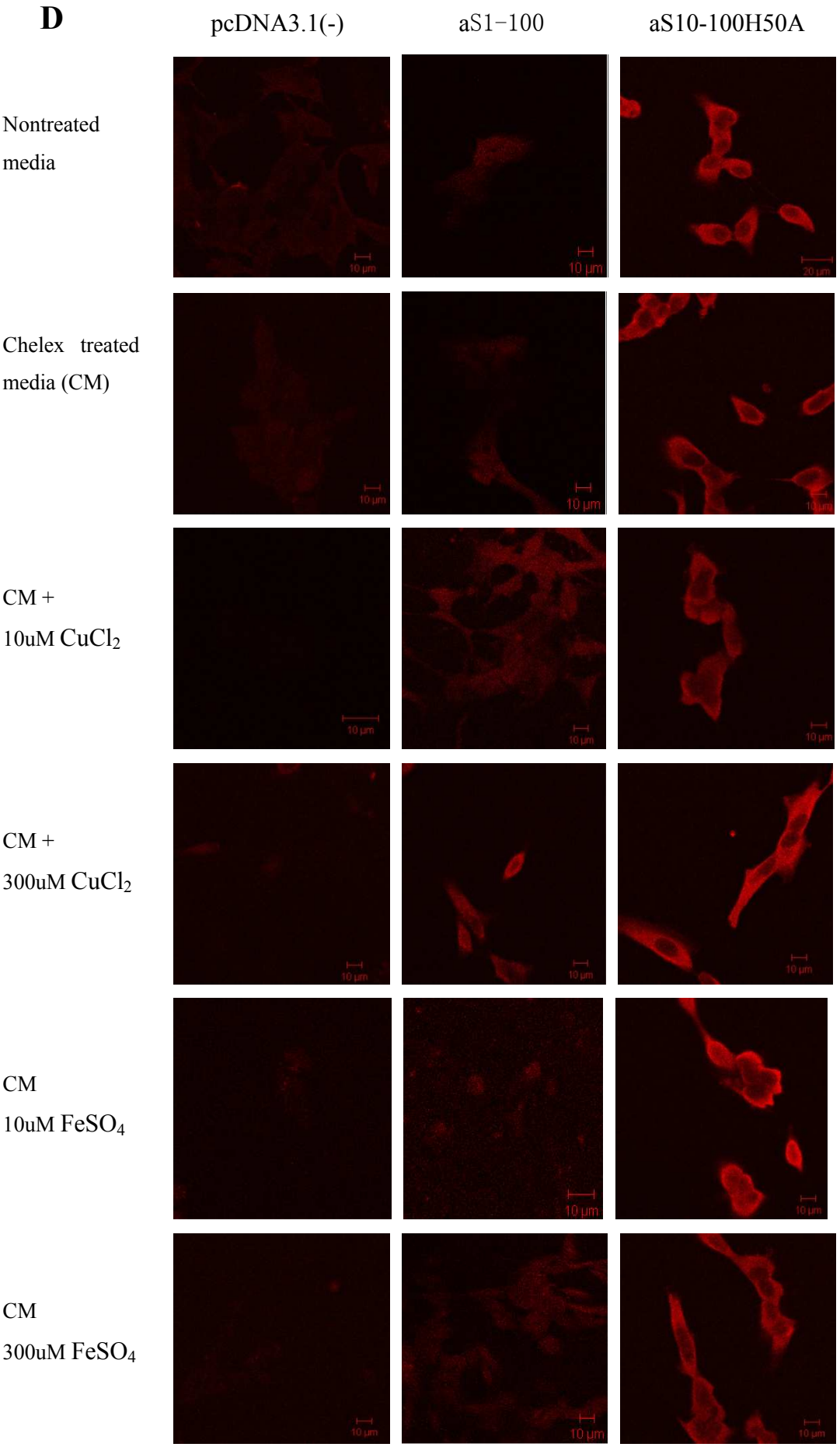
pcDNA3.1(-)
aS1−100
aS10-100H50A
Nontreated media
Chelex treated media (CM)
CM + 10uM $CuCl_2$
CM + 300uM $CuCl_2$
CM 10uM $FeSO_4$
CM 300uM $FeSO_4$

Appendix D

Programme for cation exchange column (2x5 ml HiTrap SP HP) chromatography

Volume (ml)	Buffer D (%)	Flow (ml/min)	Fraction (ml)	Buffer value	Injection value	Comment
0	0	5	-	Pos 1	Inject	Sample injected onto column
40	0	5	-	Pos 1	load	Wash column with buffer C
100	0→60	5	1	Pos 1	load	Gradient from buffer C→D
20	100	5	1	Pos 1	load	Wash column with buffer D
20	100	5	-	Pos 1	waste	End method

Programme for anion exchange column (2x5 ml HiTrap Q HP) chromatography

Volume (ml)	Buffer B (%)	Flow (ml/min)	Fraction (ml)	Buffer value	Injection value	Comment
0	0	5	-	Pos 1	Inject	Sample injected onto column
100	0	5	-	Pos 1	load	Wash column with buffer A
200	0→11	5	1	Pos 1	load	Gradient from buffer A→B
200	11	5	1	Pos 1	load	Wash column with buffer B
400	11→50	5	1	Pos 1	load	Gradient from buffer A→B
20	100	5	1	Pos 1	load	Wash column with buffer B
20	100	5	-	Pos 1	waste	End method

Appendix E

SDS-PAGE of purified synucleins

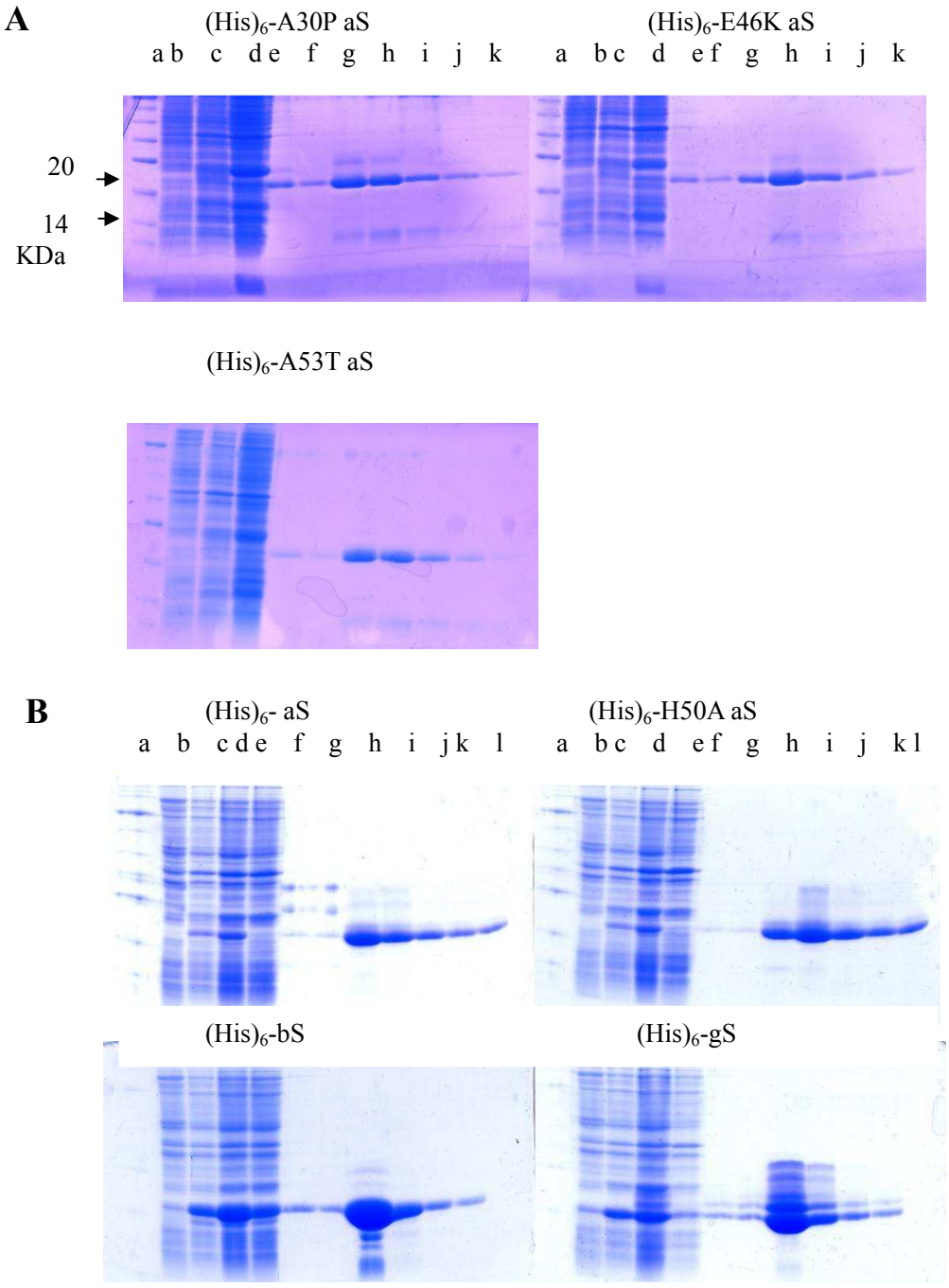

Purification of (His)$_6$-synucleins and their mutants in 12% SDS-PAGE gel.

A: Lane a, molecular weight standards (kDa); lane b and c, cellular proteins before and after (3hours) induction with IPTG; lane d, protein flow through the IMAC column; lane e, flow through column after 25 mM imidazole wash; lane f-k, fractions eluted with 100 mM imidazole.

B: Lane a, molecular weight standards (kDa); lane b and c, cellular proteins before and after (3hours) induction with IPTG; lane d, soluble proteins in urea buffer; lane e, protein flow through the IMAC column; lane f, flow through column after 25 mM imidazole wash; lane g-l, fractions eluted with 100 mM imidazole for $(His)_6$-aS and $(His)_6$-H50A aS, 300 mM imidazole for $(His)_6$-bS and $(His)_6$-gS.

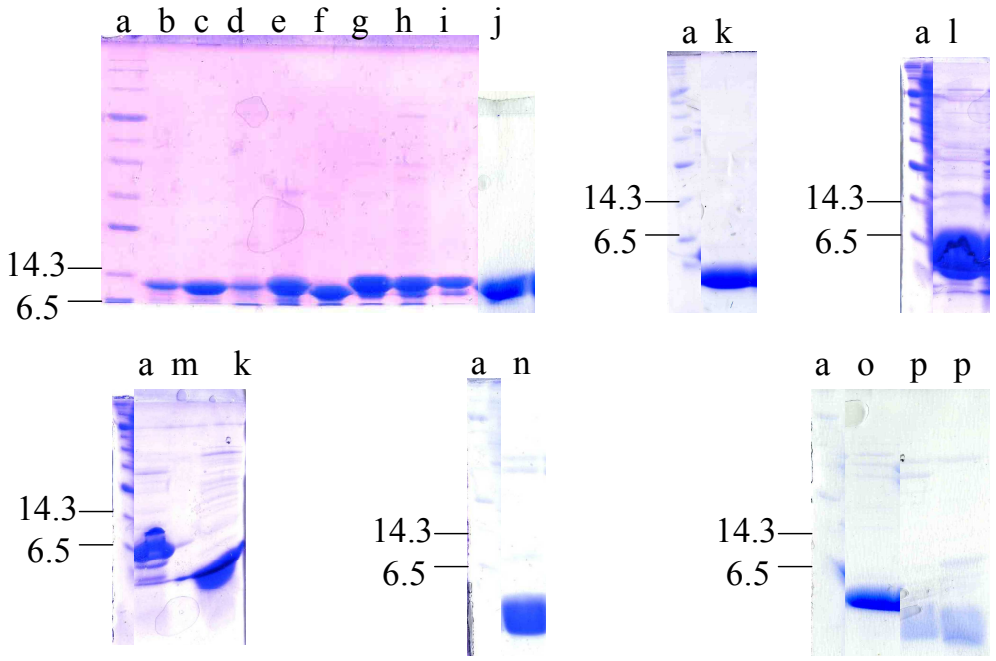

Purified synucleins and their mutants analyzed in 12% SDS-PAGE. Lane a, molecular weight standards (kDa); lane b, aS as control; lane c-p, aS, H50A aS, aS△1-9, aS△1-9 H50A, bS, H65A bS, gS, aS△119-126, bS10-100 H65A, bS△1-9, bS△1-9 H65A, aS1-100, aS△1-9 H50A △119-126, aS10-100 H50A.

Protein	Theoretical isoelectric point (pI)
aS	4.67
H50A aS	4.59
aS△1-9	4.65
aS△1-9 H50A	4.57
aS△119-126	4.98
aS△1-9 H50A aS△119-126	4.85
aS1-100	9.40
aS10-100 H50A	9.44
bS	4.41
H65A bS	4.35
bS△1-9	4.40
bS△1-9 H65A	4.33
bS10-100 H65A	5.50
gS	4.97

Isoelectric points of synuclein proteins, calculated from the amino acid sequences according to http://www.expasy.org/tools/protparam.html

Appendix F

Distribution of charge on aS

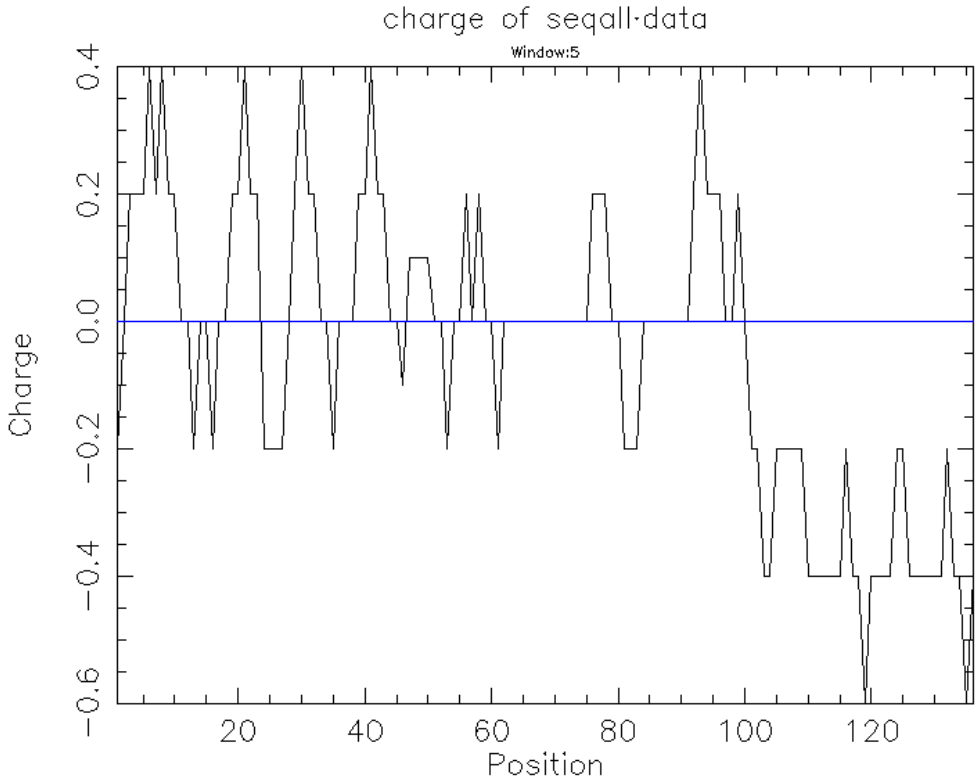

Distribution of charge on bS

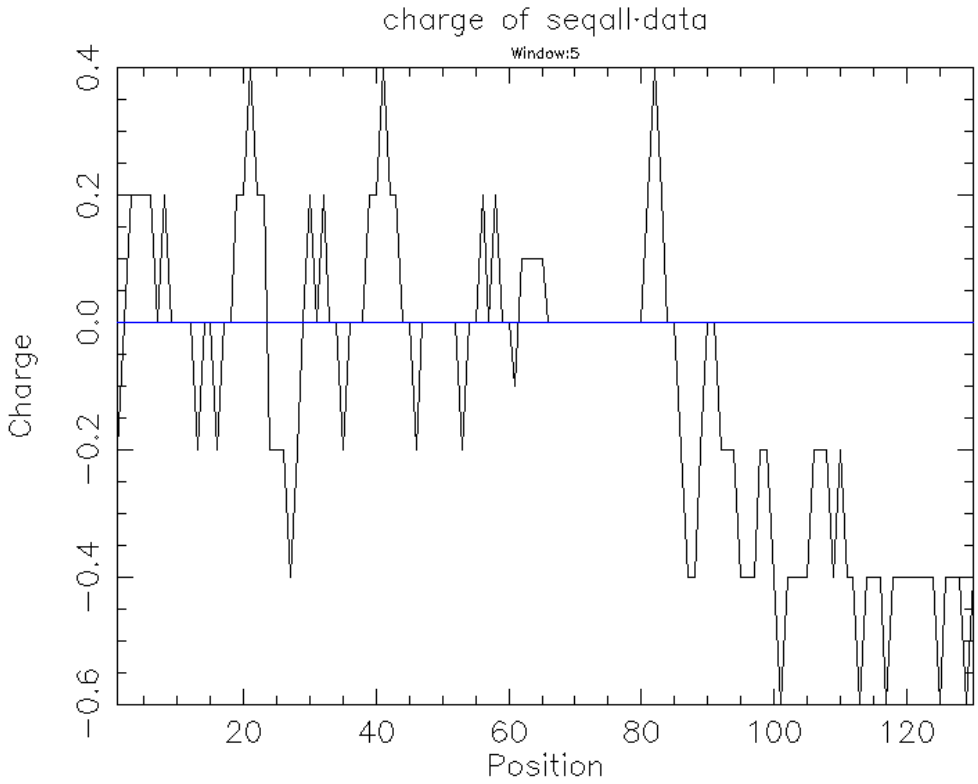

Distribution of charge on gS

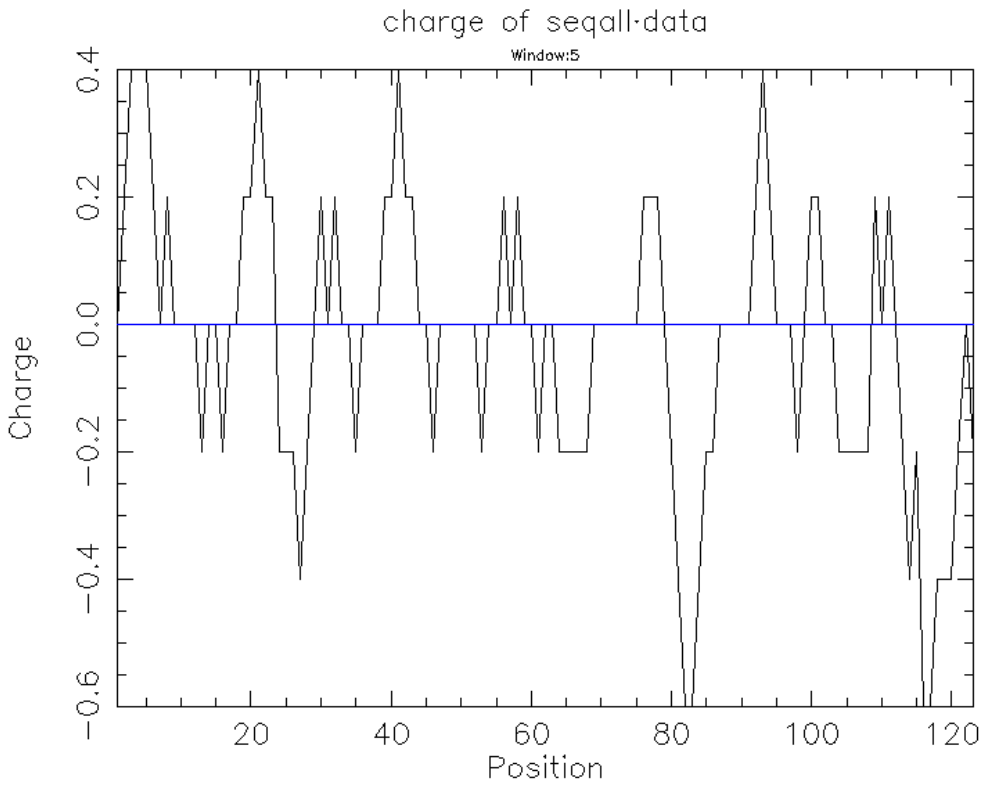

Plot of the peak current versus the scan rate for aS10-100 H50A-Cu.

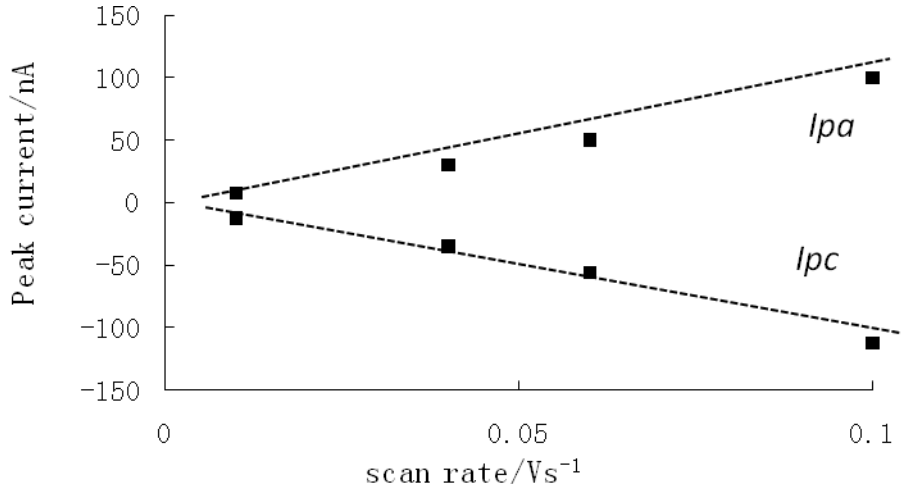

References

Abeliovich, A., Y. Schmitz, et al. (2000). "Mice lacking alpha-synuclein display functional deficits in the nigrostriatal dopamine system." Neuron **25**(1): 239-52.

Adlard, P. A., R. A. Cherny, et al. (2008). "Rapid restoration of cognition in Alzheimer's transgenic mice with 8-hydroxy quinoline analogs is associated with decreased interstitial Abeta." Neuron **59**(1): 43-55.

Ahn, M., S. Kim, et al. (2006). "Chaperone-like activities of alpha-synuclein: alpha-synuclein assists enzyme activities of esterases." Biochem Biophys Res Commun **346**(4): 1142-9.

Atwood, C. S., R. D. Moir, et al. (1998). "Dramatic aggregation of Alzheimer abeta by Cu(II) is induced by conditions representing physiological acidosis." J Biol Chem **273**(21): 12817-26.

Baba, M., S. Nakajo, et al. (1998). "Aggregation of alpha-synuclein in Lewy bodies of sporadic Parkinson's disease and dementia with Lewy bodies." Am J Pathol **152**(4): 879-84.

Bertoncini, C. W., Y. S. Jung, et al. (2005). "Release of long-range tertiary interactions potentiates aggregation of natively unstructured alpha-synuclein." Proc Natl Acad Sci U S A **102**(5): 1430-5.

Bertoncini, C. W., R. M. Rasia, et al. (2007). "Structural characterization of the intrinsically unfolded protein beta-synuclein, a natural negative regulator of alpha-synuclein aggregation." J Mol Biol **372**(3): 708-22.

Beyer, K. (2006). "Alpha-synuclein structure, posttranslational modification and alternative splicing as aggregation enhancers." Acta Neuropathol (Berl) **112**(3): 237-51.

Beyer, K. (2006). "Alpha-synuclein structure, posttranslational modification and alternative splicing as aggregation enhancers." Acta Neuropathol **112**(3): 237-51.

Beyer, K., M. Domingo-Sabat, et al. (2008). "Identification and characterization of a new alpha-synuclein isoform and its role in Lewy body diseases." Neurogenetics **9**(1): 15-23.

Beyer, K., J. I. Lao, et al. (2004). "Differential expression of alpha-synuclein isoforms in dementia with Lewy bodies." Neuropathol Appl Neurobiol **30**(6): 601-7.

Bharathi and K. S. Rao (2007). "Thermodynamics imprinting reveals differential binding of metals to alpha-synuclein: relevance to Parkinson's disease." Biochem Biophys Res Commun **359**(1): 115-20.

Bharathi and K. S. Rao (2008). "Molecular understanding of copper and iron interaction with alpha-synuclein by fluorescence analysis." J Mol Neurosci **35**(3): 273-81.

Bhatia, R., H. Lin, et al. (2000). "Fresh and globular amyloid beta protein (1-42) induces rapid cellular degeneration: evidence for AbetaP channel-mediated cellular toxicity." Faseb J **14**(9): 1233-43.

Biere, A. L., S. J. Wood, et al. (2000). "Parkinson's disease-associated alpha-synuclein is more fibrillogenic than beta- and gamma-synuclein and cannot cross-seed its homologs." J Biol Chem **275**(44): 34574-9.

Binolfi, A., G. R. Lamberto, et al. (2008). "Site-specific interactions of Cu(II) with alpha and beta-synuclein: bridging the molecular gap between metal binding and aggregation." J Am Chem Soc **130**(35): 11801-12.

Binolfi, A., R. M. Rasia, et al. (2006). "Interaction of alpha-synuclein with divalent metal ions reveals key differences: a link between structure, binding specificity and fibrillation enhancement." J Am Chem Soc **128**(30): 9893-901.

Bisaglia, M., A. Trolio, et al. (2005). "Cloning, expression, purification, and spectroscopic analysis of the fragment 57-102 of human alpha-synuclein." Protein Expr Purif **39**(1): 90-6.

Bodles, A. M., D. J. Guthrie, et al. (2001). "Identification of the region of non-Abeta component (NAC) of Alzheimer's disease amyloid responsible for its aggregation and toxicity." J Neurochem **78**(2): 384-95.

Bonifati, V. (2005). "Genetics of Parkinson's disease." Minerva Med **96**(3): 175-86.

Borghi, R., R. Marchese, et al. (2000). "Full length alpha-synuclein is present in cerebrospinal fluid from Parkinson's disease and normal subjects." Neurosci Lett **287**(1): 65-7.

Brighina, L., N. U. Okubadejo, et al. (2007). "Beta-synuclein gene variants and Parkinson's disease: a preliminary case-control study." Neurosci Lett **420**(3): 229-34.

Bruschi, M., L. De Gioia, et al. (2008). "A DFT study of EPR parameters in Cu(II) complexes of the octarepeat region of the prion protein." Phys Chem Chem Phys **10**(31): 4573-83.

Buchman, V. L., H. J. Hunter, et al. (1998). "Persyn, a member of the synuclein family, has a distinct pattern of expression in the developing nervous system." J Neurosci **18**(22): 9335-41.

Bussell, R., Jr. and D. Eliezer (2001). "Residual structure and dynamics in Parkinson's disease-associated mutants of alpha-synuclein." J Biol Chem **276**(49): 45996-6003.

Bussell, R., Jr. and D. Eliezer (2003). "A structural and functional role for 11-mer

repeats in alpha-synuclein and other exchangeable lipid binding proteins." J Mol Biol **329**(4): 763-78.

Bussell, R., Jr., T. F. Ramlall, et al. (2005). "Helix periodicity, topology, and dynamics of membrane-associated alpha-synuclein." Protein Sci **14**(4): 862-72.

Chandra, S., G. Gallardo, et al. (2005). "Alpha-synuclein cooperates with CSPalpha in preventing neurodegeneration." Cell **123**(3): 383-96.

Chen, X., H. A. de Silva, et al. (1995). "The human NACP/alpha-synuclein gene: chromosome assignment to 4q21.3-q22 and TaqI RFLP analysis." Genomics **26**(2): 425-7.

Choi, J. Y., Y. M. Sung, et al. (2002). "Rapid purification and analysis of alpha-synuclein proteins: C-terminal truncation promotes the conversion of alpha-synuclein into a protease-sensitive form in Escherichia coli." Biotechnol Appl Biochem **36**(Pt 1): 33-40.

Clayton, D. F. and J. M. George (1998). "The synucleins: a family of proteins involved in synaptic function, plasticity, neurodegeneration and disease." Trends Neurosci **21**(6): 249-54.

Cole, N. B., D. Dieuliis, et al. (2008). "Mitochondrial translocation of alpha-synuclein is promoted by intracellular acidification." Exp Cell Res **314**(10): 2076-89.

Cole, N. B., D. D. Murphy, et al. (2005). "Metal-catalyzed oxidation of alpha-synuclein: helping to define the relationship between oligomers, protofibrils, and filaments." J Biol Chem **280**(10): 9678-90.

Conway, K. A., J. D. Harper, et al. (1998). "Accelerated in vitro fibril formation by a mutant alpha-synuclein linked to early-onset Parkinson disease." Nat Med **4**(11): 1318-20.

Cookson, M. R. and M. van der Brug (2007). "Cell systems and the toxic mechanism(s) of alpha-synuclein." Exp Neurol.

Cookson, M. R. and M. van der Brug (2008). "Cell systems and the toxic mechanism(s) of alpha-synuclein." Exp Neurol **209**(1): 5-11.

Crowther, R. A., R. Jakes, et al. (1998). "Synthetic filaments assembled from C-terminally truncated alpha-synuclein." FEBS Lett **436**(3): 309-12.

da Costa, C. A., E. Masliah, et al. (2003). "Beta-synuclein displays an antiapoptotic p53-dependent phenotype and protects neurons from 6-hydroxydopamine-induced caspase 3 activation: cross-talk with alpha-synuclein and implication for Parkinson's disease." J Biol Chem **278**(39): 37330-5.

Danzer, K. M., D. Haasen, et al. (2007). "Different species of alpha-synuclein oligomers induce calcium influx and seeding." J Neurosci **27**(34): 9220-32.

Danzer, K. M., C. Schnack, et al. (2007). "Functional protein kinase arrays reveal inhibition of p-21-activated kinase 4 by alpha-synuclein oligomers." J Neurochem.

Davidson, W. S., A. Jonas, et al. (1998). "Stabilization of alpha-synuclein secondary structure upon binding to synthetic membranes." J Biol Chem **273**(16): 9443-9.

Davies, P., F. Marken, et al. (2009). "Thermodynamic and voltammetric characterization of the metal binding to the prion protein: insights into pH dependence and redox chemistry." Biochemistry **48**(12): 2610-9.

Del Mar, C., E. A. Greenbaum, et al. (2005). "Structure and properties of alpha-synuclein and other amyloids determined at the amino acid level." Proc Natl Acad Sci U S A **102**(43): 15477-82.

Dev, K. K., K. Hofele, et al. (2003). "Part II: alpha-synuclein and its molecular pathophysiological role in neurodegenerative disease." Neuropharmacology **45**(1): 14-44.

Dexter, D. T., A. Carayon, et al. (1991). "Alterations in the levels of iron, ferritin and other trace metals in Parkinson's disease and other neurodegenerative diseases affecting the basal ganglia." Brain **114 (Pt 4)**: 1953-75.

Dexter, D. T., F. R. Wells, et al. (1989). "Increased nigral iron content and alterations in other metal ions occurring in brain in Parkinson's disease." J Neurochem **52**(6): 1830-6.

Drew, S. C., S. L. Leong, et al. (2008). "Cu2+ binding modes of recombinant alpha-synuclein--insights from EPR spectroscopy." J Am Chem Soc **130**(24): 7766-73.

El-Agnaf, O. M., A. M. Bodles, et al. (1998). "The N-terminal region of non-A beta component of Alzheimer's disease amyloid is responsible for its tendency to assume beta-sheet and aggregate to form fibrils." Eur J Biochem **258**(1): 157-63.

El-Agnaf, O. M. and G. B. Irvine (2000). "Review: formation and properties of amyloid-like fibrils derived from alpha-synuclein and related proteins." J Struct Biol **130**(2-3): 300-9.

el-Agnaf, O. M. and G. B. Irvine (2002). "Aggregation and neurotoxicity of alpha-synuclein and related peptides." Biochem Soc Trans **30**(4): 559-65.

El-Agnaf, O. M., R. Jakes, et al. (1998). "Aggregates from mutant and wild-type alpha-synuclein proteins and NAC peptide induce apoptotic cell death in human neuroblastoma cells by formation of beta-sheet and amyloid-like filaments." FEBS Lett **440**(1-2): 71-5.

El-Agnaf, O. M., R. Jakes, et al. (1998). "Effects of the mutations Ala30 to Pro and Ala53 to Thr on the physical and morphological properties of alpha-synuclein protein implicated in Parkinson's disease." FEBS Lett **440**(1-2): 67-70.

El-Agnaf, O. M., S. A. Salem, et al. (2006). "Detection of oligomeric forms of alpha-synuclein protein in human plasma as a potential biomarker for Parkinson's disease." Faseb J **20**(3): 419-25.

Eliezer, D., E. Kutluay, et al. (2001). "Conformational properties of alpha-synuclein in its free and lipid-associated states." J Mol Biol **307**(4): 1061-73.

Eriksen, J. L., Z. Wszolek, et al. (2005). "Molecular pathogenesis of Parkinson disease." Arch Neurol **62**(3): 353-7.

Feany, M. B. and W. W. Bender (2000). "A Drosophila model of Parkinson's disease." Nature **404**(6776): 394-8.

Ferreon, A. C. and A. A. Deniz (2007). "Alpha-synuclein multistate folding thermodynamics: implications for protein misfolding and aggregation." Biochemistry **46**(15): 4499-509.

Fujiwara, H., M. Hasegawa, et al. (2002). "alpha-Synuclein is phosphorylated in synucleinopathy lesions." Nat Cell Biol **4**(2): 160-4.

Furukawa, K., M. Matsuzaki-Kobayashi, et al. (2006). "Plasma membrane ion permeability induced by mutant alpha-synuclein contributes to the degeneration of neural cells." J Neurochem **97**(4): 1071-7.

Gaeta, A. and R. C. Hider (2005). "The crucial role of metal ions in neurodegeneration: the basis for a promising therapeutic strategy." Br J Pharmacol **146**(8): 1041-59.

Gaggelli, E., E. Jankowska, et al. (2008). "Structural characterization of the intra- and inter-repeat copper binding modes within the N-terminal region of "prion related protein" (PrP-rel-2) of zebrafish." J Phys Chem B **112**(47): 15140-50.

Gai, W. P., J. H. Power, et al. (1999). "Alpha-synuclein immunoisolation of glial inclusions from multiple system atrophy brain tissue reveals multiprotein components." J Neurochem **73**(5): 2093-100.

George, J. M., H. Jin, et al. (1995). "Characterization of a novel protein regulated during the critical period for song learning in the zebra finch." Neuron **15**(2): 361-72.

Giasson, B. I., J. E. Duda, et al. (2000). "Oxidative damage linked to neurodegeneration by selective alpha-synuclein nitration in synucleinopathy lesions." Science **290**(5493): 985-9.

Giasson, B. I., I. V. Murray, et al. (2001). "A hydrophobic stretch of 12 amino acid residues in the middle of alpha-synuclein is essential for filament assembly." J Biol Chem **276**(4): 2380-6.

Giasson, B. I., K. Uryu, et al. (1999). "Mutant and wild type human alpha-synucleins assemble into elongated filaments with distinct morphologies in vitro." J Biol Chem

274(12): 7619-22.

Goedert, M. (1999). "Filamentous nerve cell inclusions in neurodegenerative diseases: tauopathies and alpha-synucleinopathies." Philos Trans R Soc Lond B Biol Sci **354**(1386): 1101-18.

Goedert, M. (2001). "Alpha-synuclein and neurodegenerative diseases." Nat Rev Neurosci **2**(7): 492-501.

Goers, J., A. B. Manning-Bog, et al. (2003). "Nuclear localization of alpha-synuclein and its interaction with histones." Biochemistry **42**(28): 8465-71.

Golts, N., H. Snyder, et al. (2002). "Magnesium inhibits spontaneous and iron-induced aggregation of alpha-synuclein." J Biol Chem **277**(18): 16116-23.

Gralka, E., D. Valensin, et al. (2008). "CuII binding sites located at His-96 and His-111 of the human prion protein: thermodynamic and spectroscopic studies on model peptides." Dalton Trans(38): 5207-19.

Greenbaum, E. A., C. L. Graves, et al. (2005). "The E46K mutation in alpha-synuclein increases amyloid fibril formation." J Biol Chem **280**(9): 7800-7.

Halliwell, B. and J. M. Gutteridge (1986). "Oxygen free radicals and iron in relation to biology and medicine: some problems and concepts." Arch Biochem Biophys **246**(2): 501-14.

Han, H., P. H. Weinreb, et al. (1995). "The core Alzheimer's peptide NAC forms amyloid fibrils which seed and are seeded by beta-amyloid: is NAC a common trigger or target in neurodegenerative disease?" Chem Biol **2**(3): 163-9.

Hashimoto, M., P. Bar-On, et al. (2004). "Beta-synuclein regulates Akt activity in neuronal cells. A possible mechanism for neuroprotection in Parkinson's disease." J Biol Chem **279**(22): 23622-9.

Hashimoto, M., L. J. Hsu, et al. (2002). "alpha-Synuclein protects against oxidative stress via inactivation of the c-Jun N-terminal kinase stress-signaling pathway in neuronal cells." J Biol Chem **277**(13): 11465-72.

Hashimoto, M., L. J. Hsu, et al. (1998). "Human recombinant NACP/alpha-synuclein is aggregated and fibrillated in vitro: relevance for Lewy body disease." Brain Res **799**(2): 301-6.

Hashimoto, M., L. J. Hsu, et al. (1999). "Oxidative stress induces amyloid-like aggregate formation of NACP/alpha-synuclein in vitro." Neuroreport **10**(4): 717-21.

Hashimoto, M., E. Rockenstein, et al. (2001). "beta-Synuclein inhibits alpha-synuclein aggregation: a possible role as an anti-parkinsonian factor." Neuron **32**(2): 213-23.

Hashimoto, M., A. Takeda, et al. (1999). "Role of cytochrome c as a stimulator of

alpha-synuclein aggregation in Lewy body disease." J Biol Chem **274**(41): 28849-52.

Hashimoto, M., T. Takenouchi, et al. (2003). "Alpha-synuclein up-regulates expression of caveolin-1 and down-regulates extracellular signal-regulated kinase activity in B103 neuroblastoma cells: role in the pathogenesis of Parkinson's disease." J Neurochem **85**(6): 1468-79.

Hashimoto, M., M. Yoshimoto, et al. (1997). "NACP, a synaptic protein involved in Alzheimer's disease, is differentially regulated during megakaryocyte differentiation." Biochem Biophys Res Commun **237**(3): 611-6.

Hayashita-Kinoh, H., M. Yamada, et al. (2006). "Down-regulation of alpha-synuclein expression can rescue dopaminergic cells from cell death in the substantia nigra of Parkinson's disease rat model." Biochem Biophys Res Commun **341**(4): 1088-95.

Hegde, M. L., P. Shanmugavelu, et al. (2004). "Serum trace element levels and the complexity of inter-element relations in patients with Parkinson's disease." J Trace Elem Med Biol **18**(2): 163-71.

Hirsch, E. C., J. P. Brandel, et al. (1991). "Iron and aluminum increase in the substantia nigra of patients with Parkinson's disease: an X-ray microanalysis." J Neurochem **56**(2): 446-51.

Hoyer, W., T. Antony, et al. (2002). "Dependence of alpha-synuclein aggregate morphology on solution conditions." J Mol Biol **322**(2): 383-93.

Iwai, A., E. Masliah, et al. (1995). "The precursor protein of non-A beta component of Alzheimer's disease amyloid is a presynaptic protein of the central nervous system." Neuron **14**(2): 467-75.

Iwata, A., M. Maruyama, et al. (2001). "alpha-Synuclein affects the MAPK pathway and accelerates cell death." J Biol Chem **276**(48): 45320-9.

Jakes, R., M. G. Spillantini, et al. (1994). "Identification of two distinct synucleins from human brain." FEBS Lett **345**(1): 27-32.

Jeannotte, A. M. and A. Sidhu (2007). "Regulation of the norepinephrine transporter by alpha-synuclein-mediated interactions with microtubules." Eur J Neurosci **26**(6): 1509-20.

Jellinger, K. A. (2003). "General aspects of neurodegeneration." J Neural Transm Suppl(65): 101-44.

Jenco, J. M., A. Rawlingson, et al. (1998). "Regulation of phospholipase D2: selective inhibition of mammalian phospholipase D isoenzymes by alpha- and beta-synucleins." Biochemistry **37**(14): 4901-9.

Jensen, P. H., P. Hojrup, et al. (1997). "Binding of Abeta to alpha- and beta-synucleins: identification of segments in alpha-synuclein/NAC precursor that bind Abeta and NAC." Biochem J **323 (Pt 2)**: 539-46.

Jensen, P. H., M. S. Nielsen, et al. (1998). "Binding of alpha-synuclein to brain vesicles is abolished by familial Parkinson's disease mutation." J Biol Chem **273**(41): 26292-4.

Jiang, Y., Y. E. Liu, et al. (2004). "Gamma synuclein, a novel heat-shock protein-associated chaperone, stimulates ligand-dependent estrogen receptor alpha signaling and mammary tumorigenesis." Cancer Res **64**(13): 4539-46.

Jo, E., J. McLaurin, et al. (2000). "alpha-Synuclein membrane interactions and lipid specificity." J Biol Chem **275**(44): 34328-34.

Kamiyoshihara, T., M. Kojima, et al. (2007). "Observation of multiple intermediates in alpha-synuclein fibril formation by singular value decomposition analysis." Biochem Biophys Res Commun **355**(2): 398-403.

Kawahara, M., Y. Kuroda, et al. (2000). "Alzheimer's beta-amyloid, human islet amylin, and prion protein fragment evoke intracellular free calcium elevations by a common mechanism in a hypothalamic GnRH neuronal cell line." J Biol Chem **275**(19): 14077-83.

Kim, T. D., S. R. Paik, et al. (2002). "Structural and functional implications of C-terminal regions of alpha-synuclein." Biochemistry **41**(46): 13782-90.

Kirik, D., C. Rosenblad, et al. (2002). "Parkinson-like neurodegeneration induced by targeted overexpression of alpha-synuclein in the nigrostriatal system." J Neurosci **22**(7): 2780-91.

Klajnert, B., M. Cangiotti, et al. (2007). "EPR study of the interactions between dendrimers and peptides involved in Alzheimer's and prion diseases." Macromol Biosci **7**(8): 1065-74.

Klewpatinond, M., P. Davies, et al. (2008). "Deconvoluting the Cu2+ binding modes of full-length prion protein." J Biol Chem **283**(4): 1870-81.

Kowalik-Jankowska, T., A. Rajewska, et al. (2006). "Copper(II) binding by fragments of alpha-synuclein containing M1-D2- and -H50-residues; a combined potentiometric and spectroscopic study." Dalton Trans(42): 5068-76.

Kowalik-Jankowska, T., A. Rajewska, et al. (2006). "Products of Cu(II)-catalyzed oxidation of the N-terminal fragments of alpha-synuclein in the presence of hydrogen peroxide." J Inorg Biochem **100**(10): 1623-31.

Kowalik-Jankowska, T., A. Rajewska, et al. (2005). "Coordination abilities of N-terminal fragments of alpha-synuclein towards copper(II) ions: a combined potentiometric and spectroscopic study." J Inorg Biochem **99**(12): 2282-91.

Kruger, R., W. Kuhn, et al. (1998). "Ala30Pro mutation in the gene encoding alpha-synuclein in Parkinson's disease." Nat Genet **18**(2): 106-8.

Lannfelt, L., K. Blennow, et al. (2008). "Safety, efficacy, and biomarker findings of PBT2 in targeting Abeta as a modifying therapy for Alzheimer's disease: a phase IIa, double-blind, randomised, placebo-controlled trial." Lancet Neurol **7**(9): 779-86.

Lashuel, H. A., D. Hartley, et al. (2002). "Neurodegenerative disease: amyloid pores from pathogenic mutations." Nature **418**(6895): 291.

Lashuel, H. A., B. M. Petre, et al. (2002). "Alpha-synuclein, especially the Parkinson's disease-associated mutants, forms pore-like annular and tubular protofibrils." J Mol Biol **322**(5): 1089-102.

Lavedan, C., S. Buchholtz, et al. (1998). "Absence of mutation in the beta- and gamma-synuclein genes in familial autosomal dominant Parkinson's disease." DNA Res **5**(6): 401-2.

Lavedan, C., E. Leroy, et al. (1998). "Identification, localization and characterization of the human gamma-synuclein gene." Hum Genet **103**(1): 106-12.

Lee, D., S. R. Paik, et al. (2004). "Beta-synuclein exhibits chaperone activity more efficiently than alpha-synuclein." FEBS Lett **576**(1-2): 256-60.

Lee, E. N., S. Y. Lee, et al. (2003). "Lipid interaction of alpha-synuclein during the metal-catalyzed oxidation in the presence of Cu2+ and H2O2." J Neurochem **84**(5): 1128-42.

Lee, M. K., W. Stirling, et al. (2002). "Human alpha-synuclein-harboring familial Parkinson's disease-linked Ala-53 --> Thr mutation causes neurodegenerative disease with alpha-synuclein aggregation in transgenic mice." Proc Natl Acad Sci U S A **99**(13): 8968-73.

Lee, P. H., G. Lee, et al. (2006). "The plasma alpha-synuclein levels in patients with Parkinson's disease and multiple system atrophy." J Neural Transm **113**(10): 1435-9.

Lee, S. J. (2003). "alpha-synuclein aggregation: a link between mitochondrial defects and Parkinson's disease?" Antioxid Redox Signal **5**(3): 337-48.

Leong, S. L., C. L. Pham, et al. (2009). "Formation of dopamine-mediated alpha-synuclein-soluble oligomers requires methionine oxidation." Free Radic Biol Med **46**(10): 1328-37.

Li, J., V. N. Uversky, et al. (2001). "Effect of familial Parkinson's disease point mutations A30P and A53T on the structural properties, aggregation, and fibrillation of human alpha-synuclein." Biochemistry **40**(38): 11604-13.

Li, J., V. N. Uversky, et al. (2002). "Conformational behavior of human alpha-synuclein is modulated by familial Parkinson's disease point mutations A30P and A53T." Neurotoxicology **23**(4-5): 553-67.

Lo Bianco, C., J. L. Ridet, et al. (2002). "alpha -Synucleinopathy and selective dopaminergic neuron loss in a rat lentiviral-based model of Parkinson's disease."

Proc Natl Acad Sci U S A **99**(16): 10813-8.

Lotharius, J., S. Barg, et al. (2002). "Effect of mutant alpha-synuclein on dopamine homeostasis in a new human mesencephalic cell line." J Biol Chem **277**(41): 38884-94.

Lotharius, J. and P. Brundin (2002). "Pathogenesis of Parkinson's disease: dopamine, vesicles and alpha-synuclein." Nat Rev Neurosci **3**(12): 932-42.

Lowe, R., D. L. Pountney, et al. (2004). "Calcium(II) selectively induces alpha-synuclein annular oligomers via interaction with the C-terminal domain." Protein Sci **13**(12): 3245-52.

Madine, J., A. J. Doig, et al. (2006). "A study of the regional effects of alpha-synuclein on the organization and stability of phospholipid bilayers." Biochemistry **45**(18): 5783-92.

Mandel, S., G. Maor, et al. (2004). "Iron and alpha-synuclein in the substantia nigra of MPTP-treated mice: effect of neuroprotective drugs R-apomorphine and green tea polyphenol (-)-epigallocatechin-3-gallate." J Mol Neurosci **24**(3): 401-16.

Maroteaux, L., J. T. Campanelli, et al. (1988). "Synuclein: a neuron-specific protein localized to the nucleus and presynaptic nerve terminal." J Neurosci **8**(8): 2804-15.

Maroteaux, L. and R. H. Scheller (1991). "The rat brain synucleins; family of proteins transiently associated with neuronal membrane." Brain Res Mol Brain Res **11**(3-4): 335-43.

Martin, F. L., S. J. Williamson, et al. (2003). "Fe(II)-induced DNA damage in alpha-synuclein-transfected human dopaminergic BE(2)-M17 neuroblastoma cells: detection by the Comet assay." J Neurochem **87**(3): 620-30.

Martin, L. J., Y. Pan, et al. (2006). "Parkinson's disease alpha-synuclein transgenic mice develop neuronal mitochondrial degeneration and cell death." J Neurosci **26**(1): 41-50.

Masliah, E., E. Rockenstein, et al. (2000). "Dopaminergic loss and inclusion body formation in alpha-synuclein mice: implications for neurodegenerative disorders." Science **287**(5456): 1265-9.

McLean, P. J., H. Kawamata, et al. (2000). "Membrane association and protein conformation of alpha-synuclein in intact neurons. Effect of Parkinson's disease-linked mutations." J Biol Chem **275**(12): 8812-6.

McNaught, K. S. and P. Jenner (2001). "Proteasomal function is impaired in substantia nigra in Parkinson's disease." Neurosci Lett **297**(3): 191-4.

Murphy, D. D., S. M. Rueter, et al. (2000). "Synucleins are developmentally expressed, and alpha-synuclein regulates the size of the presynaptic vesicular pool in primary hippocampal neurons." J Neurosci **20**(9): 3214-20.

Murray, I. V., B. I. Giasson, et al. (2003). "Role of alpha-synuclein carboxy-terminus on fibril formation in vitro." Biochemistry **42**(28): 8530-40.

Nakajo, S., S. Shioda, et al. (1994). "Localization of phosphoneuroprotein 14 (PNP 14) and its mRNA expression in rat brain determined by immunocytochemistry and in situ hybridization." Brain Res Mol Brain Res **27**(1): 81-6.

Nakajo, S., K. Tsukada, et al. (1996). "Distribution of phosphoneuroprotein 14 (PNP 14) in vertebrates: its levels as determined by enzyme immunoassay." Brain Res **741**(1-2): 180-4.

Nakajo, S., K. Tsukada, et al. (1993). "A new brain-specific 14-kDa protein is a phosphoprotein. Its complete amino acid sequence and evidence for phosphorylation." Eur J Biochem **217**(3): 1057-63.

Narhi, L., S. J. Wood, et al. (1999). "Both familial Parkinson's disease mutations accelerate alpha-synuclein aggregation." J Biol Chem **274**(14): 9843-6.

Neumann, M., P. J. Kahle, et al. (2002). "Misfolded proteinase K-resistant hyperphosphorylated alpha-synuclein in aged transgenic mice with locomotor deterioration and in human alpha-synucleinopathies." J Clin Invest **110**(10): 1429-39.

Nielsen, M. S., H. Vorum, et al. (2001). "Ca2+ binding to alpha-synuclein regulates ligand binding and oligomerization." J Biol Chem **276**(25): 22680-4.

Ninkina, N. N., M. V. Alimova-Kost, et al. (1998). "Organization, expression and polymorphism of the human persyn gene." Hum Mol Genet **7**(9): 1417-24.

Ninkina, N. N., E. M. Privalova, et al. (1999). "Developmentally regulated expression of persyn, a member of the synuclein family, in skin." Exp Cell Res **246**(2): 308-11.

Nishioka, K., S. Hayashi, et al. (2006). "Clinical heterogeneity of alpha-synuclein gene duplication in Parkinson's disease." Ann Neurol **59**(2): 298-309.

Ohtake, H., P. Limprasert, et al. (2004). "Beta-synuclein gene alterations in dementia with Lewy bodies." Neurology **63**(5): 805-11.

Okochi, M., J. Walter, et al. (2000). "Constitutive phosphorylation of the Parkinson's disease associated alpha-synuclein." J Biol Chem **275**(1): 390-7.

Ostrerova-Golts, N., L. Petrucelli, et al. (2000). "The A53T alpha-synuclein mutation increases iron-dependent aggregation and toxicity." J Neurosci **20**(16): 6048-54.

Paik, S. R., J. H. Lee, et al. (1997). "Aluminum-induced structural alterations of the precursor of the non-A beta component of Alzheimer's disease amyloid." Arch Biochem Biophys **344**(2): 325-34.

Paik, S. R., H. J. Shin, et al. (2000). "Metal-catalyzed oxidation of alpha-synuclein in

the presence of Copper(II) and hydrogen peroxide." Arch Biochem Biophys **378**(2): 269-77.

Paik, S. R., H. J. Shin, et al. (1999). "Copper(II)-induced self-oligomerization of alpha-synuclein." Biochem J **340 (Pt 3)**: 821-8.

Palecek, E., V. Ostatna, et al. (2008). "Changes in interfacial properties of alpha-synuclein preceding its aggregation." Analyst **133**(1): 76-84.

Pall, H. S., A. C. Williams, et al. (1987). "Raised cerebrospinal-fluid copper concentration in Parkinson's disease." Lancet **2**(8553): 238-41.

Parihar, M. S., A. Parihar, et al. (2008). "Mitochondrial association of alpha-synuclein causes oxidative stress." Cell Mol Life Sci **65**(7-8): 1272-84.

Park, J. Y. and P. T. Lansbury, Jr. (2003). "Beta-synuclein inhibits formation of alpha-synuclein protofibrils: a possible therapeutic strategy against Parkinson's disease." Biochemistry **42**(13): 3696-700.

Park, S. M., H. Y. Jung, et al. (2002). "Distinct roles of the N-terminal-binding domain and the C-terminal-solubilizing domain of alpha-synuclein, a molecular chaperone." J Biol Chem **277**(32): 28512-20.

Peisach, J. and W. E. Blumberg (1974). "Structural implications derived from the analysis of electron paramagnetic resonance spectra of natural and artificial copper proteins." Arch Biochem Biophys **165**(2): 691-708.

Perez, R. G., J. C. Waymire, et al. (2002). "A role for alpha-synuclein in the regulation of dopamine biosynthesis." J Neurosci **22**(8): 3090-9.

Periquet, M., T. Fulga, et al. (2007). "Aggregated alpha-synuclein mediates dopaminergic neurotoxicity in vivo." J Neurosci **27**(12): 3338-46.

Perrin, R. J., W. S. Woods, et al. (2000). "Interaction of human alpha-Synuclein and Parkinson's disease variants with phospholipids. Structural analysis using site-directed mutagenesis." J Biol Chem **275**(44): 34393-8.

Perrin, R. J., W. S. Woods, et al. (2001). "Exposure to long chain polyunsaturated fatty acids triggers rapid multimerization of synucleins." J Biol Chem **276**(45): 41958-62.

Petrucelli, L., C. O'Farrell, et al. (2002). "Parkin protects against the toxicity associated with mutant alpha-synuclein: proteasome dysfunction selectively affects catecholaminergic neurons." Neuron **36**(6): 1007-19.

Polymeropoulos, M. H., J. J. Higgins, et al. (1996). "Mapping of a gene for Parkinson's disease to chromosome 4q21-q23." Science **274**(5290): 1197-9.

Polymeropoulos, M. H., C. Lavedan, et al. (1997). "Mutation in the alpha-synuclein gene identified in families with Parkinson's disease." Science **276**(5321): 2045-7.

Purisai, M. G., A. L. McCormack, et al. (2005). "Alpha-synuclein expression in the substantia nigra of MPTP-lesioned non-human primates." Neurobiol Dis **20**(3): 898-906.

Ramakrishnan, M., P. H. Jensen, et al. (2003). "Alpha-synuclein association with phosphatidylglycerol probed by lipid spin labels." Biochemistry **42**(44): 12919-26.

Rasia, R. M., C. W. Bertoncini, et al. (2005). "Structural characterization of copper(II) binding to alpha-synuclein: Insights into the bioinorganic chemistry of Parkinson's disease." Proc Natl Acad Sci U S A **102**(12): 4294-9.

Ren, G., X. Wang, et al. (2007). "Translocation of alpha-synuclein expressed in Escherichia coli." J Bacteriol **189**(7): 2777-86.

Riederer, P., E. Sofic, et al. (1989). "Transition metals, ferritin, glutathione, and ascorbic acid in parkinsonian brains." J Neurochem **52**(2): 515-20.

Ritchie, C. W., A. I. Bush, et al. (2003). "Metal-protein attenuation with iodochlorhydroxyquin (clioquinol) targeting Abeta amyloid deposition and toxicity in Alzheimer disease: a pilot phase 2 clinical trial." Arch Neurol **60**(12): 1685-91.

Rochet, J. C., K. A. Conway, et al. (2000). "Inhibition of fibrillization and accumulation of prefibrillar oligomers in mixtures of human and mouse alpha-synuclein." Biochemistry **39**(35): 10619-26.

Salem, S. A., D. Allsop, et al. (2007). "An investigation into the lipid-binding properties of alpha-, beta- and gamma-synucleins in human brain and cerebrospinal fluid." Brain Res **1170**: 103-11.

Sayre, L. M., P. I. Moreira, et al. (2005). "Metal ions and oxidative protein modification in neurological disease." Ann Ist Super Sanita **41**(2): 143-64.

Serpell, L. C., J. Berriman, et al. (2000). "Fiber diffraction of synthetic alpha-synuclein filaments shows amyloid-like cross-beta conformation." Proc Natl Acad Sci U S A **97**(9): 4897-902.

Sharon, R., I. Bar-Joseph, et al. (2003). "The formation of highly soluble oligomers of alpha-synuclein is regulated by fatty acids and enhanced in Parkinson's disease." Neuron **37**(4): 583-95.

Shavali, S., H. M. Brown-Borg, et al. (2008). "Mitochondrial localization of alpha-synuclein protein in alpha-synuclein overexpressing cells." Neurosci Lett **439**(2): 125-8.

Shavali, S., E. C. Carlson, et al. (2004). "1-Benzyl-1,2,3,4-tetrahydroisoquinoline, a Parkinsonism-inducing endogenous toxin, increases alpha-synuclein expression and causes nuclear damage in human dopaminergic cells." J Neurosci Res **76**(4): 563-71.

Sherer, T. B., R. Betarbet, et al. (2001). "Pathogenesis of Parkinson's disease." Curr

Opin Investig Drugs **2**(5): 657-62.

Shin, H. J., E. K. Lee, et al. (2000). "Eosin interaction of alpha-synuclein leading to protein self-oligomerization." Biochim Biophys Acta **1481**(1): 139-46.

Singleton, A. B., M. Farrer, et al. (2003). "alpha-Synuclein locus triplication causes Parkinson's disease." Science **302**(5646): 841.

Snyder, H., K. Mensah, et al. (2005). "beta-Synuclein reduces proteasomal inhibition by alpha-synuclein but not gamma-synuclein." J Biol Chem **280**(9): 7562-9.

Snyder, H., K. Mensah, et al. (2003). "Aggregated and monomeric alpha-synuclein bind to the S6' proteasomal protein and inhibit proteasomal function." J Biol Chem **278**(14): 11753-9.

Souza, J. M., B. I. Giasson, et al. (2000). "Chaperone-like activity of synucleins." FEBS Lett **474**(1): 116-9.

Spillantini, M. G., R. A. Crowther, et al. (1998). "alpha-Synuclein in filamentous inclusions of Lewy bodies from Parkinson's disease and dementia with lewy bodies." Proc Natl Acad Sci U S A **95**(11): 6469-73.

Spillantini, M. G., A. Divane, et al. (1995). "Assignment of human alpha-synuclein (SNCA) and beta-synuclein (SNCB) genes to chromosomes 4q21 and 5q35." Genomics **27**(2): 379-81.

Spillantini, M. G., M. L. Schmidt, et al. (1997). "Alpha-synuclein in Lewy bodies." Nature **388**(6645): 839-40.

Stefanis, L., K. E. Larsen, et al. (2001). "Expression of A53T mutant but not wild-type alpha-synuclein in PC12 cells induces alterations of the ubiquitin-dependent degradation system, loss of dopamine release, and autophagic cell death." J Neurosci **21**(24): 9549-60.

Su, X., K. A. Maguire-Zeiss, et al. (2008). "Synuclein activates microglia in a model of Parkinson's disease." Neurobiol Aging **29**(11): 1690-701.

Sung, Y. H. and D. Eliezer (2006). "Secondary structure and dynamics of micelle bound beta- and gamma-synuclein." Protein Sci **15**(5): 1162-74.

Sung, Y. H. and D. Eliezer (2007). "Residual structure, backbone dynamics, and interactions within the synuclein family." J Mol Biol **372**(3): 689-707.

Sung, Y. H., C. Rospigliosi, et al. (2006). "NMR mapping of copper binding sites in alpha-synuclein." Biochim Biophys Acta **1764**(1): 5-12.

Takeda, A., M. Hashimoto, et al. (1998). "Abnormal distribution of the non-Abeta component of Alzheimer's disease amyloid precursor/alpha-synuclein in Lewy body disease as revealed by proteinase K and formic acid pretreatment." Lab Invest **78**(9): 1169-77.

Tamamizu-Kato, S., M. G. Kosaraju, et al. (2006). "Calcium-triggered membrane interaction of the alpha-synuclein acidic tail." Biochemistry **45**(36): 10947-56.

Tamo, W., T. Imaizumi, et al. (2002). "Expression of alpha-synuclein, the precursor of non-amyloid beta component of Alzheimer's disease amyloid, in human cerebral blood vessels." Neurosci Lett **326**(1): 5-8.

Tanaka, Y., S. Engelender, et al. (2001). "Inducible expression of mutant alpha-synuclein decreases proteasome activity and increases sensitivity to mitochondria-dependent apoptosis." Hum Mol Genet **10**(9): 919-26.

Thompsett, A. R., S. R. Abdelraheim, et al. (2005). "High affinity binding between copper and full-length prion protein identified by two different techniques." J Biol Chem **280**(52): 42750-8.

Tofaris, G. K. and M. G. Spillantini (2007). "Physiological and pathological properties of alpha-synuclein." Cell Mol Life Sci **64**(17): 2194-201.

Trostchansky, A., S. Lind, et al. (2006). "Interaction with phospholipids modulates alpha-synuclein nitration and lipid-protein adduct formation." Biochem J **393**(Pt 1): 343-9.

Tsigelny, I. F., P. Bar-On, et al. (2007). "Dynamics of alpha-synuclein aggregation and inhibition of pore-like oligomer development by beta-synuclein." Febs J **274**(7): 1862-77.

Turnbull, S., B. J. Tabner, et al. (2001). "alpha-Synuclein implicated in Parkinson's disease catalyses the formation of hydrogen peroxide in vitro." Free Radic Biol Med **30**(10): 1163-70.

Ueda, K., H. Fukushima, et al. (1993). "Molecular cloning of cDNA encoding an unrecognized component of amyloid in Alzheimer disease." Proc Natl Acad Sci U S A **90**(23): 11282-6.

Uversky, V. N. (2003). "A protein-chameleon: conformational plasticity of alpha-synuclein, a disordered protein involved in neurodegenerative disorders." J Biomol Struct Dyn **21**(2): 211-34.

Uversky, V. N. (2007). "Neuropathology, biochemistry, and biophysics of alpha-synuclein aggregation." J Neurochem **103**(1): 17-37.

Uversky, V. N., M. C. E, et al. (2002). "Accelerated alpha-synuclein fibrillation in crowded milieu." FEBS Lett **515**(1-3): 99-103.

Uversky, V. N., H. J. Lee, et al. (2001). "Stabilization of partially folded conformation during alpha-synuclein oligomerization in both purified and cytosolic preparations." J Biol Chem **276**(47): 43495-8.

Uversky, V. N., J. Li, et al. (2001). "Evidence for a partially folded intermediate in

alpha-synuclein fibril formation." J Biol Chem **276**(14): 10737-44.

Uversky, V. N., J. Li, et al. (2001). "Metal-triggered structural transformations, aggregation, and fibrillation of human alpha-synuclein. A possible molecular NK between Parkinson's disease and heavy metal exposure." J Biol Chem **276**(47): 44284-96.

Uversky, V. N., J. Li, et al. (2002). "Biophysical properties of the synucleins and their propensities to fibrillate: inhibition of alpha-synuclein assembly by beta- and gamma-synucleins." J Biol Chem **277**(14): 11970-8.

Volles, M. J. and P. T. Lansbury, Jr. (2002). "Vesicle permeabilization by protofibrillar alpha-synuclein is sensitive to Parkinson's disease-linked mutations and occurs by a pore-like mechanism." Biochemistry **41**(14): 4595-602.

Volles, M. J. and P. T. Lansbury, Jr. (2003). "Zeroing in on the pathogenic form of alpha-synuclein and its mechanism of neurotoxicity in Parkinson's disease." Biochemistry **42**(26): 7871-8.

Volles, M. J. and P. T. Lansbury, Jr. (2007). "Relationships between the sequence of alpha-synuclein and its membrane affinity, fibrillization propensity, and yeast toxicity." J Mol Biol **366**(5): 1510-22.

Weinreb, P. H., W. Zhen, et al. (1996). "NACP, a protein implicated in Alzheimer's disease and learning, is natively unfolded." Biochemistry **35**(43): 13709-15.

Wells, M. A., G. S. Jackson, et al. (2006). "A reassessment of copper(II) binding in the full-length prion protein." Biochem J **399**(3): 435-44.

Wolozin, B. and N. Golts (2002). "Iron and Parkinson's disease." Neuroscientist **8**(1): 22-32.

Wood, S. J., J. Wypych, et al. (1999). "alpha-synuclein fibrillogenesis is nucleation-dependent. Implications for the pathogenesis of Parkinson's disease." J Biol Chem **274**(28): 19509-12.

Wright, J. A. and D. R. Brown (2008). "Alpha-synuclein and its role in metal binding: relevance to Parkinson's disease." J Neurosci Res **86**(3): 496-503.

Wright, J. A., X. Wang, et al. (2009). "Unique copper-induced oligomers mediate alpha-synuclein toxicity." Faseb J **23**(8): 2384-93.

Wu, K. P., S. Kim, et al. (2008). "Characterization of conformational and dynamic properties of natively unfolded human and mouse alpha-synuclein ensembles by NMR: implication for aggregation." J Mol Biol **378**(5): 1104-15.

Xia, Y., H. A. Rohan de Silva, et al. (1996). "Genetic studies in Alzheimer's disease with an NACP/alpha-synuclein polymorphism." Ann Neurol **40**(2): 207-15.

Yamin, G., L. A. Munishkina, et al. (2005). "Forcing nonamyloidogenic

beta-synuclein to fibrillate." Biochemistry **44**(25): 9096-107.

Youdim, M. B., D. Ben-Shachar, et al. (1993). "The possible role of iron in the etiopathology of Parkinson's disease." Mov Disord **8**(1): 1-12.

Yu, S., X. Li, et al. (2007). "Extensive nuclear localization of alpha-synuclein in normal rat brain neurons revealed by a novel monoclonal antibody." Neuroscience **145**(2): 539-55.

Yuan, Y., J. Jin, et al. (2008). "Overexpressed alpha-synuclein regulated the nuclear factor-kappaB signal pathway." Cell Mol Neurobiol **28**(1): 21-33.

Zarranz, J. J., J. Alegre, et al. (2004). "The new mutation, E46K, of alpha-synuclein causes Parkinson and Lewy body dementia." Ann Neurol **55**(2): 164-73.

Zayed, J., S. Ducic, et al. (1990). "[Environmental factors in the etiology of Parkinson's disease]." Can J Neurol Sci **17**(3): 286-91.

Zhang, Y., S. Akilesh, et al. (2000). "Isothermal titration calorimetry measurements of Ni(II) and Cu(II) binding to His, GlyGlyHis, HisGlyHis, and bovine serum albumin: A critical evaluation." Inorganic Chemistry **39**(14): 3057-3064.

Zhang, Y., S. Akilesh, et al. (2000). "Isothermal titration calorimetry measurements of Ni(II) and Cu(II) binding to His, GlyGlyHis, HisGlyHis, and bovine serum albumin: a critical evaluation." Inorg Chem **39**(14): 3057-64.

Zhu, M., J. Li, et al. (2003). "The association of alpha-synuclein with membranes affects bilayer structure, stability, and fibril formation." J Biol Chem **278**(41): 40186-97.

Zhu, M., Z. J. Qin, et al. (2006). "Alpha-synuclein can function as an antioxidant preventing oxidation of unsaturated lipid in vesicles." Biochemistry **45**(26): 8135-42.

Zhu, Y. J., H. Lin, et al. (2000). "Fresh and nonfibrillar amyloid beta protein(1-40) induces rapid cellular degeneration in aged human fibroblasts: evidence for AbetaP-channel-mediated cellular toxicity." Faseb J **14**(9): 1244-54.